INSIGHTS IN NEPHROLOGY: 2021

EDITED BY: Maik Gollasch

PUBLISHED IN: Frontiers in Medicine

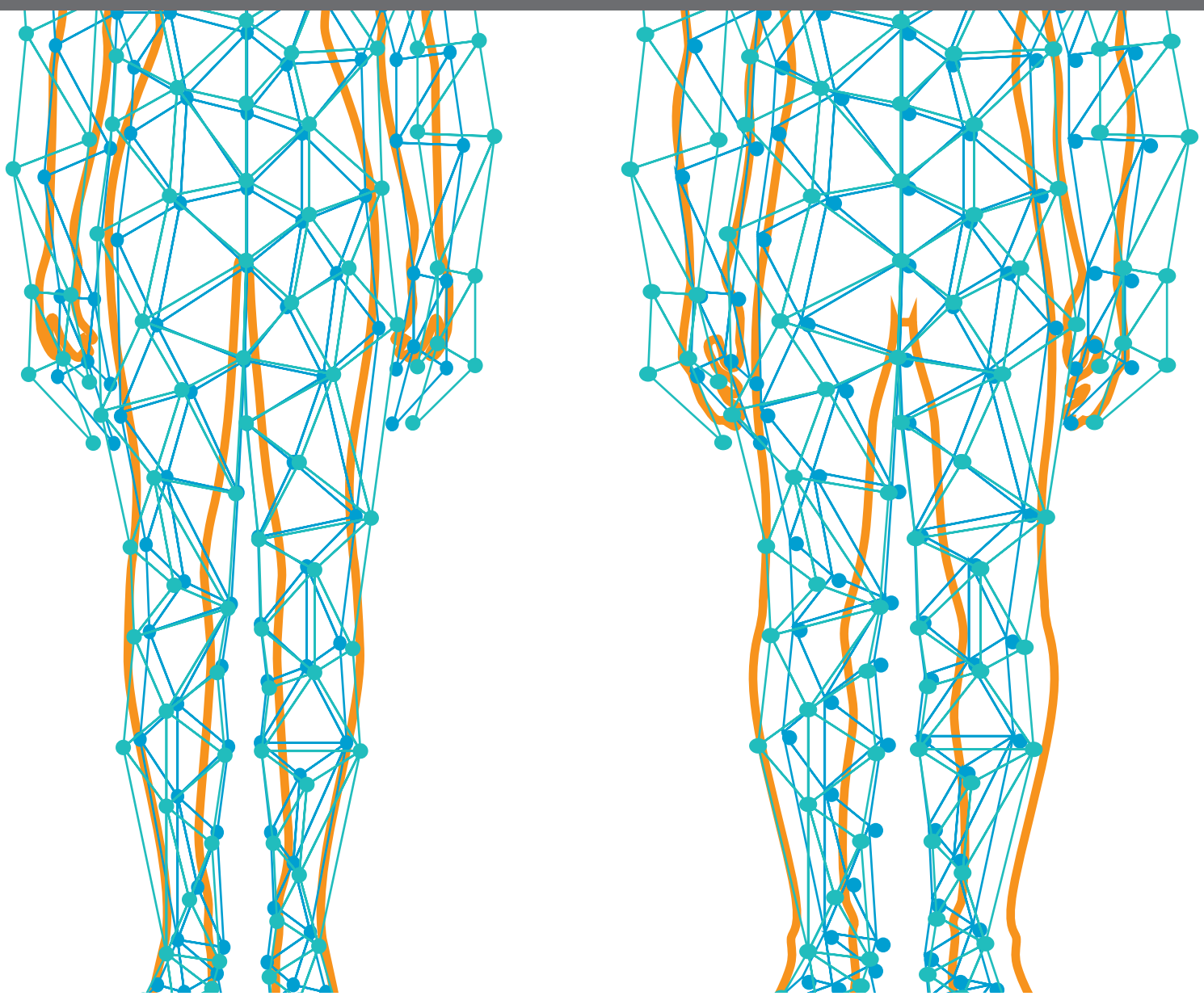

frontiers Research Topics

frontiers

ISSN 1664-8714
ISBN 978-2-83250-670-7
DOI 10.3389/978-2-83250-670-7

About Frontiers

Frontiers is more than just an open-access publisher of scholarly articles: it is a pioneering approach to the world of academia, radically improving the way scholarly research is managed. The grand vision of Frontiers is a world where all people have an equal opportunity to seek, share and generate knowledge. Frontiers provides immediate and permanent online open access to all its publications, but this alone is not enough to realize our grand goals.

Frontiers Journal Series

The Frontiers Journal Series is a multi-tier and interdisciplinary set of open-access, online journals, promising a paradigm shift from the current review, selection and dissemination processes in academic publishing. All Frontiers journals are driven by researchers for researchers; therefore, they constitute a service to the scholarly community. At the same time, the Frontiers Journal Series operates on a revolutionary invention, the tiered publishing system, initially addressing specific communities of scholars, and gradually climbing up to broader public understanding, thus serving the interests of the lay society, too.

Dedication to Quality

Each Frontiers article is a landmark of the highest quality, thanks to genuinely collaborative interactions between authors and review editors, who include some of the world's best academicians. Research must be certified by peers before entering a stream of knowledge that may eventually reach the public - and shape society; therefore, Frontiers only applies the most rigorous and unbiased reviews.
Frontiers revolutionizes research publishing by freely delivering the most outstanding research, evaluated with no bias from both the academic and social point of view. By applying the most advanced information technologies, Frontiers is catapulting scholarly publishing into a new generation.

What are Frontiers Research Topics?

Frontiers Research Topics are very popular trademarks of the Frontiers Journals Series: they are collections of at least ten articles, all centered on a particular subject. With their unique mix of varied contributions from Original Research to Review Articles, Frontiers Research Topics unify the most influential researchers, the latest key findings and historical advances in a hot research area! Find out more on how to host your own Frontiers Research Topic or contribute to one as an author by contacting the Frontiers Editorial Office: frontiersin.org/about/contact

INSIGHTS IN NEPHROLOGY: 2021

Topic Editor:
Maik Gollasch, Charité Universitätsmedizin Berlin, Germany

Citation: Gollasch, M., ed. (2022). Insights in Nephrology: 2021. Lausanne: Frontiers Media SA. doi: 10.3389/978-2-83250-670-7

Table of Contents

frontiers in Medicine

ORIGINAL RESEARCH
published: 13 January 2021
doi: 10.3389/fmed.2020.609582

Renal Expression of Light Chain Binding Proteins

Thomas Reiter[1†], Sahra Pajenda[1†], David O'Connell[2,3], Ciara Lynch[2,3], Sebastian Kapps[1], Hermine Agis[4], Alice Schmidt[1], Ludwig Wagner[1], Nelson Leung[5] and Wolfgang Winnicki[1]*

[1] Department of Medicine III, Division of Nephrology and Dialysis, Medical University of Vienna, Vienna, Austria, [2] School of Biomolecular & Biomedical Science, University College Dublin, Dublin, Ireland, [3] BiOrbic Bioeconomy Research Centre, University College Dublin, Dublin, Ireland, [4] Department of Medicine I, Division of Oncology, Medical University of Vienna, Vienna, Austria, [5] Division of Nephrology and Hypertension, Division of Hematology, Mayo Clinic Rochester, Rochester, MN, United States

Overproduction of human light chains (LCs) and immunoglobulins can result in various forms of renal disease such as cast nephropathy, monoclonal immunoglobulin deposition disease, LC proximal tubulopathy, AL amyloidosis, and crystal storing histiocytosis. This is caused by cellular uptake of LCs and overwhelmed intracellular transport and degradation in patients with high urine LC concentrations. LC kappa and lambda purification was evaluated by sodium dodecyl sulfate gel electrophoresis. LC and myeloma protein binding to immobilized renal proteins was measured by enzyme-linked immunosorbent assay (ELISA). The human protein microarray (HuProt^{TM}) was screened with purified kappa and lambda LC. Identified LC partners were subsequently analyzed *in silico* for renal expression sites using protein databases, Human Protein Atlas, UniProt, and Bgee. Binding of urinary LCs and immunoglobulins to immobilized whole renal proteins from 22 patients with myeloma or plasma cell dyscrasia was shown by ELISA. Forty lambda and 23 kappa interaction partners were identified from HuProt^{TM} array screens, of which 21 were shared interactors. Among the total of 42 interactors, 12 represented cell surface proteins. Lambda binding signals were approximately 40% higher than kappa signals. LC interaction with renal cells and disease-causing pathologies are more complex than previously thought. It involves an extended spectrum of proteins expressed throughout the nephron, and their identification has been enabled by recently developed methods of protein analysis such as protein microarray screening. Further biochemical studies on interacting proteins are warranted to elucidate their clinical relevance.

Keywords: amyloidosis, multiple myeloma, light chains, light chain associated kidney disorders, monoclonal gammopathy, protein micro array analysis

OPEN ACCESS

Edited by:
Xu-jie Zhou,
Peking University First Hospital, China

Reviewed by:
Efstathios Kastritis,
National and Kapodistrian University of Athens, Greece
Ben Sprangers,
University Hospitals Leuven, Belgium

***Correspondence:**
Sahra Pajenda
sahra.pajenda@meduniwien.ac.at

[†] These authors have contributed equally to this work

Specialty section:
This article was submitted to Nephrology, a section of the journal Frontiers in Medicine

Received: *23 September 2020*
Accepted: *03 December 2020*
Published: *13 January 2021*

Citation:
Reiter T, Pajenda S, O'Connell D, Lynch C, Kapps S, Agis H, Schmidt A, Wagner L, Leung N and Winnicki W (2021) Renal Expression of Light Chain Binding Proteins. Front. Med. 7:609582. doi: 10.3389/fmed.2020.609582

INTRODUCTION

The most frequent multiple myeloma–associated renal lesion is cast nephropathy (1, 2). This pathological entity is assumed to develop by precipitation of monoclonal free light chains (LCs) associated with uromodulin (3, 4). Cast nephropathy can also be associated with other renal lesions such as monoclonal immunoglobulin deposition disease, LC proximal tubulopathy, AL amyloidosis, and crystal storing histiocytosis (2). Thereby all parts of the nephron can be affected (5). The topology of manifestation is specific to the type and physicochemical properties

of the secreted paraprotein (6). In addition to an increased presence of LCs in urine, other factors such as a reduction in tubular flow or an increase in urine salt concentration and the intake of non-steroidal anti-inflammatory drugs (7) can negatively influence cast formation. Pharmacotherapeutic attempts have been performed to improve the outcome in cast nephropathy through modulation of urine pH (8). Also, an approach with intravenous application of a cyclic peptide to inhibit LC aggregation showed promising results in animals (9).

It is well-documented that in healthy individuals LCs appear in primary urine, but are reabsorbed by the proximal tubule through cubilin and megalin according to earlier experiments (10, 11). When the clonal disorder progresses with increasing monoclonal LC production, the reabsorption rate in the proximal tubule is overwhelmed, causing high urine concentration in the distal tubule and LC aggregation and precipitation. The impairment of urine flow in the tubule is not the only issue. Moreover, there is an interaction with tubular cell surface proteins and LCs. This protein binding induces an altered protein expression (12) and an inflammatory reaction leading to interstitial inflammation and consequently to a cast nephropathy-associated interstitial nephritis (13).

Several research reports documented that cast formation can also occur through other mechanisms than monoclonal LCs such as by the antibiotic vancomycin (14) and high concentration of bile salts (15). In this work, we concentrate on LCs, and it is of note that in particular the lambda LC tends to form oligomers (16). LCs from their nature should associate with heavy chains to form immunoglobulins. From this line of thought, it is evident that LCs, when present in high concentration, find various interaction partners even with cell surface proteins of tubular cells. Motivated by the work of previous authors, we immobilized whole renal cell protein lysate on enzyme-linked immunosorbent assay (ELISA) plates and investigated binding intensities of urinary excreted LCs/immunoglobulins obtained from patients with multiple myeloma and controls. To obtain more detailed data on specific binding partners, we purified urinary monoclonal LC kappa and lambda and sought for ways to investigate their interaction potential with renal tubular cell proteins. For this purpose, protein microarrays with 23,000 proteins originating from 16,000 human genes were screened with either purified kappa or lambda LCs. In addition, protein databases, the Human Protein Atlas, UniProt, and Bgee were studied to verify the primary structure and to identify the site and extent of expression in the renal tissue and nephron.

MATERIALS AND METHODS

Urine samples from 22 patients treated at the hematology outpatient unit for multiple myeloma or plasma cell dyscrasia were available for analysis in this study. In addition, urine samples from four patients with acute kidney injury due to delayed graft function after renal transplantation and from two healthy individuals were used as controls. Urine obtained from two patients with monoclonal LC excretion and cast nephropathy was chosen for LC purification. The study was approved by the ethics committee of the Medical University of Vienna (EK 2193/2015). All patients were adults older than 18 years and provided written informed consent.

Patient Characteristics

Patient characteristics including hematological classification and renal histology are listed in **Table 1**. The two patients with monoclonal LC excretion and cast nephropathy selected for LC purification had the following histological results.

Patient With LC Kappa

The male patient had a fine-needle biopsy of the kidney, which showed multiple tubular casts with immunohistochemical reactivity to kappa LC–specific antibodies, conversely negative for lambda LCs. Peritubular inflammatory reaction with mononuclear leukocyte infiltration and interstitial fibrosis, as well as atrophy of tubular cells, was characterized. Glomerular structure was without evidence of pathology; especially no LC deposits were present. This was confirmed by electron microscopy showing no evidence of fibrillary deposit structures.

Patient With LC Lambda

The male patient with lambda LC had a bone biopsy performed, but no kidney biopsy due to a deranged coagulation status and poor general condition. In urinary sediment cytoslides, a remarkable number of LC casts (five casts per optical field) were visualized. The individual LC casts were collected under microscope observation and were subjected to mass spectrometry. Results of these date were published recently (16).

Urine Collection

Clean-catch urine was collected in sterile containers and immediately centrifuged at 3,000 revolutions/min (RPM) for 10 min. Precleared urine was frozen in 3.5-mL aliquots at −80°C for further analysis.

LC Purification

Precleared urine was treated with saturated ammonium sulfate solution. In brief, urine was mixed with equal volume of saturated ammonium sulfate solution at room temperature. The resultant mixture turned opaque and was transferred into ultracentrifuge tubes (polycarbonate, Prod# 343778; Beckman Coulter) and fitted into the TLA120.2 rotor of an Optima™ MAX-XP ultracentrifuge. Following 1-h centrifugation at 40,000 RPM = 69,000*g*, the supernatant was separated from the pellet. The pellet was redissolved in 1/2 phosphate-buffered saline (PBS) immediately. The redissolved protein was loaded onto a sodium dodecyl sulfate–polyacrylamide gel electrophoresis (SDS-PAGE) and run under non-reducing conditions using TRIS–glycine–SDS as running buffer. The resultant gel was stained by Coomassie blue, followed by destaining in order to visualize LC oligomeric or monomeric structures.

The recovered LC protein was dialyzed in slide dialyzers (Slide-A-Lyzer Dialysis Cassette, Prod# 66330, Thermo Scientific) against PBS at 4°C for 48 h with two changes of the PBS dialysis buffer. These LCs were subsequently used for protein array screening.

TABLE 1 | Demographics of patients with monoclonal gammopathy and paraproteins.

ID	Age	Gender	LC	sCr	U[P/C]	Hematological classification	Renal histology	Disease duration
1	78	m	λ	1.03	49	MM	n.a.	10
2	71	f	κ	1.07	194	MGUS	n.a.	5
3	82	f	κ	0.90	256	MM	n.a.	3
4	81	f	λ	0.97	659	AL amyloidosis	n.a.	3
5	88	f	κ	1.15	1	MGRS	n.a.	6
6	50	m	κ	1.34	214	MM	n.a.	1
7	69	m	κ	0.99	115	MGUS	n.a.	7
8	81	f	λ	0.72	58	MM	n.a.	10
9	70	f	λ	1.11	112	MGRS	LCPT	1
10	77	f	λ	0.64	81	MM	n.a.	10
11	60	m	λ	1.07	115	MM	n.a.	2
12	79	m	λ	2.69	460	MGRS	FGN	2
13	64	f	κ	0.90	274	MM	n.a.	6
14	75	m	λ	0.79	245	MM	n.a.	6
15	84	m	κ	1.94	283	MM	n.a.	9
16	69	m	λ	0.66	1	MGUS	n.a.	6
17	81	m	κ	0.86	118	MM	n.a.	1
18	79	m	λ	1.05	228	MM	n.a.	1
19	77	m	λ	2.43	1714	MM	PGNMID	4
20	78	m	κ	2.90	1091	MGRS	no pathology	6
21	85	f	λ	0.91	254	MM	n.a.	28
22	73	m	κ	0.97	54	MM	n.a.	2

LC, light chain; λ, lambda light chain; κ, kappa light chain; FGN, monotypic fibrillary glomerulonephritis; LCPT, light-chain proximal tubulopathy; MGRS, monoclonal gammopathy with renal significance; MGUS, monoclonal gammopathy with undefined significance; MM, multiple myeloma; n.a., not available; PGNMID, proliferative glomerulonephritis and monoclonal immunoglobulin deposits; U[P/C], urinary protein/creatinine ratio given in mg/g; sCr, serum creatinine given in mg/dL after 1-year follow-up. Disease duration is given in years.

LC Binding to Renal Proteins Immobilized on ELISA Plates

Two hundred milligrams of human renal tissue was homogenized in 1× tissue lysis buffer (Prod# 9803, Cell Signaling) containing protease inhibitors (cOmplete tablets, Mini EASYpack, Prod# 04693124001, Roche). The tissue lysis was carried out in a Precellys 24 lysis and homogenization machine. Precleared lysate was diluted in PBS (1:1) containing protease inhibitors such as above, and 100 µL was applied to each well of a 96-well flat-bottomed ELISA plate for coating at 4°C overnight. Following a blocking procedure with 1× blocking solution (Prod# 50-61-01, KPL) for 1 h, urine samples were prepared. Urine samples were diluted 1:6 in PBS and incubated at 37°C for 1 h. ELISA plate washing was carried out with tween phosphate buffered saline (TPBS) on an automated ELISA washing machine applying 300-µL wash solution to each well in three cycles. For development of LC/immunoglobulin binding, rabbit anti-human immunoglobulin and LC-specific antibody (PO212, Dako), diluted 1:1,250 in 1× RayBiotech buffer (EL-ITEME2), was incubated for 1 h at 37°C. Following the second washing procedure using TPBS and the automated ELISA washing machine, the LC/immunoglobulin binding was developed using the dual-component peroxidase substrate solution (Prod# 50-65-00 and 50-76-01, KPL). The resultant signal was stopped by adding 50 µL of 2N HCl, and signals were quantitated by an ELISA reader at 450 nm. Sample and control measurements were carried out in triplicate.

Protein Array Screening

Human protein microarrays (HuProt™, Human Proteome Microarrays, Cambridge Protein Arrays) were screened at 4°C. Arrays were blocked in 5% human serum albumin (wt/vol) in Tris-buffered saline, 0.1% Tween (TBST), for 60 min followed by incubation with either purified LC protein at 1 µM for 1.5 h. Samples were applied to the microarray surface and a coverslip placed on the sample. After incubation, the microarray was washed for 5 × 2 min in TBST. Alexa Fluor 642 polyclonal goat anti-human heavy chain– and LC-specific secondary antibody (A21445, Invitrogen), diluted in 5% human serum albumin, was then incubated on the microarray at a concentration of 1 µg/mL for 60 min prior to further washing for 5 × 2 min in TBST, rinsing in deionized water, and drying by spinning in a centrifuge at 250*g* for 3 min. The microarrays were imaged on a Genepix 4000B scanner (Axon Instruments). The PMT gain settings were set at 450 for the 635-nm laser with a focus position of 10 µm. A lot-specific gal-file was used to develop.gpr result files from the array scans, and these files were analyzed with a software script developed in house.

Software and Statistical Analysis of Microarray Data

A python script called MicroarraySF was written to statistically analyze the .gpr files. The resulting files contained the calculated total fluorescence (the F635 median minus the background from

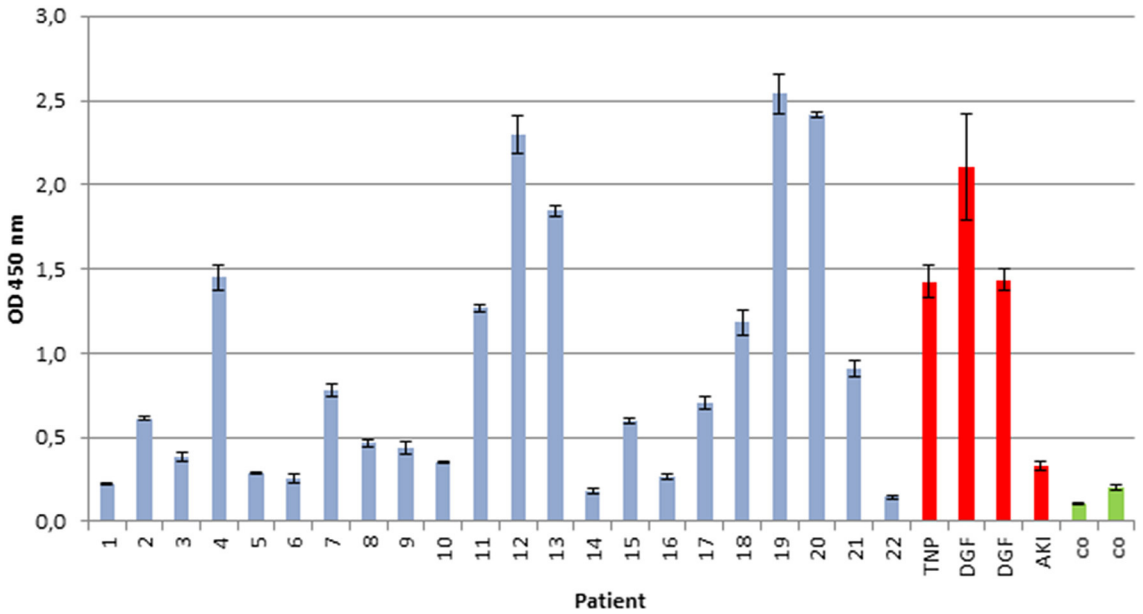

FIGURE 1 | Immunoglobulin/LC binding to immobilized renal whole-cell lysate. Urine of 22 patients with multiple myeloma and plasma cell dyscrasia was incubated in ELISA plates, coated with whole-cell renal lysate, and compared with urine of four patients with renal reperfusion injury (DGF, delayed graft function, red), transplant nephropathy (TNP, red), acute kidney injury (AKI, red), and two healthy controls (CO, green). All experiments were carried out in triplicates. Demographics of patients with multiple myeloma or plasma cell dyscrasia are given in **Table 1**.

the B635 median), as well as the *Z* scores for each protein. A signal-to-noise ratio cutoff of two was imposed, and a *Z* score cutoff of three was used, as reported previously (17). Flagged proteins with a value of <0 were also filtered out. The output file contained only the proteins that met the parameters and gave new statistical information such as the *Z* scores calculated from the F635 median value.

Data management and data analysis were conducted by GraphPad Prism (GraphPad Prism version 7.00 for Windows, GraphPad Software), as well as Microsoft Excel (Microsoft). A linear regression model was deployed to analyze the association between LC binding intensity and serum creatinine as renal function parameter at 1-year follow-up. The regression coefficient is reported with 95% confidence intervals, and a two-sided $p < 0.05$ was considered significant.

Preparation of LC Affinity Columns and Renal Protein Affinity Chromatography

The redissolved LCs were dialyzed against PBS at 4°C for 3 days applying three changes of dialysis fluid (PBS). Following swelling and washing CNBr-activated Sepharose 4B with 1 mM HCl, the LC protein was mixed with 1.5 mL gel in stopped disposable column container and rotated for 1 h at room temperature. The column was washed with PBS buffer and exposed to 1 M ethanolamine, pH 8.0, for 2 h. Following the blocking procedure, the column was mock eluted with elution buffer (50 mM glycine, 0.15 M NaCl, 0.1% Tween 20, pH 2.7). Before protein binding, the column was washed with PBS.

Renal whole-cell lysate was precleared by centrifugation at 13,000*g* for 10 min at 4°C, filtered through a 0.22-μm filter, and loaded onto the columns, followed by rotation of the column devices at room temperature for 1 h. The column was washed with 10 column volumes of PBS followed by 10 column volumes of TPBS and then eluted with elution buffer as indicated above in a stepwise mode using 100 μL for collecting in separated tubes.

Twenty microliters of each fraction was then loaded onto a 12% SDS-PAGE gel and run under denaturing conditions. Following the entrance of the loaded protein by 1 cm into the resolving gel, the electrophoresis was stopped, and the gel was stained by Coomassie blue. After destaining, the protein-containing parts of the lane were cut out of each gel separately for kappa and lambda and submitted to proteomics digestion and peptide mass spectrometry.

Peptide Mass Spectrometry

The procedure was essentially carried out as indicated in earlier work (16). In brief, following trypsin digestion, peptides were further cleaned using a C18 column and then injected into the UltiMate 3000 RSLC nano HPLC (Thermo Fisher Scientific). This HPLC system is linked to a Q Exactive HF mass spectrometer (Thermo Fisher Scientific) using a Proxeon Nanospray source (Thermo Fisher Scientific).

RESULTS

Multiple myeloma is a common cause for various renal diseases, and a high percentage of affected patients show signs of renal

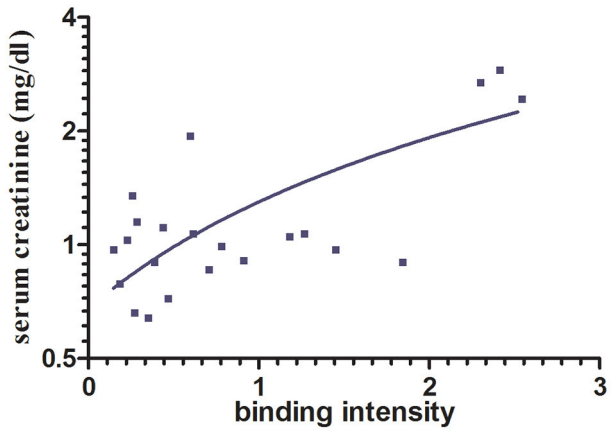

FIGURE 2 | Association between immunoglobulin/LC binding to renal whole-cell lysate by ELISA and serum creatinine after 1-year follow-up. A significant association between immunoglobulin/LC binding intensity and the serum creatinine after 12 months ($p < 0.0001$, $n = 22$) was shown. Binding intensity was measured by photometrical density (OD 450 nm).

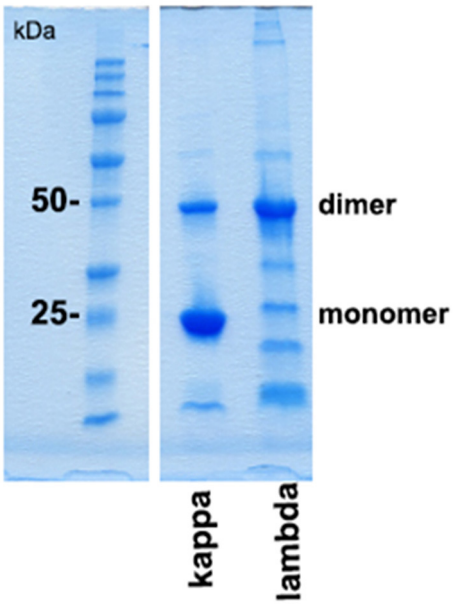

FIGURE 3 | SDS-PAGE gel analysis of purified urine light chains kappa and lambda. Dimers and monomers as well as fragments of LCs are indicated at the right lane. The protein molecular weight marker is indicated on the left lane separated from the other part of the gel. The gel was stained by Coomassie blue following electrophoresis using TRIS-glycine-SDS running buffer. This experiment represents one out of two.

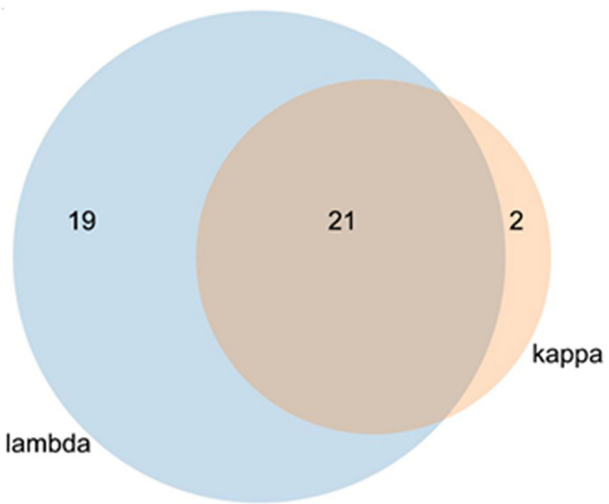

FIGURE 4 | Venn diagram of kappa and lambda overlapping stains. The lambda light chain interacted with 40 individual proteins and the kappa LC with 23 proteins. Of the total of 42 proteins, 21 interacted with both LCs.

impairment (1, 18). For this reason, patients with monoclonal gammopathies were selected from the myeloma outpatient clinic who showed different extents of protein excretion, with some of them showing signs of renal impairment. Demographic data of study patients are given in **Table 1**.

We examined whether the secreted myeloma protein LCs would bind to immobilized renal whole-cell protein on ELISA plates. As depicted in **Figure 1**, the extent of LC/immunoglobulin binding of patients with multiple myeloma or plasma cell dyscrasia was evaluated and compared with control patients (patients with ischemic–reperfusion injury following renal transplantation as well as healthy subjects). The extent of LC/immunoglobulin binding to renal whole-cell lysates varied among multiple myeloma patients and was found similar to the extent of patients suffering from renal reperfusion injury who also secrete LCs and immunoglobulins due to damage of the glomerular filtration barrier components.

To analyze whether the intensity of *in vitro* immunoglobulin/LC binding would allow prediction of the impact on progressive renal dysfunction, a linear regression analysis was performed. Hereby, a significant association between LC binding intensity to renal whole-cell lysate in the ELISA, measured by photometrical density at OD 450 nm, and serum creatinine after a 1-year follow-up was detected, $R = 0.737$ (95% confidence interval, 0.457–0.884; $p = 0.0001$) (**Figure 2**).

Protein folding as well as interprotein binding and aggregation is assumed to be involved in the pathomechanism of cast formation, intracellular LC deposition, and amyloid formation in paraprotein-associated renal disease. Of particular interest is cast nephropathy, as it represents the most frequently observed manifestation of such disorder in multiple myeloma (1). Therefore, the monoclonal LC kappa and lambda were purified from urine of patients presenting with *acute kidney injury* due to cast nephropathy. Its grade of purification was visualized by SDS-PAGE (**Figure 3**).

Using these purified LCs, the protein array HuProt™ was screened with equal concentration of lambda and kappa protein each on separate arrays. As demonstrated in **Supplementary Figure 1**, the lambda LC binding signals were

TABLE 2 | Localization and expression of proteins interacting with both kappa and lambda light chain.

Cell surface protein	Intracellular protein	Renal expression score	Nephron tubule expression score	Interacting light chain
C1QTNF2		64.79	n.a.	λ and κ
	CCNG1	99.18	99.48	λ and κ
CYAT1		n.a.	n.a.	λ and κ
DIXDC1		85.59	81.60	λ and κ
	FAM160B2	97.55	62.70	λ and κ
	GDPD5	79.12	n.a.	λ and κ
	KCNAB1	72.78	53.25	λ and κ
LPAR4		84.89	n.a.	λ and κ
	PARS2	78.19	n.a.	λ and κ
	PCSK7	89.41	74.10	λ and κ
	PPP2R5D	91.03	78.49	λ and κ
	QDPR	98.49	89.84	λ and κ
	RNF7	97.33	91.09	λ and κ
	SCLT1	92.75	n.a.	λ and κ
SIRPB1		71.03	n.a.	λ and κ
	SNX33	84.09	n.a.	λ and κ
TMEM106B		98.45	90.42	λ and κ
TMEM116		90.93	n.a.	λ and κ
TRGC1		68.89	n.a.	λ and κ
	VRK2	86.66	73.99	λ and κ
	ZADH2	89.07	n.a.	λ and κ

Kappa and lambda LC interaction proteins were categorized for membrane domain containing cell surface or intracellular/cytoplasmic localization (according to the Human Protein Atlas and UniProt database). Renal expression was ascertained and the expression score for adult kidney as well as nephron tubule was extracted from the Bgee database (n.a. = data not available). Detailed protein names are listed in ***Supplementary Table 1****.*

approximately 40% higher at most of the significant interaction partner proteins when compared with kappa signals.

In the protein array, a total of 40 interaction proteins were identified in lambda screens. The number of kappa LC interacting proteins was lower (in total 23), whereas 21 interactors were binding to both lambda and kappa LCs (**Figure 4**, **Tables 2**, **3**).

In order to evaluate the potential disease relevance of LC interactors, their subcellular localization and renal expression were verified by database mining such as the Human Protein Atlas and UniProt. The numeric kidney and nephron tubule expression extent was extracted from the Bgee database (**Tables 2**, **3**). Eight of the kappa and lambda interactors were surface proteins composed of transmembrane domains and verified cell surface structures.

A short functional description of each of the proteins interacting with the two LC subtypes kappa and lambda and a statement about their potential physiological function and involvement in the pathology of tubular epithelial cells is given in **Supplementary Data 1**.

Lambda Binding Partners

Of the HuProt™ array that identified 42 LC binding proteins, 19 proteins were found to solely bind to the lambda type LC. Four of them were cell surface proteins (first column of **Table 3**), with two (ZDHHC5, ECHDC1) being highly expressed in the kidney (expression score >94). Of particular note is the voltage-gated potassium channel subunit beta-2 (KCNAB2), a plasma membrane protein also highly expressed in the kidney (expression score >94) that functions at the cytoplasmic side of cell surface channels and is involved in ion transport.

Kappa Binding Partners

Only two of the 42 binding partners recognized by the HuProt™ array were kappa LC–specific interactors. Of note here is the cyclin-dependent kinase 10 (CDK10) that is highly expressed in the kidney (expression score >98) and that is involved in cell cycle–dependent processes such as tubular cell regeneration, a constantly ongoing mechanism in mammalian nephrons.

Protein Confirmation

Cubilin and megalin binding to LC and their uptake at the proximal tubule has been shown in previous studies (11, 19). As we could not show cubilin and megalin as interaction molecules in the HuProt™ array screening, we assumed that the recombinantly generated proteins spotted on the array did not represent the full spectrum of the *in vivo* tertiary and quaternary structure of the proteins. Therefore, we designed a LC affinity chromatography and could indeed verify cubilin and megalin (**Table 4**).

DISCUSSION

Renal amyloidosis, monoclonal immunoglobulin deposition disease, LC proximal tubulopathy, cast nephropathy, and

TABLE 3 | Localization and expression of interacting proteins unique to either lambda or kappa light chain.

Cell surface protein	Intracellular protein	Renal expression score	Nephron tubule expression score	Interacting light chain
AQP5		70.48	n.a.	λ
	CLIP4	85.19	n.a.	λ
	COX15	92.96	89.43	λ
	FAM127B	96.03	73.64	λ
	GARS	96.88	93.36	λ
IL12RB1		66.12	n.a.	λ
	KCNAB2	94.79	83.70	λ
	MECR	92.97	75.24	λ
	PRH1	72.97	n.a.	λ
	RBM47	99.70	98.71	λ
	RPRD1A	92.19	80.74	λ
	TLK1	95.59	91.95	λ
	TRIM21	83.33	n.a.	λ
	VDR	90.64	93.84	λ
	WIPF1	89.61	83.53	λ
ZDHHC5		94.03	n.a.	λ
	ALB	98.91	99.79	λ
	CRYZ	99.26	99.22	λ
ECHDC1		97.28	91.70	λ
	BAIAP2L1	84.89	n.a.	κ
	CDK10	98.99	85.38	κ

The upper part of the table demonstrates lambda specific, the lower part kappa specific binding partners.
Kappa and lambda LC interaction proteins were categorized for membrane domain containing cell surface or intracellular/cytoplasmic localization (according to the Human Protein Atlas and UniProt database). Renal expression was ascertained and the expression score for adult kidney as well as nephron tubule was extracted from the Bgee database (n.a. = data not available). Detailed protein names are listed in ***Supplementary Table 1****.*

TABLE 4 | Detection of megalin and cubilin by mass spectrometry of light chain affinity column eluates.

Accession	Description	Genes	MW [kDa]	Lambda LC		Kappa LC	
				Norm. area	No. Peptides	Norm. area	No. Peptides
P98164.3	Megalin	LRP2	521,6	7,59E+05	21	6,03E+05	20
O60494.5	Cubilin	CUBN	398,5	4,13E+05	8	3,73E+05	11

Abundance of peptides is calculated as area under the curve (norm. area) of highly specific peptide peaks. Several peptides were identified as specific for megalin and cubilin (no. peptides).

crystal storing histiocytosis are complications associated with monoclonal gammopathies and multiple myeloma. Such manifestations are associated with poor clinical outcome when not diagnosed and treated in early stages. Protein folding and LC interaction with cell surface proteins influence the site and type of LC deposition or transformation into fibrils (20). In this study, we searched for proteins that directly interact with LCs at the nephron. In a first step, this was investigated by an ELISA method using immobilized renal whole-cell protein and patients' urine. Urine immunoglobulin/LC binding could be verified and was much higher in patients who showed progressive renal failure when analyzed 1 year later by renal function parameters. In a second step, kappa and lambda LCs were purified each from a different patient with myeloma, and protein microarrays were screened for identification of potential binding partners for kappa and lambda LC. For both kappa and lambda LC binders, 21 different proteins expressed by renal cells were identified, all of them involved in renal cell activity. Of particular note is the SCLT1 protein named the sodium channel and clathrin linker 1 (21), which might act as a member of a potential transport mechanism by which the LCs are geared to the coated pits and endosomes, which later fuse with lysosomes (20). The SCLT1 is also named CAP-1 and regulates the Na(v)1.8 channel density at the cell surface, and the lysosome has been attributed a specific site for fibrillogenesis in a mouse model of LC amyloidosis (20). More interestingly, the TMEM106B protein is involved in lysosome trafficking and formation (22) and might therefore, when disturbed and partly inhibited by abundant LC presence, represent another cornerstone in LC-induced degenerative tubular nephropathy. This might also be of relevance in the mesangial transformation (23) and fibrillogenesis, which has been studied before (20). A second point of note is the KCNAB1 and KCNAB2 channel proteins involved in potassium transport. Whether the blockage

through LCs can cause the acquired Fanconi syndrome has to be left open, the relevance for paraprotein associated neuropathies is thereby more likely, and this topic deserves further research. Proteins that bind to both lambda and kappa are specifically described in **Supplementary Data 1**, both in terms of their physiological function and their potential pathomechanism in renal cells when partially inhibited or blocked by interaction with an overwhelming amount of monoclonal LC/immunoglobulin.

An interesting observation of our study is that the LCs did not bind in a direct mode to the spotted cubilin or megalin on the array. The manufactured proteins for array printing might be linearized and not glycosylated. Either a specific tertiary structure or an interaction mediator should be of relevance, because according to the previous literature these two proteins ought to represent the internalizing factors (19). However, we confirmed in LC-Sepharose affinity chromatography the binding of cubilin and megalin to both LC types kappa and lambda in almost similar quantity.

This work demonstrates the impact of recently developed tools and methods of protein analysis including microarray screening to screen for a broader range of interaction partners. Whether these newly identified interactors might be involved in cellular uptake could not be researched by these methods, but some of them including SIRPB1, VRK2, ZADH2, and others are certainly involved in signal transduction and initiation of proinflammatory processes at the tubular structures. The intracellular binding partners identified in this study might be relevant in LC protein internalization, accumulation, intracellular transport, and its way to initiate a redox signaling (24) and transformation of mesangial cells (23). In this line of thought, the seven-transmembrane spanning receptor protein LPAR4, binding to both LCs kappa and lambda, might be involved in cell activation. It has been demonstrated earlier that nuclear factor κB might be activated following LC endocytosis (24). Our screens now demonstrate that activation could already be initiated by binding to cell surface proteins via the tubular cell brush border.

The broad spectrum of interaction partners explains the notion that a high LC concentration in urine is associated with more than a single pathological entity in the kidney. The different interaction capabilities depending on the subtype of LC can influence the pathomorphological features. In this respect, intracellular interactors might be of significant relevance. Our data showing higher lambda binding levels might also reflect clinical observations that the lambda paraprotein is potentially more harmful and more likely to cause clinicopathological changes than kappa paraproteins.

The main limitation of this study is that as recombinant proteins are spotted at the HuProt™ array, only primary structure-related protein–protein interactions can be detected. Therefore, protein interactions due to tertiary and quaternary structures may not be identified, which might be a determinant factor for LC interaction *in vivo*. In our study, this applies, for example, to the two well-described transport proteins of LCs cubilin and megalin, which we could not detect by the HuProt™ array, although we could detect them by LC affinity chromatography and subsequent proteomic identification of eluted binders. However, the proteomic workup of LCs goes beyond the scope of this study and is the focus of a follow-up.

Continuous advances in protein analysis, applied to clinically relevant questions, provide detailed insight into disease-causing mechanisms. The results of our study indicate 42 cellular LC binding partners with potential pathomechanical relevance that may contribute to the induction and progression of LC-associated diseases and kidney injuries. This provides new perspectives for targeted diagnostic and therapeutic measures in the future.

DATA AVAILABILITY STATEMENT

Protein data were downloaded from the Human Protein Atlas (https://www.proteinatlas.org), UniProt (https://www.uniprot.org/) and Bgee (https://bgee.org) databases and according accession numbers are provided in **Supplementary Table 1**.

ETHICS STATEMENT

The studies involving human participants were reviewed and approved by Ethics committee of the Medical University of Vienna, Austria. The patients/participants provided their written informed consent to participate in this study.

AUTHOR CONTRIBUTIONS

TR, SP, LW, and WW conceived and designed the study. LW and CL did the statistical analysis. DO'C, CL, SK, HA, AS, and LW analyzed and interpreted the data. TR, SP, DO'C, CL, SK, HA, AS, LW, NL, and WW critically revised the manuscript for important intellectual content. All authors contributed to the article and approved the submitted version.

ACKNOWLEDGMENTS

The authors want to thank Karl Mechtler for technical support.

SUPPLEMENTARY MATERIAL

The Supplementary Material for this article can be found online at: https://www.frontiersin.org/articles/10.3389/fmed.2020.609582/full#supplementary-material

Supplementary Figure 1 | Proto Array HuProt™ screening using purified human kappa and lambda light chain. Alexa Fluo 642 polyclonal goat anti human heavy and light chain specific secondary antibody was applied as detection reagent. The blue line indicates the staining intensity of lambda and the red line of kappa for the 400 most significant proteins signals.

REFERENCES

1. Hogan JJ, Alexander MP, Leung N. Dysproteinemia and the kidney: core curriculum 2019. *Am J Kidney Dis*. (2019) 74:822–36. doi: 10.1053/j.ajkd.2019.04.029
2. Nasr SH, Valeri AM, Sethi S, Fidler ME, Cornell LD, Gertz MA, et al. Clinicopathologic correlations in multiple myeloma: a case series of 190 patients with kidney biopsies. *Am J Kidney Dis*. (2012) 59:786–94. doi: 10.1053/j.ajkd.2011.12.028
3. Huang ZQ, Sanders PW. Localization of a single binding site for immunoglobulin light chains on human Tamm-Horsfall glycoprotein. *J Clin Invest*. (1997) 99:732–6. doi: 10.1172/JCI119218
4. Ying WZ, Sanders PW. Mapping the binding domain of immunoglobulin light chains for Tamm-Horsfall protein. *Am J Pathol*. (2001) 158:1859–66. doi: 10.1016/S0002-9440(10)64142-9
5. Leung N, Bridoux F, Batuman V, Chaidos A, Cockwell P, D'Agati VD, et al. The evaluation of monoclonal gammopathy of renal significance: a consensus report of the International Kidney and Monoclonal Gammopathy Research Group. *Nat Rev Nephrol*. (2019) 15:45–59. doi: 10.1038/s41581-018-0077-4
6. Perazella MA, Finkel KW, American society of nephrology onco-nephology F. Paraprotein-related kidney disease: attack of the killer M proteins. *Clin J Am Soc Nephrol*. (2016) 11:2256–9. doi: 10.2215/CJN.02960316
7. Yadav P, Sathick IJ, Leung N, Brown EE, Cook M, Sanders PW, et al. Serum free light chain level at diagnosis in myeloma cast nephropathy-a multicentre study. *Blood Cancer J*. (2020) 10:28. doi: 10.1038/s41408-020-0295-4
8. Holland MD, Galla JH, Sanders PW, Luke RG. Effect of urinary pH and diatrizoate on Bence Jones protein nephrotoxicity in the rat. *Kidney Int*. (1985) 27:46–50. doi: 10.1038/ki.1985.8
9. Ying WZ, Allen CE, Curtis LM, Aaron KJ, Sanders PW. Mechanism and prevention of acute kidney injury from cast nephropathy in a rodent model. *J Clin Invest*. (2012) 122:1777–85. doi: 10.1172/JCI46490
10. Batuman V, Verroust PJ, Navar GL, Kaysen JH, Goda FO, Campbell WC, et al. Myeloma light chains are ligands for cubilin (gp280). *Am J Physiol*. (1998) 275:F246–54. doi: 10.1152/ajprenal.1998.275.2.F246
11. Klassen RB, Allen PL, Batuman V, Crenshaw K, Hammond TG. Light chains are a ligand for megalin. *J Appl Physiol (1985)*. (2005) 98:257–63. doi: 10.1152/japplphysiol.01090.2003
12. Hertig A, Bonnard G, Ulinski T, Colombat M, Jouanneau C, Baugey E, et al. Tubular nuclear accumulation of Snail and epithelial phenotypic changes in human myeloma cast nephropathy. *Hum Pathol*. (2011) 42:1142–8. doi: 10.1016/j.humpath.2010.11.006
13. Herrera GA, Sanders PW. Paraproteinemic renal diseases that involve the tubulo-interstitium. *Contrib Nephrol*. (2007) 153:105–15. doi: 10.1159/000096763
14. Luque Y, Louis K, Jouanneau C, Placier S, Esteve E, Bazin D, et al. Vancomycin-associated cast nephropathy. *J Am Soc Nephrol*. (2017) 28:1723–8. doi: 10.1681/ASN.2016080867
15. Leclerc M, Lanot A, Bechade C, Le Naoures C, Comoz F, Lobbedez T. Bile salt nephropathy/cholemic nephrosis. *Nephrol Ther*. (2016) 12:460–2. doi: 10.1016/j.nephro.2016.03.002
16. Reiter T, Knafl D, Agis H, Mechtler K, Wagner L, Winnicki W. Structural analysis of urinary light chains and proteomic analysis of hyaline tubular casts in light chain associated kidney disorders. *PeerJ*. (2019) 7:e7819. doi: 10.7717/peerj.7819
17. Dunning CJ, McGauran G, Willen K, Gouras GK, O'Connell DJ, Linse S. Direct high affinity interaction between Abeta42 and GSK3alpha stimulates hyperphosphorylation of tau. A New Molecular Link in Alzheimer's Disease? *ACS Chem Neurosci*. (2016) 7:161–70. doi: 10.1021/acschemneuro.5b00262
18. Leung N, Drosou ME, Nasr SH. Dysproteinemias and glomerular disease. *Clin J Am Soc Nephrol*. (2018) 13:128–39. doi: 10.2215/CJN.00560117
19. Li M, Balamuthusamy S, Simon EE, Batuman V. Silencing megalin and cubilin genes inhibits myeloma light chain endocytosis and ameliorates toxicity in human renal proximal tubule epithelial cells. *Am J Physiol Renal Physiol*. (2008) 295:F82–90. doi: 10.1152/ajprenal.00091.2008
20. Teng J, Turbat-Herrera EA, Herrera GA. An animal model of glomerular light-chain-associated amyloidogenesis depicts the crucial role of lysosomes. *Kidney Int*. (2014) 86:738–46. doi: 10.1038/ki.2014.122
21. Liu C, Cummins TR, Tyrrell L, Black JA, Waxman SG, Dib-Hajj SD. CAP-1A is a novel linker that binds clathrin and the voltage-gated sodium channel Na(v)1.8. *Mol Cell Neurosci*. (2005) 28:636–49. doi: 10.1016/j.mcn.2004.11.007
22. Brady OA, Zheng Y, Murphy K, Huang M, Hu F. The frontotemporal lobar degeneration risk factor, TMEM106B, regulates lysosomal morphology and function. *Hum Mol Genet*. (2013) 22:685–95. doi: 10.1093/hmg/dds475
23. Keeling J, Teng J, Herrera GA. AL-amyloidosis and light-chain deposition disease light chains induce divergent phenotypic transformations of human mesangial cells. *Lab Invest*. (2004) 84:1322–38. doi: 10.1038/labinvest.3700161
24. Sanders PW. Mechanisms of light chain injury along the tubular nephron. *J Am Soc Nephrol*. (2012) 23:1777–81. doi: 10.1681/ASN.2012040388

Conflict of Interest: The authors declare that the research was conducted in the absence of any commercial or financial relationships that could be construed as a potential conflict of interest.

frontiers in Medicine

SYSTEMATIC REVIEW
published: 25 January 2021
doi: 10.3389/fmed.2020.00549

Serum Total Bilirubin and Progression of Chronic Kidney Disease and Mortality: A Systematic Review and Meta-Analysis

Jia Li[1,2,3,4], *Dongwei Liu*[1,2,3,4] *and Zhangsuo Liu*[1,2,3,4]*

[1] Department of Nephrology, The First Affiliated Hospital of Zhengzhou University, Zhengzhou, China, [2] Research Institute of Nephrology, Zhengzhou University, Zhengzhou, China, [3] Key Laboratory of Precision Diagnosis and Treatment for Chronic Kidney Disease in Henan Province, Zhengzhou, China, [4] Core Unit of National Clinical Medical Research Center of Kidney Disease, Zhengzhou, China

Background: Previous studies have suggested that serum total bilirubin (STB) levels are associated with heightened chronic kidney disease (CKD) and mortality in both the general population and nephropathy patients. However, these results remain inconsistent. The aim of our study was to investigate whether STB was a predictor for progression of CKD and mortality by meta-analysis.

Methods: We performed a systematic literature search in PubMed, Web of Science, MEDLINE, EMBASE, Google Scholar, and Cochrane Library's database up to June 30, 2019. Pooled risk ratios (RR) and corresponding 95% confidence intervals (CI) were extracted for the highest vs. lowest category STB levels within the physiological range, and a random-effects model was applied to calculate the dose–response relationships. A pooled hazard ratio (HR) was used to investigate the association between STB levels and mortality in dialysis patients.

Results: A total of 16 studies, wherein participants were followed from 21 months to 7 years, were eligible for inclusion in the study. For the categorized STB, 11 studies with 41,188 participants were identified and analyzed. Patients with the highest STB levels were associated with a lower risk of CKD (RR = 0.64; 95% CI 0.55–0.73) compared to those with the lowest STB levels. Furthermore, based on seven studies, a pooled RR of 0.89, 95% CI (0.80–0.99) was observed for the continuous STB levels (per 0.2 mg/dL increase). Four studies that included 51,764 participants illustrated that there was no association between STB levels and all-cause mortality (HR = 0.77; 95% CI 0.42–1.41). A prominent negative linear relationship ($X^2 = 14.70$; $P = 0.0001$) was found between STB levels and risk of CKD. Subgroup analyses showed that there were no significant differences in the subgroup adjustment factor except for sample size.

Conclusions: Elevated STB levels within a physiological range are associated with lower risk of CKD regardless of the study characteristics and coincide with a liner dose–response relationship. However, whether high STB levels are a protective factor against mortality remains inconclusive. Large-scale randomized controlled trails are needed to target STB levels for predicting renal outcomes.

Keywords: serum total bilirubin, chronic kidney disease, disease progression, mortality, meta-analysis

OPEN ACCESS

Edited by:
Minnie M. Sarwal, University of California, San Francisco, United States

Reviewed by:
Jeffrey R. Schelling, Case Western Reserve University, United States
Amjad Khan, Quaid-I-Azam University, Pakistan

***Correspondence:**
Zhangsuo Liu
zhangsuoliu@zzu.edu.cn

Specialty section:
This article was submitted to Nephrology, a section of the journal Frontiers in Medicine

Received: *05 March 2020*
Accepted: *31 July 2020*
Published: *25 January 2021*

Citation:
Li J, Liu D and Liu Z (2021) Serum Total Bilirubin and Progression of Chronic Kidney Disease and Mortality: A Systematic Review and Meta-Analysis. Front. Med. 7:549. doi: 10.3389/fmed.2020.00549

INTRODUCTION

Chronic kidney disease (CKD), also called chronic kidney failure, is on the rise, and it has become one of the most common complications worldwide. It not only increases the risk of cardiovascular disease and can often progress to end-stage renal disease (ESRD), but it is also related to premature mortality. According to the 2013 Global Burden of Disease Study, CKD ranked 36th in the causes of total number of global deaths in 1990, but rose to 19th in 2013 (1). Much of the general population is admitted to hospital with chronic kidney disease, so early detection, diagnosis, and intervention of adverse factors that may lead to kidney disease are essential for improving the prognosis of patients with CKD. It should also be noted that a rising prevalence of comorbidities and risk factors, such as hypertension, diabetes mellitus glomerulonephritis, and infectious diseases, are also contributing to the high burden of CKD (2). However, these factors do not fully explain the variation and heterogeneity in the prevalence of CKD.

Recently, several studies have demonstrated that oxidative stress can play a crucial role in the pathogenesis of CKD (3–5). Oxidative stress imbalance is generally caused by an overproduction of reactive oxygen species (ROS) or a deficiency of the antioxidant reagent. Bilirubin is a heterogeneous group of antioxidants which derives from the heme catabolism through a complex sequence of reactions. It exists in two forms of serum, direct bilirubin and indirect bilirubin, and both are newly recognized as antioxidant, anti-inflammatory molecules under physiological conditions (6). However, the role that serum total bilirubin (STB) plays within the physiological range in the development and progression of kidney disease remains controversial. Several studies have suggested that an inverse association between STB and the progression of ESRD (7–10) plays a potential protective role in renal outcomes. A large study of the Korean population that was recently published demonstrates that individuals with higher bilirubin levels have a reduced prevalence of CKD originating from diabetes in women (11). Two studies revealed that elevated bilirubin levels have a reduced risk of progressing from urinary microalbuminuria to macroalbuminuria, as well as improved eGFR in diabetic patients (12, 13). Furthermore, Fukui et al. reported that higher circulating serum bilirubin levels were associated with reduced risk of cardiovascular disease and mortality in dialysis patients (14). Although most investigations indicate a potential beneficial effect of bilirubin on renal prognosis, there is some evidence that suggests an inconclusive relationship between bilirubin and clinical endpoints. Wang et al. noted that lower STB was not an independent protective factor in kidney disease progression among hypertensive patients who never smoke (15). Targher et al. demonstrated that higher STB levels were significantly associated with lower eGFR in both non-diabetic and diabetic individuals in unselected outpatients (16). Ryu et al. proved that neither STB nor indirect bilirubin levels were associated with the incidence of CKD (17). Additionally, it was noted that in patients with ESRD who were undergoing hemodialysis, high concentrations of bilirubin were correlated with a higher mortality rate (18). These results indicate the need for evaluating the role of STB levels on the progression of CKD and mortality.

Keeping in mind the unclear interactions between STB levels and the impact of renal outcomes, we conducted this systematic review and meta-analysis to determine whether STB independently contributes to the progression of CKD in both the general population and nephropathy patients. We also evaluate the association between STB and mortality in those who were undergoing regular dialysis and investigated the possibility of it acting as a novel biological factor to predict kidney disease progression.

MATERIALS AND METHODS

Search Strategy

The meta-analysis was conducted according to the checklist of Preferred Reporting Items for Systematic reviews and Meta-Analyses guidelines (PRISMA) (**Supplementary Table 5**). PubMed, Web of Science, MEDLINE, EMBASE, Google Scholar, and Cochrane Library were searched from January 1970 to June 2019 in order to identify relevant studies. We set the key word as "bilirubin" and ("chronic kidney disease" or "chronic renal disease" or "end-stage renal disease" or "end-stage kidney disease" or "estimated glomerular filtration rate") without language limitation. The references in relevant reports, PubMed "related articles," textbook chapters, and online clinical trial registries were searched to identify any related articles. Any unpublished data or incomplete data were requested by contacting authors through email.

Selection Criteria

The inclusion criteria was as follows: (1) the studies investigated the relationship between bilirubin concentration and kidney disease progression, (2) cohort study or random clinical trials, (3) a comparison between highest STB group and lowest STB group or per unit STB increase, (4) followed participants for at least 12 months, (5) reported any of the following renal outcomes: progression to CKD or all-cause mortality, and (6) Relative risk (RR) with 95% confidence intervals CIs or the minimum information necessary to calculate these values were provided as effect size. Liver dysfunction which could lead to elevated levels of serum bilirubin were excluded in original research studies. Studies in review, editorials, letters, and case report forms were excluded from our meta-analysis. If the study did not meet the included criteria and could not provide categories of bilirubin or sufficient data to calculate effect size, then they were also excluded. The categorization for STB levels and the units used were in line with the definition in each study. In order to keep the unit of all included studies in accordance, μmol/L was converted to mg/dL divided 17.1. CKD was defined as a decline in estimated glomerular filtration rate (eGFR) <60 ml/min/1.73 m^2 by using the CKD-EPI equation.

Data Extraction and Quality Assessment

All included studies were independently identified by two investigators (JL and ZSL). Data extracted included age, sex, country of origin, study design, populations, serum bilirubin,

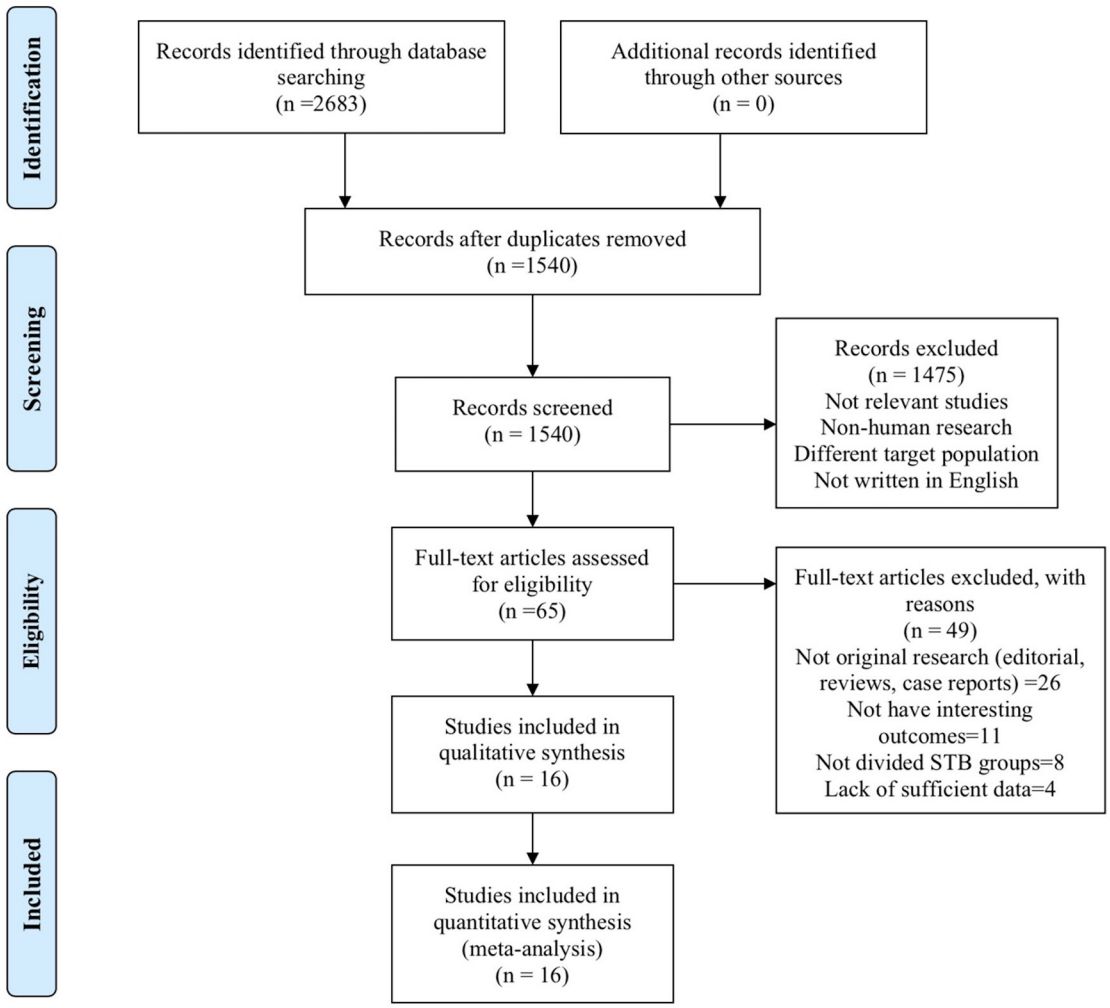

FIGURE 1 | Flow chart of study selection.

follow-up, sample size, smoking status, body mass index, No. of cases, outcome, adjusted HR or RR or OR per unit of increase in baseline serum bilirubin, and those for highest and lowest group of STB levels. The studies which had several estimates adjusted HR for different numbers of potential confounders; the greatest number of potential confounding factors was selected for analysis. The quality of all included studies was assessed by two reviewers (JL and ZSL) using the Newcastle-Ottawa scale (NOS). The scores "7–9," "4–6," and "1–3" were considered as "high," "moderate," and "low" quality, respectively. Any discrepancies between the two investigators were discussed with a third independent reviewer (DWL).

Outcomes

There were two outcomes included in this meta-analysis. The primary outcome was the assessment of kidney disease progression to CKD [defined as estimated glomerular filtration rate (eGFR) <60 ml/min/1.73 m^2, doubling of serum creatinine, or 50% decline of kidney function or end-stage renal disease (ESRD)] and the secondary outcome was assessment of all-cause mortality in patients who developed CKD and underwent hemodialysis or peritoneal dialysis. The forest plots illustrate the two outcomes reproduced from the individual studies and the size of the symbol for the estimate is proportional to the weight of each study. A dashed vertical line and diamond at the bottom of the forest plot highlights the overall estimate and its 95% confidence interval.

Statistical Analyses

In our study, the pooled RRs and 95% CIs were used for the association of STB with the risk of CKD and mortality. The hazard ratios (HR) and odds ratio (OR) in some original studies were assumed to provide accurate estimates of the risk ratio, so it was directly considered as RR (19). After certifying the connection between STB and kidney disease progression, we further clarified whether this link displays the dose–response effect and whether this dose–response relationship was nonlinear or linear. Detailed information is provided in the

TABLE 1 | Characteristics of included studies in this meta-analysis ($n = 16$).

Author	Year	Country	Populations	Cohort designation	No. of participants	Age (year)	Male (%)	Follow-up
Chin	2009	Korea	IgA nephropathy	CS	1,469	36.3	56.11%	44.9 months
Kawamoto	2014	Japan	Elderly adults	CSS	1,050	80.21	39.30%	3 years
Tanaka M (men)	2014	Japan	General population	CS	1,627	47.7 ± 9.7	100.00%	7.7 years
Tanaka M (women)	2014			CS	1,157	46.3 ± 9.7	0.00%	7.7 years
Ryu	2014	Korea	General population	CS	12,823	37.2 ± 4.9	100%	7 years
Riphagen (RENAAL)	2014	Netherland	Diabetes nephropathy	RCT	1,498	60.1 ± 7.4	63.20%	3.4 years
Riphagen (IDNT)	2014			RCT	1,707	58.9 ± 7.8	66.40%	2.6 years
Tanaka S	2015	Japan	IgA nephropathy	RCS	694	36	47.42%	4.9 years
Sakoh	2015	Japan	CKD	PCS	279	73	69.00%	21 months
Lee (men)	2015	Taiwan	General population	CSS	2,260	51.8 ± 12.2	100.00%	NA
Lee (women)	2015			CSS	1,616	49.3 ± 11.8	0%	NA
Wang	2016	China	Type 2 diabetes patients	PCS	2,958	64.06	46.55%	5 years
Ahn Hee	2017	Korea	Type 2 diabetes patients	RCS	349	55 ± 11.7	39%	41 months
Su	2017	Taiwan	Hemodialysis patients	RCS	47,650	61.4 ± 13.6	50%	3 years
Yang	2017	Taiwan	Peritoneal dialysis patients	RCS	3,704	53.5 ± 15.0	44%	2.12 ± 1.07 years
Liu	2018	China	CKD	RCS	316	61.7 ± 10.9	56%	29.09 months
Wang	2018	China	Hypertension adults	RCT	12,633	59.59	37.78%	4.4 years
Wu	2019	China	Diabetic nephropathy	RCS	118	52.58 ± 9.36	67.80%	25 months
Tsujikawa	2019	Japan	Peritoneal dialysis patients	PCS	94	55.5 ± 14.2	66.00%	3 years

CS, cohort study; CSS, cross-sectional study RCT, randomized controlled trials; PCS, prospective cohort study; RCS, retrospective cohort study; RENAAL, The Reduction in End Points in NIDDM with the Angiotensin II Antagonist Losartan study; IDNT, the Irbesartan Diabetic Nephropathy Trial; CKD, Chronic Kidney Disease; NA, not applicable.

Supplementary Material. The Chi-square based Q-test and I^2 were used to assess the heterogeneity among studies. Subgroup analysis and meta-regression were performed due to the potential impact of covariates on study heterogeneity (sample size, study design, study design, adjusted for albumin, adjusted for eGFR, adjusted for diabetes mellitus). Sensitivity analysis was also conducted by omitting each study one by one. Begg's test and Egger's test were used to evaluate publication bias. STATA and R software were used for statistical analyses and two-sided $P < 0.05$ was considered to be statistically significant.

RESULTS

Literature Selection and Study Characteristics

A total of 2,683 studies were screened from the databases described above, and 16 publications (7–10, 15, 17, 18, 20–28) (19 data points) that met our criteria were included in the final selection (**Figure 1**). The characteristics of the included studies are provided in **Table 1**. The score of quality assessment for each study is shown in **Supplementary Table 1**. Two studies provided separate data for men and women. One study included two different trials (RENAAL and IDNT). Eleven studies (14 data points) provided a comparison between highest and lowest STB levels, and seven studies (10 data points) were viable for analysis on the effect of per 0.1 mg/dl STB level increase. Further details on categories and continuous STB levels are shown in **Supplementary Table 2**.

Association of Serum Bilirubin With the Risk of CKD

The association of STB levels with risk of kidney disease progression were analyzed by the RR of the highest STB levels compared to the lowest STB levels in 11 studies (14 data points). The results highlighted that patients with the highest STB levels were associated with lower risk of CKD progression (RR = 0.64; 95% CI 0.55–0.73), as shown in **Figure 2A**. This tendency was also consistent with the results of per 0.2 mg/dl increases in STB levels. Although moderate heterogeneity among the 11 studies ($I^2 = 43.8\%$, $P = 0.04$) was found, this also demonstrates the association between the STB and the progression to CKD. The RR for per 0.1 mg/dl increases in serum bilirubin were extracted from seven studies that included 10 data points, and were used for continuous variable analysis. Considering clinical experience, each 0.1 ml/dl increase is of little significance, so we calculated the risk ratio (RR) for 0.2 mg/dl increases (29). To elaborate, each 0.2 mg/dl serum bilirubin increase was associated with an 11% decreased risk for progression to CKD. The pooled RR and 95% CI were 0.89, 95% CI (0.80–0.99), as shown in **Figure 2B** ($I^2 = 78.7\%$; $P < 0.0001$).

Association of Serum Bilirubin With the Risk of Mortality

All-cause mortality was extracted from only four studies, including 51,764 patients. The adjusted HR of all-cause mortality for highest STB levels compared to the lowest STB levels was 0.77 (95% CI 0.42–1.41) in dialysis patients with heterogeneity at 84% (**Supplementary Figure 1**). Two of the studies proved

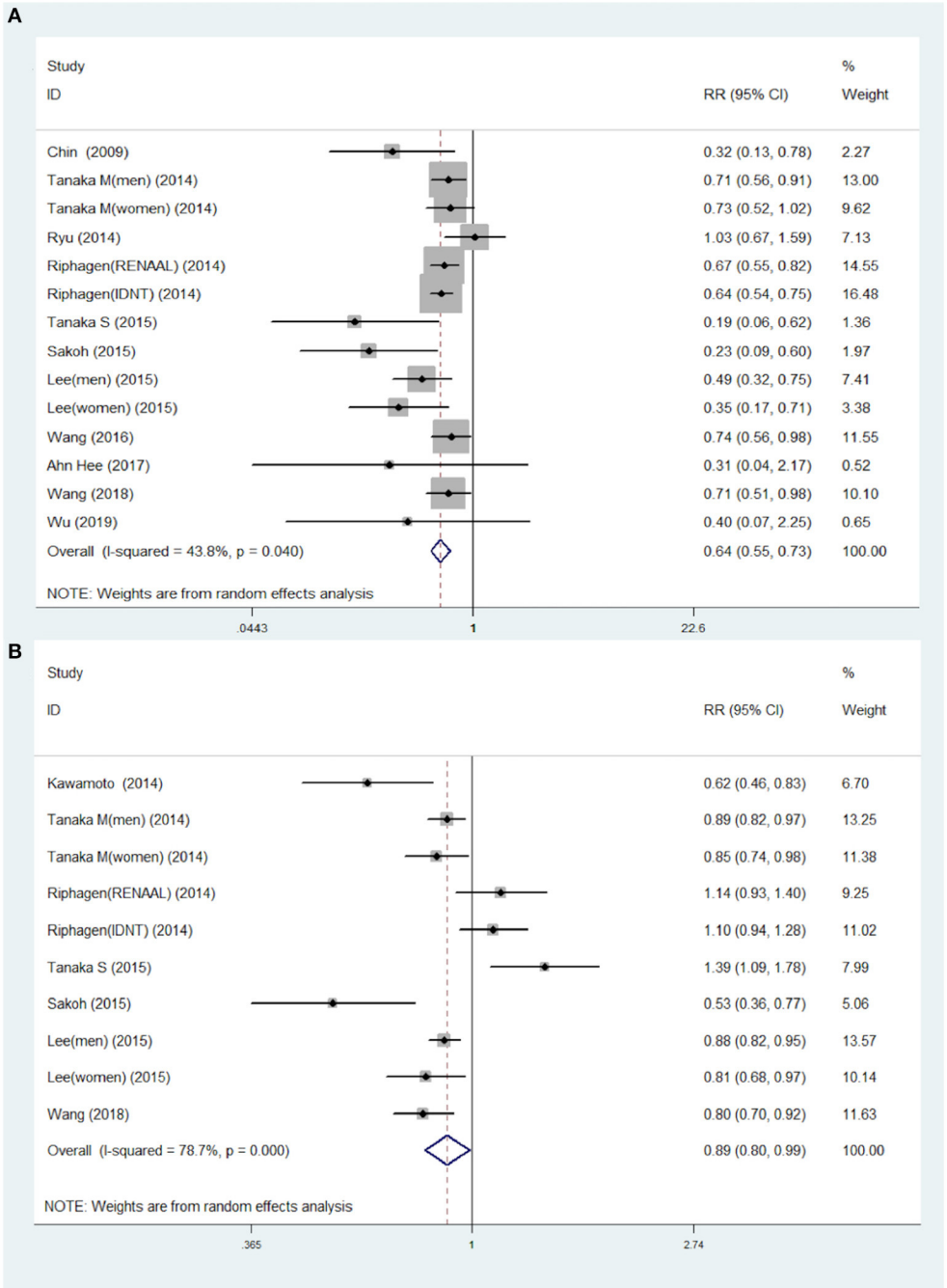

FIGURE 2 | Pooled RR with 95% CIs for the association of serum total bilirubin levels and the risk of CKD for the highest compared to the lowest category group **(A)** and for each 0.2 mg/dl increase **(B)**. The random-effects model was used and the area of each square stands for the weight of each study in the meta-analysis. The square sizes are proportional to the weight of each study in the meta-analysis; the diamond shows the overall RR; the horizontal lines indicate the 95% confidence intervals (CIs). CKD, chronic kidney diseases; RR, risk ratio.

that higher serum bilirubin was linked to a higher risk of mortality, while the other two studies had contrary conclusions. Our results illustrated that an increase of STB did not have a significant association with the risk for mortality in dialysis patients.

Publication Bias and Sensitivity Analyses

Begg's and Egger's test were performed for 11 studies on association of STB levels with disease progression. The results show that publication bias did exist, and trim and fill methods were adapted to adjust for the publication

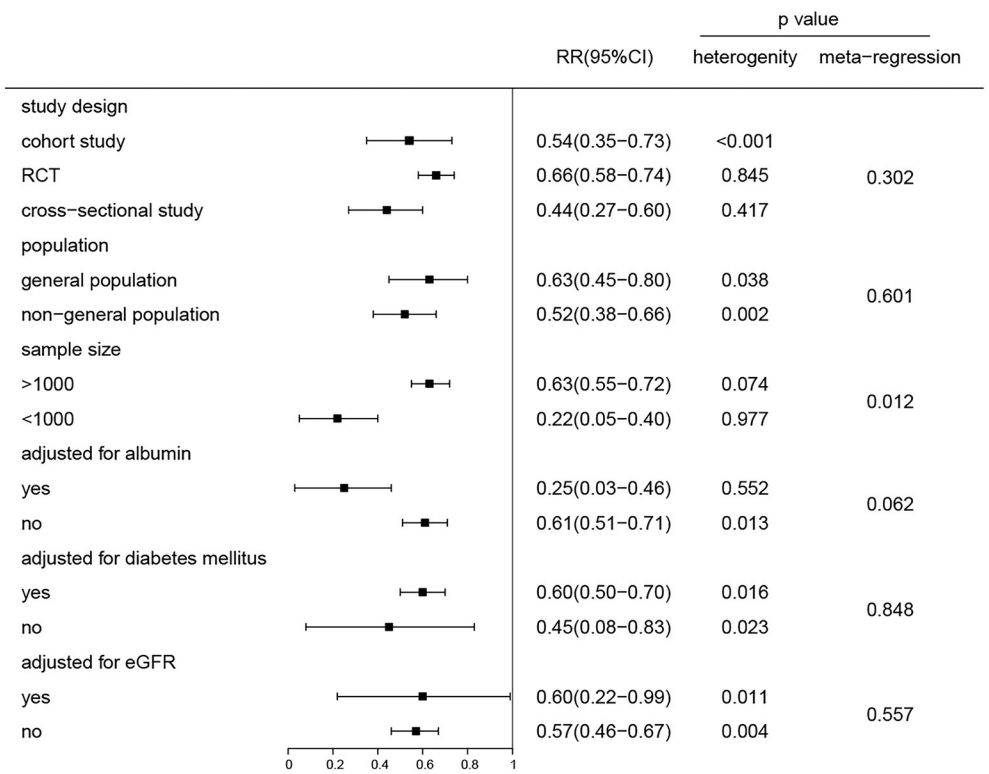

FIGURE 3 | Subgroup and regression analyses of the association between the serum total bilirubin levels and the risk of CKD for the highest compared and the lowest category group. P for the heterogeneity within each subgroup.

bias (**Supplementary Figures 2**, **3**). Sensitivity analyses were conducted to assess the extent of the influence of single studies on the pooled RR. The results indicated that there was no single study that dramatically influenced the pooled RR (**Supplementary Figure 4**). Detailed procedures and results are included in the **Supplementary Material**.

Subgroup and Regression Analyses

We analyzed the effect of potential impacts of covariates on study heterogeneity through stratified analyses and meta-regression. The gradually elevated STB levels with decreased risk of CKD remained for all factors (all RR were <1) (**Figure 3**). The negative association between the STB levels and the CKD risk was found to be significant in both the general population and nephropathy patients. Adjustment for albumin, diabetes mellitus, and eGFR were not found to have an influence on the relationship between the STB levels and risk of CKD ($P = 0.06, 0.84, 0.55$, respectively). Although there were significant differences in sample size >1,000 and <1,000 of the groups, the association between the STB levels and risk of CKD were both significant. We also conducted a regression analysis to evaluate the reason for the association between STB levels and all-cause mortality. There were no significant differences in the subgroup adjustment for albumin, diabetes mellitus, or eGFR except for sample size ($P = 0.04$) (**Supplementary Figure 5**).

Linear Dose–Response Analyses

A restricted cubic spline regression model was used to explore potential linearity. A total of seven studies that provided sufficient data were used to analyze the relationship between STB levels and risk of CKD. A linear dose–response relationship was illustrated using random-effects analysis and the results showcased a prominent, negative linear relationship ($X^2 = 14.70$; $P < 0.001$). The overall RR per 1 mg/dl increasement was associated with a 20% reduction in risk of CKD (95% CI 0.72–0.90), $P < 0.001$). No significant heterogeneity among the included studies was found ($Q = 15.13$, $P = 0.36$) (**Figure 4**).

DISCUSSION

Recently, many studies have revealed that STB levels play a critical role in CKD progression and mortality, but other studies have had inconsistent conclusions. Whether or not lower STB levels could be a biomarker of reduced kidney function is currently unclear. As far as we know, this is the first meta-analysis to focus on both CKD progression and all-cause mortality. Our meta-analysis demonstrates that higher STB levels may serve as protective factors for the development of CKD and elevated STB levels could lead to 36% of a significant decrease in the risk of CKD progression. However, the meta-analysis also concluded that there was no significant relationship between STB levels and risk of all-cause mortality.

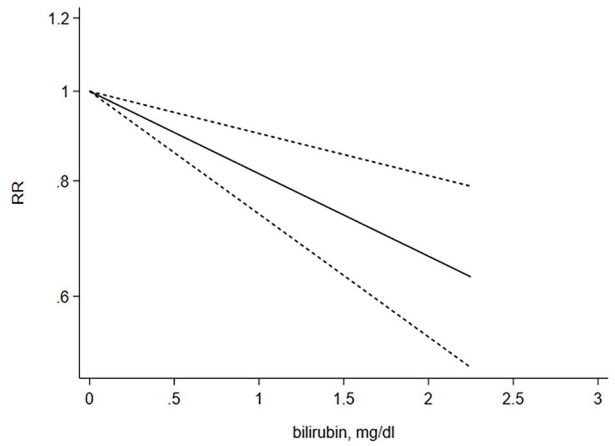

FIGURE 4 | Dose–response relationship between the serum total bilirubin levels and risk of CKD. The liner dose–response model is based on restricted cubic splines for STB concentrations at three point (25, 50, 75 percentiles). The line with short dashes represents the 95% confidence intervals.

Serum bilirubin has long been recognized as an abnormal sign of liver dysfunction. Recent data strongly indicates that slightly increased STB concentration can be a potent biological protective marker. In humans, low (<7 mmol/L) STB levels may be a risk factor for systemic diseases associated with increased oxidative stress, such as cardiovascular diseases (CVD) (30), diabetes (31), metabolic syndrome (32), certain cancers (33), and autoimmune diseases (34). However, the relationship between STB levels and kidney disease outcomes and mortality have been less certain. Based on 11 studies and 41,188 participants, our meta-analysis displayed a pooled analysis (RR = 0.64 95% CI 0.55–0.73) of the highest compared to the lowest STB group and demonstrated that STB levels were associated with CKD progression. Clinically speaking, each 0.1 ml/dL increase is of little significance, and therefore, we calculated the RR for 0.2 mg/dl, upon which the results showed a stronger association between the STB levels and renal outcomes (RR = 0.89, 95% CI 0.80–0.99). Meanwhile, a dose–response analysis showed that a 1 mg/dl increment in the STB levels led to a 20% decrease in the risk of CKD, regardless of various study characteristics. This result was consistent with a linear dose–response relationship. To assess the consistency of the association between STB levels and development of CKD, we conducted subgroup and meta-regression analysis stratified by potential confounders. STB is mainly transported in combination with albumin in the blood and a small amount is combined with α1 globulin for complex transport. Targher et al. (35) demonstrated that STB was inversely associated with eGFR in the general population in the US while Shin's et al. (36) research has concluded the opposite. Hence, according to whether the STB levels adjust for albumin and eGFR, subgroup analyses were performed and the results indicated that the significant relationship between STB and the development of CKD was not affected by stratified factors, except for sample size. When the sample size is smaller than 1,000, it has a higher heterogeneity. This could be explained by the fact that a small sample size has a different definition for the quartile of the STB levels.

Bilirubin, as the product of heme, has long been considered a symbol of liver dysfunction or a potentially harmful element that causes neonatal jaundice. Recent evidence has shown that mildly elevated bilirubin levels within the physiological range have shown to be protective against various diseases. Our meta-analysis identified higher STB levels that were validated for predicting survival of incident CKD. The potential mechanisms behind the protective role of serum bilirubin are as follows: First, serum bilirubin is seen as a potent, endogenous antioxidant reagent because of persistent recovery in intracellular bilirubin redox metabolism. Second, it has been previously demonstrated that STB has a positive association with anti-inflammatory effects, which are a protective factor of CKD (37). Zucker et al. supported the finding that bilirubin could prevent an inflammatory reaction in a mice model of inflammatory colitis by preventing vascular cell adhesion molecule 1 (VCAM-1) - mediated leukocyte infiltration in target tissues (38). Third, renal endothelial dysfunction plays a critical role in progression of CKD and renal fibrosis through the process of endothelial-to-mesenchymal transition (End MT) (39). Higher STB levels are associated with lower levels of oxidative stress and enhancement of endothelium-dependent vasodilation in Gilbert's syndrome patients (40). Vogel M.E reported that bilirubin inhibits monocyte migration across activated human endothelial cells by disrupting the VCAM-1/ICAM-1 signaling pathway but does not affect the expression of the two *in vitro* or *in vivo* (41). Finally, diabetic nephropathy is the most common cause of ESRD, which accounts for >40% of patients on renal replacement therapy (42). One study depicts that in diabetic db/db mice, hyperbilirubinemia has a protective effect against the mesangial expansion and progression of CKD (43). Moreover, biliverdin and conjugated bilirubin may have an anticomplement role (44). More specifically, the protective effects of STB are complex and include multiple stages of cell and tissue biology. These biological properties of bilirubin support the finding that it plays a protective role for STB levels associated with the renal outcomes.

Patients with ESRD often undergo renal replacement therapy, including hemodialysis and peritoneal dialysis. The dialysis removes water-soluble circulating antioxidants, including uric acid and ascorbate, but does not remove hydrophobic substances, such as unconjugated bilirubin, which is plasma albumin-bound (18). There is a need to find appropriate biomarkers that indicate the clinical outcomes of dialysis patients. Therefore, we analyzed the relationship between STB levels and mortality in ESRD patients who underwent dialysis. The results showed no significant improvement in mortality outcomes within this dialysis population. There may be a few reasons behind this. First, only four studies and 51,764 participants were included in our meta-analysis, which led to high heterogeneity and publication bias. The way of dialysis, study design, adjusted items, and precise detecting time of STB could have influenced the negative outcomes. Second, Liu and Tsujikawa's studies have 316 and 94 patients, respectively. This could have caused low quality of the two studies. Third, in patients with ESRD, muscle wasting is accelerated by several catabolic factors. Higher bilirubin levels are often associated with lower triglycerides and cholesterol levels, low testosterone levels (45), and abnormalities in the

insulin growth factor-1 pathway (46). Vitek et al. demonstrated that there was a strong negative association between bilirubin levels and total mortality in the general population, especially in men. There are significant differences between dialysis and non-dialysis patients in regards to metabolic syndrome (47). It is postulated that patients with dialysis have higher mortality rates possibly because of the potent confounding effect of malnutrition and inflammation in hemodialysis patients with a low BMI index. Mortality rates for maintenance dialysis patients are much higher than the general population and this may preclude identification of small effect size risk factors. Thus, clinical trials and further research into this matter are needed to evaluate whether higher STB levels can reduce mortality rates in dialysis patients.

This study did have several strengths. Specifically speaking, this is the first meta-analysis of studies that examined associations of STB levels for renal outcomes among different subgroup populations and also examined associations between STB and mortality in dialysis populations. Furthermore, we not only conducted the highest STB groups verse reference groups analyses but also continuous variables (per 0.2 mg/dl increase) were used to certify the dose–response relationship.

Nonetheless, there are potential limitations to this study. First, our meta-analysis was restricted to published aggregate data. Individual participant-level data were not available, which is the primary limitation of this meta-analysis. Unpublished data or incomplete retrieval of identified studies led to an incomplete set of evidence and produced biased effects in the summary results. Funnel plot and "trim and fill" methods were used for assessment to balance out the publication bias and the relationship between the STB levels, and the risk of CKD remained statistically significant. Second, the included studies do not directly report on the data information required for meta-analysis, which can cause reporting bias. Third, potential confounding factors, such as age, sex, history of smoking, and/or alcohol intake (all of which could potentially influence the STB levels or risk of disease progression to CKD), could not be excluded. The studies did not adjust for same risk factors. Considering this fact, we included these factors in the multiple adjust models as much as possible. Fourth, only a few studies have differentiated the conjugated bilirubin and unconjugated bilirubin, and therefore the accurate role of separating bilirubin could not be investigated. Fifth, only STB levels in a narrow range (1.5 times the upper limit of normal) were studied. To translate these findings to clinical practice, future studies are needed to define an optimal range of STB. Finally, there was only one study involving a European population, which makes it difficult to definitively assess the association between STB levels and CKD in American and African populations.

In conclusion, our study indicates that individuals with reduced bilirubin concentrations, in the absence of liver pathology, are at a higher risk of CKD. This association was confirmed to be a linear dose–response relationship. Whether high STB levels serve as a protective factor of mortality or the risk of renal replacement therapy among the patients that underwent dialysis remains inconclusive. High-quality randomized controlled trials are needed to target STB levels for predicting renal outcomes. Considering that multiple mechanisms likely explain the protective properties of bilirubin and that bilirubin measurement is performed routinely for most patients, bilirubin might be a potential predictor for renal prognosis. It also highlights the importance of monitoring biomarkers related to serum bilirubin homeostasis in early prevention, diagnosis, and treatment of CKD and provides evidence to further multicenter validation research for bilirubin levels in routine risk stratification of CKD.

AUTHOR CONTRIBUTIONS

JL: conceptualization, formal analysis, methodology, software, and writing—original draft. JL, DL, and ZL: data curation. DL and ZL: investigation and supervision. ZL: project administration, validation, and writing—review and editing. All authors contributed to the article and approved the submitted version.

FUNDING

This study was supported by grants from the Science and Technology Huimin Project of Henan Province (No. 162207310001) and the Pathogenesis & Precision diagnosis and treatment of Chronic Kidney Disease (No. 182101510002).

SUPPLEMENTARY MATERIAL

The Supplementary Material for this article can be found online at: https://www.frontiersin.org/articles/10.3389/fmed.2020.00549/full#supplementary-material

REFERENCES

1. GBD 2013 Mortality and Causes of Death Collaborators. Global, regional, and national age-sex specific all-cause and cause-specific mortality for 240 causes of death, 1990-2013: a systematic analysis for the Global Burden of Disease Study 2013. *Lancet*. (2015) 385:117–71. doi: 10.1016/S0140-6736(14)61682-2
2. Jha V, Garcia-Garcia G, Iseki K, Li Z, Naicker S, Plattner B, et al. Chronic kidney disease: global dimension and perspectives. *Lancet*. (2013) 382:260–72. doi: 10.1016/S0140-6736(13)60687-X
3. Krata N, Zagozdzon R, Foroncewicz B, Mucha KJAIeTE. Oxidative stress in kidney diseases: the cause or the consequence? *Arch Immunol Ther Exp*. (2018) 66:211–20. doi: 10.1007/s00005-017-0496-0
4. Duni A, Liakopoulos V, Roumeliotis S, Peschos D, Dounousi E. Oxidative stress in the pathogenesis and evolution of chronic kidney disease: untangling ariadne's thread. *Int J Mol Sci*. (2019) 20:3711. doi: 10.3390/ijms20153711
5. Miranda-Diaz AG, Pazarin-Villasenor L, Yanowsky-Escatell FG, Andrade-Sierra J. Oxidative stress in diabetic nephropathy with early chronic kidney disease. *J Diabetes Res*. (2016) 2016:7047238. doi: 10.1155/2016/7047238
6. Zelenka J, Dvorak A, Alan L, Zadinova M, Haluzik M, Vitek L. Hyperbilirubinemia protects against aging-associated inflammation and metabolic deterioration. *Oxidative Med Cell Longevity*. (2016) 2016:6190609. doi: 10.1155/2016/6190609
7. Chin HJ, Cho HJ, Lee TW, Na KY, Oh KH, Joo KW, et al. The mildly elevated serum bilirubin level is negatively associated with the incidence of end stage

renal disease in patients with IgA nephropathy. *J Korean Med Sci*. (2009) 24(Suppl):S22–9. doi: 10.3346/jkms.2009.24.S1.S22
8. Riphagen IJ, Deetman PE, Bakker SJ, Navis G, Cooper ME, Lewis JB, et al. Bilirubin and progression of nephropathy in type 2 diabetes: a post hoc analysis of RENAAL with independent replication in IDNT. *Diabetes*. (2014) 63:2845–53. doi: 10.2337/db13-1652
9. Wang J, Li Y, Han X, Hu H, Wang F, Yu C, et al. Association between serum bilirubin levels and decline in estimated glomerular filtration rate among patients with type 2 diabetes. *J Diabetes Complications*. (2016) 30:1255–60. doi: 10.1016/j.jdiacomp.2016.05.013
10. Ahn KH, Kim SS, Kim WJ, Kim JH, Nam YJ, Park SB, et al. Low serum bilirubin level predicts the development of chronic kidney disease in patients with type 2 diabetes mellitus. *Korean J Internal Med*. (2017) 32:875–82. doi: 10.3904/kjim.2015.153
11. Han SS, Na KY, Chae DW, Kim YS, Kim S, Chin HJ. High serum bilirubin is associated with the reduced risk of diabetes mellitus and diabetic nephropathy. *Tohoku J Exp Med*. (2010) 221:133–40. doi: 10.1620/tjem.221.133
12. Toya K, Babazono T, Hanai K, Uchigata Y. Association of serum bilirubin levels with development and progression of albuminuria, and decline in estimated glomerular filtration rate in patients with type 2 diabetes mellitus. *J Diabetes Investig*. (2014) 5:228–35. doi: 10.1111/jdi.12134
13. Mashitani T, Hayashino Y, Okamura S, Tsujii S, Ishii H. Correlations between serum bilirubin levels and diabetic nephropathy progression among Japanese type 2 diabetic patients: a prospective cohort study (Diabetes Distress and Care Registry at Tenri [DDCRT 5]). *Diabetes Care*. (2014) 37:252–8. doi: 10.2337/dc13-0407
14. Fukui M, Tanaka M, Yamazaki M, Hasegawa G, Nishimura M, Iwamoto N, et al. Low serum bilirubin concentration in haemodialysis patients with Type 2 diabetes. *Diabet Med*. (2011) 28:96–9. doi: 10.1111/j.1464-5491.2010.03173.x
15. Wang J, Wang B, Liang M, Wang G, Li J, Zhang Y, et al. Independent and combined effect of bilirubin and smoking on the progression of chronic kidney disease. *Clin Epidemiol*. (2018) 10:121–32. doi: 10.2147/CLEP.S150687
16. Targher G, Zoppini G, Cesare Guidi G, Lippi G. Relationship between serum bilirubin and kidney function in non-diabetic and diabetic individuals. *Kidney Int*. (2009) 75:863. doi: 10.1038/ki.2008.677
17. Ryu S, Chang Y, Zhang Y, Woo HY, Kwon MJ, Park H, et al. Higher serum direct bilirubin levels were associated with a lower risk of incident chronic kidney disease in middle aged Korean men. *PLoS ONE*. (2014) 9:e75178. doi: 10.1371/journal.pone.0075178
18. Su HH, Kao CM, Lin YC, Lin YC, Kao CC, Chen HH, et al. Relationship between serum total bilirubin levels and mortality in uremia patients undergoing long-term hemodialysis: a nationwide cohort study. *Atherosclerosis*. (2017) 265:155–61. doi: 10.1016/j.atherosclerosis.2017.09.001
19. Willi C, Bodenmann P, Ghali WA, Faris PD, Cornuz J. Active smoking and the risk of type 2 diabetes: a systematic review and meta-analysis. *JAMA*. (2007) 298:2654–64. doi: 10.1001/jama.298.22.2654
20. Kawamoto R, Ninomiya D, Hasegawa Y, Kasai Y, Kusunoki T, Ohtsuka N, et al. Association between serum bilirubin and estimated glomerular filtration rate among elderly persons. *PLoS ONE*. (2014) 9:e115294. doi: 10.1371/journal.pone.0115294
21. Tanaka M, Fukui M, Okada H, Senmaru T, Asano M, Akabame S, et al. Low serum bilirubin concentration is a predictor of chronic kidney disease. *Atherosclerosis*. (2014) 234:421–5. doi: 10.1016/j.atherosclerosis.2014.03.015
22. Lee AT, Wang YY, Lin SY, Liang JT, Sheu WH, Song YM, et al. Higher serum total bilirubin concentration is associated with lower risk of renal insufficiency in an adult population. *Int J Clin Exp Med*. (2015) 8:19212–22.
23. Sakoh T, Nakayama M, Tanaka S, Yoshitomi R, Ura Y, Nishimoto H, et al. Association of serum total bilirubin with renal outcome in Japanese patients with stages 3-5 chronic kidney disease. *Metab Clin Exp*. (2015) 64:1096–102. doi: 10.1016/j.metabol.2015.06.006
24. Tanaka S, Ninomiya T, Masutani K, Nagata M, Tsuchimoto A, Tsuruya K, et al. Prognostic impact of serum bilirubin level on long-term renal survival in IgA nephropathy. *Clin Exp Nephrol*. (2015) 19:1062–70. doi: 10.1007/s10157-015-1096-0
25. Yang TL, Lin YC, Lin YC, Huang CY, Chen HH, Wu MS. Total bilirubin in prognosis for mortality in end-stage renal disease patients on peritoneal dialysis therapy. *J Am Heart Assoc*. (2017) 6:e007507. doi: 10.1161/JAHA.117.007507
26. Liu Y, Li M, Song Y, Liu X, Zhao J, Deng B, et al. Association of serum bilirubin with renal outcomes in Han Chinese patients with chronic kidney disease. *Clin Chim Acta Int J Clin Chem*. (2018) 480:9–16. doi: 10.1016/j.cca.2018.01.041
27. Tsujikawa H, Tanaka S, Hara M, Kawai Y, Matsukuma Y, Torisu K, et al. Association of lower serum bilirubin with loss of residual kidney function in peritoneal dialysis patients. *Therap Apheresis Dialysis*. (2019) 24:202. doi: 10.1111/1744-9987.12865
28. Wu Y, Zhang J, Wang J, Wang Y, Han Q, Li H, et al. The association of serum bilirubin on kidney clinicopathologic features and renal outcome in patients with diabetic nephropathy: a biopsy-based study. *Endocrine Pract*. (2019) 25:554–61. doi: 10.4158/EP-2018-0560
29. Liu X, Luo X, Liu Y, Sun X, Han C, Zhang L, et al. Resting heart rate and risk of metabolic syndrome in adults: a dose-response meta-analysis of observational studies. *Acta Diabetol*. (2017) 54:223–35. doi: 10.1007/s00592-016-0942-1
30. Lin JP, Vitek L, Schwertner HA. Serum bilirubin and genes controlling bilirubin concentrations as biomarkers for cardiovascular disease. *Clin Chem*. (2010) 56:1535–43. doi: 10.1373/clinchem.2010.151043
31. Inoguchi T, Sasaki S, Kobayashi K, Takayanagi R, Yamada T. Relationship between Gilbert syndrome and prevalence of vascular complications in patients with diabetes. *JAMA*. (2007) 298:1398–400. doi: 10.1001/jama.298.12.1398-b
32. Lee MJ, Jung CH, Kang YM, Hwang JY, Jang JE, Leem J, et al. Serum bilirubin as a predictor of incident metabolic syndrome: a 4-year retrospective longitudinal study of 6205 initially healthy Korean men. *Diabetes Metab*. (2014) 40:305–9. doi: 10.1016/j.diabet.2014.04.006
33. Ching S, Ingram D, Hahnel R, Beilby J, Rossi E. Serum levels of micronutrients, antioxidants and total antioxidant status predict risk of breast cancer in a case control study. *J Nutr*. (2002) 132:303–6. doi: 10.1093/jn/132.2.303
34. Wagner KH, Wallner M, Molzer C, Gazzin S, Bulmer AC, Tiribelli C, et al. Looking to the horizon: the role of bilirubin in the development and prevention of age-related chronic diseases. *Clin Sci*. (2015) 129:1–25. doi: 10.1042/CS20140566
35. Targher G, Bosworth C, Kendrick J, Smits G, Lippi G, Chonchol M. Relationship of serum bilirubin concentrations to kidney function and albuminuria in the United States adult population. Findings from the National Health and Nutrition Examination Survey 2001-2006. *Clin Chem Lab Med*. (2009) 47:1055–62. doi: 10.1515/CCLM.2009.244
36. Shin HS, Jung YS, Rim H. Relationship of serum bilirubin concentration to kidney function and 24-hour urine protein in Korean adults. *BMC Nephrol*. (2011) 12:29. doi: 10.1186/1471-2369-12-29
37. Tsai MT, Tarng DC. Beyond a measure of liver function-bilirubin acts as a potential cardiovascular protector in chronic kidney disease patients. *Int J Mol Sci*. (2018) 20:117. doi: 10.3390/ijms20010117
38. Zucker SD, Vogel ME, Kindel TL, Smith DL, Idelman G, Avissar U, et al. Bilirubin prevents acute DSS-induced colitis by inhibiting leukocyte infiltration and suppressing upregulation of inducible nitric oxide synthase. *Am J Physiol Gastrointestinal Liver Physiol*. (2015) 309:G841–54. doi: 10.1152/ajpgi.00149.2014
39. Lipphardt M, Song JW, Matsumoto K, Dadafarin S, Dihazi H, Muller G, et al. The third path of tubulointerstitial fibrosis: aberrant endothelial secretome. *Kidney Int*. (2017) 92:558–68. doi: 10.1016/j.kint.2017.02.033
40. Maruhashi T, Soga J, Fujimura N, Idei N, Mikami S, Iwamoto Y, et al. Hyperbilirubinemia, augmentation of endothelial function, and decrease in oxidative stress in Gilbert syndrome. *Circulation*. (2012) 126:598–603. doi: 10.1161/CIRCULATIONAHA.112.105775
41. Vogel ME, Idelman G, Konaniah ES, Zucker SD. Bilirubin prevents atherosclerotic lesion formation in low-density lipoprotein receptor-deficient mice by inhibiting endothelial VCAM-1 and ICAM-1 signaling. *J Am Heart Assoc*. (2017) 6:e004820. doi: 10.1161/JAHA.116.004820
42. Alicic RZ, Rooney MT, Tuttle KR. Diabetic kidney disease: challenges, progress, and possibilities. *Clin J Am Soc Nephrol*. (2017) 12:2032–45. doi: 10.2215/CJN.11491116
43. Fujii M, Inoguchi T, Sasaki S, Maeda Y, Zheng J, Kobayashi K, et al. Bilirubin and biliverdin protect rodents against diabetic nephropathy by downregulating NAD(P)H oxidase. *Kidney Int*. (2010) 78:905–19. doi: 10.1038/ki.2010.265

44. Nakagami T, Toyomura K, Kinoshita T, Morisawa S. A beneficial role of bile pigments as an endogenous tissue protector: anti-complement effects of biliverdin and conjugated bilirubin. *Biochim Biophys Acta*. (1993) 1158:189–93. doi: 10.1016/0304-4165(93)90013-X
45. Carrero JJ, Qureshi AR, Nakashima A, Arver S, Parini P, Lindholm B, et al. Prevalence and clinical implications of testosterone deficiency in men with end-stage renal disease. *Nephrol Dialysis Transpl*. (2011) 26:184–90. doi: 10.1093/ndt/gfq397
46. Bailey JL, Zheng B, Hu Z, Price SR, Mitch WE. Chronic kidney disease causes defects in signaling through the insulin receptor substrate/phosphatidylinositol 3-kinase/Akt pathway: implications for muscle atrophy. *J Am Soc Nephrol*. (2006) 17:1388–94. doi: 10.1681/ASN.2004100842
47. Vitek L, Hubacek JA, Pajak A, Doryńska A, Kozela M, Eremiasova L, et al. Association between plasma bilirubin and mortality. *Ann Hepatol*. (2019) 18:379–85. doi: 10.1016/j.aohep.2019.02.001

Conflict of Interest: The authors declare that the research was conducted in the absence of any commercial or financial relationships that could be construed as a potential conflict of interest.

frontiers in Medicine

BRIEF RESEARCH REPORT
published: 01 February 2021
doi: 10.3389/fmed.2020.617786

Anticoagulant Related Nephropathy Only Partially Develops in C57BL/6 Mice: Hematuria Is Not Accompanied by Red Blood Cell Casts in the Kidney

Ajay K. Medipally[1†], Min Xiao[1†], Shahzeb Qaisar[1], Anjali A. Satoskar[1], Iouri Ivanov[1], Brad Rovin[2] and Sergey V. Brodsky[1]*

[1] Department of Pathology, The Ohio State University Wexner Medical Center, Columbus, OH, United States, [2] Department of Medicine, The Ohio State University Wexner Medical Center, Columbus, OH, United States

Anticoagulant-related nephropathy (ARN) may develop in patients that are on anticoagulation therapy. Rats with 5/6 nephrectomy treated with different anticoagulants showed acute kidney injury (AKI) and red blood cell (RBC) casts in the tubules similar to ARN in humans. The aim of the current study was to investigate the feasibility of inducing ARN in mice. C57BL/6 5/6 nephrectomy mice were treated with warfarin and dabigatran 3 weeks after ablative surgery for 7 days. Two doses of each anticoagulant were used. All anticoagulants resulted in serum creatinine and hematuria increase. Mortality was 63% in 5.0 mg/kg/day of warfarin but only 13% in 2.5 mg/kg/day of warfarin or in 400 mg/kg/day of dabigatran and 0% in 200 mg/kg/day of dabigatran. In spite of increasing hematuria, RBC tubular casts were not seen in mice treated with any anticoagulant. The 5/6 nephrectomy murine model in C57BL/6 mice only partially reproduced ARN in terms of increasing serum creatinine and hematuria, but there were no RBC tubular casts in the remnant kidney.

Keywords: anticoagulant related nephropathy, acute kidney injury, mouse model, 5/6 nephrectomy, anticoagulation

OPEN ACCESS

Edited by:
Xiao-ming Meng,
Anhui Medical University, China

Reviewed by:
Ben Sprangers,
University Hospitals Leuven, Belgium
Hoon Young Choi,
Yonsei University, South Korea

****Correspondence:***
Sergey V. Brodsky
sergey.brodsky@osumc.edu

† These authors have contributed equally to this work

Specialty section:
This article was submitted to Nephrology, a section of the journal Frontiers in Medicine

Received: *15 October 2020*
Accepted: *31 December 2020*
Published: *01 February 2021*

Citation:
Medipally AK, Xiao M, Qaisar S, Satoskar AA, Ivanov I, Rovin B and Brodsky SV (2021) Anticoagulant Related Nephropathy Only Partially Develops in C57BL/6 Mice: Hematuria Is Not Accompanied by Red Blood Cell Casts in the Kidney. Front. Med. 7:617786. doi: 10.3389/fmed.2020.617786

INTRODUCTION

After our first description of warfarin-related nephropathy [later defined as anticoagulant-related nephropathy (ARN)] in humans (1, 2), we developed an animal model in rats that has close fidelity to the human disease (3, 4). Rats with 5/6 nephrectomy developed glomerular hemorrhage, red blood cell (RBC) tubular casts, and acute kidney injury (AKI) when treated with vitamin K antagonists or a thrombin inhibitor (3, 5). The mechanisms of this AKI include disruption of the glomerular filtration barrier that allows RBC crossing into the urine, increased oxidative stress in the kidney, and acute tubular necrosis (6). The rat model is useful to evaluate the morphological changes in the kidney associated with anticoagulation, but it is difficult to study molecular mechanisms that lead to the glomerular filtration barrier disruption. A murine model could be more useful to study the pathogenesis of ARN because of easier knockout of different genes in mice as compared to rats. The aim of the current study was to investigate the feasibility of ARN induction in C57BL/6 mice.

MATERIALS AND METHODS

These studies were approved by the Institutional Animal Care and Use Committees (IACUC) at the Ohio State University.

C57BL/6 mice were obtained from the Charles River Laboratories (Wilmington, MA). A 5/6 nephrectomy was performed in 25–30 g mice as we described previously for rats (3). Briefly, mice were anesthetized with isoflurane/oxygen (1:5), a middle laparotomy was performed, the right kidney was removed, as well as 2/3 of the left kidney at the same time. Kidney tissue from the nephrectomy was frozen at −80°C for further studies. Hemostasis was achieved by hemostatic sponges (Quick clot; Z-medica Corporation, Wallingford, CT). The incision was closed with 4.0 proline, and the animals were kept on a 12/12 h light/dark cycle and on the standard rodent diet with free access to water.

Three weeks later, treatment with an anticoagulant was begun, and daily blood and urine samples were collected. Warfarin sodium (Sigma-Aldrich, St. Louis, MO) and dabigatran etexilate (Boehringer Ingelheim Pharmaceuticals, Inc., Ridgefield, CT) were given once a day *per os via* gavage. Animals were sacrificed on day 7 of the treatment; the remnant kidney was dissected for histological and molecular studies. The histology of the kidney was evaluated on 2–3 mcm sections of paraffin-embedded tissue stained with hematoxylin-eosinophil.

Serum creatinine was measured based on the Jaffe reaction using a creatinine reagent assay (Pointe Scientific, Inc., Canton, MI) as we described earlier. Briefly, 10 μL of serum was mixed with 200 μL of working reagent at 37°C in a 96-well plate, and the absorbance was read at 510 nm at 40 and 100 s using a Molecular Devices Versa Max plate reader (Molecular Devices, Sunnyvale, CA).

Hematuria and proteinuria were evaluated by dipsticks (Siemens reagent strips; Tarrytown, NY) and expressed in a semiquantitative scale from 0 to 3, where 0 is absent, 1 is mild, 2 is moderate, and 3 is severe.

Coagulation parameters [prothrombin time (PT) and activated partial thromboplastin time (aPTT)] were measured using the Biobase coagulation analyzer (model COA01; Genprice Inc., San Jose, CA) based on the manufacturer's protocol. Briefly, blood was collected into a tube containing 3.8% sodium citrate in a ratio of 9:1. The blood was centrifuged at 3,500 RPM for 10 min. Twenty microliters of plasma was placed in the incubation station with 20 μL of the aPTT reagent (Fisher Scientific, Middletown, VA). Then, after 3 min, preheated at 37°C for 10 min and 20 μL of 0.025 M calcium chloride was added. Clotting time was recorded in seconds. For PT, 20 μL of plasma was placed in the incubation station; after 2 min, preheated at 37°C for 10 min and 40 μL of PT reagent (Fisher scientific, Middletown, VA) was added. Clotting time was recorded in seconds. sINR was calculated as changes of PT to the "standard" PT (mean PT calculated from all baselines measurements from all groups), as we described earlier (3).

Statistical Analysis

Descriptive statistics were used to analyze differences between experimental groups. Data are presented as mean ± standard deviation (SD), unless otherwise specified. Student's two-tailed *t*-test was used to analyze differences between two different time points within the same animal group; one-way ANOVA was used to analyze dynamic changes associated with the treatment. Survival plots were built by using Kaplan–Meier curves. Survival curves were compared by using the Mantel–Haenszel (logrank) test.

RESULTS

Changes in Coagulation and Mortality

C57BL/6 mice were subjected to ablative surgery (5/6 nephrectomy) and treated with warfarin and dabigatran 3 weeks after the surgery as described in Materials and Methods. Both warfarin and dabigatran in mice had anticoagulation effects that are similar to humans. Thus, treatment with 5.0 mg/kg/day of warfarin resulted in a rapid increase in sINR above 3 a.u. by day 3 of treatment and remained elevated above 3 a.u. until the end of the study (**Figure 1A**). Treatment with 2.5 mg/kg/day of warfarin resulted in a modest elevation in sINR, and it was in the range 1.5–2 a.u. since day 4 (**Figure 1A**). Dabigatran increased aPTT above 50 s (upper limit of the reading range for the coagulometer) on day 3 for 400 mg/kg/day and day 4 for 200 mg/kg/day (**Figure 1B**). Mortality in warfarin-treated animals was high in the 5.0 mg/kg/day group (62.5% of mice died by day 7), whereas it was modest in the 2.5 mg/kg/day group (12.5% died by day 7, $p = 0.0311$) (**Figure 1C**). Among animals treated with dabigatran, only one mouse died at day 4 in the 400 mg/kg/day group, whereas all mice survived in the 200 mg/kg/day group after 7 days ($p = 0.2801$) (**Figure 1D**). The main cause of death was hemorrhage to the gastrointestinal tract; no gross evidence of intracranial hemorrhage was noted.

Changes in Serum Creatinine and Hematuria

All mice had an increase in serum creatinine after 5/6 nephrectomy (from 0.50 ± 0.04 to 0.58 ± 0.1 mg/dL 3 weeks after the surgery, $p = 0.004$). In mice treated with warfarin, serum creatinine was increased in both groups. Treatment with 2.5 mg/kg/day resulted in a significant increase in serum creatinine by day 5 of treatment (0.64 ± 0.03 mg/dL, $p = 0.009$). Treatment with 5.0 mg/kg/day resulted in a more rapid increase in serum creatinine (significantly elevated at day 4 of treatment, 0.76 ± 0.11 mg/dL, $p = 0.042$) (**Figure 2A**). In control (vehicle-treated) mice, serum creatinine remained unchanged 7 days after the treatment (0.60 ± 0.05 mg/dL). Simultaneously with the increase in serum creatinine, there was an increase in hematuria that was more prominent in mice treated with 5 mg/kg/day of warfarin (**Figure 2C**). In the control (vehicle-treated) group, hematuria did not change by day 7 (0.1 ± 0.11 and 0.1 ± 0.21 a.u. days 0 and 7, respectively).

Similarly to warfarin, treatment with dabigatran resulted in an increase in serum creatinine in 5/6 nephrectomy mice (**Figure 2B**). Both 200 and 400 mg/kg/day of dabigatran resulted in serum creatinine increase, but only with 400 mg/kg/day of dabigatran was such increase significant at day 6 (0.69 ± 0.11 mg/dL, $p = 0.0355$), whereas serum creatinine elevation in mice

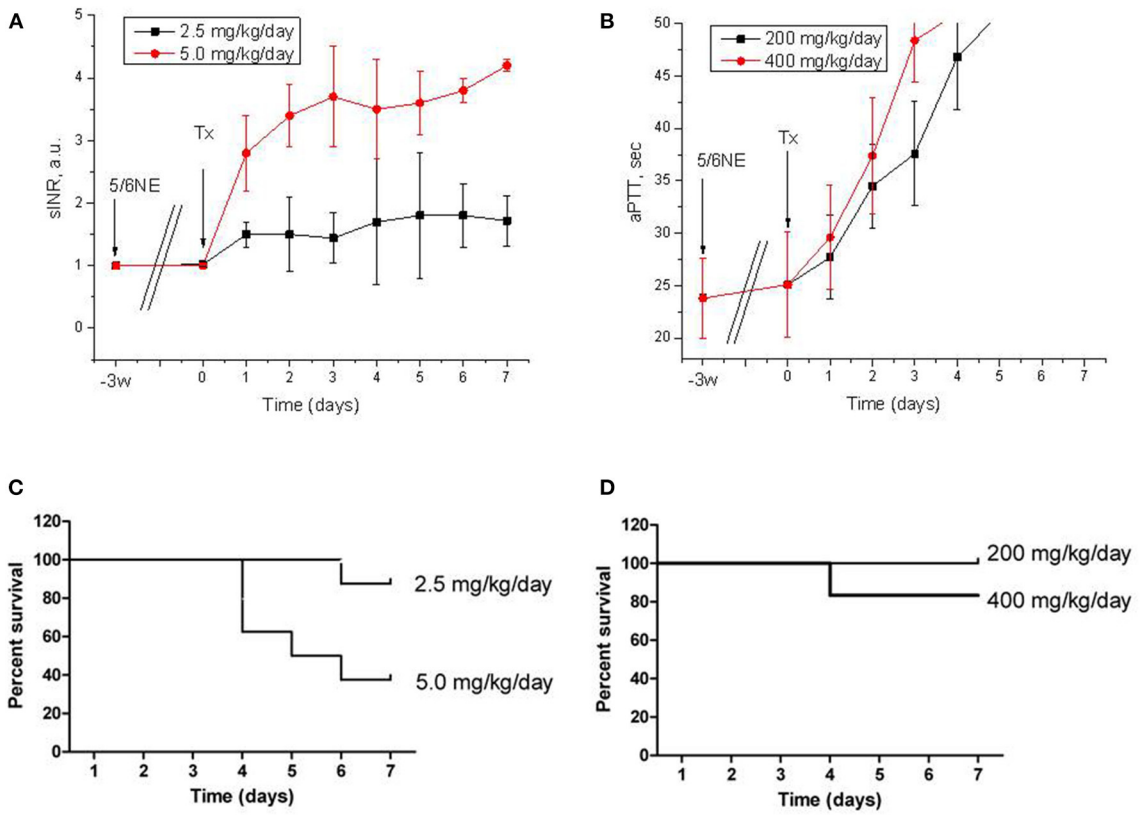

FIGURE 1 | Anticoagulation effects and mortality of warfarin and dabigatran treatments in 5/6 nephrectomy mice. **(A,B)** Changes in prothrombin time calculated as sINR in 5/6 nephrectomy mice treated with 2.5 mg/kg/day ($n = 8$) and 5.0 mg/kg/day ($n = 8$) of warfarin **(A)** or with 200 mg/kg/day ($n = 7$) and 400 mg/kg/day ($n = 6$) of dabigatran **(B)**. **(C,D)** Kaplan-Meier curves of mortality rate in 5/6 nephrectomy mice treated with 2.5 mg/kg/day ($n = 8$) and 5.0 mg/kg/day ($n = 8$) of warfarin **(C)** or with 200 mg/kg/day ($n = 7$) and 400 mg/kg/day ($n = 6$) of dabigatran **(D)**. 5/6NE, 5/6 nephrectomy; Tx, beginning of treatment.

treated with 200 mg/kg/day of dabigatran was not significant (**Figure 2B**). Hematuria was increased in both dabigatran treatment groups (**Figure 2D**).

Morphologic Changes in the Kidney

Morphological changes in the kidney in mice treated with both anticoagulants included mild acute tubular epithelial cell injury (more pronounced in high dosage groups), but no RBC casts in the tubules or RBC in the Bowman's space were seen.

DISCUSSION

Since our kidney biopsy findings in patients treated with warfarin were described over 10 years ago (2), many cases of ARN in humans have since been reported (7). The pathogenesis of this condition is unclear, and it requires further studies. We had demonstrated that 5/6 nephrectomy rats treated with anticoagulants (warfarin and dabigatran) 3 weeks after the ablative surgery have an increase in serum creatinine and morphological changes in the kidney that are similar to the human disease (3, 5). Unfortunately, it is not easy to control gene and protein expression in rats; therefore, there is a need for a murine model of ARN. Here, we report our findings when we treated C57BL/6 5/6 nephrectomy mice with warfarin and dabigatran.

Our data indicate that C57BL/6 mice require higher doses of anticoagulants as compared to rats, which corresponds to literature data (8). Thus, in our previous works, we used 0.75 mg/kg/day of warfarin and 50 mg/kg/day of dabigatran in rats, and we achieved anticoagulation levels similar to those in humans. These treatments resulted in ARN in rats with an increase in serum creatinine and RBC casts in the tubules. In mice, we had to use 2.5 mg/kg/day of warfarin to increase PT two-fold and 5.0 mg/kg/day to increase PT four times and higher. The high warfarin dose was fatal for mice, and there was over 50% mortality (**Figure 1C**). Similarly, dabigatran in the dose of 200 mg/kg/day increased aPTT two-fold in mice (**Figure 1B**), whereas in rats a similar effect was achieved with only 50 mg/kg/day (5). Effects on the kidney function were different in mice and rats. Even though there was the increase in serum creatinine and hematuria which were associated with treatment with both anticoagulants in C57BL/6 mice, the morphological hallmark of ARN such as occlusive red blood casts in the

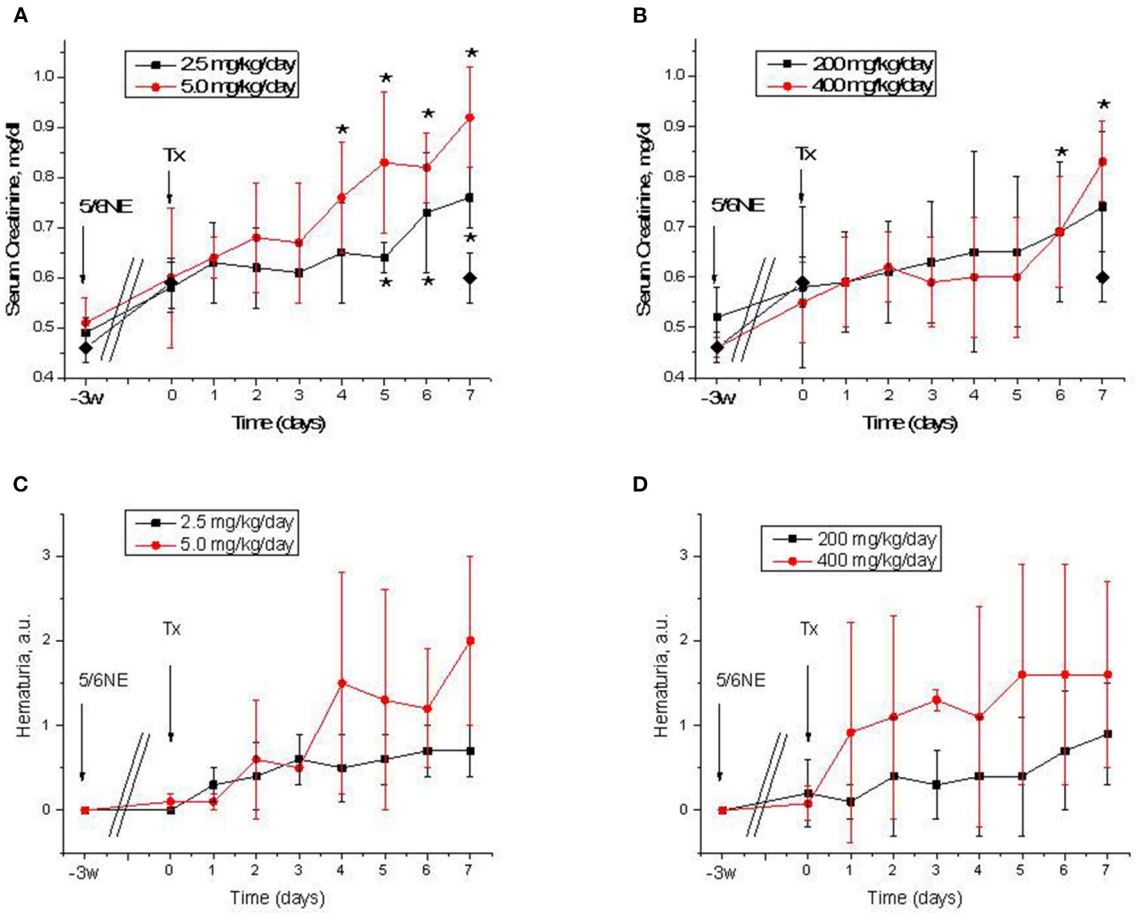

FIGURE 2 | Serum creatinine changes and hematuria in 5/6 nephrectomy mice treated with warfarin and dabigatran. **(A,B)** Serum creatinine changes in 5/6 nephrectomy mice treated with 2.5 mg/kg/day ($n = 8$) and 5.0 mg/kg/day ($n = 8$) of warfarin **(A)** or with 200 mg/kg/day ($n = 7$) and 400 mg/kg/day ($n = 6$) of dabigatran **(B)**. Control (vehicle-treated group) data on day 0 and 7 are shown in a solid diamond on both **(A,B)**. **(C,D)** Hematuria in 5/6 nephrectomy mice treated with 2.5 mg/kg/day ($n = 8$) and 5.0 mg/kg/day ($n = 8$) of warfarin **(C)** or with 200 mg/kg/day ($n = 7$) and 400 mg/kg/day ($n = 6$) of dabigatran **(D)**. 5/6NE, 5/6 nephrectomy; Tx, beginning of treatment. *$p < 0.05$ as compared to day 0 of treatment. Hematuria was quantitated by a semiquantitative scale from 0 to 3, where 0 is absent, 1 is mild, 2 is moderate, and 3 is severe.

tubules was lacking in mice but was present in rats. One possible explanation of such a difference could be related to the fact that mice are more resistant to 5/6 nephrectomy compared to rats and the decline in kidney function in C57BL/6 mice is less pronounced than in other mouse strains (9). Even though we observed a significant increase in serum creatinine 3 weeks after the ablative surgery in C57BL/6 mice, the kidney function was probably still not impaired enough to develop RBC casts in the tubules. Other mouse strains, such as BALB/c mice, could be more susceptible to developing ARN, but since many knockout mice are developed based on the C57BL/6 strain, it is desirable to develop a model to study ARN using the C57BL/6 mice. One possible solution would be to induce hypertension by using angiotensin II in C57BL/6 mice after 5/6 nephrectomy and to study ARN after the treatment; this requires further investigation (9). However, even in the absence of occlusive tubular RBC casts, we achieved a dose-dependent increase in serum creatinine and hematuria, indicating that C57BL/6 5/6 nephrectomy mice, at least partially, could be used to study ARN.

DATA AVAILABILITY STATEMENT

The raw data supporting the conclusions of this article will be made available by the authors, without undue reservation.

ETHICS STATEMENT

The animal study was reviewed and approved by the Institutional Animal Care and Use Committees (IACUC) at the Ohio State University.

AUTHOR CONTRIBUTIONS

AM conducted animals studies (surgeries), collected and analyzed samples, and participated in data analysis, writing,

and reviewing the manuscript. MX conducted animals studies, collected and analyzed samples, and participated in data analysis, writing, and reviewing the manuscript. SQ collected and analyzed samples, participated in data analysis, writing, and reviewing the manuscript. AS, II, and BR participated in study design, data analysis, writing, and reviewing the manuscript. SB oversees the entire study, designed experiments, and performed data analysis, writing, and reviewing the manuscript. All authors contributed to the article and approved the submitted version.

FUNDING

This study was supported by a grant from NIH (NIDDK grant R01DK117102) to SB.

REFERENCES

1. Brodsky SV, Collins M, Park E, Rovin BH, Satoskar AA, Nadasdy G, et al. Warfarin therapy that results in an International Normalization Ratio above the therapeutic range is associated with accelerated progression of chronic kidney disease. *Nephron Clin Pract*. (2010) 115:c142–6. doi: 10.1159/000312877
2. Brodsky SV, Satoskar A, Chen J, Nadasdy G, Eagen JW, Hamirani M, et al. Acute kidney injury during warfarin therapy associated with obstructive tubular red blood cell casts: a report of 9 cases. *Am J Kidney Dis*. (2009) 54:1121–6. doi: 10.1053/j.ajkd.2009.04.024
3. Ozcan A, Ware K, Calomeni E, Nadasdy T, Forbes R, Satoskar AA, et al. 5/6 nephrectomy as a validated rat model mimicking human warfarin-related nephropathy. *Am J Nephrol*. (2012) 35:356–64. doi: 10.1159/000337918
4. Ware K, Brodsky P, Satoskar AA, Nadasdy T, Nadasdy G, Wu H, et al. Warfarin-related nephropathy modeled by nephron reduction and excessive anticoagulation. *J Am Soc Nephrol*. (2011) 22:1856–62. doi: 10.1681/ASN.2010101110
5. Ryan M, Ware K, Qamri Z, Satoskar A, Wu H,. Nadasdy G, et al. Warfarin-related nephropathy is the tip of the iceberg: direct thrombin inhibitor dabigatran induces glomerular hemorrhage with acute kidney injury in rats. *Nephrol Dial Transplant*. (2014) 29:2228–34. doi: 10.1093/ndt/gft380
6. Ware K, Qamri Z, Ozcan A, Satoskar AA, Nadasdy G, Rovin BH, et al. N-acetylcysteine ameliorates acute kidney injury but not glomerular hemorrhage in an animal model of warfarin-related nephropathy. *Am J Physiol Renal Physiol*. (2013) 304:F1421–7. doi: 10.1152/ajprenal.00689.2012
7. Glassock RJ. Anticoagulant-related nephropathy: it's the real McCoy. *Clin J Am Soc Nephrol*. (2019) 14:935–7. doi: 10.2215/cjn.02470319
8. Sato K, Taniuchi Y, Kawasaki T, Hirayama F, Koshio H, Matsumoto Y, et al. Comparison of the anticoagulant and antithrombotic effects of YM-75466, a novel orally-active factor Xa inhibitor, and warfarin in mice. *Jpn J Pharmacol*. (1998) 78:191–7. doi: 10.1254/jjp.78.191
9. Leelahavanichkul A, Yan Q, Hu X, Eisner C, Huang Y, Chen R, et al. Angiotensin II overcomes strain-dependent resistance of rapid CKD progression in a new remnant kidney mouse model. *Kidney Int*. (2010) 78:1136–53. doi: 10.1038/ki.2010.287

Conflict of Interest: SB received a grant from NIH (NIDDK grant R01DK117102).

The remaining authors declare that the research was conducted in the absence of any commercial or financial relationships that could be construed as a potential conflict of interest.

frontiers in Medicine

ORIGINAL RESEARCH
published: 09 April 2021
doi: 10.3389/fmed.2021.592357

Natural History of Clinical, Laboratory, and Echocardiographic Parameters of a Primary Hyperoxaluria Cohort on Long Term Hemodialysis

David J. Sas[1,2,3], Felicity T. Enders[4], Tina M. Gunderson[4], Ramila A. Mehta[4], Julie B. Olson[3], Barbara M. Seide[3], Carly J. Banks[3], Bastian Dehmel[5], Patricia A. Pellikka[6], John C. Lieske[2,3] and Dawn S. Milliner[1,3]*

[1] Division of Pediatric Nephrology and Hypertension, Mayo Clinic, Rochester, MN, United States, [2] Department of Laboratory Medicine and Pathology, Mayo Clinic, Rochester, MN, United States, [3] Division of Nephrology and Hypertension, Mayo Clinic, Rochester, MN, United States, [4] Division of Biomedical Statistics and Informatics, Mayo Clinic, Rochester, MN, United States, [5] OxThera AB, Stockholm, Sweden, [6] Department of Cardiovascular Medicine, Mayo Clinic, Rochester, MN, United States

OPEN ACCESS

Edited by:
Michael L. Moritz,
University of Pittsburgh, United States

Reviewed by:
Elizabeth Harvey,
Hospital for Sick Children, Canada
Kirsten Kusumi,
Akron Children's Hospital,
United States

****Correspondence:***
David J. Sas
sas.david@mayo.edu

Specialty section:
This article was submitted to Nephrology, a section of the journal Frontiers in Medicine

Received: *28 August 2020*
Accepted: *12 March 2021*
Published: *09 April 2021*

Citation:
Sas DJ, Enders FT, Gunderson TM, Mehta RA, Olson JB, Seide BM, Banks CJ, Dehmel B, Pellikka PA, Lieske JC and Milliner DS (2021) Natural History of Clinical, Laboratory, and Echocardiographic Parameters of a Primary Hyperoxaluria Cohort on Long Term Hemodialysis. Front. Med. 8:592357. doi: 10.3389/fmed.2021.592357

Background: Primary hyperoxaluria type 1 (PH1) is a rare monogenic disorder characterized by excessive hepatic production of oxalate leading to recurrent nephrolithiasis, nephrocalcinosis, and progressive kidney damage, often requiring renal replacement therapy (RRT). Though systemic oxalate deposition is well-known, the natural history of PH1 during RRT has not been systematically described. In this study, we describe the clinical, laboratory, and echocardiographic features of a cohort of PH1 patients on RRT.

Methods: Patients with PH1 enrolled in the Rare Kidney Stone Consortium PH Registry who progressed to require RRT, had ≥2 plasma oxalate (pOx) measurements 3–36 months after start of RRT, and at least one pair of pOx measurements between 6 and 18 months apart were retrospectively analyzed. Clinical, echocardiographic, and laboratory results were obtained from the Registry.

Results: The 17 PH1 patients in our cohort had a mean total HD hours/week of 17.4 (SD 7.9; range 7.5–36) and a range of age of RRT start of 0.2–75.9 years. The average change in plasma oxalate (pOx) over time on RRT was −0.74 [−2.9, 1.4] μmol/L/month with the mean pOx never declining below 50 μmol/L. Over time on RRT, oxalosis progressively developed in multiple organ systems. Echocardiography performed on 13 subjects showed worsening of left ventricular global longitudinal strain correlated with pOx ($p < 0.05$).

Conclusions: Even when a cohort of PH1 patients were treated with intensified RRT, their predialysis pOx remained above target and they developed increasing evidence of oxalosis. Echocardiographic data suggest that cardiac dysfunction could be related to elevated pOx and may worsen over time.

Keywords: primary hyperoxaluria, oxalosis, echocardiography, dialysis, renal replacement therapy 2

INTRODUCTION

The primary hyperoxalurias are a group of genetic diseases that result in excessive hepatic oxalate production producing increased urinary oxalate excretion, which can cause severe urinary stone disease, nephrocalcinosis, and progressive chronic kidney disease (CKD). Systemic oxalosis can occur with end-stage kidney disease (ESKD) if patients are maintained on routine renal replacement therapy (RRT) long term. The 3 known genetic causes of primary hyperoxaluria (PH) are caused by mutations in *AGXT* (PH1), *GRHPR* (PH2), and *HOGA1* (PH3).

On average, PH1 manifests the most severe hyperoxaluria and the greatest risk of ESKD. In the cohort of PH1 patients enrolled in the Rare Kidney Stone Consortium (RKSC) registry, 57% progressed to ESKD by 40 years of age and 88% by age 60 (1, 2). Since the vast majority of oxalate is eliminated by the kidney, once patients progress to ESKD plasma oxalate (pOx) concentrations dramatically increase. Once pOx exceeds a critical threshold (believed to be 30–45 μmol/L) (3, 4), systemic oxalosis can occur due to deposition of calcium oxalate crystals in a variety of tissues, including the heart, bone, eyes, skin, blood vessels, endocrine, and nervous systems (2).

Little is known about the natural history of PH1 patients maintained on RRT for a prolonged period of time. Thus, in this study, we characterized the progression of clinical, laboratory, and echocardiographic features of a cohort of PH1 patients maintained on RRT to better understand the expected clinical course including changes in pOx, oxalosis findings, and echocardiogram findings over time.

MATERIALS AND METHODS

Study Population

This was a retrospective observational study. Clinical, laboratory, and echocardiographic information were abstracted from PH1 patients enrolled in the RKSC PH registry between 2003 and 2018 (5) and augmented by review of the medical records as necessary. Informed consent for registry participation was obtained from each subject after Mayo Clinic Institutional Review Board approval. All patients in the current study had confirmed mutations of the *AGXT* gene. We anticipated that pOx would increase over time on RRT as any remaining endogenous kidney function was lost and oligoanuria ensued.

Renal Replacement Therapy

A major objective of this study was to define the natural history of pOx over time on RRT. Therefore, in order for to be included in this study, PH1 patients were required to have at least 2 pOx measurements by Mayo Clinic Renal Testing Laboratory between 3 and 36 months after initiation of RRT, with at least one pair of measurements between 6 and 18 months apart (**Figure 1**). One patient was homozygous for the G170R mutation known to confer responsiveness to this pyridoxine and was receiving pyridoxine at the time of pOx measurements. The 82 PH patients seen at Mayo Clinic on RRT represent heterogenous scenarios which accounts for the decreased sample size meeting our inclusion criteria. For example, some of these patients came to Mayo for a brief period for second opinions or follow-up rather than longer-term care.

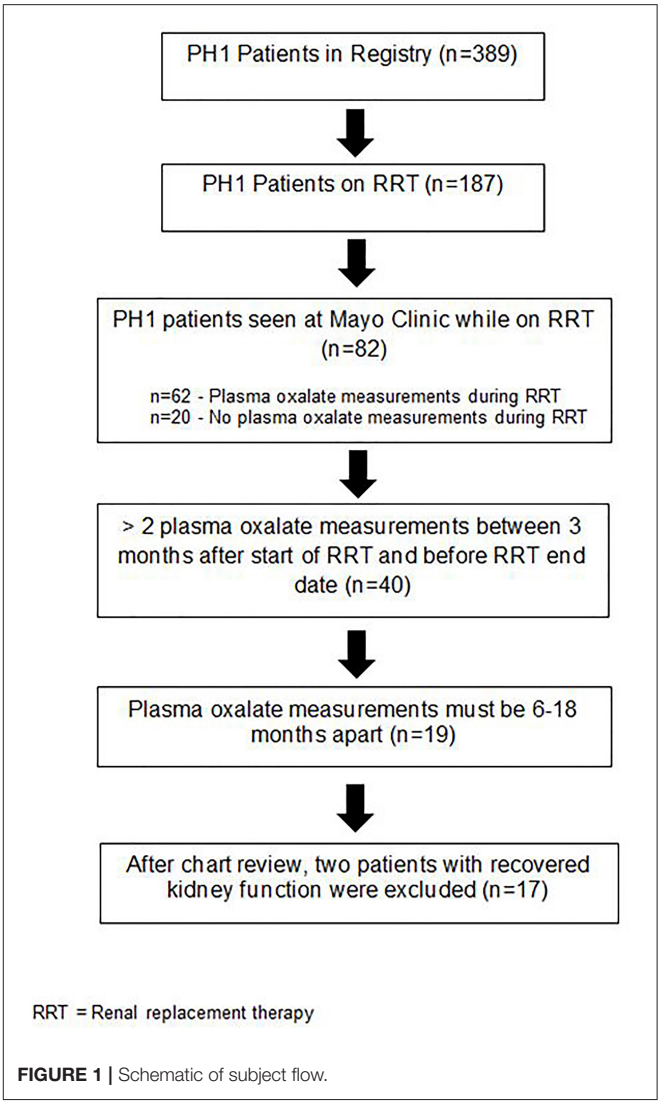

FIGURE 1 | Schematic of subject flow.

Descriptive statistics are provided as counts, mean/standard deviation (SD) and/or median/interquartile range (IQR), and range for continuous variables or counts and percentages for categorical variables. All pOx samples were obtained immediately prior to RRT sessions and measurements were made in a single reference laboratory, Mayo Clinic Renal Testing Laboratory (normal <1.6 μmol/L) (6). Plasma and urine oxalate was measured using an enzymatic oxalate oxidase method (Trinity Biotech, Wicklow, Ireland), as previously described for plasma (6) and urine (7). The test is based upon oxalate reduction by oxalate oxidase yielding hydrogen peroxide, which in the presence of peroxidase reacts with an indamine dye. This colored end point is measured using a sensitive Beckman Coulter DU800 Spectrophotometer at 590 nm.

Of note, though kidney transplant is considered a form of RRT, post-transplant patients were not included in this study.

TABLE 1 | Investigations used to evaluate for oxalate deposition in specific tissues.

Tissue	Investigation
Bone	DEXA scan, radiographs, evidence of pathologic fractures, bone, or bone marrow biopsy
Cardiac	ECG, chest radiographs, echocardiography, persistent hypotension
Musculoskeletal	Persistent musculoskeletal pain and weakness
Neurological	Exam or nerve conduction confirming neuropathy
Retina	Funduscopic examination for crystals by ophthalmologist
Skin	Livedo reticularis, subcutaneous nodules resembling oxalate deposits, non-healing ulcers

DEXA, dual energy x-ray absorptiometry; ECG, electrocardiogram.

TABLE 2 | Baseline demographic characteristics of PH1 patients at RRT start date.

	***N* = 17**
Age at PH1 diagnosis (years)	
Mean (SD)	22.4 (21.9)
Median (IQR)	18.9 (4.1, 28.9)
Range	0.3–74.0
Age at RRT start date (years)	
Mean (SD)	37.4 (24.3)
Median (IQR)	27.4 (21.2, 61.5)
Range	0.2–75.9
Gender	
Female	11 (64.7%)
Male	6 (35.3%)

"Standard" RRT regimen is considered 12 h per week, given a typical prescription of 3 weekly sessions, 4 h each, while weekly durations >12 h are considered "intensified."

Investigations for Tissue-Specific Oxalosis

Since few patients had undergone biopsies to definitively document the presence of oxalate crystals in extrarenal body tissues clinical findings associated with oxalosis were abstracted as a surrogate. **Table 1** details investigations used to evaluate for evidence of systemic oxalosis in specific tissues. Evaluation of bone density by dual energy X-ray absorptiometry (DEXA), cardiac function by electrocardiography (ECG) and echocardiography, and presence of retinal oxalate by funduscopic examination were obtained for clinical indications or as screening for systemic oxalosis. Medical records were reviewed for clinical indicators of systemic oxalate deposition including pathologic fractures, erythropoiesis-stimulating agents (ESA) refractory anemia (defined as significant and persistent anemia despite management with erythropoietin stimulating agents, requiring periodic transfusions), cardiac arrhythmias or cardiomyopathy, livedo reticularis, non-healing ulcers, subcutaneous nodules resembling oxalate deposits, peripheral neuropathy, and persistent musculoskeletal pain and weakness. Bone manifestations for this analysis were limited to pathologic fractures, radiographic evidence suggesting oxalate osteopathy, or bone biopsy showing oxalate induced changes in osteoclasts or trabecular architecture. The majority of patients had these tests performed on a repeated basis while on RRT, although they were not done on a protocolized schedule.

Echocardiography

Of the 17 subjects, 13 had at least one echocardiogram during follow-up on RRT. All echocardiograms were reviewed by a Mayo Clinic cardiologist (PP). For the purposes of demographics and analysis, a subject's first echocardiogram was designated as the echocardiogram after the start of the RRT. Descriptive statistics are provided as counts, median/IQR, and range. Data were treated as independent points for analysis. Association of echocardiographic indices with duration of RRT was examined using linear regression models.

Windows were treated as 60 day rolling periods. If multiple echocardiograms were performed within the time window, the first was included, as follow up studies were frequently abbreviated.

Indices abstracted for the echocardiogram analysis included left ventricular and right ventricular global longitudinal peak systolic strain (LV global strain, RV global strain), left ventricular ejection fraction (LVEF), left ventricular stroke volume index (LVSVI), left ventricular mass index (LVMI), left atrial volume index (LAVI), the ratio of the mitral inflow early diastolic velocity /medial mitral annulus early diastolic velocity (E/e', an indicator of left ventricular filing pressure), right ventricular systolic pressure (RVSP), and relative apical strain. Because of the young age of our 2 pediatric subjects who had echocardiograms and the age-related differences in echocardiographic measurements, this analysis was only performed on data from adult subjects. Relative apical strain was calculated as:

$$(\textit{mean of apical LV strain segments})/[(\textit{mean of six basal LV strain segments}) + (\textit{mean of six mid LV strain segments})].$$

RESULTS

Patient demographics are shown in **Table 2**. Nineteen subjects with PH1 requiring RRT initially met criteria for inclusion in the analysis, of whom two patients recovered kidney function during RRT. Since this improved kidney function likely altered oxalate dynamics and risk for systemic deposition, these subjects were excluded from the cohort.

The majority (88.2%) of the cohort was white; 58.8% were white non-Hispanic or Latino, while ethnicity was unknown or not reported in 41.2%. The median age (range) for diagnosis was 19 (0.3–74) years and start of RRT was 27 (0.2–75.9) years. Eleven of the 17 members of our cohort had a diagnosis of PH prior to initiation of RRT; 4 were first known to have PH within 3 months before or after starting RRT (including both infants who first presented in ESKD), and there were 2 in whom the PH diagnosis was made >3 months after the start of dialysis.

TABLE 3 | PH1 patients' RRT regimen, plasma oxalate concentration, and urine output.

	Baseline (*N* = 17)	1 year (*N* = 12)	2 years (*N* = 6)	3+ years (*N* = 5)
Type of RRT				
HD + PD	0 (0.0%)	2 (16.7%)	0 (0.0%)	0 (0.0%)
HD only	16 (94.1%)	10 (83.3%)	6 (100.0%)	5 (100.0%)
PD only	1 (5.9%)	0 (0.0%)	0 (0.0%)	0 (0.0%)
RRT treatments/week				
N	15	11	6	5
Median (IQR)	4.0 (3.0, 5.5)	6.0 (4.0, 6.0)	5.0 (3.5, 5.8)	5.0 (3.0, 5.0)
Range	3.0–6.0	3.0–6.0	2.0–6.0	2.0–6.0
Hours/RRT session				
N	13	11	6	5
Median (IQR)	4.0 (3.5, 4.0)	3.5 (3.0, 4.0)	3.0 (3.0. 3.4)	3.0 (3.0, 3.5)
Range	2.5–6.0	2.5–4.0	3.0–4.0	3.0–4.0
Hours RRT/week				
N	13	11	6	5
Median (IQR)	18.0 (11.2, 20.0)	18.0 (13.5, 24.0)	15.0 (11.6, 17.2)	15.0 (10.5, 15.0)
Range	7.5–36.0	7.5–24.0	6.0–24.0	6.0–24.0
First pOx measured after starting RRT (μmol/L)*				
N	17	12	6	5
Median (IQR)	75.0 (40.3, 150.7)	76.0 (37.0, 145.7)	80.1 (44.9, 133.8)	77.0 (34.2, 83.2)
Range	16.1–187.5	16.1–159.8	16.1–159.8	16.1–150.7
Urine (mL/24 h)**				
N	6	7	3	1
Median (IQR)	3,582 (2,380, 4,243)	1,300 (798, 1,848)	2,250 (1,204, 2,409)	1,658 (1,658, 1,658)
Range	28.0–4,637	384–2,392	157–2,568	1,658–1,658

**pOx reference range <1.6 μmol/L.*
***A single data point in this set is from a pediatric patient and this volume was not corrected for BSA.*

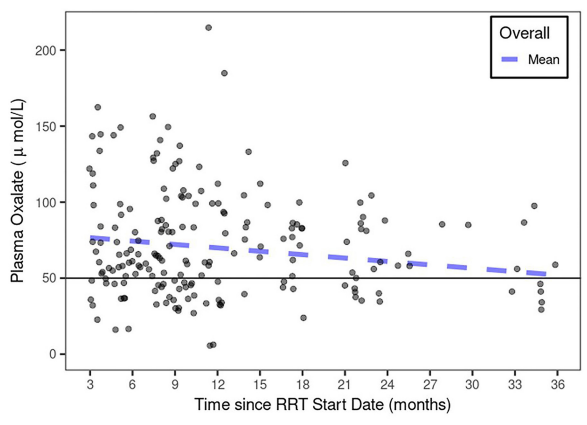

FIGURE 2 | pOx over the course of RRT in PH1. The mean pOx declined slightly over time (though not statistically significant) with RRT, but remained above 50 μmol/L using a linear mixed-effects model with subject-specific intercept and slopes.

Baseline characteristics, RRT regimen, and clinical parameters over time on RRT are shown in **Table 3**. At baseline, 16 subjects received HD only and one subject received PD only. The mean (SD) days of treatment per week was 4.3 (1.3) (range 3–6 days) and session lengths averaged 3.8 (0.8) h (range 2.5–6.0). Total HD was 17.4 (7.9) h/week (range 7.5–36). Over the course of dialysis, three patients received PD either alone or in conjunction with HD; the remainder received HD only. The decline in sample size each year represents patients discontinuing RRT due to transplant. By 2 years after initiation of dialysis, 11 subjects had been transplanted. A single subject was transplanted between 2 and 3 years and 5 subjects continued on RRT beyond 3 years.

The average change in pOx over the course of RRT was −0.74 [−2.9, 1.4] μmol/L/month with the mean pOx never decreasing below 50 μmol/L despite RRT regimens with greater weekly duration than are standard (**Figure 2**). Median pOx was slightly lower immediately after initiation of RRT compared to the first

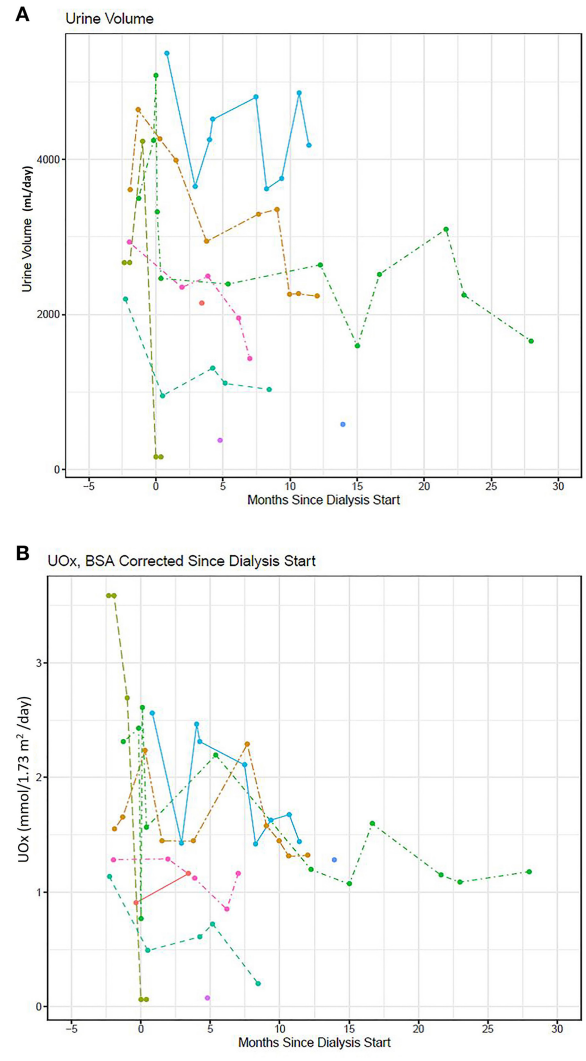

FIGURE 3 | (A) Urine output (mL/day) and **(B)** urine oxalate excretion/BSA (mmol/1.73m^2/day) over time since initiating RRT (n = 9).

measurement included in the analysis (i.e., >90 days after start of RRT) (75.0–80.3 μmol/L). Urine output was maintained in 6/17 subjects, 3 of whom still had >2000 ml/day after 1 year on dialysis (**Figure 3A**). Oxalate excretion ranged from 0.85 to 2.3 mmol/1.73 m^2/day measured in 5 subjects 6 months after the start of dialysis and 1.2–1.4 mmol/1.73m^2/day at 1 year ($n = 3$) (**Figure 3B**).

As a group, PH1 patients had increasing symptoms or clinical testing evidence of progressive systemic oxalate deposition over time on RRT in all body systems including bone, cardiovascular, musculoskeletal, neurological, retina, and skin (**Figure 4**).

Among the 17 patients studied, 9 had no oxalosis-related symptoms. Three of these 9 also had no objective findings suggestive of systemic oxalosis on clinical, laboratory, nor imaging studies. An additional 5 had findings that were thought related to ESKD or other causes rather than to oxalate deposition (osteopenia alone, grade 1–2 diastolic dysfunction on echocardiography, advanced degenerative joint disease, mild sensory neuropathy). The remaining asymptomatic patient had retinal oxalate deposits without change in vision.

Among 7 patients who had symptoms and findings consistent with systemic oxalosis, severe hypotension complicating dialysis was observed in 3, overt cardiomyopathy or complete heart block in 4, marked musculoskeletal pain and weakness with or without neuropathy in 4, compromise of vision related to retinal oxalate deposits in 1, and complex metabolic bone disease with fractures in 2.

One remaining patient, an infant, had complex metabolic bone disease, growth, and developmental delay that were consistent with ESKD in this age group, though could have been complicated by systemic oxalate deposition.

Five of the patients underwent biopsies during the course of RRT, among whom 3 had calcium oxalate crystals confirmed by bone marrow biopsy. One of the 3 also had documented calcium oxalate crystals in a myocardial biopsy. The remaining biopsies of bone and a thyroid mass were negative for calcium oxalate crystals.

Of the 17 subjects in this cohort, 13 had echocardiograms during the RRT period (**Table 4**). Reference ranges for echocardiographic indices are found in **Table 5** and descriptive statistics for the cohort are displayed in **Table 6**. There were

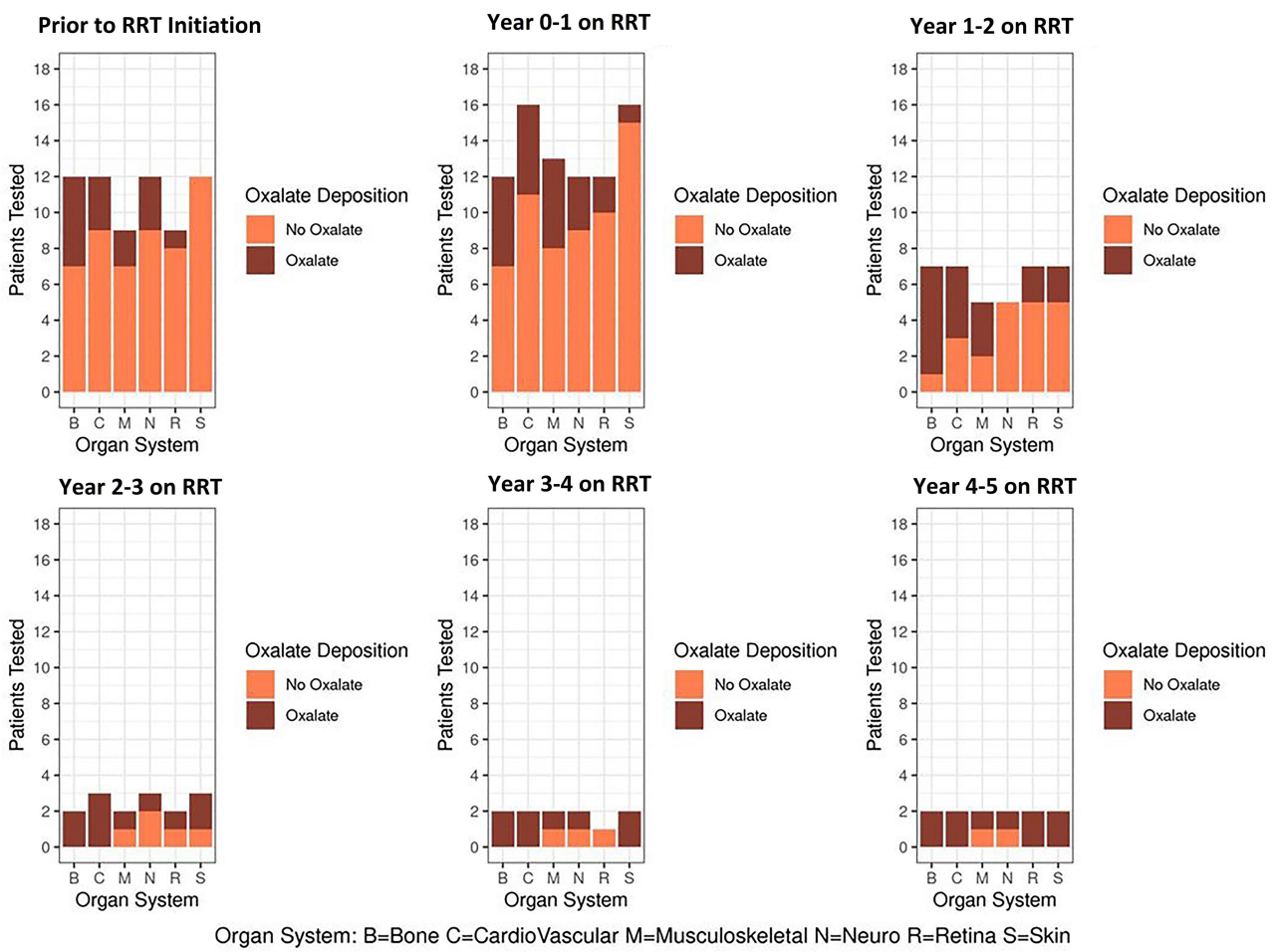

FIGURE 4 | Clinical evidence of oxalosis over time on RRT.

TABLE 4 | Demographic data for PH1 patients on RRT who underwent echocardiography.

	Overall (*N* = 13)
Age at RRT Start Date	
Median (IQR)	30.7 (22.5, 66.0)
Range	18.5–75.9
Age at Diagnosis	
Median (IQR)	18.9 (5.0, 28.1)
Range	3.3–74.0
Gender	
Female	7 (53.8%)
Male	6 (46.2%)
Race	
White	12 (92.3%)
Unknown	1 (7.7%)
Ethnicity	
Non-Hispanic or Latino	7 (53.8%)
Unknown or not reported	6 (46.2%)
Echocardiograms/subject	
Median (IQR)	1.0 (1.0, 3.0)
Range	1.0–7.0
Months to first echocardiogram	
Median (IQR)	3.4 (2.8, 4.8)
Range	0.6–12.5
Months to last echocardiogram	
Median (IQR)	9.9 (2.9, 19.7)
Range	1.2–33.6

TABLE 5 | Reference ranges for echocardiography measures.

Echocardiogram parameter	Reference range
Left ventricular ejection fraction	>50%
Left ventricular stroke volume	N/A – reference LVSVI
Left ventricular stroke volume index	>35 mL/m2
Left atrial volume index	<=34 mL/m2
Left ventricular mass index	Women 43–95 g/m2, men 49–115 g/m2
E/e'	Normal <10, 10–14 indeterminate, >14 abnormal
RV global strain	No lower limit to <-20
LV global strain	No lower limit to <-18
Right ventricular systolic pressure	>35 mmHg

RV, Right Ventricular; LV, Left Ventricular; LVSVI, Left Ventricular Stroke Volume Index.

a total of 30 echocardiography periods with at least partial data. The timing of the echocardiograms ranged from 0.6 to 33.6 months after the start of RRT [mean(SD) 11(8.6)], with time of first echocardiogram observation ranging from 0.6 to 12.5 months after RRT start and time to last echocardiogram observation 1.2–33.6 months after start of the RRT interval.

TABLE 6 | Descriptive echocardiographic data for PH1 patients on RRT.

	Overall (*N* = 30)
Left ventricular ejection fraction	
N	30
Median (IQR)	60.5 (56.0, 65.0)
Range	32.0–69.0
LVEF in ref range	
N	30
No	3 (10.0%)
Yes	27 (90.0%)
Left ventricular stroke volume	
N	28
Median (IQR)	87.0 (72.0, 99.5)
Range	63.0–152.0
Left ventricular stroke volume index	
N	28
Median (IQR)	43.0 (38.0, 51.5)
Range	33.0–72.0
LVSVI in ref. range	
N	28
No	2 (7.1%)
Yes	26 (92.9%)
Left atrial volume index	
N	26
Median (IQR)	33.5 (27.0, 43.2)
Range	16.0–64.0
LAVI in ref. range	
N	26
No	14 (53.8%)
Yes	12 (46.2%)
Left ventricular mass index	
N	29
Median (IQR)	94.5 (74.5, 112.0)
Range	55.0–169.0
LVMI in ref. range	
N	29
No	10 (34.5%)
Yes	19 (65.5%)
E/e'	
N	28
Median (IQR)	11.3 (8.0, 13.7)
Range	5.4–27.5
E/e' interpretation	
N	28
Normal	11 (39.3%)
Indeterminate	11 (39.3%)
Abnormal	6 (21.4%)
RV global longitudinal strain	
N	20
Median (IQR)	−24.5 (−28.0, −22.8)
Range	−32.0–−18.0
RVGS in ref. range	
N	20

(Continued)

TABLE 6 | Continued

	Overall (*N* = 30)
4 (20.0%)	
Yes	16 (80.0%)
LV global longitudinal strain	
N	21
Median (IQR)	−19.0 (-20.0, −15.5)
Range	−22.0–−10.0
LVGS in ref. range	
N	21
No	9 (42.9%)
Yes	12 (57.1%)
Right ventricular systolic pressure	
N	28
Median (IQR)	34.0 (30.0, 39.0)
Range	18.0–73.0
RVSP in ref. range	
N	28
No	11 (39.3%)
Yes	17 (60.7%)
Basal Mean	
N	21
Median (IQR)	−16.3 (−19.5, −14.2)
Range	−22.8–−7.2
BMS in ref. range	
N	21
No	14 (66.7%)
Yes	7 (33.3%)
Relative apical strain	
N	21
Median (IQR)	0.6 (0.5, 0.7)
Range	0.3–0.9
AS ratio <1	
N	21
Yes	21 (100.0%)
SBP	
N	30
Median (IQR)	126.0 (110.0, 137.5)
Range	88.0–170.0
DBP	
N	30
Median (IQR)	71.0 (60.0, 78.0)
Range	52.0–92.0

(N reflects echocardiography readings; some individual patients had multiple readings).

Regression model analysis results related to time on RRT and pOx are shown in **Table 7**. Only DBP showed a statistically significant change, with decline over time on RRT (estimate [95%CI] −0.54 [−0.97, −0.11], $p < 0.05$). Sensitivity analyses of subject-specific influence on model estimates indicated one subject contributed significant decreases in model estimates for E/e', LAVI, LVMI, and nearly significant for RVSP, and another subject contributed significant positive increases for LVEF, as well as large positive increases for LVMI and LVSVI. By contrast,

TABLE 7 | Association of changes in echocardiography measures related to time and pOx on RRT in PH patients in linear regression models (up to 30 time points in 13 patients).

CV parameter	Est(months on RRT)	CI	p-value
RV global longitudinal strain	0.014	−0.192, 0.219	0.89
LV global longitudinal strain	−0.041	−0.187, 0.105	0.57
E/e'	0.118	−0.114, 0.35	0.31
LVEF	−0.252	−0.596, 0.092	0.14
LVMI	0.445	−0.842, 1.732	0.49
LVSVI	0.119	−0.423, 0.661	0.66
LAVI	0.303	−0.255, 0.861	0.27
RVSP	0.1	−0.379, 0.579	0.67
basal mean	−0.09	−0.291, 0.112	0.36
Apical mean	0.037	−0.125, 0.199	0.64
Relative apical strain	−0.002	−0.009, 0.004	0.44
SBP	−0.619	−1.551, 0.313	0.18
DBP	−0.539	−0.987, −0.092	0.020
CV parameter	**Est(pOx)**	**CI**	**p-value**
RV global longitudinal strain	0.061	0.012, 0.109	0.018
LV global longitudinal strain	0.046	0.006, 0.086	0.025
E/e'	−0.027	−0.089, 0.036	0.39
LVEF	−0.065	−0.155, 0.025	0.15
LVMI	−0.002	−0.337, 0.334	0.99
LVSVI	−0.184	−0.306, −0.061	0.005
LAVI	0.126	−0.033, 0.286	0.12
RVSP	−0.04	−0.172, 0.093	0.55
Basal mean	0.072	0.021, 0.124	0.008
Apical mean	0.029	−0.018, 0.076	0.21
Relative apical strain	0.002	0, 0.003	0.070
SBP	−0.283	−0.509, −0.056	0.016
DBP	−0.11	−0.232, 0.012	0.075

RV, Right ventricular; LV, left ventricular; LVEF, left ventricular ejection fraction; LVMI, left ventricular mass index; LVSV, left ventricular stroke volume; LVSVI, left ventricular stroke volume index; LAVI, left atrial volume index; RVSP, right ventricular systolic pressure; SBP, Systolic Blood Pressure; DBP, Diastolic Blood Pressure.

regression models using pOx demonstrated decreasing systolic blood pressure as pOx increased ($p < 0.05$) (**Figure 5A**), lower LVSVI ($p < 0.05$), worsening of LV ($p < 0.05$), and RV global longitudinal strain ($p < 0.05$), as well as a trend toward lower DBP ($p = 0.075$). The mean longitudinal strain of the basal segments of the LV and RV worsened ($p < 0.05$) (**Figure 5B**) with a trend toward apical sparing ($p = 0.07$) (**Figure 5C**).

Echocardiography was performed in two additional pediatric patients according to a pediatric echocardiography protocol. Values were not included in the averages because of the young ages of these patients and age-related differences in echocardiographic measurements. One patient, age 11 months, had left ventricular ejection fraction of 65% and mild-moderate concentric left ventricular hypertrophy. There was no evidence of coarctation of the aorta. Medial e' was low at 0.05 m/s and E/e' was indeterminate at 12. Strain was not measured. The other patient, age 2 years, had left ventricular ejection fraction ranging between 64 and 69% on two serial echocardiograms. Medial e'

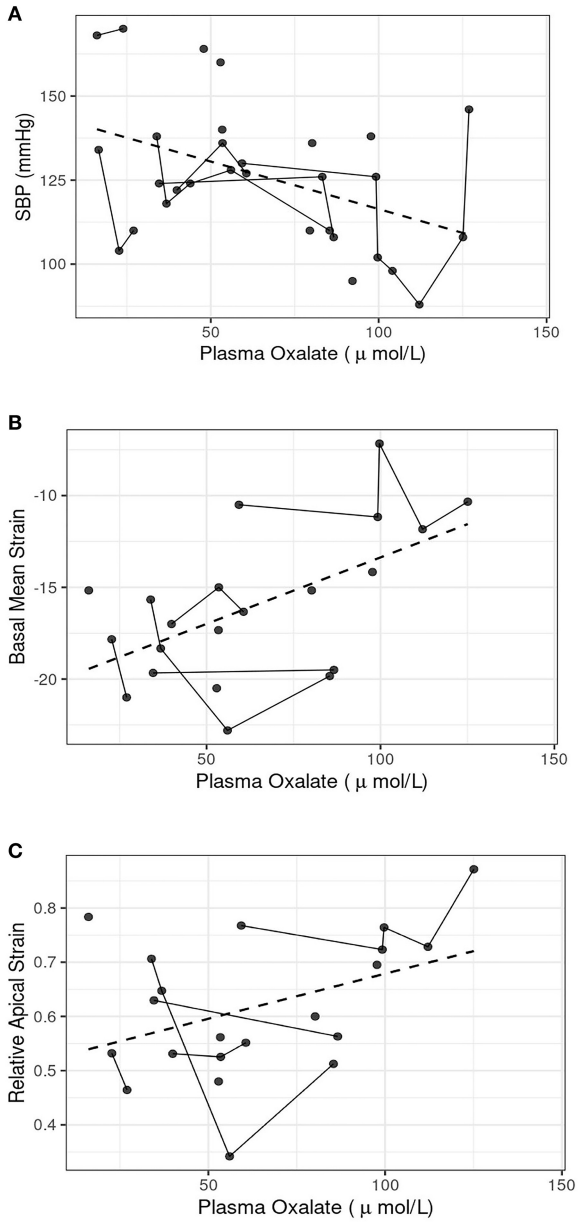

FIGURE 5 | Regression models of selected markers of cardiac function as a function of pOx. Dashed line represents a simple linear regression fit. **(A)** Systolic blood pressure: Systolic blood pressure decreased at higher pOx, $p < 0.05$, $n = 30$ readings in 13 subjects. **(B)** Basal mean strain: Mean longitudinal strain of the basal segments of the LV plus RV worsened at higher pOx, $p < 0.05$, $n = 21$ readings in 10 subjects. **(C)** Relative apical strain: Trend toward apical sparing, $p = 0.070$, $n = 21$ readings in 10 subjects.

was normal at 0.10 and E/e' was normal at 6. Left ventricular GLS was attempted on the second echocardiogram and an average value of the 12 visualized segments was normal at −22.

DISCUSSION

Supersaturation of calcium oxalate in blood leading to systemic oxalosis is thought to occur when pOx increases to >30–45 μmol/L (3, 4). Our data show that most patients with PH1 maintain pOx concentrations above this limit of supersaturation with no clinically significant decline over time despite intensified RRT. Standard hemodialysis prescriptions likely lead to unacceptably high pOx and high risk for worsening systemic oxalosis. This observation alone highlights the challenge for both clinicians and patients in managing PH1, the need for thoughtful, individualized management including regular pOx measurement to determine the efficacy of the dialysis prescription, and the urgent need for more efficacious therapy. Our data also show that PH1 patients are at risk for developing cardiac dysfunction while on RRT, illustrating one potential consequence from systemic oxalosis.

Previous work from the Rare Kidney Stone Consortium and other investigators has shown that, even though HD effectively clears oxalate from plasma during a given treatment, pre-dialysis pOx concentrations are variable and often remain quite elevated due to oxalate re-entering circulation from other compartments (3, 8, 9). Our study expands upon these observations by providing an analysis of serial pOx values obtained from a relatively large cohort of PH1 patients maintained on RRT for 1–5 years. Our previous work illustrated the importance of maintenance of residual urine output given the decline in oxalate excretion as urine output diminishes, and data from this study are consistent with this, though our sample size is too small to generate statistical significance (8).

When treating patients with PH1 and ESKD, the clinician is challenged with balancing the risks of systemic oxalosis with the burden more frequent and longer dialysis sessions impose on a patient. While nocturnal home HD might be another option to manage ESKD (10), it has not been rigorously studied and the efficacy might depend largely upon the dialysis system available for use since volume flows of dialysate vary in home systems (11). The risks of elevated pOx and prolonged time to transplant from starts of RRT are associated with an increased risk of post-transplant complications in PH, particularly in regards to rapid recurrence of oxalosis in the transplanted kidney (12).

The current study demonstrates that clinically evident manifestations of oxalate on bone, skin, nervous system, and eyes vary from patient to patient over time on dialysis (13–18). Due to our small sample size and retrospective review of clinically-indicated testing for oxalosis, we cannot draw statistically significant conclusions regarding prevalence. However, our data suggest that this patient population is susceptible to multi-tissue involvement from oxalate deposition and that the number of organ systems per subject increases over time on dialysis. The dynamic equilibrium between oxalate in plasma and deposits of oxalate in tissue is not well-understood; it is possible that accumulating oxalate tissue deposits attenuate the amount of oxalate circulating in plasma.

Most symptoms as well as laboratory and imaging findings of systemic oxalosis can mimic those of ESKD. For example, complex metabolic bone disease and cardiac dysfunction are characteristic of all patients maintained on chronic RRT. Tissue biopsies are not often performed, thus indirect methods that lack specificity are usually relied upon for oxalosis detection. Thus, our retrospective study may overestimate the frequency of certain aspects of oxalosis.

Cardiac manifestations in PH1 patients are described in the literature, though most are anecdotal observations. Mookadam et al. found that 82% of PH patients had cardiac abnormalities by either echocardiography or electrocardiography, with increased LVMI and left atrial enlargement being most common (19). Conduction disturbances including bundle branch block and atrioventricular block were also observed in that study. Quan and Biblo described a PH patient with ventricular tachycardia and valvular dysfunction (20). In 2013, Lagies et al. described a PH1 patient with apical sparing of longitudinal strains, left ventricular rotational abnormalities, and short-axis dysfunction along with characteristics of infiltrative cardiomyopathy with restrictive physiology (21). A more recent publication from the same group reports impaired global longitudinal strain despite preserved left ventricular ejection fraction in 15 PH patients (13 PH1, 1 PH2, and 1 PH3) not on RRT, demonstrating subclinical myocardial disease and supporting early monitoring of cardiac function in PH patients (22).

Intracardiac deposition of calcium oxalate crystals would be expected to result in progressive worsening of cardiac function. Mode sensitive markers of ventricular function, namely left ventricular and right ventricular global longitudinal strain did not worsen over the course of RRT in the group as a whole. However, worse global longitudinal strain was associated with higher plasma oxalate. This is of particular concern given that abnormal global longitudinal strain leads to increased risk for cardiovascular morbidity and mortality (23, 24). Basal strain showed particular worsening, with a trend toward apical sparing as pOx increased in our patients. Thus, the functional consequences of calcium oxalate deposition in cardiac tissue appear similar to that of infiltration with amyloid proteins. In cardiac amyloidosis, longitudinal strain in the basal ventricular segments typically deteriorates first; apical segments may be spared despite the systemic nature of the disease (25, 26). We also observed a decline in blood pressure over the course of RRT overall, with 3 patients developing severe hypotension that complicated dialysis. Systolic blood pressure correlated inversely with pOx with a similar trend for diastolic pressure.

Published reports of echocardiography in non-PH patients maintained on HD describe some degree of myocardial impairment despite preserved ejection fraction (27–29). Lagies et al. also reported abnormal longitudinal cardiac rotation and left ventricular longitudinal strain in a significant proportion of a cohort of HD patients (30). It is possible that oxalosis may impact myocardial function differently from general ESKD and RRT. Further investigation regarding impaired myocardial function in PH patients on HD compared to non-PH patients on HD is warranted to further delineate the impact of PH on cardiac function compared to HD alone. Our findings showing worsening diastolic function and worsening of left ventricular global longitudinal strain correlating with pOx suggest the importance of serial echography for this patient population.

Our data demonstrating a sustained elevation in pOx and progressive systemic oxalate deposition over the duration of intensive RRT highlight the urgency for new innovative therapies for PH. Standard RRT alone is not effective for many PH patients to achieve an acceptable pOx; thus, treatment options that reduce oxalate production or enhance removal would greatly benefit this patient population. Moreover, data show that after PH1 patients maintained on HD receive a liver and kidney transplant, urinary oxalate excretion remains quite high for a long period of time (31), posing potential risk to the transplanted allograft, providing further evidence that strategies to more effectively lower pOx while maintained on HD are needed.

Urine volume and oxalate excretion were maintained in a subset of our PH1 patients despite markedly reduced GFR. Thus, renal excretion provides another critical opportunity for additional elimination of oxalate. Strategies to maintain urine volume, including avoidance of aggressive fluid removal during dialysis sessions and generous oral intake between dialysis sessions should be considered where appropriate.

Our study has some limitations. Most importantly, the retrospective nature limited the number and timing of clinical variables and tests that were available for analysis. These patients also were seen at a single tertiary medical center though ongoing care was provided by local dialysis centers, so the results and frequency of outcomes might not transfer to all settings. In addition, there may have been selection bias regarding who received which tests over time based upon the clinical situation. Our data set lacks objective measures of dialysis delivery like Kt/V, so we relied on hours of dialysis, acknowledging that it would have been more meaningful to show suboptimal pOx in the context of proven adequate Kt/V. Also, our echocardiography cohort had a wide range of ages, so we cannot exclude that some of our findings may be related to age differences. Nevertheless, this is one of the largest PH1 cohorts reported to date maintained on HD for a prolonged period of time.

CONCLUSIONS

Patients with PH1 are exposed to persistently high pOx concentrations even when they receive an intensified dialysis regimen. Thus, they are increasingly at risk for systemic oxalosis in multiple organ systems over time on RRT. Failure to recognize the risks of insufficient dialysis in PH1 patients may have significant consequences. Echocardiographic data suggests worsening of diastolic dysfunction over time. Decline in blood pressure and worsening of basal ventricular strain consistent with an ongoing infiltrative process correlated with higher pOx. These observations support an urgent need for improved management strategies for PH1 patients who develop ESKD.

DATA AVAILABILITY STATEMENT

The raw data supporting the conclusions of this article will be made available by the authors, without undue reservation.

ETHICS STATEMENT

The studies involving human participants were reviewed and approved by Mayo Clinic Institutional Review Board. Written informed consent to participate in this study was provided by the participants' legal guardian/next of kin.

AUTHOR CONTRIBUTIONS

DS, JL, DM, and FE: contributed to the research idea, study design, data analysis, interpretation, and manuscript preparation. FE, TG, and RM contributed to data analysis, interpretation, and performed statistical analysis. JO, BS, and CB contributed data acquisition and subject recruitment. BD provided research idea, data analysis, interpretation, and content feedback. PP contributed expertise in cardiology content and data analysis, interpretation. Each author contributed important intellectual content during manuscript drafting or revision and accepts accountability for the overall work by ensuring that questions pertaining to the accuracy or integrity of any portion of the work are appropriately investigated and resolved.

FUNDING

This work was funded by the Rare Kidney Stone Consortium (U54DK83908), which is part of Rare Diseases Clinical Research Network (RDCRN), an initiative of the Office of Rare Diseases Research (ORDR), National Center for Advancing Translational Sciences (NCATS). This consortium was funded through collaboration between NCATS, and the National Institute of Diabetes and Digestive and Kidney Diseases. This work was also supported by an industry grant from OxThera.

REFERENCES

1. Hopp K, Cogal AG, Bergstralh EJ, Seide BM, Olson JB, Meek AM, et al. Phenotype-genotype correlations and estimated carrier frequencies of primary hyperoxaluria. *J Am Soc Nephrol.* (2015) 26:2559–70. doi: 10.1681/ASN.2014070698
2. Sas DJ, Harris PC, Milliner DS. Recent advances in the identification and management of inherited hyperoxalurias. *Urolithiasis.* (2019) 47:79–89. doi: 10.1007/s00240-018-1093-3
3. Hoppe B, Kemper MJ, Bokenkamp A, Portale AA, Cohn RA, Langman CB. Plasma calcium oxalate supersaturation in children with primary hyperoxaluria and end-stage renal failure. *Kidney Int.* (1999) 56:268–74. doi: 10.1046/j.1523-1755.1999.00546.x
4. Marangella M, Cosseddu D, Petrarulo M, Vitale C, Linari F. Thresholds of serum calcium oxalate supersaturation in relation to renal function in patients with or without primary hyperoxaluria. *Nephrol Dial Transplant.* (1993) 8:1333–7.
5. Lieske JC, Monico CG, Holmes WS, Bergstralh EJ, Slezak JM, Rohlinger AL, et al. International registry for primary hyperoxaluria. *Am J Nephrol.* (2005) 25:290–6. doi: 10.1159/000086360
6. Ladwig PM, Liedtke RR, Larson TS, Lieske JC. Sensitive spectrophotometric assay for plasma oxalate. *Clin Chem.* (2005) 51:2377–80. doi: 10.1373/clinchem.2005.054353
7. Koch GH, Strong FM. Determination of oxalate in urine. *Anal Biochem.* (1969) 27:162–71. doi: 10.1016/0003-2697(69)90227-9
8. Illies F, Bonzel KE, Wingen AM, Latta K, Hoyer PF. Clearance and removal of oxalate in children on intensified dialysis for primary hyperoxaluria type 1. *Kidney Int.* (2006) 70:1642–48. doi: 10.1038/sj.ki.5001806
9. Tang X, Voskoboev NV, Wannarka SL, Olson JB, Milliner DS, Lieske JC. Oxalate quantification in hemodialysate to assess dialysis adequacy for primary hyperoxaluria. *Am J Nephrol.* (2014) 39:376–82. doi: 10.1159/000360624
10. Plumb TJ, Swee ML, Fillaus JA. Nocturnal home hemodialysis for a patient with type 1 hyperoxaluria. *Am J Kidney Dis.* (2013) 62:1155–9. doi: 10.1053/j.ajkd.2013.05.013
11. Haroon S, Davenport A. Haemodialysis at home: review of current dialysis machines. *Expert Rev Med Devices.* (2018) 15:337–47. doi: 10.1080/17434440.2018.1465817
12. Jamieson NV, European PHITSG. A 20-year experience of combined liver/kidney transplantation for primary hyperoxaluria (PH1): the European PH1 transplant registry experience 1984-2004. *Am J Nephrol.* (2005) 25:282–9. doi: 10.1159/000086359
13. Ardemani G, Govaert P, Oussoren E, Dorresteijn E, Wildschut E, Lequin M, et al. Crystal clear cerebral ultrasound images mimicking acute asphyxia in an infant with primary hyperoxaluria. *Eur J Paediatr Neurol.* (2017) 21:792–4. doi: 10.1016/j.ejpn.2017.06.003
14. Bacchetta J, Boivin G, Cochat P. Bone impairment in primary hyperoxaluria: a review. *Pediatr Nephrol.* (2016) 31:1–6. doi: 10.1007/s00467-015-3048-z
15. Berini SE, Tracy JA, Engelstad JK, Lorenz EC, Milliner DS, Dyck PJ. Progressive polyradiculoneuropathy due to intraneural oxalate deposition in type 1 primary hyperoxaluria. *Muscle Nerve.* (2015) 51:449–54. doi: 10.1002/mus.24495
16. Derveaux T, Delbeke P, Walraedt S, Raes A, Van Laecke S, Leroy BP, et al. Detailed clinical phenotyping of oxalate maculopathy in primary hyperoxaluria type 1 and review of the literature. *Retina.* (2016) 36:2227–35. doi: 10.1097/IAE.0000000000001058
17. Moorhead PJ, Cooper DJ, Timperley WR. Progressive peripheral neuropathy in patient with primary hyperoxaluria. *Br Med J.* (1975) 2:312–3. doi: 10.1136/bmj.2.5966.312
18. Shreberk-Hassidim R, Zaguri R, Maly A, Zlotogorski A, Ramot Y. Skin manifestations of primary hyperoxaluria: a case report. *Int J Dermatol.* (2015) 54:e478–9. doi: 10.1111/ijd.13036
19. Mookadam F, Smith T, Jiamsripong P, Moustafa SE, Monico CG, Lieske JC, et al. Cardiac abnormalities in primary hyperoxaluria. *Circ J.* (2010) 74:2403–9. doi: 10.1253/circj.CJ-10-0107
20. Quan KJ, Biblo LA. Type I primary hyperoxaluria: an unusual presentation of ventricular tachycardia. *Cardiol Rev.* (2003) 11:318–9. doi: 10.1097/01.crd.0000065421.50549.21
21. Lagies R, Beck BB, Hoppe B, Sreeram N, Udink Ten Cate FE. Apical sparing of longitudinal strain, left ventricular rotational abnormalities, and short-axis dysfunction in primary hyperoxaluria type 1. *Circ Heart Fail.* (2013) 6:e45–7. doi: 10.1161/CIRCHEARTFAILURE.113.000432
22. Lagies R, Udink Ten Cate FEA, Feldkotter M, Beck BB, Sreeram N, Hoppe B, et al. Subclinical myocardial disease in patients with primary hyperoxaluria and preserved left ventricular ejection fraction: a two-dimensional speckle-tracking imaging study. *Pediatr Nephrol.* (2019) 34:2591–600. doi: 10.1007/s00467-019-04330-7
23. Fujikura K, Peltzer B, Tiwari N, Shim HG, Dinhofer AB, Shitole SG, et al. Reduced global longitudinal strain is associated with increased risk of cardiovascular events or death after kidney transplant. *Int J Cardiol.* (2018) 272:323–8. doi: 10.1016/j.ijcard.2018.07.088
24. Ravera M, Rosa GM, Fontanive P, Bussalino E, Dorighi U, Picciotto D, et al. Impaired left ventricular global longitudinal strain among patients with chronic kidney disease and end-stage renal disease and renal transplant recipients. *Cardiorenal Med.* (2019) 9:61–8. doi: 10.1159/000494065
25. Bellavia D, Pellikka PA, Abraham TP, Al-Zahrani GB, Dispenzieri A, Oh JK, et al. Evidence of impaired left ventricular systolic function by Doppler myocardial imaging in patients with systemic amyloidosis and no evidence of cardiac involvement by standard two-dimensional and Doppler echocardiography. *Am J Cardiol.* (2008) 101:1039–45. doi: 10.1016/j.amjcard.2007.11.047
26. Phelan D, Collier P, Thavendiranathan P, Popović ZB, Hanna M, Plana JC, et al. Relative apical sparing of longitudinal strain using two-dimensional speckle-tracking echocardiography is both sensitive and specific for the diagnosis of cardiac amyloidosis. *Heart.* (2012) 98:1442–48. doi: 10.1136/heartjnl-2012-302353

27. Green D, Kalra PR, Kalra PA. Echocardiographic abnormalities in dialysis patients with normal ejection fraction. *Nephrol Dial Transplant*. (2012) 27:4256–9. doi: 10.1093/ndt/gfs357
28. Rakha S, Hafez M, Bakr A, Hamdy N. Changes of cardiac functions after hemodialysis session in pediatric patients with end-stage renal disease: conventional echocardiography and two-dimensional speckle tracking study. *Pediatr Nephrol*. (2020) 35:861–70. doi: 10.1007/s00467-019-04460-y
29. Wang H, Liu J, Yao XD, Li J, Yang Y, Cao T, et al. Multidirectional myocardial systolic function in hemodialysis patients with preserved left ventricular ejection fraction and different left ventricular geometry. *Nephrol Dial Transplant*. (2012) 27:4422–9. doi: 10.1093/ndt/gfs090
30. Lagies R, Beck BB, Hoppe B, Sheta SS, Verena Weiß ARDCS, Sreeram N, et al. Inhomogeneous longitudinal cardiac rotation and impaired left ventricular longitudinal strain in children and young adults with end-stage renal failure undergoing hemodialysis. *Echocardiography*. (2015) 32:1250–60. doi: 10.1111/echo.12842
31. Bergstralh EJ, Monico CG, Lieske JC, Herges RM, Langman CB, Hoppe B, et al. Transplantation outcomes in primary hyperoxaluria. *Am J Transplant*. (2010) 10:2493–501. doi: 10.1111/j.1600-6143.2010.03271.x

Conflict of Interest: BD is an employee of OxThera.

The remaining authors declare that the research was conducted in the absence of any commercial or financial relationships that could be construed as a potential conflict of interest.

frontiers in Medicine

ORIGINAL RESEARCH
published: 12 May 2021
doi: 10.3389/fmed.2021.657073

Serum-Urine Matched Metabolomics for Predicting Progression of Henoch-Schonlein Purpura Nephritis

Qian Zhang[1†], *Ling-Yun Lai*[2†], *Yuan-Yuan Cai*[1†], *Ma-Jie Wang*[1], *Gaoxiang Ma*[1], *Lian-Wen Qi*[1*], *Jun Xue*[2*] *and Feng-Qing Huang*[1*]

[1] *The Clinical Metabolomics Center, China Pharmaceutical University, Nanjing, China,* [2] *Division of Nephrology, Huashan Hospital, Fudan University, Shanghai, China*

Henoch-Schonlein purpura nephritis (HSPN) is a common glomerulonephritis secondary to Henoch-Schonlein purpura (HSP) that affects systemic metabolism. Currently, there is a rarity of biomarkers to predict the progression of HSPN. This work sought to screen metabolic markers to predict the progression of HSPN via serum-urine matched metabolomics. A total of 90 HSPN patients were enrolled, including 46 HSPN (+) patients with severe kidney damage (persistent proteinuria >0.3 g/day) and 44 HSPN (–) patients without obvious symptoms (proteinuria < 0.3 g/day). Untargeted metabolomics was determined by liquid chromatography-quadrupole time-of-flight mass spectrometry (LC-Q/TOF-MS). A total of 38 and 50 differential metabolites were, respectively, identified in serum and urine from the comparison between HSPN (+) and HSPN (–) patients. Altered metabolic pathways in HSPN (+) mainly included glycerophospholipid metabolism, pyruvate metabolism, and citrate cycle. A panel of choline and *cis*-vaccenic acid gave areas under the curve of 92.69% in serum and 72.43% in urine for differential diagnosis between HSPN (+) and HSPN (–). In addition, the two metabolites showed a significant association with clinical indices of HSPN. These results suggest that serum-urine matched metabolomics comprehensively characterized the metabolic differences between HSPN (+) and HSPN (–), and choline and *cis*-vaccenic acid could serve as biomarkers to predict HSPN progression.

Keywords: choline and *cis*-vaccenic acid, differential diagnosis, Henoch-Schonlein purpura nephritis, nephrotic proteinuria, serum-urine matched metabolomics

OPEN ACCESS

Edited by:
Tara Sigdel,
University of California, San Francisco, United States

Reviewed by:
Seung Seok Han,
Seoul National University, South Korea
Shijia Liu,
The Affiliated Hospital of Nanjing University of CM, China

***Correspondence:**
Lian-Wen Qi
Qilw@cpu.edu.cn
Jun Xue
xuejun@fudan.edu.cn
Feng-Qing Huang
1620194561@cpu.edu.cn

[†] *These authors have contributed equally to this work*

Specialty section:
This article was submitted to Nephrology, a section of the journal Frontiers in Medicine

Received: *22 January 2021*
Accepted: *15 April 2021*
Published: *12 May 2021*

Citation:
Zhang Q, Lai L-Y, Cai Y-Y, Wang M-J, Ma G, Qi L-W, Xue J and Huang F-Q (2021) Serum-Urine Matched Metabolomics for Predicting Progression of Henoch-Schonlein Purpura Nephritis. Front. Med. 8:657073. doi: 10.3389/fmed.2021.657073

INTRODUCTION

Henoch-schonlein purpura (HSP) is a common systemic vasculitis affecting the skin, joints, gastrointestinal tract, and kidney (1). Henoch-Schonlein purpura nephritis (HSPN) is the most severe complication of HSP accompanied by renal injury that accounts for 20–80% of HSP incidence (2). Epidemiological investigations showed that renal involvement may be the principal cause of morbidity in HSPN patients (3, 4). Under physiological conditions, protein levels in urine is <150 mg/L per 24 h (5). In patients with HSPN, the filtration barrier is damaged pathologically, resulting in proteinuria. In clinic, the degree of proteinuria has been proposed as being symptomatic of kidney damage in HSPN.

Clinically, routine urinalysis and renal biopsy are the two main diagnostic methods for HSPN. Urinalysis is simple, non-invasive and speedy, but lacks sensitivity and specificity. Although renal

biopsy is the gold standard to assess the degree of renal damage, its invasiveness, potential damage and possible complications limit its application. The 24 h urine protein test combined with renal biopsy provides a reliable strategy to assess kidney damage in HSPN, however, proteinuria can only be detected after severe kidney damage has occurred and could sometimes be detected within 1–3 months of onset, thereby hindering early intervention (6).

Metabolomics measures the alteration of endogenous low-molecular-weight metabolites in response to stress stimulation and diseases. It has shown potential in diagnosing occurrence and progress of diseases (7). Metabolomics shows advantages in comprehensive profiling, high-throughput analysis, and non-invasive sampling (8). In this work, 90 HSPN patients comprising 46 HSPN (+) patients with severe kidney damage (persistent proteinuria >0.3 g/day) and 44 HSPN (–) patients without obvious symptoms (proteinuria <0.3 g/day) were recruited. A serum-urine matched metabolomics strategy was developed with the following underlying goals: (1) to comprehensively characterize the metabolic differences between HSPN (+) and HSPN (–) patients, and (2) to screen for potential metabolic biomarkers for assessing the progression of renal damage in HSPN patients.

MATERIALS AND METHODS

Study Participants

All the subjects in this study were recruited from Huashan Hospital of Fudan University (Shanghai, China). The patients were subjected to serological antibody tests prior to diagnosis, including anti-neutrophil cytoplasmic antibody (ANCA), anti-nuclear antibody (ANA), and anti-double-stranded DNA antibody (dsDNA) tests. Negative outcomes of these tests excluded the possibility of these patients having vasculitis or lupus erythematosus. In accordance with guidelines of the American College of Rheumatology, HSPN was confirmed by renal biopsy and was defined as those HSP patients with evidence of kidney damage such as hematuria, proteinuria, and/or renal failure. IgA deposits in the glomeruli were observed in all biopsies of the HSPN patients. The 2012 Kidney Disease: Improving Global Outcomes (KDIGO) Clinical Practice Guideline categorized the patients with proteinuria <0.3 g per 24 h as complete remission. In this study, the HSPN patients with severe kidney damage (persistent proteinuria >0.3 g/day) were regarded as HSPN (+) patients, while those without obvious symptoms (proteinuria <0.3 g/day) were defined as HSPN (–). The exclusion criterion included patients with hepatitis B nephritis, diabetes mellitus, systemic lupus erythematosus, any form of malignancy, and liver cirrhosis. Clinical information of the enrolled participants was systematically collected at baseline, including age, sex, routine blood tests, 24-h urine protein tests, and clinical symptoms such as purpura and renal damage.

Sample Collection

The blood and urine samples were collected from the patients prior to biopsy. All blood samples were collected in the morning after a 12-h fast. After storing at room temperature for 1 h, the whole blood was centrifuged at 3,000 rpm at 4°C for 20 min. The supernatant serum was then immediately transferred and stored at −80°C before use. The 24-h urine samples were collected by patients at the Huashan Hospital of Fudan University. Samples were frozen and stored at −80°C until metabolomics analysis.

Sample Preparation

Serum

After thawing at 4°C, an aliquot of 135 μL methanol/acetonitrile (3:1, v/v) (containing 0.4 μg/mL L-2-chlorophenylalanine and 10 μg/mL ketoprofen as the internal standards for the positive and negative ion modes, respectively) was added to 45 μL serum and vortexed for 2 min. The mixture was then centrifuged at 13,000 rpm at 4°C for 10 min. The supernatant fraction was divided into two 60-μL aliquots (for ESI^+ and ESI^- mode) and subsequently dried under nitrogen gas at room temperature. Finally, 60 μL of 50% acetonitrile was chosen to redissolve the residue and 1 μL supernatant was injected for further liquid chromatography-quadrupole time-of-flight mass spectrometry (LC-Q/TOF-MS) analysis. Quality control (QC) samples were prepared by pooling equal volumes (10 μL) from each sample and pretreated under the same procedure as study samples.

Urine

Briefly, an aliquot of 150 μL methanol was added to 50 μL urine to extract the metabolites. After vortexing for 2 min, the mixture was centrifuged (13,000 rpm, 4°C, 10 min). Then, 150 μL of the supernatant was divided into two parts and dried under nitrogen gas at room temperature. The residues were redissolved in 75 μL of 50% aqueous acetonitrile and 2 μL injection was analyzed.

Chromatographic and Mass Spectrometric Conditions

Chromatographic separation of the serum and urine samples were achieved on an Agilent 1290 UPLC system equipped with an ACQUITY UPLC HSST3 column (2.1 × 100 mm, 1.8 μm) at 40°C. All the analytical batches were run with a randomly generated sequence and one injection of QC sample was analyzed after every 10 test samples to evaluate the stability of the analytical platform. The mobile phase of ESI^+ mode consisted of 0.1% formic acid/water (A) and acetonitrile (B). For ESI^- mode, water and acetonitrile/water (9:1, v/v) both containing 10 mM ammonium acetate were used as phases A and B, respectively. In serum metabolomics, the gradient of elution was programmed as follows: 1% B at 0–1 min, 1–15% B at 1–3 min, 15–70% B at 3–5 min, 70–85% B at 5–9 min, 85–100% B at 9–10 min, 100% B at 10–12 min, and then back to initial conditions, with 3 min for equilibration. For the urine analysis, the gradient elution program was 1% B at 0–1 min, 1–15% B at 1–4 min, 15–50% B at 4–10 min, 50–95% B at 10–12 min, 95% B at 12–14.5 min, and then back to initial conditions for equilibration with 3 min. The flow rate was set at 0.4 ml/min. Detection of metabolite ions was performed on a 6545 Quadrupole time-of-flight spectrometric system (Agilent Technologies, USA) operated in both positive and negative ion modes. The detailed MS parameters were set as follows: fragmental voltage, 120 V; capillary voltage, 3,500 V; nozzle voltage, 1,000 V; drying gas flow rate, 8 L/min; drying gas

temperature, 320°C; sheath gas temperature, 250°C; sheath gas flow, 11 L/min. A full scan with mass ranges from m/z 50 to 1,050 was performed for the raw data acquisition.

Data Processing

All the raw spectral data acquired from LC-Q/TOF-MS were first transformed to "mz data" format using data reprocess analysis software (DA Reprocessor, Agilent, 6.0 version) with the threshold of the peak height set at 1,000 counts. Data pretreatment including nonlinear retention time alignment, peak discrimination, filtering and alignment were subsequently processed by running the XCMS package in R-3.3.3 platform. The ion features with more than 20% missing values across all samples were deleted. Data normalization of sera were done through internal standard while urine data were normalized by area abundance. Identification of differential metabolite signatures were performed based on the accurate mass and MS/MS fragments by searching through online databases such as Human Metabolome Database (HMDB; https://hmdb.ca/) and METLIN (http://metlin.scripps.edu). Some of them were unambiguously confirmed with available reference compounds. The pathway enrichment analyses were conducted with MetaboAnalyst 4.0 software (https://www.metaboanalyst.ca/) based on KEGG database.

Statistical Analysis

Multivariate analysis was carried out with R-3.3.3 platform. Mann–Whitney *U*-test combined with hochberg false discovery rate (FDR) correction was performed for the statistical measurement of each metabolite between the comparisons. FDR-adjusted $p < 0.05$ was considered statistically significant. Unsupervised principal component analysis (PCA) was performed to provide information on the overall distribution of the analyzed data matrix. Supervised orthogonal partial least-squares discriminant analysis (OPLS-DA) was applied to identify the differences in metabolic phenotypes between groups. Those metabolic features with an adjusted $p < 0.05$ and variable importance in the projection (VIP) value >1.0 in the OPLS-DA model were screened as differential metabolites. The relative levels of the differential metabolites between the groups were visualized as heatmap by hierarchical clustering analysis. Receiver operating characteristic (ROC) analysis and other statistical analyses were performed with R-3.3.3.

RESULTS

Participants' Clinical Characteristics

A total of 90 HSPN patients (≥15 years old) were enrolled in this work. Their detailed clinical baseline characteristics are summarized in **Table 1**. The 46 patients identified as HSPN (+) showed severe kidney damage with persistent proteinuria of 1.95 ± 1.73 g/day. The 44 patients identified as HSPN (–) showed no obvious symptoms with proteinuria of 0.15 ± 0.16 g/day. Among the HSPN (+) patients, 43.18% had segmental sclerosis and 70.45% had crescent formation, while for the HSPN (–) patients, no segmental sclerosis or crescent formation was observed. Statistical significance in the levels of blood creatinine, urinary red blood cells, and urinary white cells between the two groups indicated that kidney damage may be linked to inflammatory cytokines and the immune system.

TABLE 1 | Clinical baseline characteristics of the study subjects.

Characteristic	HSPN (+) ($n = 46$)	HSPN (–) ($n = 44$)	p-value
Male (%)	27 (59%)	20 (45%)	0.296
Age, years	42.15 ± 18.91	32.36 ± 14.20	0.007
Proteinuria/24 h	1.95 ± 1.73	0.15 ± 0.16	<0.001
Blood creatinine, μmol/L	90.59 ± 78.35	65.45 ± 12.58	0.038
Urea nitrogen, mmol/L	8.04 ± 12.56	4.60 ± 1.17	0.075
Uric acid, mmol/L	0.37 ± 0.13	0.33 ± 0.06	0.093
IgG, g/L	10.04 ± 3.45	13.00 ± 2.09	<0.001
IgA, g/L	3.37 ± 1.54	3.50 ± 1.22	0.690
IgM, g/L	1.07 ± 0.48	1.20 ± 0.58	0.298
Urinary red blood cell counts/μl	278.36 ± 421.95	81.19 ± 148.52	0.006
Urinary white blood cell counts/μl	40.16 ± 42.76	17.07 ± 22.43	0.003
Urinary ACR mg/g	1,359.95 ± 1,601.95	77.28 ± 158.11	<0.001
Segmental sclerosis (%)	19 (43.18%)	0 (0%)	
Crescent formation (%)	31 (70.45%)	0 (0%)	

IgG, immunoglobulin G; IgA, immunoglobulin A; IgM, immunoglobulin M; Urinary ACR, urinary albumin-to-creatinine ratio.

Metabolomics Analysis

The solvents for metabolites extraction and redissolution were optimized. For serum, methanol/acetonitrile (3:1, v/v) was found to show the best extraction efficiency over methanol (100%), acetonitrile (100%), methanol/acetonitrile (1:1, v/v), and methanol/acetonitrile (1:3, v/v) based on the total number of ion features (**Supplementary Figure 1**). For urine, methanol (100%) was selected as the best solvent for metabolite extraction. During the re-dissolution stage, 50% aqueous acetonitrile exhibited highest efficiency by producing more metabolites both in the serum and urine samples (**Supplementary Figure 2**). The typical total ion chromatograms of HSPN serum and urine samples both in positive and negative ion modes are presented in **Supplementary Figure 3**. Totally, 2,770 ions were captured in the serum, and 3,992 ion features were detected in urine.

Serum Metabolic Differences Between HSPN (+) and HSPN (–) Patients

The unsupervised PCA showed a clear separation between HSPN (+) and HSPN (–) with PC1 at 76.2% and PC2 at 11.1% (**Figure 1A**). An OPLS-DA model further confirmed the significant distinction in metabolic patterns (**Figure 1B**). The cumulative R2Y and Q2 were 0.855 and 0.675, respectively. With the selection criterion of VIP >1.0 and adjusted-$p < 0.05$, a total of 587 differential ions were screened out. Among them, 38 metabolites were identified. The details of the differential metabolites including name, retention time, mass-to-charge ratio, VIP value, fold change, and p-value are provided in **Table 2**. Their relative levels are summarized in a heatmap in **Figure 1C**.

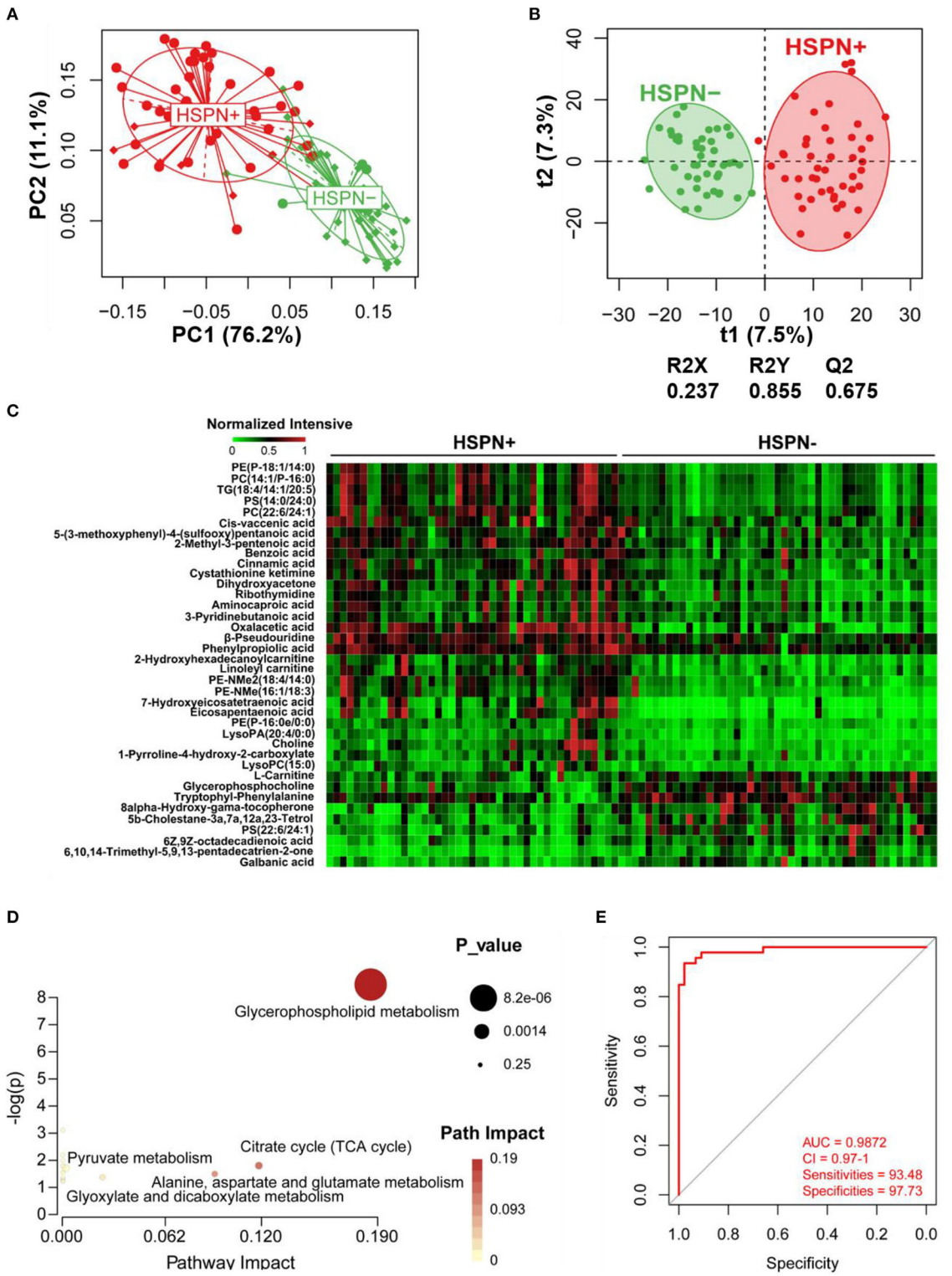

FIGURE 1 | Serum metabolic comparison of HSPN (+) and HSPN (–) patients. **(A)** PCA score plots of HSPN (+) vs. HSPN (–). **(B)** OPLS-DA score plots of HSPN (+) vs. HSPN (–). **(C)** Heatmap of the 38 metabolites identified from the comparison of HSPN (+) vs. HSPN (–). The colors from green to red in the heatmap indicate the elevation in levels of metabolites. **(D)** Disturbed metabolic pathways identified from the comparison of HSPN (+) vs. HSPN (–) using serum samples. **(E)** ROC curve analysis of the top 10 differential metabolites with highest VIP values in serum for HSPN (+) vs. HSPN (–). PCA, principal component analysis; OPLS-DA, orthogonal partial least-squares discriminant analysis; ROC, receiver operating characteristic.

TABLE 2 | Statistical analysis of 38 differential metabolites in serum identified from the comparison of HSPN (+) vs. HSPN (–).

Differential metabolites	Retention time (min)	Mass-to-charge ratio	VIP	Fold change	*p*-value[a]	Adjusted *p*-value[b]	Adduct
Oxalacetic acid	0.95	133.0135	2.70	2.14	<0.001	<0.001	M+H
PE-NMe (16:1/18:3)	7.28	726.5133	2.56	1.81	<0.001	<0.001	M+H
2-Methyl-3-pentenoic acid	1.89	132.1014	2.45	1.34	<0.001	<0.001	$M+NH_4$
PE-NMe2 (18:4/14:0)	6.62	712.4977	2.47	1.81	<0.001	<0.001	M+H
Eicosapentaenoic acid*	7.25	303.2329	2.35	7.02	<0.001	<0.001	M+H
7-Hydroxyeicosatetraenoic acid[c]	6.52	319.2283	2.30	7.50	<0.001	<0.001	M–H
PS (14:0/24:0)	7.13	820.6026	2.29	1.38	<0.001	<0.001	M+H
TG (18:4/14:1/20:5)	7.04	865.6317	2.27	1.38	<0.001	<0.001	M+Na
Glycerophosphocholine	0.66	280.0938	2.18	0.65	<0.001	<0.001	M+Na
PC (14:1/P-16:0)	7.52	688.5217	2.23	1.35	<0.001	<0.001	M+H
Linoleyl carnitine	6.15	424.344	2.22	1.80	<0.001	<0.001	M+H
PC (22:6/24:1)	6.52	938.6656	2.17	1.37	<0.001	<0.001	M+Na
PE (P-18:1/14:0)	6.96	674.5069	2.14	1.34	<0.001	<0.001	M+H
5b-Cholestane-3a,7a,12a,23-Tetrol	11.04	437.3639	2.11	0.58	<0.001	<0.001	M+H
PS (22:6/24:1)	11.79	935.6486	2.10	0.76	<0.001	<0.001	$M+NH_4$
8alpha-Hydroxy-gama-tocopherone	10.41	433.3692	2.09	0.61	<0.001	<0.001	M+H
6,10,14-Trimethyl-5,9,13-Pentadecatrien-2-one	11.90	263.2382	2.08	0.42	<0.001	<0.001	M+H
Phenylpropiolic acid	1.25	147.0443	2.04	1.32	<0.001	<0.001	M+H
Cystathionine ketimine	3.04	204.0329	2.04	1.25	<0.001	<0.001	M+H
2-Hydroxyhexadecanoylcarnitine	6.47	426.3589	1.97	1.66	<0.001	<0.001	M+H
Ribothymidine[c]	0.64	257.0788	1.96	1.73	<0.001	<0.001	M–H
Cinnamic acid	3.04	149.0594	1.95	1.16	<0.001	<0.001	M+H
6Z,9Z-octadecadienoic acid	10.70	281.2483	1.94	0.62	<0.001	<0.001	M+H
Choline*	0.65	104.1074	1.89	1.46	<0.001	<0.001	M+H
Dihydroxyacetone[c]	0.65	89.02451	1.88	1.63	<0.001	<0.001	M–H
β-Pseudouridine[c*]	1.29	243.0626	1.82	1.44	<0.001	<0.001	M–H
Cis-vaccenic acid*	8.59	300.2904	1.77	1.26	<0.001	<0.001	$M+NH_4$
LysoPA (20:4/0:0)[c]	6.65	457.2372	1.76	2.28	<0.001	<0.001	M–H
5-(3-methoxyphenyl)-4-(sulfooxy) Pentanoic acid	0.58	327.0523	1.64	1.29	<0.001	<0.001	M+Na
L-Carnitine*	0.67	162.1129	1.64	0.82	<0.001	<0.001	M+H
Tryptophyl-Phenylalanine	4.63	352.1637	1.62	0.70	<0.001	<0.001	M+H
PE (P-16:0e/0:0)	7.05	438.2994	1.62	1.65	<0.001	<0.001	M+H
Benzoic acid	1.69	123.0436	1.62	1.25	<0.001	<0.001	M+H
Galbanic acid[c]	5.36	397.2054	1.52	0.55	<0.001	<0.001	M–H
LysoPC (15:0)*	7.83	482.3255	1.51	1.47	<0.001	<0.001	M+H
3-Pyridinebutanoic acid[c]	2.87	164.0721	1.46	1.31	<0.001	0.001	M–H
1-Pyrroline-4-hydroxy-2-Carboxylate[c]	0.68	128.0356	1.44	1.47	<0.001	<0.001	M–H
Aminocaproic acid[c]	1.23	130.0877	1.35	1.24	0.008	0.034	M–H

**means that the metabolites were confirmed with reference compounds.*

The metabolites were listed in a decreasing order based on variable importance in the projection (VIP) values.

Fold change with a value >1 indicates a relatively higher concentration present in the HSPN (+) patients.

[a]p-values from Mann–Whitney U-test; [b]Adjusted by false discovery rate correction across all the metabolites within the comparison. [c]means that the metabolite was detected in the negative ion mode. PE, Phosphatidylethanolamine; PS, Phosphatidylserine; TG, Triglyceride; PC, Phosphatidylcholine; LysoPA, Lysophosphatidic acid; LysoPC, lysophosphatidylcholine.

On the basis of the altered metabolites, the perturbed pathways between the two groups mainly related to glycerophospholipid metabolism, citrate cycle, pyruvate metabolism and alanine, aspartate, and glutamate metabolism (**Figure 1D**). A panel of the top 10 metabolites with the highest VIP values were selected to evaluate their diagnostic potentials based on receiver operating characteristic (ROC) curve analyses. The results showed that the combination of the 10 metabolites provided an area under curve (AUC) of 0.9872 with high sensitivity (93.48%) and specificity (97.73%) at a cutoff value of 0.912 (**Figure 1E**).

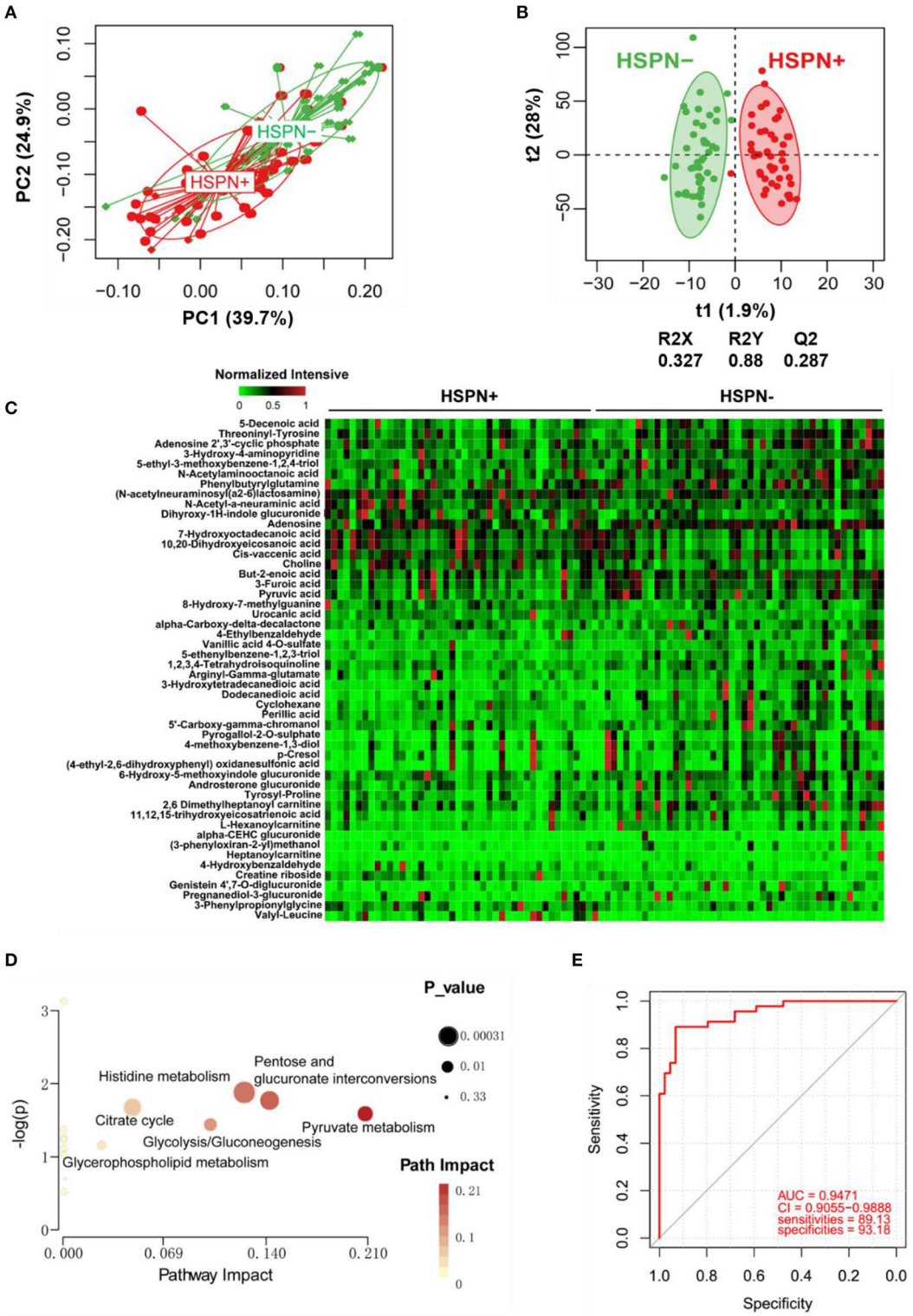

FIGURE 2 | Urine metabolic comparison of HSPN (+) and HSPN (–) patients. **(A)** PCA score plots of HSPN (+) vs. HSPN (–). **(B)** OPLS-DA score plots of HSPN (+) vs. HSPN (–). **(C)** Heatmap of the 50 differential metabolites identified from the comparison of HSPN (+) vs. HSPN (–) using urine samples. The colors from green to red in the heatmap indicate the elevation in levels of metabolites. **(D)** Disturbed metabolic pathways identified from the comparison of HSPN (+) vs. HSPN (–). **(E)** ROC curve analyses of the top 10 differential metabolites with highest VIP values for HSPN (+) vs. HSPN (–). PCA, principal component analysis; OPLS-DA, orthogonal partial least-squares discriminant analysis; ROC, receiver operating characteristic.

Urine Metabolic Differences Between HSPN (+) and HSPN (–) Patients

A clear discrimination from the unsupervised PCA scores plots (PC1 at 39.7%, PC2 at 24.9%) was observed between HSPN (+) and HSPN (–) patients, indicating that the two groups have distinctly different metabolic phenotypes (**Figure 2A**). In the OPLS-DA model, HSPN (–) were significantly separated from HSPN (+) patients with R2Y of 0.88 and Q2 of 0.287, suggesting that the model had good predictability for discovering potential biomarkers (**Figure 2B**). A total of 396 differential metabolite features were screened out, of which, 50 differential metabolites were identified (**Table 3**). Their relative levels across the samples were visualized in a heatmap (**Figure 2C**). The metabolic perturbations in urine between the two groups mainly focused on pyruvate, pentose, and glucuronate interconversions, histidine metabolism and citrate cycle (**Figure 2D**). With the same criterion, ROC analysis was performed to evaluate the diagnostic capacity of the top 10 metabolites in terms of VIP values. The panel provided AUC of 0.9471 (CI: 0.9055–0.9888, sensitivity: 89.13%, specificity: 93.18%) at a cutoff value of 0.823 (**Figure 2E**).

Metabolic Markers for the Prediction of HSPN Progression

To simplify the metabolic biomarker panel for potential clinical application, we focused on the metabolites that: (1) have commercially available reference compounds and (2) are present as differential metabolites both in serum and urine. In line with this, two differential metabolites namely choline and *cis*-vaccenic acid were screened out as biomarkers for predicting HSPN progression. As compared to HSPN (–), HSPN (+) patients showed an elevated level of choline in both serum (**Figure 3A**) and urine (**Figure 3B**). The results of spearman correlation analysis indicated that the levels of choline in serum and urine exhibited a significant correlation with *p*-value of 0.0059 (**Figure 3C**). Similarly, *cis*-vaccenic acid was significantly increased in HSPN (+) patients (**Figures 3D,E**) and showed a significant correlation in serum and urine (**Figure 3F**). Through ROC analysis, the calculated area under curve (AUC) of choline, *cis*-vaccenic acid, and their combination were 88.69% (95% CI: 0.8155–0.9582), 79.15% (95% CI: 0.6968–0.8862) and 92.69% (95% CI: 0.8687–0.9851), respectively (**Figures 4A–C**). Obviously, the combined panel showed a better predictive potential for distinguishing the HSPN (–) from HSPN (+) group. In urine, choline, *cis*-vaccenic acid, and their combination provided area under curve (AUC) values of 72.53% (95% CI: 0.6213–0.8293), 63.51% (95% CI: 0.5160–0.7543) and 72.43% (95% CI: 0.6203–0.8284), respectively (**Supplementary Table 1**).

Besides proteinuria, the urinary albumin excretion rate (ACR) and blood creatinine are also considered as important indicators to justify the renal involvement of HSPN in clinic. We then performed correlation analysis to assess the association between the metabolic markers and these clinical indices (**Figure 4D**). We found that the level of *cis*-vaccenic acid in serum and choline in urine were correlated with proteinuria. Meanwhile, the choline in both serum and urine, and *cis*-vaccenic acid in serum showed a positive correlation with urinary ACR. Also, choline in serum showed a positive correlation with blood creatinine. These findings further confirmed the potential of choline and *cis*-vaccenic acid as biomarkers for predicting HSPN progression.

DISCUSSION

HSPN is the most common and severe form of HSP complication that could lead to chronic kidney disease. Clinically, it is important to assess the risk of developing renal complications in HSPN. Routine urinalysis and renal biopsy are commonly used to diagnose HSPN, albeit some shortcomings. Although the degree of proteinuria reflects the severity of kidney damage, its detection in the latter phase of the disease makes it unreliable for early intervention of HSPN. Metabolomics has the advantages of dynamic detection and non-invasiveness, and shows potential in diagnosing occurrence and progress of diseases. The occurrence of kidney diseases has been shown to be closely related to metabolic disorders (9, 10). Hence, we conducted a comprehensive untargeted metabolomics to identify markers that could predict HSPN progression. Biofluids including blood, urine, and saliva are most commonly used as pools of endogenous metabolites for metabolomics studies (11, 12). In contrast to the use of one biofluid type, our use of serum-urine matched samples provided a wider coverage of metabolite information with more than 6,000 metabolic features.

The perturbed metabolic pathways both identified from serum and urine metabolomics mainly included glycerophospholipid metabolism, citrate cycle, and pyruvate metabolism, which is indicative of abnormal lipid metabolism and energy metabolism in the progress of renal damage. These results are consistent with previous studies on kidney diseases (12–14). In addition, serum metabolomics supplied other disturbed pathways such as alanine, aspartate, and glutamate metabolism, glyoxylate, and dicarboxylate metabolism. Urine metabolomics provided histidine metabolism, glycolysis/gluconeogenesis, and purine metabolism as the disturbed pathways. These findings suggest that the diverse pathophysiological changes inherent during renal damage in HSPN is reflective of the varied metabolic phenotypes in serum and urine.

Lipid accumulation has been proposed as a risk factor of renal injury (15). In this work, we found significant increase of phosphatidylethanolamines (PE) including (PE)-NMe (16:1/18:3), PE-NMe2 (18:4/14:0), PE (P-18:1/14:0), and PE (P-16:0e:/0:0). PE is a key phospholipid of cytomembrane and its externalization has been regarded as a signal of early apoptosis (16). The up-regulation of PE in HSPN (+) indicates that cell apoptosis possibly accelerates the decline in renal function. Under physiological conditions, the kidney is exposed to a wide range of fluctuation in terms of extracellular solutes and responds to hypertonic stress through the accumulation of the organic osmolytes (17). Glycerophosphorylcholine, a choline derivative, is one of the four major organic osmolytes in renal medullary cells. During cellular osmoadaptation, an increased intracellular glycerophosphorylcholine level contributes in maintaining osmotic equilibrium (18). The

TABLE 3 | Statistical analysis of 50 differential metabolites in urine identified from the comparison of HSPN (+) vs. HSPN (–).

Differential metabolites	Retention time (min)	Mass-to-charge ratio	VIP	Fold change	*P*-value[a]	Adduct
10,20-Dihydroxyeicosanoic acid	10.71	362.3240	3.41	1.37	<0.001	M+NH_4
7-Hydroxyoctadecanoic acid	10.63	318.3003	3.16	1.27	<0.001	M+NH_4
Choline*	0.65	104.1070	3.15	1.44	<0.001	M+H
5-Ethenylbenzene-1,2,3-triol[b]	4.52	151.0406	2.84	0.58	0.002	M–H
Valyl-Leucine	4.48	231.1698	2.83	6.08	0.005	M+H
Dodecanedioic acid	7.23	231.1581	2.83	0.48	0.006	M+H
1,2,3,4-Tetrahydroisoquinoline	7.27	134.0961	2.71	0.67	0.008	M+H
Dihydroxy-1H-indole glucuronide I[b]	2.94	324.0731	2.67	1.45	0.036	M–H
N-Acetyl-a-neuraminic acid	0.75	310.1136	2.55	1.29	0.014	M+H
Perillic acid	5.99	167.1063	2.41	0.57	0.007	M+H
Genistein 4′,7-O-diglucuronide	5.18	623.1245	2.37	0.31	<0.001	M+H
3-Phenylpropionylglycine[b]	4.31	206.0827	2.36	1.69	0.004	M–H
3-Hydroxytetradecanedioic acid[b]	6.91	273.1709	2.19	0.51	0.001	M–H
Cyclohexane	6.00	107.0838	2.15	0.71	0.039	M+Na
2,6-Dimethylheptanoyl carnitine	8.71	302.2325	2.10	0.62	0.008	M+H
Urocanic acid[b]	2.41	137.0355	2.06	1.28	0.003	M–H
(3-Phenyloxiran-2-yl) methanol[b]	7.46	149.0609	2.06	0.55	0.032	M–H
[N-acetylneuraminosyl (a2–6) lactosamine]	0.83	675.2462	2.05	1.19	0.027	M+H
5-Ethyl-3-methoxybenzene-1,2,4-triol	3.65	202.1068	2.03	0.78	0.037	M+NH_4
Alpha-CEHC glucuronide[b]	7.58	453.1770	1.98	0.32	0.042	M–H
N-Acetylaminooctanoic acid[b]	6.41	200.1296	1.97	1.29	0.002	M–H
5′-Carboxy-gamma-chromanol	9.12	324.2163	1.91	0.64	0.023	M+NH_4
Creatine riboside	0.75	264.1179	1.91	1.74	0.003	M+H
Pyruvic acid[b*]	0.56	87.00843	1.90	0.77	0.003	M–H
Vanillic acid 4-O-sulfate[b]	2.94	246.9922	1.85	0.61	0.010	M–H
Adenosine 2′,3′-cyclic phosphate	2.79	330.0597	1.84	0.74	0.017	M+H
Androsterone glucuronide	10.02	484.2900	1.82	0.64	0.049	M+NH_4
L-Hexanoylcarnitine	5.93	260.1856	1.67	0.59	0.014	M+H
Adenosine*	2.60	268.1037	1.64	0.74	0.006	M+H
Tyrosyl-Proline	3.86	279.1333	1.62	0.66	0.018	M+H
6-Hydroxy-5-methoxyindole Glucuronide	4.65	340.1028	1.60	0.72	0.013	M+H
8-Hydroxy-7-methylguanine	2.89	182.0670	1.60	1.24	0.020	M+H
Threoninyl-Tyrosine	6.32	283.1282	1.59	0.76	0.021	M+H
3-Hydroxy-4-aminopyridine	0.74	111.0552	1.58	0.84	0.004	M+H
3-Furoic acid[b]	0.55	111.0082	1.58	0.83	0.032	M–H
Alpha-Carboxy-delta-decalactone[b]	3.90	213.1135	1.55	0.67	0.017	M–H
4-Methoxybenzene-1,3-diol[b]	4.33	139.0403	1.53	0.71	0.004	M–H
4-Hydroxybenzaldehyde[b]	4.17	121.0294	1.50	1.74	0.007	M–H
Cis-vaccenic acid*	11.56	300.2875	1.48	1.10	0.028	M+NH_4
(4-Ethyl-2,6-dihydroxyphenyl) Oxidanesulfonic acid[b]	5.20	233.0127	1.48	0.64	0.017	M–H
Phenylbutyrylglutamine	8.21	315.1326	1.41	0.78	0.040	M+Na
Pyrogallol-2-O-sulfate[b]	2.77	204.9817	1.39	0.67	0.002	M–H
But-2-enoic acid[b]	0.57	85.02898	1.39	0.87	0.024	M–H
Arginyl-Gamma-glutamate	3.85	320.2052	1.38	0.75	0.019	M+NH_4
4-Ethylbenzaldehyde[b]	7.89	133.0658	1.37	0.69	0.011	M–H
Heptanoylcarnitine	7.10	274.2012	1.36	0.42	0.009	M+H
Pregnanediol-3-glucuronide[b]	9.36	495.2969	1.31	0.64	0.005	M–H
p-Cresol[b]	5.20	153.0557	1.21	0.72	0.011	M+FA–H
5-Decenoic acid	8.73	171.1369	1.21	0.75	0.045	M+H
11,12,15-Trihydroxyeicosatrienoic acid	8.75	372.2741	1.13	0.61	0.022	M+NH_4

**means that the metabolites were confirmed with reference compounds.*

The metabolites were listed in a decreasing order based on VIP values.

Fold change with a value >1 indicates a relatively higher concentration present in the HSPN (+) patients.

[a]p-values from Mann–Whitney U-test; [b]means that the metabolite was detected in negative ion mode.

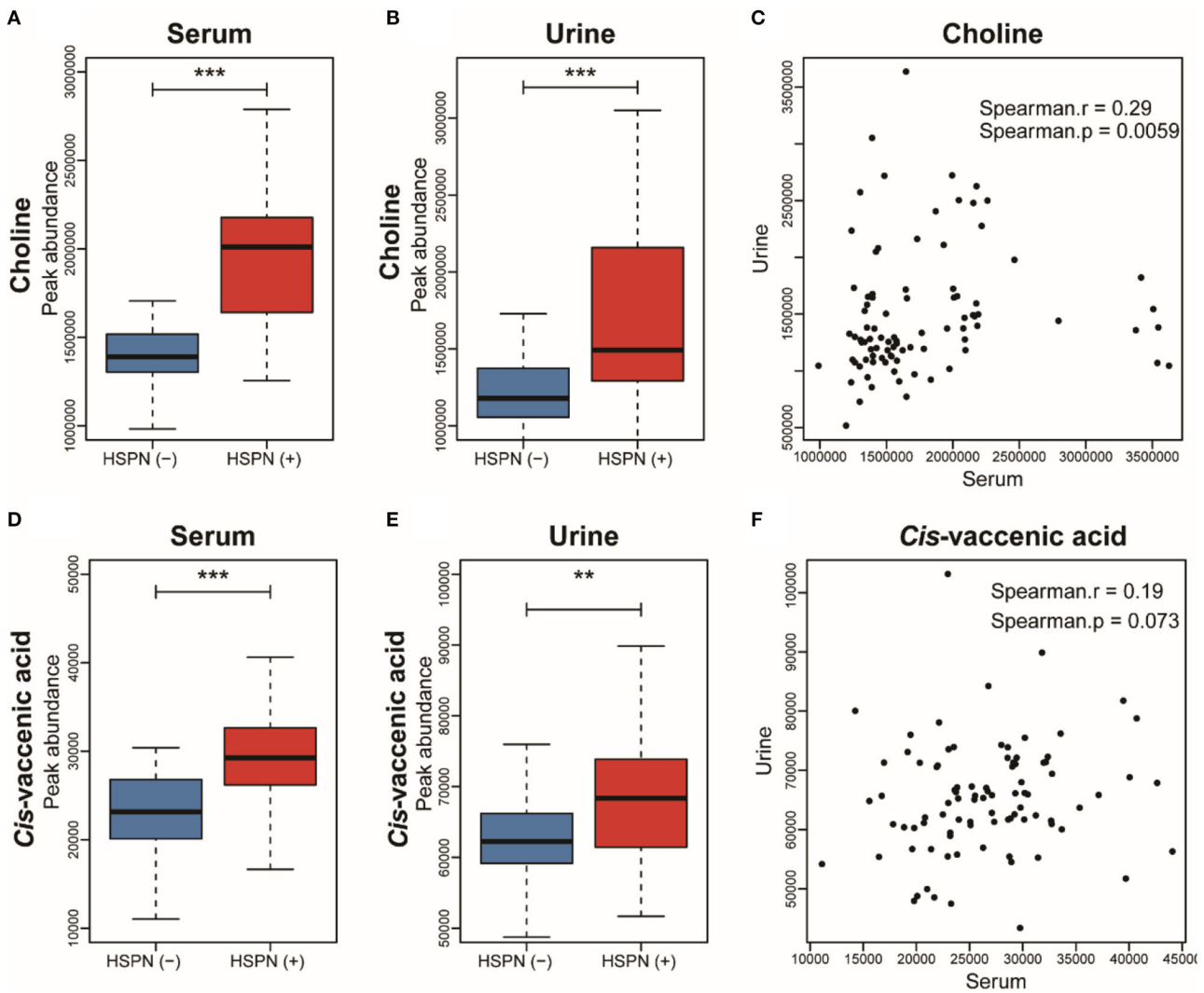

FIGURE 3 | Boxplot analysis of choline in **(A)** serum and **(B)** urine between HSPN (–) and HSPN (+) patients. **(C)** Spearman correlation analysis of the levels of choline in serum and urine. Boxplot analysis of *cis*-vaccenic acid in **(D)** serum and **(E)** urine between HSPN (–) and HSPN (+) patients. **(F)** Spearman correlation analysis of the levels of *cis*-vaccenic acid in serum and urine. $^{**}p < 0.01$ and $^{***}p < 0.001$.

decreased glycerophosphorylcholine may indicate cell osmolar dysfunction was involved in HSPN (+). Free fatty acids (FFAs) are harmful to the kidneys. We observed some FFAs including 6Z,9Z-octadecadienoic acid and *cis*-vaccenic acid were significantly elevated in the HSPN (+) group. High FFA levels accelerate the production of reactive oxygen species (ROS), a phenomenon that could induce mitochondrial damage and tissue inflammation, resulting in renal damage (19, 20).

Abnormal energy metabolism is associated with a decline in renal function (21). Pyruvate, the end-product of glycolysis, is down-regulated in serum, which indicates the possible occurrence of renal ischemia in HSPN (+) patients (22). We found that the tricarboxylic acid cycle (TCA) intermediate oxaloacetate was significantly up-regulated in serum but decreased in the urine of HSPN (+) patients. These contrasting levels of TCAs in the serum and urine may be an indication of renal dysfunction (23).

Choline is the precursor of trimethylamine N-oxide and acts as a methyl donor in various metabolic processes, especially in lipid metabolism. In our study, the level of choline in both serum and urine were up-regulated in HSPN (+) patients. It has been reported that elevated levels of choline could lead to an increase in KIM-1 level—a marker of early kidney damage resulting in an increased risk of developing renal fibrosis (24). In addition, a long-term hypercholinergic state can induce an increase in plasma cystatin C level, which is a sensitive indicator of renal function impairment (25).

Cis-vaccenic acid is a monounsaturated fatty acid derived from intestinal flora. A cross-sectional cohort study showed *cis*-vaccenic acid to be positively associated with reduced estimated

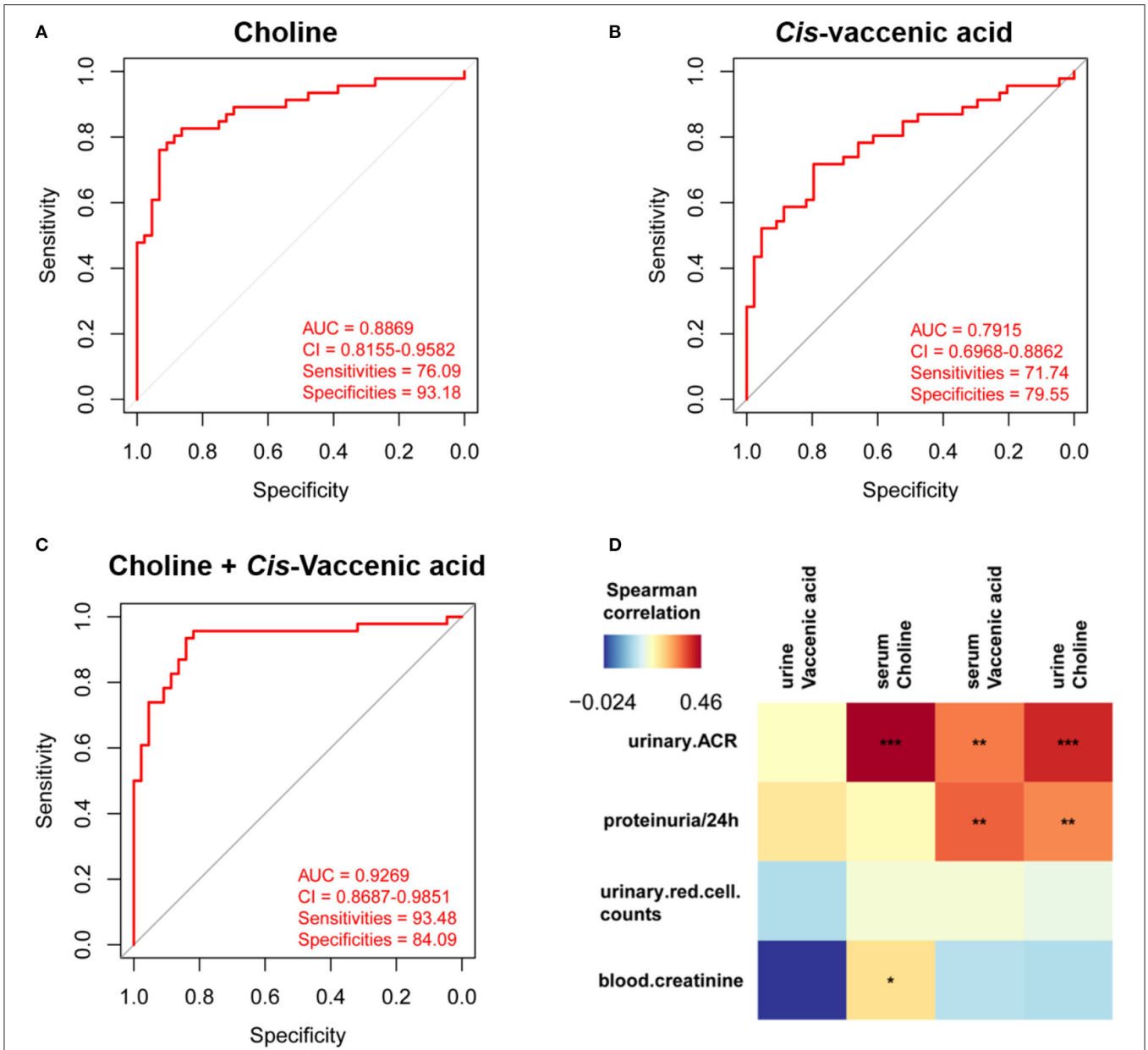

FIGURE 4 | Differential diagnosis and correlation analysis of the metabolic biomarkers. ROC analysis of **(A)** choline, **(B)** *cis*-vaccenic acid, and **(C)** the combination of choline and *cis*-vaccenic acid for HSPN (+) vs. HSPN (–) in serum. **(D)** Correlation analysis of HSPN clinical indices and metabolic markers (choline and *cis*-vaccenic acid) in serum and urine. Color units denoted the value of Spearman correlation coefficient. The red color indicates a positive correlation and the blue represents a negative correlation. $^{*}p < 0.05$, $^{**}p < 0.01$, and $^{***}p < 0.001$. ROC, receiver operating characteristic.

glomerular filtration rate (eGFR), an important indicator of renal function (26). In our results, the increased level of *cis*-vaccenic acid in HSPN (+) patients further confirmed this observation.

Identification of novel biomarkers contributes to early detection and prediction of diseases. The moderate sample size, integrative analysis of serum and urine, and biopsy-proven cohort in this study contributed to screening for the reliable biomarkers for HSPN. The panel of choline and *cis*-vaccenic acid exhibited differential capacity with area under the curve value of 92.69% in serum and 72.43% in urine between HSPN (+) and HSPN (–), and showed significant correlations with clinical indices of HSPN. These results highlight the early diagnostic potential of the metabolic biomarkers as an alternative method to predict HSPN progression.

This work has some limitations. First, the single cohort of HSPN patients constitutes the primary limitation. In

future studies, a large sample size from multi-centers including healthy controls could be considered to validate our results or otherwise. Second, due to the unavailability of reference compounds, the confirmation of the metabolites mainly depended on the databases and this remains a challenge for accurate identification. Finally, targeted quantification of the metabolic markers is necessary in future and a suitable animal model could be applied for further biological validation.

CONCLUSIONS

In this work, we described an untargeted metabolomics by LC-Q/TOF-MS to characterize the underlying metabolic differences between HSPN (+) and HSPN (–) patients. The use of serum-urine matched samples provided a broad-scope for detection of metabolic information. Choline and *cis*-vaccenic acid that were both identified in serum and urine were screened as markers to predict HSPN progression. The panel of choline and *cis*-vaccenic acid showed the potential to differentiate between HSPN (+) and HSPN (–) patients with area under the curve value of 92.69% in serum and 72.43% in urine. In addition, choline and *cis*-vaccenic acid showed a significant association with the clinical indices of HSPN. These results suggest that choline and *cis*-vaccenic acid could serve as biomarkers to predict HSPN progression, and we do believe that following further studies with larger cohorts, the findings of this study hold great promise for clinical application.

DATA AVAILABILITY STATEMENT

The raw data supporting the conclusions of this article will be made available by the authors, without undue reservation.

ETHICS STATEMENT

The studies involving human participants were reviewed and approved by Ethics Committee of the Affiliated Huashan Hospital, Fudan University. Written informed consent to participate in this study was provided by the participants' legal guardian/next of kin.

AUTHOR CONTRIBUTIONS

F-QH, JX, and L-WQ: conceptualization. Y-YC, M-JW, and GM: data curation. QZ, L-YL, and GM: investigation. QZ: methodology. F-QH: project administration. JX and L-YL: resources. L-WQ: supervision. QZ: writing – original draft. L-WQ and F-QH: writing – review and editing. All authors contributed to the article and approved the submitted version.

FUNDING

This work was financially supported in part by the National Natural Science Foundation of China (No. 82003979) and the China Postdoctoral Science Foundation (No. 2020M671660).

ACKNOWLEDGMENTS

We thank Dr. Raphael N. Alolga of China pharmaceutical University for editing the manuscript.

SUPPLEMENTARY MATERIAL

The Supplementary Material for this article can be found online at: https://www.frontiersin.org/articles/10.3389/fmed.2021.657073/full#supplementary-material

REFERENCES

1. Yu Y, Chen J, Yin H, Deng Z, Xie Y, Yuan Q, et al. Efficacy of steroid and immunosuppressant combined therapy in Chinese patients with Henoch-Schonlein purpura nephritis: a retrospective study. *Int Immunopharmacol.* (2020) 81:106229. doi: 10.1016/j.intimp.2020.106229
2. Hetland LE, Susrud KS, Lindahl KH, Bygum A. Henoch-Schonlein purpura: a literature review. *Acta Derm Venereol.* (2017) 97:1160–6. doi: 10.2340/00015555-2733
3. Davin JC. Henoch-Schonlein purpura nephritis: pathophysiology, treatment, and future strategy. *Clin J Am Soc Nephrol.* (2011) 6:679–89. doi: 10.2215/CJN.06710810
4. Audemard-Verger A, Pillebout E, Guillevin L, Thervet E, Terrier B. IgA vasculitis (Henoch-Shonlein purpura) in adults: diagnostic and therapeutic aspects. *Autoimmun Rev.* (2015) 14:579–85. doi: 10.1016/j.autrev.2015.02.003
5. Fang X, Wu H, Lu M, Cao Y, Wang R, Wang M, et al. Urinary proteomics of Henoch-Schonlein purpura nephritis in children using liquid chromatography-tandem mass spectrometry. *Clin Proteomics.* (2020) 17:10. doi: 10.1186/s12014-020-09274-x
6. Buscatti IM, Casella BB, Aikawa NE, Watanabe A, Farhat SCL, Campos LMA, et al. Henoch-Schonlein purpura nephritis: initial risk factors and outcomes in a Latin American tertiary center. *Clin Rheumatol.* (2018) 37:1319–24. doi: 10.1007/s10067-017-3972-3
7. Johnson CH, Ivanisevic J, Siuzdak G. Metabolomics: beyond biomarkers and towards mechanisms. *Nat Rev Mol Cell Biol.* (2016) 17:451–9. doi: 10.1038/nrm.2016.25
8. Kalim S, Rhee EP. Metabolomics and kidney precision medicine. *Clin J Am Soc Nephrol.* (2017) 12:1726–7. doi: 10.2215/CJN.09480817
9. Nishi H, Higashihara T, Inagi R. Lipotoxicity in kidney, heart, and skeletal muscle dysfunction. *Nutrients.* (2019) 11:1664. doi: 10.3390/nu11071664
10. Mika A, Wojtowicz W, Zabek A, Młynarz P, Chmielewski M, Sledzinski T, et al. Application of nuclear magnetic resonance spectroscopy for the detection of metabolic disorders in patients with moderate kidney insufficiency. *J Pharm Biomed Anal.* (2018) 149:1–8. doi: 10.1016/j.jpba.2017.10.037
11. Ma T, Liu T, Xie P, Jiang S, Yi W, Dai P, et al. UPLC-MS-based urine nontargeted metabolic profiling identifies dysregulation of pantothenate and CoA biosynthesis pathway in diabetic kidney disease. *Life Sci.* (2020) 258:118160. doi: 10.1016/j.lfs.2020.118160
12. Lee H, Jang HB, Yoo MG, Park SI, Lee HJ. Amino acid metabolites associated with chronic kidney disease: an eight-year follow-up Korean epidemiology study. *Biomedicines.* (2020) 8:222. doi: 10.3390/biomedicines8070222
13. Lee HS. Mechanisms and consequences of hypertriglyceridemia and cellular lipid accumulation in chronic kidney disease and metabolic syndrome. *Histol Histopathol.* (2011) 26:1599–610. doi: 10.14670/HH-26.1599

14. Luo S, Coresh J, Tin A, Rebholz CM, Appel LJ, Chen J, et al. Serum metabolomic alterations associated with proteinuria in CKD. *Clin J Am Soc Nephrol.* (2019) 14:342–53. doi: 10.2215/CJN.10010818
15. van der Mijn JC, Fu L, Khani F, Zhang T, Molina AM, Barbieri CE, et al. Combined metabolomics and genome-wide transcriptomics analyses show multiple HIF1α-induced changes in lipid metabolism in early stage clear cell renal cell carcinoma. *Transl Oncol.* (2020) 13:177–85. doi: 10.1016/j.tranon.2019.10.015
16. Wang X, Li N, Liu B, Sun H, Chen T, Li H, et al. A novel human phosphatidylethanolamine-binding protein resists tumor necrosis factor-α-induced apoptosis by inhibiting mitogen-activated protein kinase pathway activation and phosphatidylethanolamine externalization. *J Biol Chem.* (2004) 279:45855–64. doi: 10.1074/jbc.M405147200
17. Burg MB. Coordinate regulation of organic osmolytes in renal cells. *Kidney Int.* (1996) 49:1684–5. doi: 10.1038/ki.1996.247
18. Sizeland PC, Chambers ST, Lever M, Bason LM, Robson RA. Organic osmolytes in human and other mammalian kidneys. *Kidney Int.* (1993) 43:448–53. doi: 10.1038/ki.1993.66
19. Gai Z, Wang T, Visentin M, Kullak-Ublick GA, Fu X, Wang Z. Lipid accumulation and chronic kidney disease. *Nutrients.* (2019) 11:722. doi: 10.3390/nu11040722
20. Liu ZX, Hong Q, Peng DH, Yang Y, Yu WL, Shuai H, et al. Evaluation of serum free fatty acids in chronic renal failure: evidence from a rare case with undetectable serum free fatty acids and population data. *Lipids Health Dis.* (2019) 18:151. doi: 10.1186/s12944-019-1093-5
21. Packer M. Role of deranged energy deprivation signaling in the pathogenesis of cardiac and renal disease in states of perceived nutrient overabundance. *Circulation.* (2020) 141:2095–105. doi: 10.1161/CIRCULATIONAHA.119.045561
22. Weld KJ, Montiglio C, Bush AC, Patricia SD, Schwertner HA, Hensley DM, et al. Predicting irreparable renal ischemic injury using a real-time marker in the porcine model. *J Urol.* (2008) 180:2218–25. doi: 10.1016/j.juro.2008.07.017
23. Li M, Wang X, Aa J, Qin W, Zha W, Ge Y, et al. GC/TOFMS analysis of metabolites in serum and urine reveals metabolic perturbation of TCA cycle in db/db mice involved in diabetic nephropathy. *Am J Physiol Renal Physiol.* (2013) 304:F1317–24. doi: 10.1152/ajprenal.00536.2012
24. Runyan CE, Schnaper HW, Poncelet AC. Smad3 and PKCdelta mediate TGF-beta1-induced collagen I expression in human mesangial cells. *Am J Physiol Renal Physiol.* (2003) 285:F413–22. doi: 10.1152/ajprenal.00082.2003
25. Tang WH, Wang Z, Kennedy DJ, Wu Y, Buffa JA, Agatisa-Boyle B, et al. Gut microbiota-dependent trimethylamine N-oxide (TMAO) pathway contributes to both development of renal insufficiency and mortality risk in chronic kidney disease. *Circ Res.* (2015) 116:448–55. doi: 10.1161/CIRCRESAHA.116.305360
26. Bloc R, Kakinami L, Liebman S, Shearer GC, Kramer H, Tsai M. *Cis*-vaccenic acid and the Framingham risk score predict chronic kidney disease: The multi-ethnic study of atherosclerosis (MESA). *Prostag Leukotr Ess.* (2012) 86:175–82. doi: 10.1016/j.plefa.2012.02.009

Conflict of Interest: The authors declare that the research was conducted in the absence of any commercial or financial relationships that could be construed as a potential conflict of interest.

frontiers in Medicine

ORIGINAL RESEARCH
published: 25 May 2021
doi: 10.3389/fmed.2021.632097

Deep Learning-Based Quantification of Visceral Fat Volumes Predicts Posttransplant Diabetes Mellitus in Kidney Transplant Recipients

Ji Eun Kim[1], Sang Joon Park[2], Yong Chul Kim[3], Sang-Il Min[4], Jongwon Ha[4], Yon Su Kim[3], Soon Ho Yoon[2,5] and Seung Seok Han[3]**

[1] Department of Internal Medicine, Korea University Guro Hospital, Seoul, South Korea, [2] Department of Radiology, Seoul National University College of Medicine, Seoul, South Korea, [3] Department of Internal Medicine, Seoul National University College of Medicine, Seoul, South Korea, [4] Department of Surgery, Seoul National University College of Medicine, Seoul, South Korea, [5] Department of Radiology, UMass Memorial Medical Center, Worcester, MA, United States

OPEN ACCESS

Edited by:
Marian Klinger,
Opole University, Poland

Reviewed by:
Hoon Young Choi,
Yonsei University, South Korea
Katarzyna Madziarska,
Wroclaw Medical University, Poland

***Correspondence:**
Seung Seok Han
hansway80@gmail.com
Soon Ho Yoon
yshoka@gmail.com

Specialty section:
This article was submitted to Nephrology, a section of the journal Frontiers in Medicine

Received: *22 November 2020*
Accepted: *30 April 2021*
Published: *25 May 2021*

Citation:
Kim JE, Park SJ, Kim YC, Min S-I, Ha J, Kim YS, Yoon SH and Han SS (2021) Deep Learning-Based Quantification of Visceral Fat Volumes Predicts Posttransplant Diabetes Mellitus in Kidney Transplant Recipients. Front. Med. 8:632097. doi: 10.3389/fmed.2021.632097

Background: Because obesity is associated with the risk of posttransplant diabetes mellitus (PTDM), the precise estimation of visceral fat mass before transplantation may be helpful. Herein, we addressed whether a deep-learning based volumetric fat quantification on pretransplant computed tomographic images predicted the risk of PTDM more precisely than body mass index (BMI).

Methods: We retrospectively included a total of 718 nondiabetic kidney recipients who underwent pretransplant abdominal computed tomography. The 2D (waist) and 3D (waist or abdominal) volumes of visceral, subcutaneous, and total fat masses were automatically quantified using the deep neural network. The predictability of the PTDM risk was estimated using a multivariate Cox model and compared among the fat parameters using the areas under the receiver operating characteristic curves (AUROCs).

Results: PTDM occurred in 179 patients (24.9%) during the median follow-up period of 5 years (interquartile range, 2.5–8.6 years). All the fat parameters predicted the risk of PTDM, but the visceral and total fat volumes from 2D and 3D evaluations had higher AUROC values than BMI did, and the best predictor of PTDM was the 3D abdominal visceral fat volumes [AUROC, 0.688 (0.636–0.741)]. The addition of the 3D abdominal VF volume to the model with clinical risk factors increased the predictability of PTDM, but BMI did not.

Conclusions: A deep-learning based quantification of visceral fat volumes on computed tomographic images better predicts the risk of PTDM after kidney transplantation than BMI.

Keywords: artificial intelligence, body mass index, fat, deep learning, kidney transplantation, post-transplant diabetes mellitus

INTRODUCTION

Posttransplant diabetes mellitus (PTDM), a metabolic complication after kidney transplantation, occurs in 10–40% of kidney recipients depending on the patient characteristics (1–4). Because PTDM correlates with adverse outcomes such as cardiovascular events and death, it is crucial to predict PTDM precisely and manage its occurrence in advance (4–6). Several risk factors for PTDM have been identified, such as obesity (7, 8), high blood pressure (9), immunosuppressive agents (10–12), infection with hepatitis C virus (4, 13), hyperuricemia (13), and hypertriglyceridemia (13). High values of body mass index (BMI), one of the crude measures for body fat, predict the risk of DM (14), but this relationship has not necessarily happened in PTDM (4, 15–18).

BMI is a simple and convenient measure for adiposity but does not reflect body shape and fat distribution, which leads to inevitable limitations in the precise estimation of visceral fat (VF) volumes (19). Furthermore, the relationship with worse outcomes may depend on the race as Asians have a higher proportion of body fat mass for a given BMI than Caucasians (20). A bioelectrical impedance analysis, dual-energy X-ray absorptiometry, and cross-sectional computed tomography (CT) have been used to substitute BMI (21–25). Analyzing body components in cross-sectional CT imaging is regarded as a reference standard. However, its clinical use remains limited because the analysis requires a considerable amount of time and effort of specialists.

The introduction of a deep-learning algorithm in medicine attempts to change the paradigm of the clinical process (26, 27), particularly of diagnostic imaging (28). Deep learning algorithms have shown potential in automatic fat quantification on CT images and thus can reduce the laborious work involved in fat segmentation (29). Herein, we addressed whether deep-learning-based volumetric fat quantification on CT images after segmenting body fat distribution predicted the risk of PTDM more precisely than BMI.

METHODS

Study Subjects

The study was approved by the institutional review board of the Seoul National University Hospital (no. H-1907-072-1047) and complied with the Declaration of Helsinki. Among 1,377 adults (aged $\geq$ 18 years) who consecutively underwent kidney transplantation at Seoul National University Hospital between 2003 and 2017, 983 patients who underwent abdominal CT scans within 1 year before transplantation were initially reviewed. Of these, 38 patients in whom the CT scan did not sufficiently cover the abdominal waist from the iliac crest to the lower margin of the ribs and 227 patients who had DM before transplantation were excluded. Accordingly, 718 patients were analyzed in the present study. Under the review board's approval, informed consent was waived.

Data Collection and Definition

Baseline information such as age, sex, weight, height, type of pretransplant dialysis, donor type (living or deceased), ABO incompatibility, positivity for hepatitis B surface antigen and anti-hepatitis C virus antibody, the number of human leukocyte antigen mismatches, and the immunosuppressive regimens for induction (e.g., basiliximab and anti-thymocyte globulin) and maintenance (e.g., steroid, calcineurin inhibitor, and mycophenolic acid) were collected. A combination therapy of steroids, tacrolimus, and mycophenolic acid was primarily used for maintenance in our center. BMI was calculated as weight (kg)/height (m^2). Laboratory findings such as total cholesterol, high-density lipoprotein cholesterol, triglyceride, and uric acid were collected in the fasting state before kidney transplantation.

TABLE 1 | Baseline characteristics of the study subjects.

Variables	Total (n = 718)
Age (years)	45.2 ± 12.6
Male sex (%)	60.0
Body mass index (kg/m^2)	22.5 ± 3.4
Deceased donor (%)	34.5
Type of pre-transplant dialysis (%)	
Preemptive	14.4
Hemodialysis	66.4
Peritoneal dialysis	19.2
Pre-transplant dialysis duration, months	23 [2–79]
Cause of kidney failure (%)	
Hypertension	9.5
Glomerulonephritis	51.7
Polycystic kidney disease	10.3
Others	28.6
Hypertension (%)	81.8
Positivity for anti-hepatitis C virus antibody (%)	2.1
Positivity for hepatitis B surface antigen (%)	6.7
ABO incompatibility (%)	9.6
Number of HLA mismatch > 3 (%)	39.7
Induction agent (%)	
None	11.8
Basiliximab	85.8
Anti-thymocyte globulin	2.4
Calcineurin inhibitor (%)	
None	2.9
Cyclosporine	8.6
Tacrolimus	88.4
Mycophenolic acid (%)	98.6
Laboratory findings	
Total cholesterol (mg/dL)	159.0 ± 36.7
Triglyceride (mg/dL)	123.7 ± 80.3
HDL cholesterol (mg/dL)	50.2 ± 16.5
LDL cholesterol (mg/dL)	92.4 ± 32.5
Uric acid (mg/dL)	6.0 ± 2.0

HLA, human leukocyte antigen; HDL, high-density lipoprotein; LDL, low-density lipoprotein.

Low-density lipoprotein cholesterol was calculated using the following formula: total cholesterol – high-density lipoprotein cholesterol – (triglyceride/5).

The primary outcome was PTDM. PTDM was diagnosed when recipients needed antidiabetic medications because of high blood glucose levels. The secondary outcomes were delayed graft function (i.e., the requirement of dialysis within 7 days after transplantation) and biopsy-proven acute rejection such as acute T-cell-mediated and antibody-mediated rejections.

Deep Learning-Based Measurement of 2D and 3D Fat Volumes

All abdominal CT scans were performed using multidetector CT scanners without the intravenous administration of contrast media. The mean interval between CT scanning and transplantation was 91.1 ± 54.5 days. After uploading precontrast volumetric abdominal CT images to commercially available segmentation software (MEDIP Deep Catch v1.0.0.0, MEDICALIP Co. Ltd., Seoul, Korea), a 3D U-Net automatically generated a volumetric mask of 7 compartments in <1.5 min with the recommended specifications (30): skin, bone, muscle, VF, subcutaneous fat (SF), internal organs with vessels, and central nervous system. The network was developed using 39,286 labeled whole-body CT images and provided an average segmentation accuracy for VF and SF of 92.4–98.9% and 94.1–99.7%, respectively, in internal and external validation datasets of whole-body CT scans. After the volumetric segmentation of VF and SF, the range of the whole abdominal waist was automatically extracted between the iliac crest and the margin of the lowest rib, with subsequent calculation of the 3D volumes of VF and SF in the whole abdominal or waist area and 2D volumes at the midpoint of the abdominal waist (31). An experienced body radiologist (SH Yoon) identified whether the results of segmentation and the range of the abdominal waist were appropriate. VF and SF volumes were summed to calculate total fat (TF) volumes. All of the TF, VF, and SF volumes were normalized by the height squared (m^2) (32).

Statistical Analysis

All statistical analyses were performed with the STATA (version 15.1; StataCorp, College Station, TX, USA) and R (version 3.5.0; R Core Team) software. Continuous variables are

TABLE 2 | 2D and 3D fat volumes and their correlations with body mass index.

Parameters	Mean ± standard deviation	r^2	*P*
2D volume of waist TF	0.66 ± 0.41 m^2/m^2	0.539	<0.001
2D volume of waist VF	0.28 ± 0.23 m^2/m^2	0.426	<0.001
2D volume of waist SF	0.38 ± 0.23 m^2/m^2	0.420	<0.001
3D volume of waist TF	0.41 ± 0.36 m^3/m^2	0.448	<0.001
3D volume of waist VF	0.17 ± 0.18 m^3/m^2	0.399	<0.001
3D volume of waist SF	0.24 ± 0.21 m^3/m^2	0.381	<0.001
3D volume of abdominal TF	2.08 ± 1.42 m^3/m^2	0.526	<0.001
3D volume of abdominal VF	0.76 ± 0.57 m^3/m^2	0.466	<0.001
3D volume of abdominal SF	1.32 ± 0.90 m^3/m^2	0.454	<0.001

TF, total fat; VF, visceral fat; SF, subcutaneous fat.

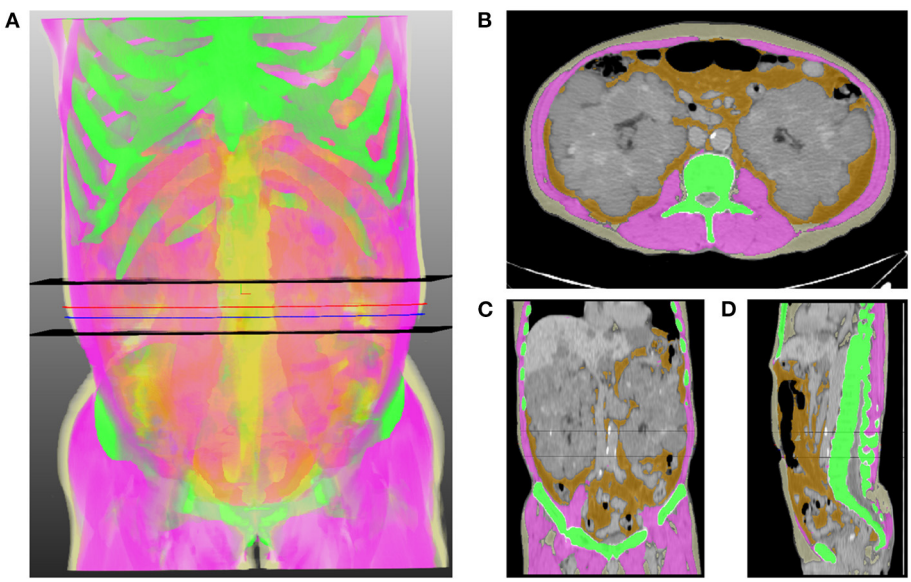

FIGURE 1 | Representative image of the volumetric extraction of body compositions. **(A)** 3D translucent image shows a volumetric segmentation of muscle (pink), subcutaneous fat (light yellow), abdominal visceral fat (orange), and bone (green) using a deep neural network. Two black horizontal planes indicate the range of the abdominal waist between the lowest end of the rib cage and the uppermost end of the iliac crest. Blue and red lines indicate the levels of the umbilicus and the middle of the abdominal waist, respectively. Axial **(B)**, coronal **(C)**, and sagittal **(D)** images show the results of segmentation, which are overlaid on orthogonal cross-sectional images.

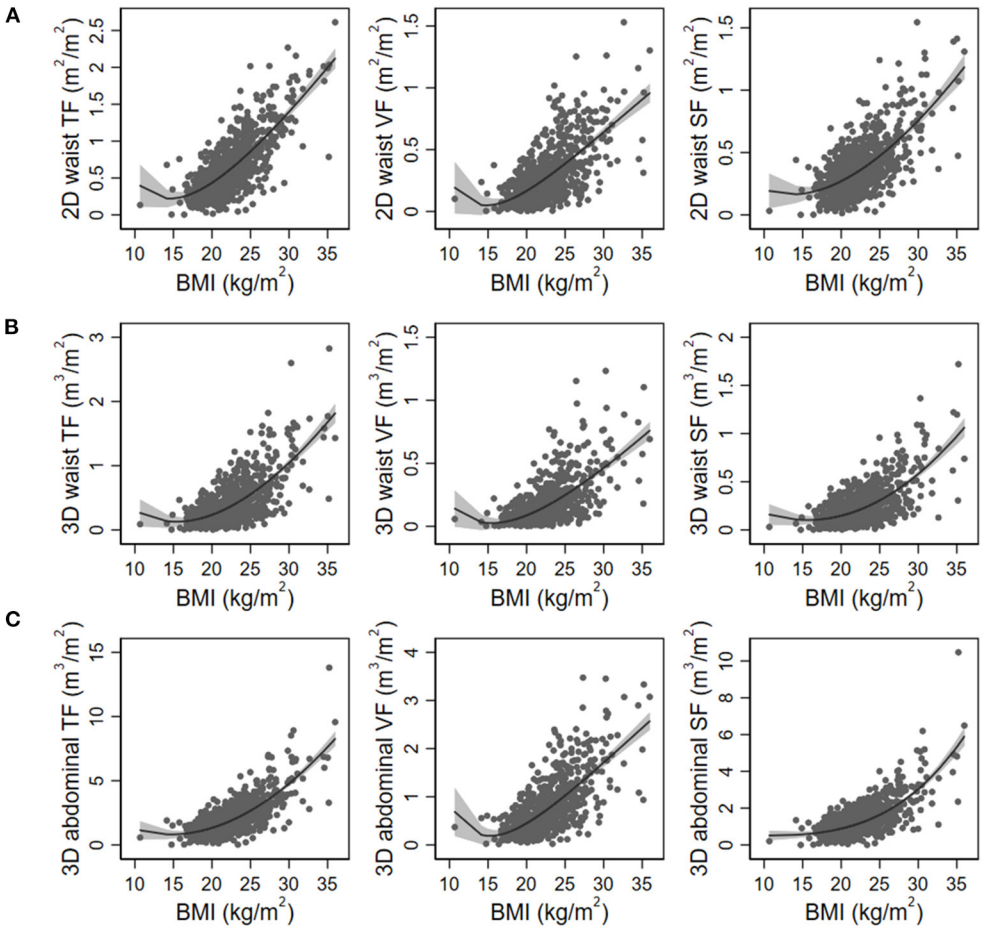

FIGURE 2 | Nonlinear regression models of body mass index (BMI) with 2D waist **(A)**, 3D waist **(B)**, and 3D abdominal fat volumes **(C)**. The gray area indicates 95% confidence intervals. TF, total fat; VF, visceral fat; SF, subcutaneous fat.

TABLE 3 | Risk of posttransplant diabetes mellitus according to the fat parameters.

	Model 1		Model 2		Model 3	
Parameters	**HR (95% CI)**	***P***	**HR (95% CI)**	***P***	**HR (95% CI)**	*P*
2D volume of waist TF (per 1 m^2/m^2)	3.71 (2.74–5.04)	<0.001	3.22 (2.31–4.48)	<0.001	3.01 (2.07–4.36)	<0.001
2D volume of waist VF (per 1 m^2/m^2)	8.73 (5.36–14.22)	<0.001	5.88 (3.44–10.05)	<0.001	5.74 (3.07–10.73)	<0.001
2D volume of waist SF (per 1 m^2/m^2)	5.64 (3.25–9.79)	<0.001	6.45 (3.50–11.90)	<0.001	4.94 (2.55–9.57)	<0.001
3D volume of waist TF (per 1 m^3/m^2)	3.05 (2.26–4.11)	<0.001	2.98 (2.17–4.09)	<0.001	2.47 (1.74–3.50)	<0.001
3D volume of waist VF (per 1 m^3/m^2)	9.45 (5.36–16.65)	<0.001	7.41 (4.04–13.62)	<0.001	6.45 (3.15–13.23)	<0.001
3D volume of waist SF (per 1 m^3/m^2)	5.31 (3.04–9.26)	<0.001	6.24 (3.49–11.16)	<0.001	4.02 (2.15–7.53)	<0.001
3D volume of abdominal TF (per 1 m^3/m^2)	1.34 (1.24–1.44)	<0.001	1.30 (1.21–1.41)	<0.001	1.24 (1.14–1.35)	<0.001
3D volume of abdominal VF (per 1 m^3/m^2)	2.41 (1.98–2.94)	<0.001	2.22 (1.78–2.77)	<0.001	2.10 (1.64–2.70)	<0.001
3D volume of abdominal SF (per 1 m^3/m^2)	1.42 (1.27–1.59)	<0.001	1.40 (1.25–1.57)	<0.001	1.29 (1.13–1.46)	<0.001
Body mass index (per 1 kg/m^2)	1.12 (1.07–1.16)	<0.001	1.10 (1.05–1.15)	<0.001	1.08 (1.03–1.13)	0.001

Model 1: Unadjusted.

Model 2: Adjusted for age and sex.

Model 3: Adjusted for age, sex and variables which had P < 0.1 in univariate analysis (ABO incompatibility, induction agents, triglyceride level, high density lipoprotein cholesterol level and positivity for anti-hepatitis C virus antibody).

HR, hazard ratio; CI, confidence interval; TF, total fat; VF, visceral fat; SF, subcutaneous fat.

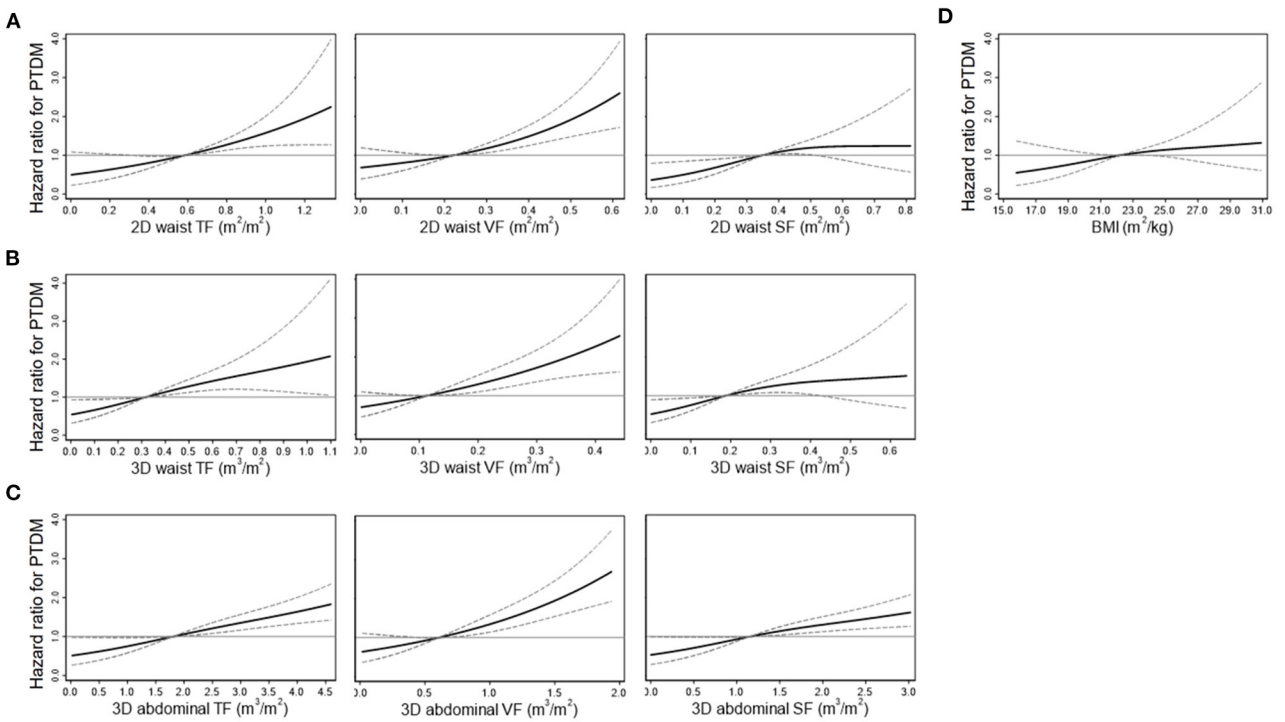

FIGURE 3 | Restricted cubic spline curves for the risk of posttransplant diabetes mellitus (PTDM) according to the 2D waist **(A)**, 3D waist **(B)**, 3D abdominal fat volumes **(C)**, and body mass index (BMI) **(D)**. Curves were adjusted by multiple variables, such as age, sex, ABO incompatibility, anti-hepatitis C virus antibody, the induction agents, and serum levels of high-density lipoprotein cholesterol. Solid and dashed lines indicate hazard ratios and 95% confidence intervals, respectively. TF, total fat; VF, visceral fat; SF, subcutaneous fat.

presented as the mean and standard deviation or median and interquartile ranges and compared by Student's *t*-test or the Wilcoxon rank-sum test, respectively. Categorical variables are presented as percentages and compared by the chi-squared test. Ordinary least-squares linear regression and fractional polynomial regression with continuous variables were used to determine a nonlinear relationship. Univariate and multivariable Cox regression models were applied to estimate the hazard ratio of the risks of outcomes. The Stata function *mkspline* was used to create a restricted cubic spline function to describe the hazard ratio of outcomes according to the fat parameters. The areas under the receiver operating characteristic curves (AUROCs) for predicting the risk of PTDM were compared between fat parameters using permutation tests (33, 34). The AUROCs for cumulative predictive probability depending on the follow-up duration were drawn using the *survivalROC* package in R. For the risk of delayed graft function, a multivariate logistic regression model was applied. A *P*-value of < 0.05 was considered significant.

RESULTS

Baseline Characteristics

The mean age was 45.2 ± 12.6 years old, and 431 patients (60.0%) were male. A total of 81.8% of patients were treated with anti-hypertensive agents. A total of 65.5% of patients received transplants from living donors. The mean preoperative BMI was 22.5 ± 3.4 kg/m^2. Other baseline characteristics of kidney recipients are shown in **Table 1**.

Fat Volume Parameters and Their Correlation With BMI

Figure 1 shows the schematic diagram to measure 2D waist, 3D waist, and 3D abdominal fat volumes using the deep neural network algorithm on 3D-reconstructed CT images. The mean values of 2D waist, 3D waist, and 3D abdominal TF volumes were 0.66 ± 0.41, 0.41 ± 0.36, and 2.08 ± 1.42 m^3/m^2, respectively. Although all the 2D and 3D fat volumes correlated with BMI (**Table 2**), their coefficients of determination (r^2) in linear regression models were <0.6. When the nonlinear relationship was subsequently applied, a J-shaped relationship, but not a linear one, was shown between them (**Figure 2**).

Fat Volume Parameters and the Risk of PTDM

During the median follow-up duration of 5 years (2.5–8.6 years), PTDM occurred in 179 patients (24.9%). The prevalence of PTDM was 13.2 and 18.1% at 1 year and 3 years after transplantation, respectively. Among the baseline

clinical variables, age, ABO incompatibility, induction regimens, and serum levels of high-density lipoprotein cholesterol were associated with the risk of PTDM (**Supplementary Table 1**). All 2D and 3D fat parameters and BMI were associated with the risk of PTDM irrespective of adjustment for multiple variables (**Table 3**). When a nonlinear relationship was applied, the relationship with the PTDM risk seemed to be more prominent in the VF and TF volumes compared with the SF volumes and BMI (**Figure 3**).

The AUROCs for predicting the 3-year risk of PTDM were higher in VF and TF volumes from 2D and 3D quantification than in BMI (**Table 4**). The highest value was identified in 3D abdominal VF volumes. The corresponding curves support these results (**Supplementary Figure 1**). When the cumulative AUROCs were evaluated, VF volumes had higher values than BMI irrespective of the follow-up period (**Supplementary Figure 2**). We evaluated whether the addition of fat parameters to the risk model with other clinical factors, which had $P < 0.05$ in **Supplementary Table 1**, increased the overall predictability for the 3-year PTDM. The 3D abdominal VF volumes elevated the predictability of the model when added ($P = 0.015$), but BMI did not ($P = 0.206$). The corresponding ROC curves support these results (**Figure 4**).

TABLE 4 | Area under the receiver operating characteristic curves of fat parameters in predicting 3-year posttransplant diabetes mellitus.

Parameters	AUROC (95% CI)	*P*
2D volume of waist TF	0.684 (0.632–0.735)	0.001
2D volume of waist VF	0.688 (0.635–0.740)	0.001
2D volume of waist SF	0.628 (0.576–0.679)	0.532
3D volume of waist TF	0.669 (0.617–0.720)	0.023
3D volume of waist VF	0.685 (0.634–0.735)	0.002
3D volume of waist SF	0.628 (0.575–0.681)	0.561
3D volume of abdominal TF	0.672 (0.619–0.724)	0.008
3D volume of abdominal VF	0.688 (0.636–0.741)	< 0.001
3D volume of abdominal SF	0.634 (0.581–0.687)	0.378
Body mass index	0.612 (0.559–0.664)	Reference

AUROC, area under the receiver operating characteristic curve; CI, confidence interval; TF, total fat; VF, visceral fat; SF, subcutaneous fat.

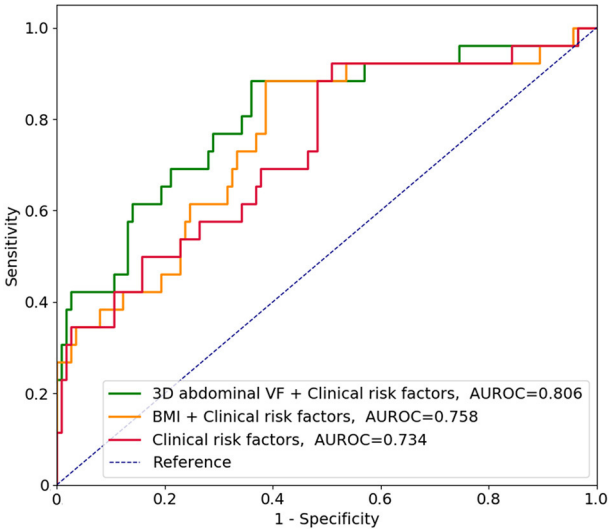

FIGURE 4 | Receiver operating characteristic curves in predicting the 3-year risk of posttransplant diabetes mellitus along with clinical risk factors. According to **Supplementary Table 1**, clinical risk factors included age, ABO incompatibility, induction regimens, and serum levels of high-density lipoprotein cholesterol. VF, visceral fat; AUROC, area under the receiver operating characteristic curve; BMI, body mass index.

Association With Other Transplant Outcomes

Because high fat volumes may confer the risk of rejection and delayed graft function according to previous studies (35, 36), other risks such as delayed graft function and rejections were assessed. For delayed graft function, the 3D volumes of abdominal VF and TF were predictors with odds ratios of 2.08 (1.12–3.87) and 1.33 (1.01–1.75) per 1-unit increase, respectively, but other fat parameters, including BMI, were not (**Supplementary Table 2**). None of the fat parameters were associated with the risk of rejections in the present cohort (**Supplementary Table 3**).

DISCUSSION

The present study used the deep learning algorithm to quantify the 2D and 3D fat volumes in pretransplant CT images and identified that their relationship with BMI was not linear. Although all the fat parameters were associated with the risk of PTDM, the predictability was greater in VF volumes than in BMI. The addition of 3D abdominal VF volume to the model with clinical risk factors increased the predictability of PTDM, but BMI did not. The present results indicate that precise quantification of fat volumes by deep learning algorithm may help to alert clinicians of the risk of PTDM.

Precise measurement of fat components is a critical issue in classifying risky patients based on obesity-related outcomes. BMI, which is based on weight and height, is a commonly used method to measure fat mass, but it does not take into account other body compositions such as muscle and bone. BMI seems to be an insufficient marker to assess PTDM based on inconsistent research results (16–18). VF components have been revealed as a risk factor for metabolic and cardiovascular diseases in the general population, independent of BMI (37). VF was related to glucose intolerance in kidney recipients (38). Based on both the previous and present results, the estimation of VF volumes is needed to predict the risk of PTDM more precisely than BMI.

Abdominal imaging methods, including CT, have been used to assess the volumes of fat components using computer calculator more than before (9, 39–41). This method has been validated in several studies, but optimization is needed to reduce bias and the time consumed by the task (42–44). The present study applied

a deep learning algorithm to automatically segment the VF and SF components and exclude muscle and bone, which eventually detected the fat volumes quickly and unbiasedly for a number of images. Because kidney transplant recipients undergo abdominal CT scans for routine preoperative work-up, our approach using readily available software is implementable for more accurate prediction of PTDM than BMI, which may help in designing a plan to prevent PTDM occurrence.

Despite the valuable findings of our study, there are some limitations that need to be addressed. Waist circumference, a useful method for fat volume, was not evaluated. Follow-up CT images may be helpful to predict the risk of PTDM, but the present study could not obtain these data. Other unidentified factors, such as diet and exercise information, could have an interacting effect on the relationships observed in the study. Only Korean patients were analyzed, and no other populations were analyzed. Nevertheless, the primary purpose of the study was to address the application of the deep-learning-algorithm-based quantification of 2D and 3D fat volumes in kidney recipients, not to build a final model. A prospective application and adjustment of our algorithm to other cohorts is warranted in future studies.

Quantification of VF components with a deep learning algorithm successfully predicts PTDM, which is better than the measurement of BMI. Deep-learning-based approaches are increasingly used in many clinical aspects, and the present results will be a basis for application in the transplant field.

DATA AVAILABILITY STATEMENT

The raw data supporting the conclusions of this article will be made available by the authors, without undue reservation.

ETHICS STATEMENT

The studies involving human participants were reviewed and approved by the Institutional Review Board of the Seoul National University Hospital. Written informed consent for participation was not required for this study in accordance with the national legislation and the institutional requirements.

AUTHOR CONTRIBUTIONS

JK: data analysis and interpretation and manuscript drafting. SP: technical support. YCK, S-IM, and JH: data collection. YSK: technical support and supervision. SY and SH: project development, data interpretation, supervision, and manuscript editing. All authors contributed to the article and approved the submitted version.

SUPPLEMENTARY MATERIAL

The Supplementary Material for this article can be found online at: https://www.frontiersin.org/articles/10.3389/fmed.2021.632097/full#supplementary-material

REFERENCES

1. Baron PW, Infante S, Peters R, Tilahun J, Weissman J, Delgado L, et al. Post-transplant diabetes mellitus after kidney transplant in hispanics and caucasians treated with tacrolimus-based immunosuppression. *Ann Transplant.* (2017) 22:309–14. doi: 10.12659/AOT.903079
2. Terjimanian MN, Underwood PW, Cron DC, Augustine JJ, Noon KA, Cote DR, et al. Morphometric age and survival following kidney transplantation. *Clin Transplant.* (2017) 31:e13066. doi: 10.1111/ctr.13066
3. David-Neto E, Lemos FC, Fadel LM, Agena F, Sato MY, Coccuza C, et al. The dynamics of glucose metabolism under calcineurin inhibitors in the first year after renal transplantation in nonobese patients. *Transplantation.* (2007) 84:50–5. doi: 10.1097/01.tp.0000267647.03550.22
4. Kasiske BL, Snyder JJ, Gilbertson D, Matas AJ. Diabetes mellitus after kidney transplantation in the United States. *Am J Transplant.* (2003) 3:178–85. doi: 10.1034/j.1600-6143.2003.00010.x
5. Hjelmesaeth J, Hartmann A, Leivestad T, Holdaas H, Sagedal S, Olstad M, et al. The impact of early-diagnosed new-onset post-transplantation diabetes mellitus on survival and major cardiac events. *Kidney Int.* (2006) 69:588–95. doi: 10.1038/sj.ki.5000116
6. Ducloux D, Kazory A, Chalopin JM. Posttransplant diabetes mellitus and atherosclerotic events in renal transplant recipients: a prospective study. *Transplantation.* (2005) 79:438–43. doi: 10.1097/01.TP.0000151799.98612.EB
7. Chang S, Jiang J. Association of body mass index and the risk of new-onset diabetes after kidney transplantation: a meta-analysis. *Transplant Proc.* (2018) 50:1316–25. doi: 10.1016/j.transproceed.2018.02.075
8. Parikh CR, Klem P, Wong C, Yalavarthy R, Chan L. Obesity as an independent predictor of posttransplant diabetes mellitus. *Transplant Proc.* (2003) 35:2922–6. doi: 10.1016/j.transproceed.2003.10.074
9. Cron DC, Noon KA, Cote DR, Terjimanian MN, Augustine JJ, Wang SC, et al. Using analytic morphomics to describe body composition associated with post-kidney transplantation diabetes mellitus. *Clin Transplant.* (2017) 31:e13040. doi: 10.1111/ctr.13040
10. Ciancio G, Burke GW, Gaynor JJ, Ruiz P, Roth D, Kupin W, et al. A randomized long-term trial of tacrolimus/sirolimus versus tacrolimums/mycophenolate versus cyclosporine/sirolimus in renal transplantation: three-year analysis. *Transplantation.* (2006) 81:845–52. doi: 10.1097/01.tp.0000203894.53714.27
11. Ekberg H, Bernasconi C, Noldeke J, Yussim A, Mjornstedt L, Erken U, et al. Cyclosporine, tacrolimus and sirolimus retain their distinct toxicity profiles despite low doses in the symphony study. *Nephrol Dial Transplant.* (2010) 25:2004–10. doi: 10.1093/ndt/gfp778
12. Laskow DA, Vincenti F, Neylan JF, Mendez R, Matas AJ. An open-label, concentration-ranging trial of FK506 in primary kidney transplantation: a report of the United States multicenter FK506 kidney transplant group. *Transplantation.* (1996) 62:900–5. doi: 10.1097/00007890-199610150-00005
13. Sharif A, Cohney S. Post-transplantation diabetes-state of the art. *Lancet Diabetes Endocrinol.* (2016) 4:337–49. doi: 10.1016/S2213-8587(15)00387-3
14. Hanson RL, Narayan KM, McCance DR, Pettitt DJ, Jacobsson LT, Bennett PH, et al. Rate of weight gain, weight fluctuation, and incidence of NIDDM. *Diabetes.* (1995) 44:261–6. doi: 10.2337/diab.44.3.261
15. Numakura K, Satoh S, Tsuchiya N, Horikawa Y, Inoue T, Kakinuma H, et al. Clinical and genetic risk factors for posttransplant diabetes mellitus in adult renal transplant recipients treated with tacrolimus. *Transplantation.* (2005) 80:1419–24. doi: 10.1097/01.tp.0000181142.82649.e3
16. Sumrani NB, Delaney V, Ding ZK, Davis R, Daskalakis P, Friedman EA, et al. Diabetes mellitus after renal transplantation in the cyclosporine era–an analysis of risk factors. *Transplantation.* (1991) 51:343–7. doi: 10.1097/00007890-199102000-00014

17. Montori VM, Basu A, Erwin PJ, Velosa JA, Gabriel SE, Kudva YC. Posttransplantation diabetes: a systematic review of the literature. *Diabetes Care.* (2002) 25:583–92. doi: 10.2337/diacare.25.3.583
18. Gourishankar S, Jhangri GS, Tonelli M, Wales LH, Cockfield SM. Development of diabetes mellitus following kidney transplantation: a Canadian experience. *Am J Transplant.* (2004) 4:1876–82. doi: 10.1111/j.1600-6143.2004.00591.x
19. Zafon C. Oscillations in total body fat content through life: an evolutionary perspective. *Obes Rev.* (2007) 8:525–30. doi: 10.1111/j.1467-789X.2007.00377.x
20. Deurenberg P, Deurenberg-Yap M, Guricci S. Asians are different from caucasians and from each other in their body mass index/body fat per cent relationship. *Obes Rev.* (2002) 3:141–6. doi: 10.1046/j.1467-789X.2002.00065.x
21. Browning LM, Mugridge O, Chatfield MD, Dixon AK, Aitken SW, Joubert I, et al. Validity of a new abdominal bioelectrical impedance device to measure abdominal and visceral fat: comparison with MRI. *Obesity.* (2010) 18:2385–91. doi: 10.1038/oby.2010.71
22. Ryo M, Maeda K, Onda T, Katashima M, Okumiya A, Nishida M, et al. A new simple method for the measurement of visceral fat accumulation by bioelectrical impedance. *Diabetes Care.* (2005) 28:451–3. doi: 10.2337/diacare.28.2.451
23. Kim SK, Kim HJ, Hur KY, Choi SH, Ahn CW, Lim SK, et al. Visceral fat thickness measured by ultrasonography can estimate not only visceral obesity but also risks of cardiovascular and metabolic diseases. *Am J Clin Nutr.* (2004) 79:593–9. doi: 10.1093/ajcn/79.4.593
24. Klopfenstein BJ, Kim MS, Krisky CM, Szumowski J, Rooney WD, Purnell JQ. Comparison of 3 T MRI and CT for the measurement of visceral and subcutaneous adipose tissue in humans. *Br J Radiol.* (2012) 85:e826–30. doi: 10.1259/bjr/57987644
25. Borkan GA, Gerzof SG, Robbins AH, Hults DE, Silbert CK, Silbert JE. Assessment of abdominal fat content by computed tomography. *Am J Clin Nutr.* (1982) 36:172–7. doi: 10.1093/ajcn/36.1.172
26. Patel VL, Shortliffe EH, Stefanelli M, Szolovits P, Berthold MR, Bellazzi R, et al. The coming of age of artificial intelligence in medicine. *Artif Intell Med.* (2009) 46:5–17. doi: 10.1016/j.artmed.2008.07.017
27. Darcy AM, Louie AK, Roberts LW. Machine learning and the profession of medicine. *JAMA.* (2016) 315:551–2. doi: 10.1001/jama.2015.18421
28. Jha S, Topol EJ. Adapting to artificial intelligence: radiologists and pathologists as information specialists. *JAMA.* (2016) 316:2353–4. doi: 10.1001/jama.2016.17438
29. Weston AD, Korfiatis P, Kline TL, Philbrick KA, Kostandy P, Sakinis T, et al. Automated abdominal segmentation of CT scans for body composition analysis using deep learning. *Radiology.* (2019) 290:669–79. doi: 10.1148/radiol.2018181432
30. *MEDICAL IP.* (2018). Available online at: http://www.medicalip.com/sub.php?p=deepcatch (accessed June 18, 2020).
31. Lean ME, Han TS, Deurenberg P. Predicting body composition by densitometry from simple anthropometric measurements. *Am J Clin Nutr.* (1996) 63:4–14. doi: 10.1093/ajcn/63.1.4
32. Schutz Y, Kyle UU, Pichard C. Fat-free mass index and fat mass index percentiles in caucasians aged 18-98 y. *Int J Obes Relat Metab Disord.* (2002) 26:953–60. doi: 10.1038/sj.ijo.0802037
33. Bandos AI, Rockette HE, Gur D. A permutation test sensitive to differences in areas for comparing ROC curves from a paired design. *Stat Med.* (2005) 24:2873–93. doi: 10.1002/sim.2149
34. Bandos AI, Rockette HE, Gur D. A permutation test for comparing ROC curves in multireader studies a multi-reader ROC, permutation test. *Acad Radiol.* (2006) 13:414–20. doi: 10.1016/j.acra.2005.12.012
35. Kwan JM, Hajjiri Z, Metwally A, Finn PW, Perkins DL. Effect of the obesity epidemic on kidney transplantation: obesity is independent of diabetes as a risk factor for adverse renal transplant outcomes. *PLoS ONE.* (2016) 11:e0165712. doi: 10.1371/journal.pone.0165712
36. Molnar MZ, Kovesdy CP, Mucsi I, Bunnapradist S, Streja E, Krishnan M, et al. Higher recipient body mass index is associated with post-transplant delayed kidney graft function. *Kidney Int.* (2011) 80:218–24. doi: 10.1038/ki.2011.114
37. Zhang M, Hu T, Zhang S, Zhou L. Associations of different adipose tissue depots with insulin resistance: a systematic review and meta-analysis of observational studies. *Sci Rep.* (2015) 5:18495. doi: 10.1038/srep18495
38. von During ME, Jenssen T, Bollerslev J, Asberg A, Godang K, Eide IA, et al. Visceral fat is better related to impaired glucose metabolism than body mass index after kidney transplantation. *Transpl Int.* (2015) 28:1162–71. doi: 10.1111/tri.12606
39. Englesbe MJ, Lee JS, He K, Fan L, Schaubel DE, Sheetz KH, et al. Analytic morphomics, core muscle size, and surgical outcomes. *Ann Surg.* (2012) 256:255–61. doi: 10.1097/SLA.0b013e31826028b1
40. Krishnamurthy V, Zhang P, Ethiraj S, Enchakalody B, Waljee AK, Wang L, et al. Use of analytic morphomics of liver, spleen, and body composition to identify patients at risk for cirrhosis. *Clin Gastroenterol Hepatol.* (2015) 13:360–8 e5. doi: 10.1016/j.cgh.2014.07.042
41. Smith SR, Lovejoy JC, Greenway F, Ryan D, deJonge L, de la Bretonne J, et al. Contributions of total body fat, abdominal subcutaneous adipose tissue compartments, and visceral adipose tissue to the metabolic complications of obesity. *Metabolism.* (2001) 50:425–35. doi: 10.1053/meta.2001.21693
42. Sjostrom L, Kvist H, Cederblad A, Tylen U. Determination of total adipose tissue and body fat in women by computed tomography, 40K, and tritium. *Am J Physiol.* (1986) 250(6 Pt 1):E736–45. doi: 10.1152/ajpendo.1986.250.6.E736
43. Maurovich-Horvat P, Massaro J, Fox CS, Moselewski F, O'Donnell CJ, Hoffmann U. Comparison of anthropometric, area- and volume-based assessment of abdominal subcutaneous and visceral adipose tissue volumes using multi-detector computed tomography. *Int J Obes.* (2007) 31:500–6. doi: 10.1038/sj.ijo.0803454
44. Kvist H, Chowdhury B, Grangard U, Tylen U, Sjostrom L. Total and visceral adipose-tissue volumes derived from measurements with computed tomography in adult men and women: predictive equations. *Am J Clin Nutr.* (1988) 48:1351–61. doi: 10.1093/ajcn/48.6.1351

Conflict of Interest: SP is the CEO of MEDICALIP Co. Ltd., Seoul, Korea.

The remaining authors declare that the research was conducted in the absence of any commercial or financial relationships that could be construed as a potential conflict of interest.

frontiers in Medicine

ORIGINAL RESEARCH
published: 26 May 2021
doi: 10.3389/fmed.2021.671798

Sphingomyelin and Medullary Sponge Kidney Disease: A Biological Link Identified by Omics Approach

*Simona Granata[1], Maurizio Bruschi[2], Michela Deiana[3], Andrea Petretto[4], Gianmarco Lombardi[1], Alberto Verlato[1], Rossella Elia[1], Giovanni Candiano[2], Giovanni Malerba[3], Giovanni Gambaro[1] and Gianluigi Zaza[1]**

[1] Renal Unit, Department of Medicine, University-Hospital of Verona, Verona, Italy, [2] Laboratory of Molecular Nephrology, Istituto Pediatrico di Ricovero e Cura a Carattere Scientifico (IRCCS) Istituto Giannina Gaslini, Genova, Italy, [3] Section of Biology and Genetics, Department of Neuroscience, Biomedicine and Movement Sciences, University of Verona, Verona, Italy, [4] Core Facilities - Clinical Proteomics and Metabolomics, Istituto Pediatrico di Ricovero e Cura a Carattere Scientifico (IRCCS) Istituto Giannina Gaslini, Genoa, Italy

Background: Molecular biology has recently added new insights into the comprehension of the physiopathology of the medullary sponge kidney disease (MSK), a rare kidney malformation featuring nephrocalcinosis and recurrent renal stones. Pathogenesis and metabolic alterations associated to this disorder have been only partially elucidated.

Methods: Plasma and urine samples were collected from 15 MSK patients and 15 controls affected by idiopathic calcium nephrolithiasis (ICN). Plasma metabolomic profile of 7 MSK and 8 ICN patients was performed by liquid chromatography combined with electrospray ionization tandem mass spectrometry (UHPLC–ESI-MS/MS). Subsequently, we reinterrogated proteomic raw data previously obtained from urinary microvesicles of MSK and ICN focusing on proteins associated with sphingomyelin metabolism. Omics results were validated by ELISA in the entire patients' cohort.

Results: Thirteen metabolites were able to discriminate MSK from ICN (7 increased and 6 decreased in MSK vs. ICN). Sphingomyelin reached the top level of discrimination between the two study groups (FC: −1.8, $p < 0.001$). Ectonucleotide pyrophophatase phosphodiesterase 6 (ENPP6) and osteopontin (SPP1) resulted the most significant deregulated urinary proteins in MSK vs. ICN ($p < 0.001$). ENPP6 resulted up-regulated also in plasma of MSK by ELISA.

Conclusion: Our data revealed a specific high-throughput metabolomics signature of MSK and indicated a pivotal biological role of sphingomyelin in this disease.

Keywords: medullary sponge kidney, idiopathic calcium nephrolithiasis, metabolomics, sphingomyelin, proteomics

OPEN ACCESS

Edited by:
Min Chen,
Peking University First Hospital, China

Reviewed by:
Xiaojing Sun,
Peking University First Hospital, China
Tarak Srivastava,
Children's Mercy Hospital, United States

***Correspondence:**
Gianluigi Zaza
gianluigi.zaza@univr.it

Specialty section:
This article was submitted to Nephrology, a section of the journal Frontiers in Medicine

Received: *24 February 2021*
Accepted: *03 May 2021*
Published: *26 May 2021*

Citation:
Granata S, Bruschi M, Deiana M, Petretto A, Lombardi G, Verlato A, Elia R, Candiano G, Malerba G, Gambaro G and Zaza G (2021) Sphingomyelin and Medullary Sponge Kidney Disease: A Biological Link Identified by Omics Approach. Front. Med. 8:671798. doi: 10.3389/fmed.2021.671798

INTRODUCTION

Medullary sponge kidney disease (MSK) is a kidney malformation with a rare frequency in the general population but relatively common in renal stone formers (1). This clinical condition is associated with nephrocalcinosis and renal stones, urinary acidification and concentration alterations, and cysts formation in the precalyceal ducts (1). Its pathogenesis is complex and not fully understood.

MSK development in childhood and its relationship with developmental disorders (e.g., congenital hemihypertrophy and Beckwith–Wiedemann syndrome) and with kidney anomalies (e.g., horse-shoe kidney, unilateral renal aplasia, contralateral congenital small kidney) (2–4) support the hypothesis of an inherited condition. Genetic studies revealed that familial clustering of MSK is common and has an autosomal dominant inheritance with a reduced penetrance and variable expressivity (5, 6). Additionally, mutations in the glial cell line-derived neurotrophic factor (GDNF) and receptor tyrosine kinase (RET) genes, disrupting the "ureteric bud–metanephric mesenchyme" interface, could be responsible of the disease pathogenesis (7, 8).

Moreover, as demonstrated by urinary proteomic analysis, some regulators of epithelial cell differentiation, kidney development, cell migration/adhesion, extracellular matrix organization, and complement may be deregulated in MSK and could serve as non-invasive MSK diagnostic biomarkers (9, 10). Among them laminin subunit alpha 2 (LAMA-2) seems a good candidate.

Laminin, a family of at least 15 αβγ heterotrimeric proteins of the extracellular matrix and a major constituent of the basement membrane (11), mediates the attachment, migration, and organization of cells into tissues during embryonic development by interacting with other extracellular matrix components. Additionally, laminin may have a role in the cysts' formation being responsible of cellular apical pole orientation (12–14). LAMA-2 and other selected proteins could be proposed as diagnostic biomarkers to replace invasive procedures or imaging techniques with low sensitivity (e.g., Intravenous Urography and CT urography).

A subsequent analysis of the protein content of microvesicles/exosomes isolated from urine of MSK and idiopathic calcium nephrolithiasis (ICN) patients identified a core panel of 20 proteins that distinguished the two study groups (15). Among them, three exosome proteins involved in the lectin complement pathway maximized the discrimination between MSK and ICN: Ficolin 1, Mannan-binding lectin serine protease 2 and Complement component 4-binding protein β. This revealed, for the first time, a possible involvement of the complement pathway in MSK. In particular the downregulation of MASP2 together with the upregulation of C4BPB that inhibits the activation of the complement cascade by preventing the formation of the classical C3 and C5 convertases, may reflect the physiological attempt of the kidneys to mitigate the activation of the lectin complement pathway, also to preserve renal function. Indeed, the hyperactivation of complement may induce glomerular and tubulointerstitial injury (16).

Additionally, our group has recently described extra-renal alterations involving the cardiovascular apparatus, the central nervous system, and bone metabolism (17, 18) in MSK patients suggesting that it may be considered a systemic disease. These patients are more prone to develop hypertrophic cardiomyopathy with adipose metaplasia and mitral valve prolapse and bone mineralization defects.

Therefore, to obtain additional information on the molecular mechanisms underlying MSK and to discover systemic factors of this disease, we used an untargeted approach to compare the plasma metabolomic profile of MSK vs. idiopathic calcium nephrolithiasis (ICN) patients, used as control group, and we reinterrogated proteomic raw data previously obtained from urinary microvesicles of MSK and ICN (15) focusing on proteins associated with sphingomyelin metabolism.

TABLE 1 | Main demographic and clinical characteristics of the patients.

	MSK ($n = 15$)	ICN ($n = 15$)	p
Males, *n* (%)	10 (66.7)	8 (53.3)	0.709
Age, years, mean (SD)	55.80 (15.50)	57.33 (14.80)	0.784
Serum creatinine, mg/dL, mean (SD)	0.86 (0.17)	0.82 (0.12)	0.420
Urinary Ca, mg/die, mean (SD)	317 (107)	222 (107)	0.045
Urinary protein, mg/dL, median (IQR)	0.11 (0.06, 0.13)	0.09 (0.00, 0.15)	0.835
Urinary volume, ml/die, mean (SD)	2136 (450)	1635 (542)	0.026

MATERIALS AND METHODS

Patients

A total of 15 adult patients with medullary sponge kidney disease (MSK) and 15 with idiopathic calcium nephrolithiasis (ICN) matched for age, gender, and geographical origin followed up at Renal Unit of University/Hospital of Verona were included in the study. The main demographic and clinical characteristics of the patients have been reported in **Table 1**.

The inclusion criteria for the MSK group were the same as described in our previous study (9). Particularly, patients had both kidneys involved, nephrocalcinosis and/or cysts in at least 2 papillae in each kidney. For MSK, patients had papillary precalyceal ectasias on films obtained at least 10 min after contrast medium injection in the absence of compression maneuvers and signs of obstruction. The X-ray films were reviewed by an independent radiologist to confirm the diagnosis. For ICN patients the inclusion criteria were as follows: calcium stone disease, normal serum creatinine and electrolyte concentrations, and urinary pH $\leq$ 5.5 measured in spot morning urine (after overnight fasting) to exclude tubular acidosis. Major exclusion criteria for ICN were as follows: the presence of endocrine diseases and cystic kidney disorders, nephrocalcinosis, and obstructive nephropathy.

Plasma and urine samples were obtained from all patients enrolled in the study. Whole-blood samples were collected in EDTA-coated tubes. The tubes were centrifuged (1,800 × g for 10 min), and the plasma was extracted and aliquoted. Second morning urine were collected and centrifuged to eliminate cells and debris. The supernatants were divided into aliquots and stored at −80°C until use.

Laboratory data were electronically registered for all patients enrolled. All subjects gave their informed consent for inclusion before they participated in the study. The study was conducted in accordance with the Declaration of Helsinki, and the protocol was approved by the Local Ethics Committee (AOUI Verona, 1312CESC).

Sample Preparation and Set-Up for Metabolomics

Plasma samples from 7 MSK patients and 8 controls affected by idiopathic calcium nephrolithiasis (ICN) were used for metabolomics using liquid chromatography combined with electrospray ionization tandem mass spectrometry (UHPLC–ESI-MS/MS).

Sample preparation was performed according to standard protocols (19). MS setup: plasma metabolites were detected using liquid chromatography combined with electrospray ionization tandem mass spectrometry (HPLC–ESI-MS/MS). The analytic system consists of an Accela 1250 pump, Accela autosampler and a LTQ Orbitrap Velos mass spectrometer (Thermo Scientific, USA). The analytes were separated on Kinetex C18 100 mm × 2.1 mm × 1.7 um and mobile phase [solvent A: aqueous solution of acetic acid (pH 2); solvent B: methanol] in gradient elution at a flow rate of 300 ul/min. The HPLC elution program was as follows: 5% B (2 Min), 30% B (linear increase in 1 Min), 30% B (5 Min), 5% B (linear decrease in 1 min), 5% B (3 min). The column temperature was maintained at 25°C. The injection volume was 5 ul. The metabolites were detected both in the positive (ESI +) and in the negative (ESI –) ionization mode (20).

Processing of Raw Data

Raw mass spectrometry (MS) files were processed using XCMS software version 3.2.7.1. Features were associated with known metabolites, when possible, searching their M/Z and RT values in the Metlin data base. Features presenting a missing value rate >20% were removed. Variables showing a poor variation in their values and outlier values were removed through a filtering based on Inter Quartile Range (IQR). Each feature was normalized by median-normalization and scaled by Auto scaling (mean-centered and divided by the standard deviation of each variable) (21). Statistical analyses were performed with MetaboAnalyst software version 4.0 (22).

ELISA

The concentration of sphingomyelin in plasma and urine, of the entire cohort of patients was determined by ELISA (Abcam, AB133118 and LifeSpan BioScience, LS-F30127) following the protocols provided by the manufacturer. ELISA kits were also used to measure the content of SPP1 and ENPP6 (Abcam, ab100618 and MyBiosource, MBS9327272).

Statistical and Bioinformatics Analyses

For ELISA data analysis, U-Mann-Whitney test was used to assess differences in the protein levels of sphingomyelin, SPP1 and ENPP6 between the 2 study groups. Results were expressed as median and IQ range. A value of $P < 0.05$ was considered to be statistically significant.

For metabolomics, differences in feature mean values between paired samples (i.e., pre and post run) were tested by estimating a fold-change value between groups and an associated p-value. Dysregulated features (fold change $\geq$ 1.5 and nominal $p \leq$ 0.05, arbitrarily chosen) were plotted in a Cloud plot, reporting intensities of signals between groups.

For t-test analysis p-values were adjusted for multiple testing using the Benjamini-Hochberg false discovery rate. Principal component analysis (PCA) was used to explore the data and identify any possible resemblances among subjects, based on the value of all features. Statistical analysis of metabolite-associated features was performed using XCMS and MetaboAnalyst (v.4.0) (22).

Enrichment analysis of the biological process was performed using information of the Kegg database.

For urine proteomic analysis, we have re-interrogated our previous proteomic datasets obtained from whole urinary and urinary microvesicles isolated from 15 MSK and 15 ICN (9, 15).

In particular, mass spectrometry data were analyzed as previously reported (15). Then, the fold change of the identified proteins associated to the sphingomyelin metabolism (23–25) and their −Log10 P-values were visualized in a volcano plot. The proteomic profile, after Z-score normalization, of these associated proteins were visualized by Heatmap diagram. Finally, Support Vector Machine (SVM) was used to identify a rank list of sphingomyelin metabolism proteins for discrimination between MSK and ICN samples. Proteins were considered to be significantly differentially expressed between the two conditions with power of 80% and an adjusted $P \leq 0.05$ in the T-test after correction for multiple interactions (Benjamini-Hochberg) and a fold change of ≥2. In addition, the proteins needed to show at least 70% identity in the samples in one of two conditions. In SVM a 4-fold cross-validation approach was applied to estimate the prediction and classification accuracy of ranked list of statistically significant proteins. All proteomic statistical analysis were performed using OriginLab and the latest version of software package R available at the time of the experiments.

RESULTS

Metabolomic Profiling Discriminated MSK From ICN Patients

After missing values estimation, 4,005 signals have been obtained and subjected to statistical analysis. Thirteen metabolites were able to clearly discriminate MSK from ICN (7 metabolites increased and 6 decreased in MSK compared to ICN patients) (**Figure 1A**). Using the principal Component Analysis (PCA) plot of the selected 13 metabolites, it was possible to clearly differentiate MSK from ICN (**Figure 1B**).

Sphingomyelin, which level was significantly decreased in MSK vs. ICN, reached the higher level of discrimination between the two study groups (Log2 fold change: −1.8, $p < 0.001$).

ELISA for Sphingomyelin Confirmed Metabolomics Results

To validate metabolomics data, we performed ELISA on plasma samples collected from all enrolled patients (15 MSK and 15 ICN).

Data analysis clearly demonstrated that the level of sphingomyelin was significantly lower in MSK patients than in ICN [Median/(IQR) MSK vs. ICN, 28.33 (12.73, 30.76) vs. 36.52 (33.48, 41.67), $p < 0.01$] (**Figure 2A**). ROC curve showed that

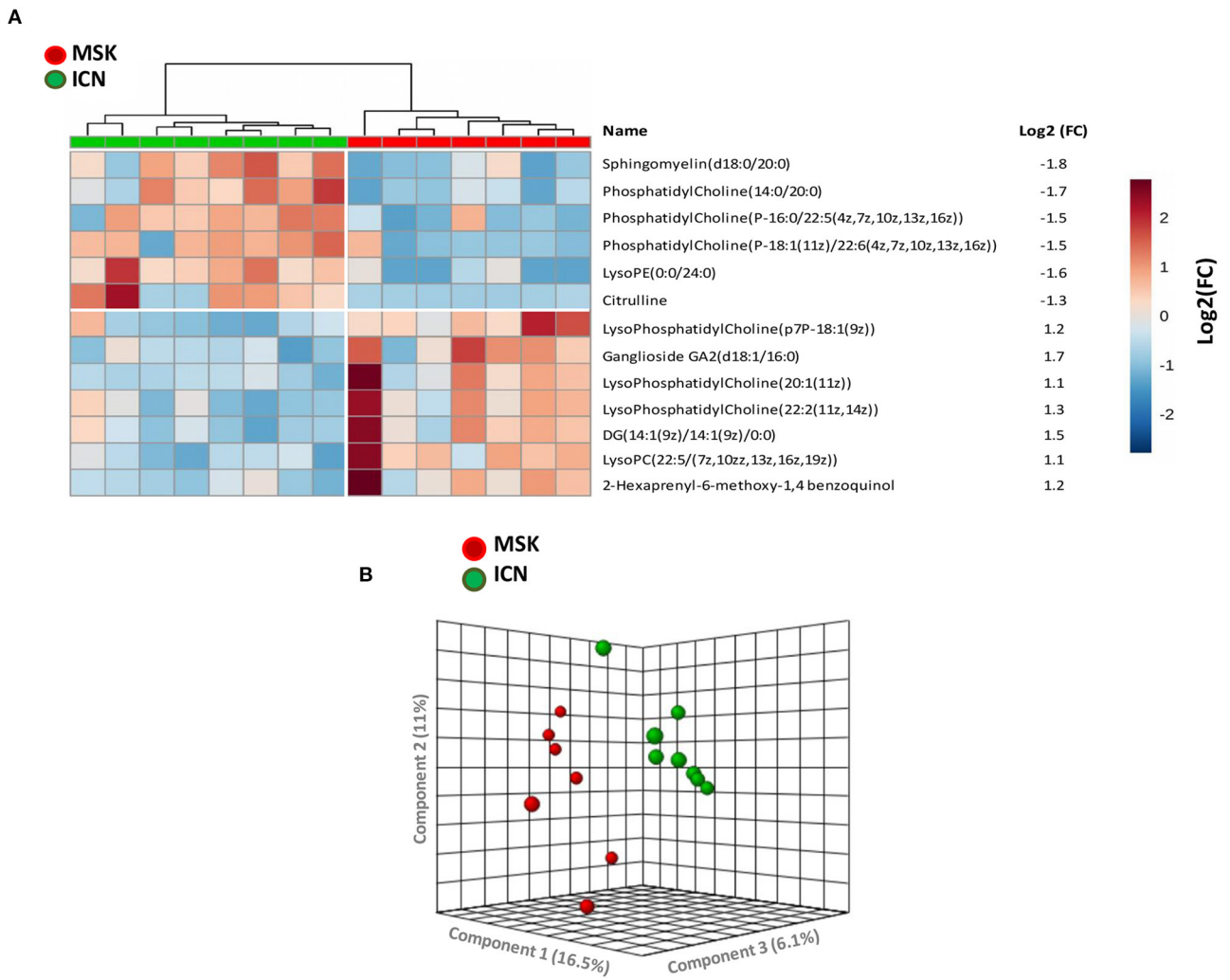

FIGURE 1 | 2-D Supervised hierarchical clustering and Principal Component Analysis (PCA) discriminating MSK from ICN patients. **(A)** 2-D Supervised hierarchical clustering able to discriminate patients with Medullary Sponge Kidney (MSK) from controls (ICN, nephrolithiasis). Patients are represented as vertical columns, with red symbols indicating MSK patients ($n = 7$) and green symbols ICN ($n = 8$). Thirteen metabolites (rows) were used for hierarchical grouping. The scale intensity of the metabolites is depicted according to the color key shown on the right. Red indicates high intensity level; blue, low intensity level. The figure also shows the mean levels of the fold change of expression of each metabolite in the MSK group compared to controls. **(B)** PCA plot built using the 13 metabolites selected by statistical analysis showed high discrimination accuracy between the two study groups.

the level of sphingomyelin can discriminate MSK from ICN patients (**Figure 2B**). The AUC, 95% CI and p values for the ROC analysis were 0.913, 0.808–1.000, and $p < 0.001$, respectively. The cutoff, sensitivity, specificity were 31.5 mg/dl, 87%, 87%, respectively.

To confirm whether sphingomyelin was reduced also in kidney, we decided to measure its urinary level by ELISA in MSK and ICN patients.

According to the results obtained in plasma, the level of sphingomyelin in urine was lower in MSK patients than in ICN (**Figure 3A**) [Median/(IQR) MSK vs. ICN, 1.13(1.08–1.21) ng/ml vs. 1.25 (1.23–1.31) ng/ml $p < 0.0001$]. The AUC, 95% CI and p values in ROC analysis were 0.960, 0.902–1.000, and $p < 0.001$, respectively (**Figure 3B**). The cutoff, sensitivity, specificity were 1.2 ng/ml, 93%, 87% respectively.

Proteomic Profile of Urinary Microvesicles Differentiated MSK From ICN

The analysis of urinary proteomic data of MSK and ICN focused on proteins associated with sphingomyelin metabolism did not show any statistically significant difference (**Supplementary Methods** and **Supplementary Figure 1**).

Then, since microvesicles seem to be involved in the complex biological machinery associated with MSK (15) and appear highly enriched in sphingomyelin (26), we decided to re-interrogate proteomic raw data previously obtained (15) from urinary

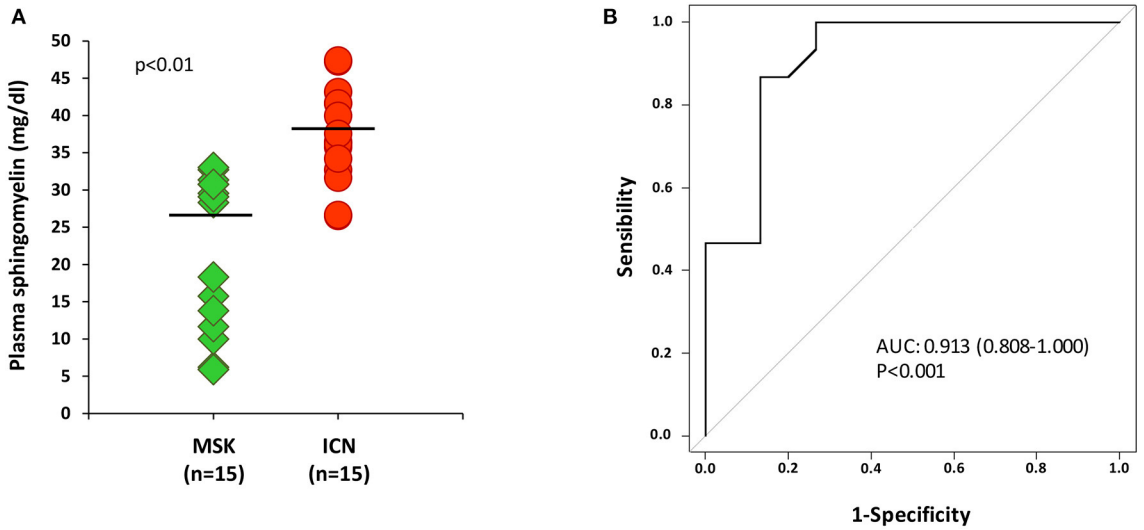

FIGURE 2 | ELISA for sphingomyelin validated metabolomic results. **(A)** Dot plot shows sphingomyelin plasma levels (mg/dl) in 15 patients with MSK (green) and 15 with nephrolithiasis (ICN, red). Solid lines indicate median values. The *p* value was calculated using the *t*-test. **(B)** ROC curve analysis of plasma sphingomyelin revealed that the reported values allow to discriminate MSK from the ICN.

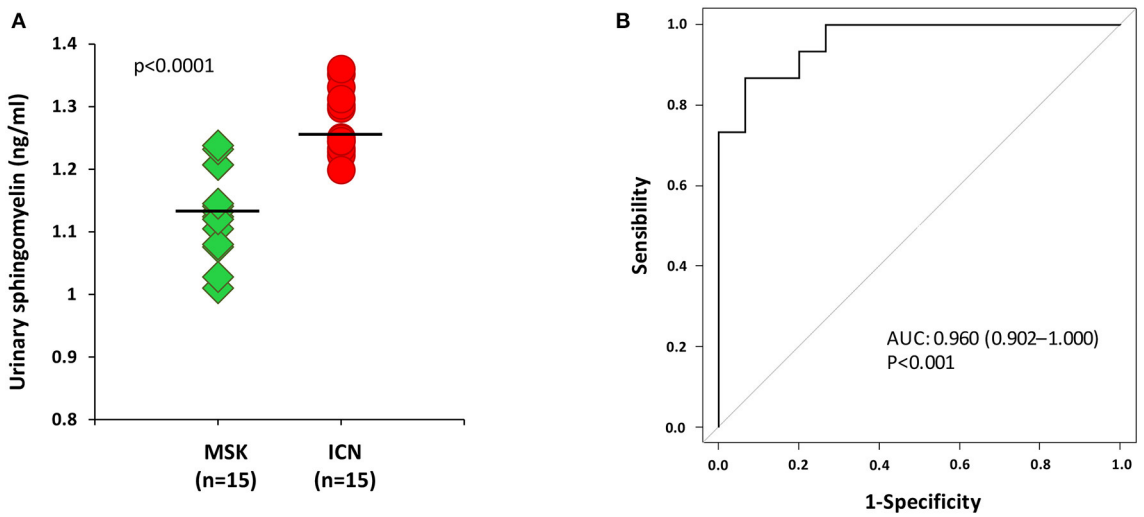

FIGURE 3 | ELISA for the urinary content of sphingomyelin was in accordance with the results obtained in plasma. **(A)** Dot plot shows sphingomyelin urinary levels (ng/ml) measured in 15 patients with MSK and 15 with ICN. Solid lines indicate median values. The *p* value was calculated using the *U* Mann-Whitney test. **(B)** ROC curve analysis of urinary sphingomyelin revealed that the reported values allow to discriminate MSK from the ICN.

microvesicles isolated from MSK and ICN focusing on proteins associated with sphingomyelin metabolism (**Supplementary Methods**).

As shown in **Figure 4**, twenty-nine proteins associated to sphingomyelin metabolism were identified. Among these, 14 proteins were able to discriminate MSK from ICN patients. SPP1 (Osteopontin) and ENPP6 (Ectonucleotide Pyrophosphatase/Phosphodiesterase 6), two proteins involved in renal morphogenesis, were the top de-regulated proteins identified by the SVM to distinguish between urinary microvesicles isolated from MSK and ICN. In particular, SPP1, in four isoforms (2, 3, 4, and 5) appeared over-expressed, while ENPP6 under-expressed in MSK compared to ICN (**Figures 4A,B**). ENPP6 down-regulation in MSK was also confirmed by urinary ELISA (**Figure 5**). Instead, SPP1 levels did not reach statistical differences

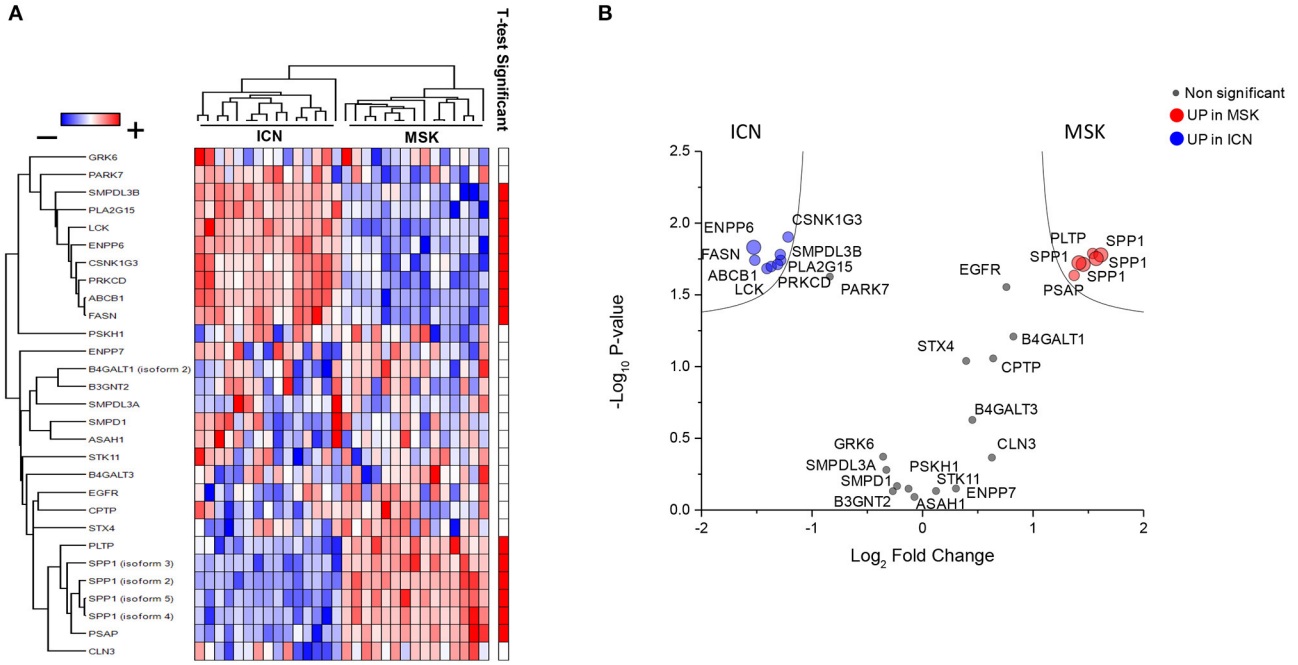

FIGURE 4 | Proteomic profile. **(A)** Heatmap of the 29 proteins associated to sphingomyelin metabolism identified in urinary microvesicles of MSK and ICN patients. Each row represents a protein and each column a sample. Normalized Z-scores of protein abundance are depicted using a pseudocolor scale (red, white, and blue indicating positive equal and negative expression, respectively) compared to each protein value. The dendrogram displays unsupervised hierarchical clustering analysis. Similar sample/proteome-profile values are next to each other. **(B)** Volcano plot of the 29 proteins associated to sphingomyelin metabolism. The plot is based on the relative abundance ratio (log2 fold change) and the *p* value (−log10). Gray, red and blue circles indicate the changes for the non-significant, significant up and down regulated proteins in MSK samples. Black line indicates the limits of statistically significant.

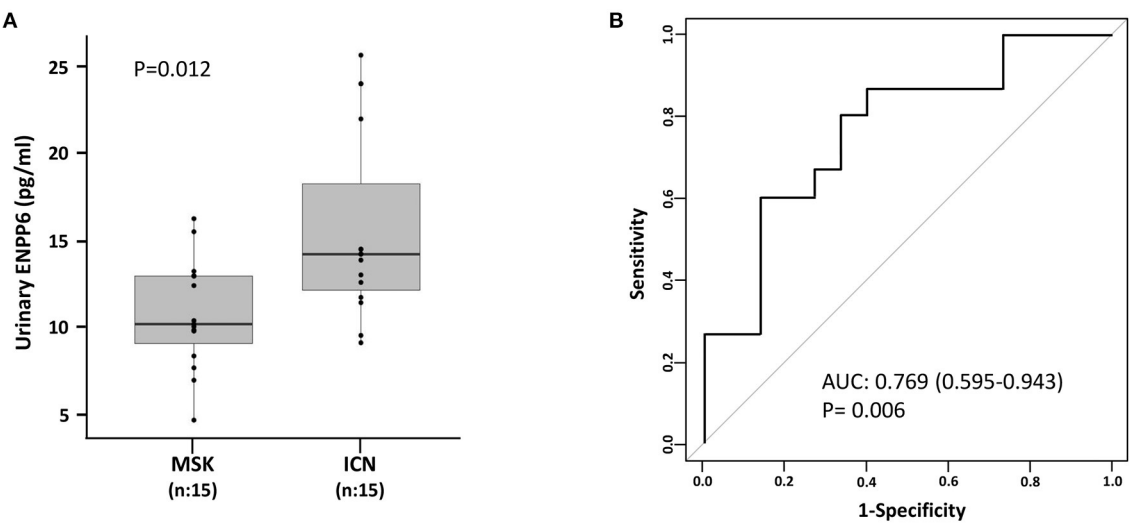

FIGURE 5 | ELISA for the urinary content of ENPP6 confirmed proteomics results. **(A)** Box plot shows ENPP6 urinary levels (pg/ml) measured in 15 patients with MSK and 15 with ICN. Solid lines indicate median values. The *p* value was calculated using the *U* Mann-Whitney test. **(B)** ROC curve analysis of urinary ENPP6 revealed that the reported values allow to discriminate MSK from the ICN.

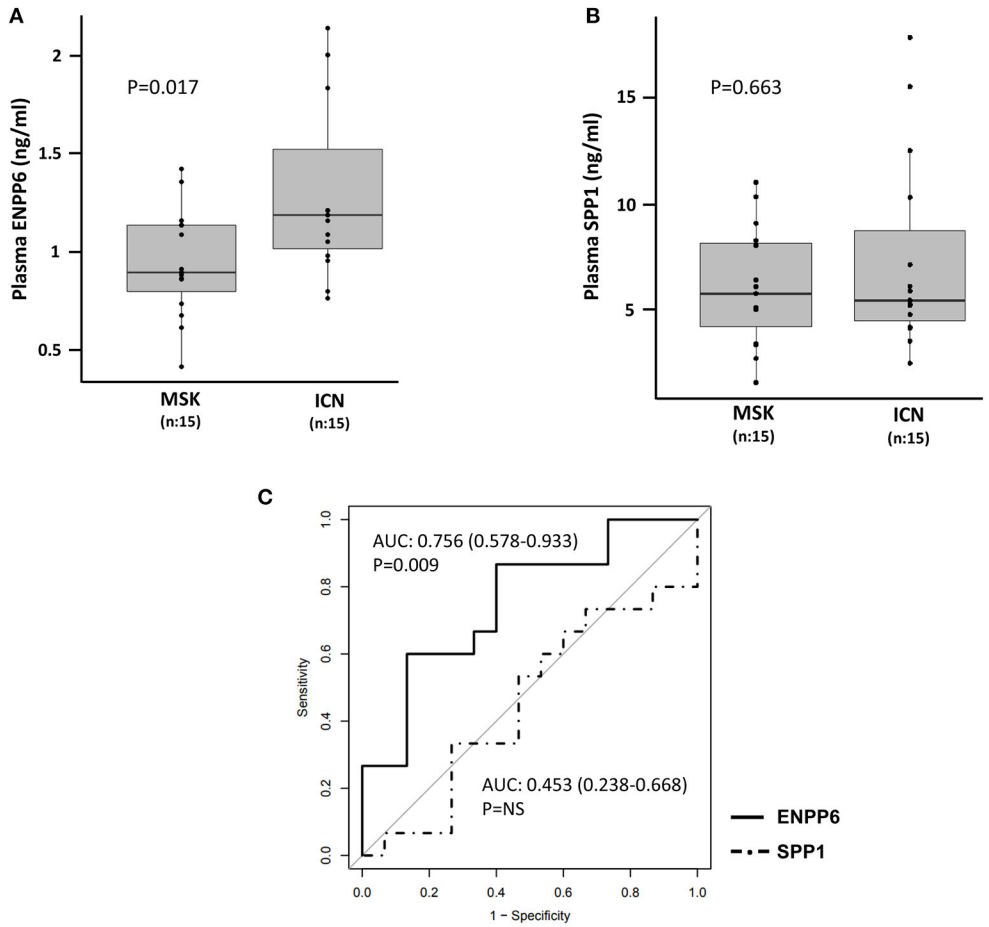

FIGURE 6 | Quantification of ENPP6 and SPP1 by ELISA. Box plots revealed **(A)** higher level of ENPP6 (ng/ml) in ICN vs. MSK and **(B)** no significant difference in the level of SPP1 (ng/ml) in plasma of MSK and ICN. The *p* values were calculated using the *t*-test. **(C)** Analysis of the ROC curve for plasma ENPP6 and SPP1.

in MSK vs. ICN (see whole urinary proteomics results in **Supplementary Figure 1**).

ELISA Demonstrated Low Levels of ENPP6 in Plasma of MSK vs. ICN Patients

Statistical analysis showed that the ENPP6 was under-expressed in plasma of patients with MSK compared to ICN (controls) [Median/(IQR) MSK vs. ICN, 0.9 (0.8, 1.1) vs. 1.2 (1.0, 1.5), $p = 0.017$]. ROC analysis revealed the power of discrimination of this biological factor (**Figure 6A**). The AUC, 95% CI and *p*-values for the ROC analysis were 0.756, 0.578–0.933, and $p = 0.009$, respectively. The cutoff, sensitivity, specificity were 0.93 ng/ml, 87%, 60% respectively.

Contrarily, no difference was found at plasma level in SPP1 between the two groups [Median/(IQR) MSK vs. ICN, 7.06 (6.18, 10.00) vs. 7.34 (5.93, 9.48), $p = 0.663$] (**Figure 6B**). The AUC and 95% CI for the ROC analysis were 0.453, 0.238–0.668. The cutoff, sensitivity, specificity were 5.3 ng/ml, 93%, 27% respectively (**Figure 6C**).

DISCUSSION

This study demonstrated, for the first time, the involvement of the sphingolipid metabolic pathway in medullary sponge kidney (MSK) disease pathogenesis and offered new insights into the biological machinery associated with this complex and neglected disorder.

Results of our omics research strategy revealed that several metabolites (sphingomyelin, phosphatidylcholine, lysophosphatidylethanolamine, citrulline, lysophosphatidylcholine, Ganglioside GA2, diglyceride, 2-Hexaprenyl-6-methoxy-1,4-benzoquinol) were able to clearly discriminate MSK from ICN. Sphingomyelin, a sphingolipid and major component of mammalian cells, resulted the most down-regulated.

Sphingomyelin can be synthesized from ceramide by sphingomyelin synthase (SMS) types 1 and 2 (27). SMS1 is constitutively expressed in the Golgi apparatus and is involved in the homeostatic synthesis of SM (28), while the expression of SMS2 in the Golgi depends on numerous stimuli (29).

The reverse process of sphingomyelin hydrolysis to ceramide and phosphorylcholine is induced by different isoforms of sphingomyelinase and represents an alternative route for the synthesis of ceramide (30).

At our knowledge, this is the first report describing a specific metabolic fingerprint of MSK and the possible involvement of sphingomyelin in the MSK-associated biological impairment. Instead, alterations in the metabolism of sphingomyelin and other sphingolipids have been extensively reported in other diseases including neurodegenerative [Alzheimer's disease (31), Parkinson's (32), multiple sclerosis (33), Lewy body dementia (34)], vascular (35), and bone disorders (30).

Sphingomyelin and ceramide are implicated in the survival of osteoclasts (36) and in the mineralization of the extracellular matrix. As demonstrated in animal models, a neutral Sphingomyelinase 2 deficiency is responsible for defects in bone and dental mineralization, probably due to deficiencies in ceramide and phosphocholine synthesis secondary to the degradation of sphingomyelin (37).

The involvement of sphingomyelin in MSK could partially explain the pathogenesis of systemic alterations observed in these patients. MSK patients, in fact, seem to have an altered neuroprotection capability against oxidative stress/ischemia and several bone metabolic defects (17, 18). As previously reported by our group, some MSK patients may develop central nervous system alterations (17) with the genetic derangement of the RET–GDNF axis having a possible pathogenetic role (38). Sphingomyelin, involved in several neurodegenerative disorders (39), may also contribute to the development of these clinical features.

As previously pointed out, about 75% of patients with MSK have alterations in bone mineralization (60% osteopenia and about 15% osteoporosis) in the absence of common risk factors such as menopause or hyperparathyroidism and also due to the persistent hypercalciuria (18). This high secretion of calcium may be the result of the renal calcium-handling defect (1), absorptive hypercalciuria (40), and defective urinary acidification (41) that characterize these patients.

The reduction of sphingomyelin, observed in MSK patients, could represent an adaptive response of the bone tissue to modulate osteoblastic/osteoclastic activity in the presence of a negative calcium balance and altered tubular acidification typical changes in the kidneys of these patients.

Sphingomyelin and some of its associated proteins, enriched in microvesicles [characterized by a high content of sphingolipids (42)] resulted also deregulated in the urines of our MSK patients demonstrating a possible ubiquitously alteration of this pathway in these patients. The absence of statistical difference in the level of the proteins associated with sphingomyelin metabolism in whole urinary proteomics may be due to the fact that it is mainly synthesized/compartmentalized in Golgi by the biological/biochemical machinery of the renal epithelial tubular cells and then, probably, excreted in urine. Additionally, we cannot exclude that part of the sphingomyelin detected in urine by ELISA could derive from plasma. Further studies are necessary to better understand this issue.

Interestingly, ectonucleotide pyrophophatase phosphodiesterase 6 (ENPP6) and osteopontin (SPP1) resulted the most down- and high-regulated protein, respectively.

ENPP6 belongs to a family of 7 phosphodiesterases involved in multiple cellular processes. ENPP6 hydrolyzes only choline-containing lysophospholipids to phosphocholine and monoacylglyceride (43). It is expressed in multiple tissues including the heart, central nervous system, kidney and bone tissue. In the kidney it is mostly expressed on the luminal side of proximal tubular epithelial cells. It is possible that ENPP6 in the kidney contributes to the reabsorption of choline by hydrolyzing glycerophosphocholine in the primary urine (43).

ENPP6, then, would participate in the synthesis of inorganic phosphate, a constituent of the bone matrix, through the metabolism of phosphocholine (44) and its higher level in ICN could predispose these patients to stone forming (45).

SPP1 is a widely expressed and multifunctional phosphorylated acid glycoprotein, it regulates the synthesis of bone matrix and the activity of osteoclasts. Osteopontin increases bone resorption by stimulating osteoclastogenesis and by anchoring osteoclasts to the matrix (46, 47). SPP1 in physiological conditions is expressed in the distal nephron, especially at the level of the thick segment of the loop of Henle.

In humans, there is an increased expression of osteopontin in the urine in several kidney diseases: hypertensive nephropathy, renal carcinoma, membranous glomerulonephritis, IgA nephropathy, lupus nephritis and in mouse models of ADPKD.

In addition, high expression of osteopontin in urine from MSK has been already reported by our group (48). Then, Ricci et al., have described a similar up-regulation in a group of pediatric patients suffering from ADTKD (Autosomal dominant Tubulointerstitial Kidney Disease) associated with a mutation of HNF1B, a hereditary tubulointerstitial nephritis with cystic dilatation of the renal tubules (49) and in kidney from rat model of ADPKD (50). It is possible that this protein could mediate the cyst formation in MSK patients similarly to ADPKD. The absence of a significant difference in its plasma level in our MSK vs. ICN patients could be explained by a possible paracrine urinary effect of this protein in MSK.

Therefore, our study, although performed on a small cohort of patients (particularly in metabolomics), highlighted a specific metabolic profile associated with MSK and confirmed our hypothesis that this disease could have systemic implications. Sphingomyelin, then, could represent a new disease pathogenetic element and a potential novel biomarker or therapeutic target. Further studies that could employ urinary metabolomics and *in vitro/in vivo* functional experiments, need to be undertaken to validate our research hypothesis and to translate our results into the daily clinical practice.

DATA AVAILABILITY STATEMENT

The datasets presented in this study can be found in online repositories. The names of the repository/repositories and accession numbers can be found below: Proteomics data are

available at PRIDE repository, https://www.ebi.ac.uk/pride/. Accession: PXD025744 and PXD025547. Metabolomics data supporting the conclusions of this article will be made available by the authors, without undue reservation.

ETHICS STATEMENT

The studies involving human participants were reviewed and approved by Comitato Etico per la Sperimentazione Clinica delle Province di Verona e Rovigo Azienda Ospedaliera Universitaria Integrata Verona. The patients/participants provided their written informed consent to participate in this study.

AUTHOR CONTRIBUTIONS

SG and GZ: conceptualization and draft of the manuscript. SG, MB, MD, AP, AV, and RE: investigation. SG, MB, MD, GL, GC, and GZ: formal analysis. GM: critical revision of the final version of the manuscript. GZ, GG, and GM: review and editing of the manuscript. GZ: project administration. All authors contributed to the article and approved the submitted version.

FUNDING

This study was performed (in part) in the LURM (Laboratorio Universitario di Ricerca Medica) Research Center, University of Verona.

SUPPLEMENTARY MATERIAL

The Supplementary Material for this article can be found online at: https://www.frontiersin.org/articles/10.3389/fmed.2021.671798/full#supplementary-material

REFERENCES

1. Gambaro G, Feltrin GP, Lupo A, Bonfante L, D'Angelo A, Antonello A. Medullary sponge kidney (LenarduzziCacchi-Ricci disease): a Padua medical school discovery in the 1930s. *Kidney Int*. (2006) 69:663–70. doi: 10.1038/sj.ki.5000035
2. Lambrianides AL, John DR. Medullary sponge disease in horseshoe kidney. *Urology*. (1987) 29:426–7. doi: 10.1016/0090-4295(87)90516-4
3. Fabris A, Anglani F, Lupo A, Gambaro G. Medullary sponge kidney: state of the art. *Nephrol Dial Transplant.* (2013) 28:1111–9. doi: 10.1093/ndt/gfs505
4. Gambaro G, Fabris A, Citron L, Tosetto E, Anglani F, Bellan F, et al. An unusual association of contralateral congenital small kidney reduced renal function and hyperparathyroidism in sponge kidney patients: on the track of the molecular basis. *Nephrol Dial Transplant.* (2005) 20:1042–7. doi: 10.1093/ndt/gfh798
5. Torregrossa R, Anglani F, Fabris A, Gozzini A, Tanini A, Del Prete D, et al. Identification of GDNF gene sequence variations in patients with medullary sponge kidney disease. *Clin J Am Soc Nephrol*. (2010) 5:1205–10. doi: 10.2215/CJN.07551009
6. Fabris A, Lupo A, Ferraro PM, Anglani F, Pei Y, Danza FM, et al. Familial clustering of medullary sponge kidney is autosomal dominant with reduced penetrance and variable expressivity. *Kidney Int*. (2013) 83:272–7. doi: 10.1038/ki.2012.378
7. Diouf B, Ka EH, Calender A, Giraud S, Diop TM. Association of medullary sponge kidney disease and multiple endocrine neoplasia type IIA due to RET gene mutation: is there a causal relationship? *Nephrol Dial Transplant*. (2000) 15:2062–3. doi: 10.1093/ndt/15.12.2062
8. Janjua MU, Long XD, Mo ZH, Dong CS, Jin P. Association of medullary sponge kidney and hyperparathyroidism with RET G691S/S904S polymorphism: a case report. *J Med Case Rep.* (2018) 12:197. doi: 10.1186/s13256-018-1736-6
9. Fabris A, Bruschi M, Santucci L, Candiano G, Granata S, Dalla Gassa A, et al. Proteomic-based research strategy identified laminin subunit alpha 2 as a potential urinary-specific biomarker for the medullary sponge kidney disease. *Kidney Int.* (2017) 91:459–68. doi: 10.1016/j.kint.2016.09.035
10. Panfoli I, Granata S, Candiano G, Verlato A, Lombardi G, Bruschi M, et al. Analysis of urinary exosomes applications for rare kidney disorders. *Expert Rev Proteomics*. (2020) 17:735–49. doi: 10.1080/14789450.2020.1866993
11. Guldager Kring Rasmussen D, Karsdal MA. Chapter 29 – Laminins. In: Morten A, editor. *Biochemistry of Collagens*. Karsdal Laminins and Elastin: Academic Press (2016). p. 163–96. doi: 10.1016/B978-0-12-809847-9.00029-5
12. O'Brien LE, Jou TS, Pollack AL, Zhang Q, Hansen SH, Yurchenco P, et al. Rac1 orientates epithelial apical polarity through effects on basolateral laminin assembly. *Nat Cell Biol.* (2001) 3:831–8. doi: 10.1038/ncb0901-831
13. Shannon MB, Patton BL, Harvey SJ, Miner JH. A hypomorphic mutation in the mouse laminin alpha5 gene causes polycystic kidney disease. *J Am Soc Nephrol.* (2006) 17:1913–22. doi: 10.1681/ASN.2005121298
14. Vijayakumar S, Dang S, Marinkovich MP, Lazarova Z, Yoder B, Torres VE, et al. Aberrant expression of laminin-332 promotes cell proliferation and cyst growth in ARPKD. *Am J Physiol Renal Physiol.* (2014) 306:F640–54. doi: 10.1152/ajprenal.00104.2013
15. Bruschi M, Granata S, Candiano G, Fabris A, Petretto A, Ghiggeri GM, et al. Proteomic analysis of urinary extracellular vesicles reveals a role for the complement system in medullary sponge kidney disease. *Int J Mol Sci.* (2019) 20:5517. doi: 10.3390/ijms20215517
16. Chen SF, Chen M. Complement activation in progression of chronic kidney disease. *Adv Exp Med Biol.* (2019) 1165:423–41. doi: 10.1007/978-981-13-8871-2_20
17. Ria P, Fabris A, Dalla Gassa A, Zaza G, Lupo A, Gambaro G. New non-renal congenital disorders associated with medullary sponge kidney (MSK) support the pathogenic role of GDNF and point to the diagnosis of MSK in recurrent stone formers. *Urolithiasis*. (2017) 45:359-62. doi: 10.1007/s00240-016-0913-6
18. Fabris A, Bernich P, Abaterusso C, Marchionna N, Canciani C, Nouvenne A, et al. Bone disease in medullary sponge kidney and effect of potassium citrate treatment. *Clin J Am Soc Nephrol.* (2009) 4:1974–9. doi: 10.2215/CJN.02360409
19. Yuan M, Breitkopf SB, Yang X, Asara JM. A positive/negative ion-switching, targeted mass spectrometry-based metabolomics platform for bodily fluids, cells, and fresh and fixed tissue. *Nat Protoc*. (2012) 7:872–81. doi: 10.1038/nprot.2012.024
20. Kubesova A, Tejkalova H, Syslova K, Kacer P, Vondrousova J, Tyls F, et al. Biochemical, histopathological and morphological profiling of a rat model of early immune stimulation: relation to psychopathology. *PLoS ONE*. (2015) 10:e0115439. doi: 10.1371/journal.pone.0115439
21. Xia J, Wishart DS. Web-based inference of biological patterns, functions and pathways from metabolomic data using MetaboAnalyst. *Nat Protoc.* (2011) 6:743–60. doi: 10.1038/nprot.2011.319
22. Xia J, Wishart DS. Using MetaboAnalyst 3.0 for comprehensive metabolomics data analysis. *Curr Protoc Bioinformat.* (2016) 55:14.10.1–14.10.91. doi: 10.1002/cpbi.11
23. UniProt Consortium. UniProt: a worldwide hub of protein knowledge. *Nucleic Acids Res*. (2019) 47:D506–15. doi: 10.1093/nar/gky1049
24. Kanehisa M, Furumichi M, Tanabe M, Sato Y, Morishima K. KEGG: new perspectives on genomes, pathways, diseases and drugs. *Nucleic Acids Res.* (2017) 45:D353–61. doi: 10.1093/nar/gkw1092
25. Jassal B, Matthews L, Viteri G, Gong C, Lorente P, Fabregat A, et al. The reactome pathway knowledgebase. *Nucleic Acids Res*. (2020) 48:D498–D503. doi: 10.1093/nar/gkz1031

26. Bruno S, Porta S, Bussolati B. Extracellular vesicles in renal tissue damage and regeneration. *Eur J Pharmacol*. (2016) 790:83–91. doi: 10.1016/j.ejphar.2016.06.058
27. Tafesse FG, Ternes P, Holthuis JC. The multigenic sphingomyelin synthase family. *J Biol Chem*. (2006) 281:29421–5 doi: 10.1074/jbc.R600021200
28. Villani M, Subathra M, Im YB, Choi Y, Signorelli P, Del Poeta M, et al. Sphingomyelin synthases regulate production of diacylglycerol at the Golgi. *Biochem J*. (2008) 414:31–41. doi: 10.1042/BJ20071240
29. Taniguchi M, Okazaki T. The role of sphingomyelin and sphingomyelin synthases in cell death, proliferation and migration-from cell and animal models to human disorders. *Biochim Biophys Acta*. (2014) 1841:692–703. doi: 10.1016/j.bbalip.2013.12.003
30. Khavandgar Z, Murshed M. Sphingolipid metabolism and its role in the skeletal tissues. *Cell Mol Life Sci*. (2015) 72:959–69. doi: 10.1007/s00018-014-1778-x
31. Han X, Rozen S, Boyle SH, Hellegers C, Cheng H, Burke JR, et al. Metabolomics in early Alzheimer's disease: identification of altered plasma sphingolipidome using shotgun lipidomics. *PLoS ONE*. (2011) 6:e21643. doi: 10.1371/journal.pone.0021643
32. Hu L, Dong MX, Huang YL, Lu CQ, Qian Q, Zhang CC, et al. Integrated metabolomics and proteomics analysis reveals plasma lipid metabolic disturbance in patients with parkinson's disease. *Front Mol Neurosci*. (2020) 13:80. doi: 10.3389/fnmol.2020.00080
33. Villoslada P, Alonso C, Agirrezabal I, Kotelnikova E, Zubizarreta I, Pulido-Valdeolivas I, et al. Metabolomic signatures associated with disease severity in multiple sclerosis. *Neurol Neuroimmunol Neuroinflamm*. (2017) 4:e321. doi: 10.1212/NXI.0000000000000321
34. Savica R, Murray ME, Persson XM, Kantarci K, Parisi JE, Dickson DW, et al. Plasma sphingolipid changes with autopsy-confirmed Lewy Body or Alzheimer's pathology. *Alzheimers Dement*. (2016) 3:43–50. doi: 10.1016/j.dadm.2016.02.005
35. Borodzicz S, Czarzasta K, Kuch M, Cudnoch-Jedrzejewska A. Sphingolipids in cardiovascular diseases and metabolic disorders. *Lipids Health Dis*. (2015) 14:55. doi: 10.1186/s12944-015-0053-y
36. Iwamoto T, Fukumoto S, Kanaoka K, Sakai E, Shibata M, Fukumoto E, et al. Lactosylceramide is essential for the osteoclastogenesis mediated by macrophage-colony-stimulating factor and receptor activator of nuclear factor-kappa B ligand. *J Biol Chem*. (2001) 276:46031–8. doi: 10.1074/jbc.M104464200
37. Stoffel W, Hammels I, Jenke B, Schmidt-Soltau I, Niehoff A. Neutral sphingomyelinase 2 (SMPD3) deficiency in mice causes chondrodysplasia with unimpaired skeletal mineralization. *Am J Pathol*. (2019) 189:1831–45. doi: 10.1016/j.ajpath.2019.05.008
38. Ibáñez CF, Andressoo JO. Biology of GDNF and its receptors - Relevance for disorders of the central nervous system. *Neurobiol Dis*. (2017) 97(Pt B):80–9. doi: 10.1016/j.nbd.2016.01.021
39. Bouscary A, Quessada C, René F, Spedding M, Turner BJ, Henriques A, et al. Sphingolipids metabolism alteration in the central nervous system: amyotrophic lateral sclerosis (ALS) and other neurodegenerative diseases. *Semin Cell Dev Biol*. (2021) 112:82–91. doi: 10.1016/j.semcdb.2020.10.008
40. O'Neill M, Breslau NA, Pak CY. Metabolic evaluation of nephrolithiasis in patients with medullary sponge kidney. *JAMA*. (1981) 245:1233–6. doi: 10.1001/jama.245.12.1233
41. Osther PJ, Mathiasen H, Hansen AB, Nissen HM. Urinary acidification and urinary excretion of calcium and citrate in women with bilateral medullary sponge kidney. *Urol Int*. (1994) 52:126–30. doi: 10.1159/000282590
42. Zaborowski MP, Balaj L, Breakefield XO, Lai CP. Extracellular vesicles: composition, biological relevance, and methods of study. *Bioscience*. (2015) 65:783–97. doi: 10.1093/biosci/biv084
43. Morita J, Kano K, Kato K, Takita H, Sakagami H, Yamamoto Y, et al. Structure and biological function of ENPP6, a choline-specific glycerophosphodiester-phosphodiesterase. *Sci Rep*. (2016) 6:20995. doi: 10.1038/srep20995
44. Stewart AJ, Leong DTK, Farquharson C. PLA2 and ENPP6 may act in concert to generate phosphocholine from the matrix vesicle membrane during skeletal mineralization. *FASEB J*. (2018) 32:20–25. doi: 10.1096/fj.201700521r
45. Khan SR, Glenton PA, Backov R, Talham DR. Presence of lipids in urine, crystals and stones: implications for the formation of kidney stones. *Kidney Int*. (2002) 62:2062–72. doi: 10.1046/j.1523-1755.2002.00676.x
46. McKee MD, Nanci A. Osteopontin: an interfacial extracellular matrix protein in mineralized tissues. *Connect Tissue Res*. (1996) 35:197–205. doi: 10.3109/03008209609029192
47. Reinholt FP, Hultenby K, Oldberg A, Heinegård D. Osteopontin–a possible anchor of osteoclasts to bone. *Proc Natl Acad Sci USA*. (1990) 87:4473–5. doi: 10.1073/pnas.87.12.4473
48. Bruschi M, Granata S, Santucci L, Candiano G, Fabris A, Antonucci N, et al.. Proteomic analysis of urinary microvesicles and exosomes in medullary sponge kidney disease and autosomal dominant polycystic kidney disease. *Clin J Am Soc Nephrol*. (2019) 14:834–43. doi: 10.2215/CJN.12191018
49. Ricci P, Magalhães P, Krochmal M, Pejchinovski M, Daina E, Caruso MR, et al. Urinary proteome signature of Renal Cysts and Diabetes syndrome in children. *Sci Rep*. (2019) 9:2225. doi: 10.1038/s41598-019-38713-5
50. Cowley BD Jr, Ricardo SD, Nagao S, Diamond JR. Increased renal expression of monocyte chemoattractant protein-1 and osteopontin in ADPKD in rats. *Kidney Int*. (2001) 60:2087–96. doi: 10.1046/j.1523-1755.2001.00065.x

Conflict of Interest: The authors declare that the research was conducted in the absence of any commercial or financial relationships that could be construed as a potential conflict of interest.

frontiers in Medicine

ORIGINAL RESEARCH
published: 09 June 2021
doi: 10.3389/fmed.2021.679171

Urinary Extracellular Vesicles for Renal Tubular Transporters Expression in Patients With Gitelman Syndrome

*Chih-Chien Sung[1], Min-Hsiu Chen[1], Yi-Chang Lin[2], Yu-Chun Lin[3], Yi-Jia Lin[3], Sung-Sen Yang[1] and Shih-Hua Lin[1]**

[1] Division of Nephrology, Department of Medicine, National Defense Medical Center, Tri-Service General Hospital, Taipei, Taiwan, [2] Division of Cardiovascular Surgery, Department of Surgery, National Defense Medical Center, Tri-Service General Hospital, Taipei, Taiwan, [3] Deparment of Pathology, National Defense Medical Center, Tri-Service General Hospital, Taipei, Taiwan

Background: The utility of urinary extracellular vesicles (uEVs) to faithfully represent the changes of renal tubular protein expression remains unclear. We aimed to evaluate renal tubular sodium (Na^+) or potassium (K^+) associated transporters expression from uEVs and kidney tissues in patients with Gitelman syndrome (GS) caused by inactivating mutations in *SLC12A3*.

Methods: uEVs were isolated by ultracentrifugation from 10 genetically-confirmed GS patients. Membrane transporters including Na^+-hydrogen exchanger 3 (NHE3), $Na^+/K^+/2Cl^-$ cotransporter (NKCC2), NaCl cotransporter (NCC), phosphorylated NCC (p-NCC), epithelial Na^+ channel β (ENaCβ), pendrin, renal outer medullary K1 channel (ROMK), and large-conductance, voltage-activated and Ca^{2+}-sensitive K^+ channel (Maxi-K) were examined by immunoblotting of uEVs and immunofluorescence of biopsied kidney tissues. Healthy and disease (bulimic patients) controls were also enrolled.

Results: Characterization of uEVs was confirmed by nanoparticle tracking analysis, transmission electron microscopy, and immunoblotting. Compared with healthy controls, uEVs from GS patients showed NCC and p-NCC abundance were markedly attenuated but NHE3, ENaCβ, and pendrin abundance significantly increased. ROMK and Maxi-K abundance were also significantly accentuated. Immunofluorescence of the representative kidney tissues from GS patients also demonstrated the similar findings to uEVs. uEVs from bulimic patients showed an increased abundance of NCC and p-NCC as well as NHE3, NKCC2, ENaCβ, pendrin, ROMK and Maxi-K, akin to that in immunofluorescence of their kidney tissues.

Conclusion: uEVs could be a non-invasive tool to diagnose and evaluate renal tubular transporter adaptation in patients with GS and may be applied to other renal tubular diseases.

Keywords: Gitelman syndrome, renal tubular transporters, hypokalemia, renal tubular disease, urinary extracellular vesicles (exosomes)

OPEN ACCESS

Edited by:
Zaid A. Abassi, Technion Israel Institute of Technology, Israel

Reviewed by:
Gerardo Gamba, National Autonomous University of Mexico, Mexico
Gautam Bhave, Vanderbilt University, United States

***Correspondence:**
Shih-Hua Lin
l521116@ndmctsgh.edu.tw

Specialty section:
This article was submitted to Nephrology, a section of the journal Frontiers in Medicine

Received: *11 March 2021*
Accepted: *11 May 2021*
Published: *09 June 2021*

Citation:
Sung C-C, Chen M-H, Lin Y-C, Lin Y-C, Lin Y-J, Yang S-S and Lin S-H (2021) Urinary Extracellular Vesicles for Renal Tubular Transporters Expression in Patients With Gitelman Syndrome. Front. Med. 8:679171. doi: 10.3389/fmed.2021.679171

INTRODUCTION

Gitelman syndrome (GS) is one of the most common inherited tubulopathy with a prevalence ranging from 0.25 to 4/10,000 per population. It is caused by biallelic inactivating mutations in the *SLC12A3* gene encoding thiazide-sensitive sodium-chloride cotransporter (NCC) expressed in the apical membrane of distal convoluted tubules (DCT) (1, 2). To date, more than 450 different mutations scattered throughout *SLC12A3* have been identified in GS (1, 3, 4). Clinical characteristics include renal sodium (Na^+) wasting with secondary hyperreninemia and hyperaldosteronism, renal potassium (K^+) wasting with chronic hypokalemia and metabolic alkalosis, and renal magnesium wasting with hypomagnesemia, but hypocalciuria (5). The defective NCC function caused by different classes of *SLC12A3* mutations leads to the reduced sodium chloride (NaCl) reabsorption in DCT with increased luminal NaCl delivery to downstream collecting ducts (CD) responsible for NaCl reabsorption via epithelial Na^+ channel (ENaC) and K^+ secretion via renal outer medullary K1 channel (ROMK) and large-conductance, voltage-activated and Ca^{2+}-sensitive K^+ channel (Maxi-K). Although the expression of ENaCβ, ROMK and Maxi-K in mouse GS model has been reported to be significantly increased in both immunoblotting and immunofluorescence of mouse kidney (6), the adaptive response of upstream and downstream Na^+ and K^+ associated transporters in response to renal Na^+ and K^+ wasting in GS patients remains unknown.

Urinary extracellular vesicles (uEVs) containing membrane and cytosolic proteins, mRNAs, miRNA and signaling molecules from each renal epithelial cell type may reflect the physiological state of their cells of origin (7, 8). The isolation of uEVs had the potential to shed much insight on the health status of the kidney and expression of urinary proteins (9–11). Knepper et al. has identified more than one thousand proteins including solute and water transporters, vacuolar H^+-ATPase subunits, and disease related proteins (12). It has been also reported that the isolated uEVs had an increased NCC abundance in patients with primary aldosteronism (13, 14) and Cushing syndrome (15) as well as a rapid increase in abundance of NCC and p-NCC in healthy subjects following the mineralocorticoid administration (16). In the inherited renal tubular disorders, uEVs have been used as a non-invasive tool to detect the defect of mutated renal tubular transporter such as NCC and $Na^+/K^+/2Cl^-$ cotransporter (NKCC2) expression in patients with GS and Bartter syndrome, respectively (17, 18). Nevertheless, uEVs for other renal Na^+ and K^+ associated transporters expression has not been also investigated in GS.

The aim of this study was to evaluate the changed expression of NCC, phosphorylated NCC (p-NCC), upstream DCT such as Na^+-hydrogen exchanger 3 (NHE3), NKCC2, downstream DCT such as ENaCβ, pendrin, as well as K^+-secreting channels such as ROMK and Maxi-K from uEVs and representative kidney tissues in patients with GS. Results to be reported indicated that a marked attenuation of NCC and p-NCC expression from uEVs could be used as a non-invasive diagnostic biomarker for GS. Both upstream NHE3 and downstream ENaCβ and pendrin from uEVs were increased in response to salt-losing and an enhanced ROMK and Maxi-K expression were associated with renal K^+ wasting in GS patients. These findings from uEVs were similar to those obtained from renal biopsied tissues in GS patients.

MATERIALS AND METHODS

Study Design

The study protocol was approved by the Ethics Committee on Human Studies at Tri-Service General Hospital (TSGHIRB No.2-103-05-160 and TSGHIRB No.2-105-05-062). We prospectively collected 10 genetically confirmed GS patients. Their mutations included homozygous intronic mutation ($n = 2$), compound heterozygous mutati on ($n = 8$) in the *SLC12A3* gene encoding NCC (**Table 1**). Five healthy controls and three bulimic patients as hypokalemic disease controls were also enrolled. The diagnosis of bulimia was based on the American Psychiatric Association's Diagnostic and Statistical Manual, Fifth Edition (19). Clinical characteristics and laboratory examination were collected and determined. Renal biopsied tissues were collected from three different GS patients with definite *SLC12A3* mutations (compound heterozygous mutation of intronic c1670-191/p.I888_H916del, p.T60M/p.R959fs, and p.T60M/splicing c.965-1G>A+c965-977gcggacattttgt>accgaaaattttt) and one bulimic patient. All of them had long-standing, severe hypokalemia refractory to aggressive K^+ supplementation and significant proteinuria. Control kidney tissue was obtained from normal part of kidney in one patient with renal cell carcinoma undergoing total nephrectomy.

uEVs Studies

Urine Collection and uEVs Isolation

Secondary morning spot urine with forty milliliters with protease inhibitors were collected for uEVs isolation by ultracentrifugation-based protocol. The urine sample was centrifuged at 17,000 × g for 10 min at 37°C. Supernatant was then ultracentrifuged at 200,000 × g for 2 h at 4°C. The pellet was resuspended in PBS or laemmli buffer with dithiothreitol.

Nanoparticle Tracking Analysis

Nanoparticles from isolated uEVs were analyzed using the NanoSight NS300 instrument (NanoSight Ltd, Amesbury, UK). Following published method (20), all experiments were carried out at a 1:1,000 dilution, yielding particle concentrations in the region of 1×10^8 particles ml^{-1} in accordance with the manufacturer's recommendations.

Transmission Electron Microscopy

uEVs pellet was carefully fixed the with enough volume of 2.5% glutaraldehyde (G5882, Sigma-Aldrich) in 0.1 M sodium cacodylate, pH 7.4 and 4% paraformaldehyde mix buffer (1:1) for 1 h at 4°C and then washed with PBS. Pre-fix the sample with 1 ml of 1% Osmium tetroxide (in ddH_2O) for 50 min at 4°C in dark. Post-fix the sample with 5% uranyl acetate (UA) blocking overnight at 4°C. Incubate for 10 min with a graded EtOH series (50, 70, 90, 95, 100%) and followed by EPON (Resin 20 ml, DDSA 7 ml, NMA 14 ml, DMP-30 0.8 ml). The uEVs samples

TABLE 1 | Characteristics of *SLC12A3* mutation among 10 patients with Gitelman syndrome.

Patients	Genotypes	Nucleotide change (NM_000339.3)	AA change (NP_000330.3)	Topological localization
1	Compound heterozygous	c.1924C>T + c.2548+253	p.R642C + Intronic	Transmembrane + C-terminal
2	Homozygous	c.1670-191C>T + c.1670-C>T	Intronic + Intronic	Transmembrane + Transmembrane
3	Compound heterozygous	c.2875_76delAG + c.2548+253	p.R959fs + Intronic	C-terminal + C-terminal
4	Compound heterozygous	c.2129C>A + c.2875-76delAG	p.S710X + p.R959fs	C-terminal + C-terminal
5	Compound heterozygous	c.488C>T+c.2660+1G>A	p.T163M + splicing	Transmembrane + C-terminal
6	Compound heterozygous	c.1000C>T+c.1326C>G	p.R334W + p.N442K	Transmembrane + Transmembrane
7	Homozygous	c.1670-191C>T + c.1670-C>T	Intronic+ Intronic	Transmembrane + Transmembrane
8	Compound heterozygous	c.2129C>A + c.2875_76delAG	p.S710X + p.R959fs	C-terminal + C-terminal
9	Compound heterozygous	c.911C>T/c.2875_76delAG	p.T304M + p.R959fs	Transmembrane + C-terminal
10	Compound heterozygous	c.2532G>A+c.805-06insTTGGCGTGGTCTCGG	p.W844X + p.T269delinsIGVVSA	C-terminal + Transmembrane

were analyzed with a Hitachi TEM HT7700 electron microscope operated at 60 kV.

Immunoblotting

For immunoblotting, the loading volume of each uEVs sample was adjusted so that the loaded amount of creatinine was constant (21, 22). SDS/PAGE was carried out on an 8% polyacrylamide gel, and proteins were transferred to Immobilon®-P membranes (Millipore, Amsterdam, The Netherlands). The primary antibodies were as follows: NSE (ab254088, Abcam, Cambridge, UK), TSG101 (ab125011, Abcam, Cambridge, UK), CD9 (GTX55564, Genetex, HsinChu City), AQP2 (sc-515770, Santa Cruz Biotechnology, Santa Cruz, CA), NHE3 (NHE31-A, Alpha Diagnostic Intl Inc., San Antonio, TX) (6), NKCC2 (AB2281, Millipore, Temecula, CA), NCC (AB3553, Millipore, Temecula, CA) (23), ENaCβ (ASC-019, Alomone labs, Jerusalem, Israel) (23), p-NCC (17T, in-house antibody) (23), Maxi-K (APC-021, Alomone labs, Jerusalem, Israel) (6), ROMK (APC-001, Alomone labs, Jerusalem, Israel) (6), and pendrin (ARP41739_P050, Aviva system biology, San Diego, CA). The membranes were incubated with the secondary antibody. Immunoreactive proteins were detected by the enhanced chemiluminescence method (Pierce, Rockford, IL, USA). The immunopositive bands from immunoblotting were quantified using pixel density scanning and calculated using Image J and the relative band intensity was normalized to the healthy controls.

Immunofluorescence of Kidney Tissue

After paraffin removal and rehydration, the slides were heated in 1× citrate buffer (ThermoFisher) and exposed to 3% H_2O_2 (ThermoFisher) at room temperature and then the blocking solution. After washing with PBS plus 0.1% Tween 20 (J.T. Baker), the tissue was incubated with primary antibodies at 4°C overnight. The primary antibodies of AQP2, NHE3, NKCC2, NCC, p-NCC, ENaCβ, Maxi-K, ROMK, and pendrin were used. The tissues were exposed to species-specific secondary antibodies conjugated to Alexa Fluor fluorophores (ThermoFisher). Immunofluorescence images were obtained by Zeiss LSM880 confocal microscope.

Statistical Analyses

Serum and urine biochemistry data were expressed as mean ± standard deviation. Correlation between uEVs particles and urine creatinine were calculated by Pearson's correlation coefficient statistic in Excel. Data analyses were performed with the Prism (v5) software (GraphPad Software). Group comparisons of renal transporters from uEVs between GS patients and healthy controls were made using a two-tailed unpaired Student's *t*-test. Statistical significance was defined as p-values <0.05.

RESULTS

Clinical Characteristics in GS

As shown in **Table 2**, all GS patients (Male/Female = 9/1, age 33.4 ± 7.8 years old) were normotensive with renal Na^+ and Cl^- wasting and secondary hyperreninemia (plasma renin activity, PRA 28.9 ± 14.4 ng/mL/h) but normal to high plasma aldosterone concentration (PAC) (229.4 ± 69.6 pg/mL), chronic hypokalemia (K^+, 2.34 ± 0.45 mmol/L) with higher urinary K^+ excretion (transtubular potassium gradient, 13.46 ± 10.91), metabolic alkalosis ($HCO3^-$, 28.7 ± 3.9 mmol/L), hypomagnesemia (Mg^{2+} 0.63 ± 0.07 mmol/L), and hypocalciuria (Ca^{2+}/Creatinine 0.07 ± 0.06 mmol/mmol).

Characterization of uEVs

Characterization of the uEVs in healthy controls was validated by nanoparticle tracking analysis (NTA), transmission electron microscopy (TEM), and immunoblotting of uEVs makers. NTA identified size distribution of particles in the expected uEVs size range of 20–120 nm shown in **Figures 1A,B**. The mean particle size and concentration were 132.9 ± 65.8 nm and 6.6 × 10^{14}/ml,

TABLE 2 | Clinical characteristics and biochemistries in patients with Gitelman syndrome.

Patients		1	2	3	4	5	6	7	8	9	10	Mean ± SD
SBP/DBP (mmHg)		123/65	111/68	120/80	114/78	128/70	120/64	126/64	120/70	105/84	115/68	116.2 ± 7.5/69.7 ± 7.4
Serum	Reference											
BUN (mmol/L)	2.50–8.93	5.71	5.36	7.85	4.64	6.07	5.36	7.14	4.64	4.28	5.71	5.68 ± 1.12
Creatinine (μmol/L)	61.9–106.1	79.6	88.4	114.9	53 0	106.1	106.1	88.4	97.2	70.7	97.2	90.17.0 ± 18.54
Sodium (mmol/L)	136–145	135	135	138	132	140	142	138	137	134	134	137.1 ± 3.1
Potassium (mmol/L)	3.5–5.1	2.6	1.9	2.4	2.9	2.8	2.3	2.1	2.1	1.5	2.8	2.34 ± 0.45
Chloride (mmol/L)	98–107	97	100	98	94	97	99	97	98	96	96	97.2 ± 1.7
Total Calcium (mmol/L)	2.15–2.55	2.33	2.20	2.33	2.35	2.53	2.45	2.50	2.23	2.45	2.45	2.38 ± 0.11
Magnesium (mmol/L)	0.7–1.05	0.53	0.66	0.62	0.62	0.70	0.66	0.74	0.58	0.62	0.53	0.63 ± 0.67
Hematocrit (%)	38.0–47.0	45.7	49.0	46.3	39.9	53.9	54.0	48.3	46.8	44.4	45.6	47.4 ± 4.3
Albumin (g/L)	35–57	43	37	43	48	47	46	43	38	46	45	44 ± 4
PRA (ng/ml/hr)	1.31–3.95	17.15	10.29	47.13	6.32	50.00	31.97	38.35	29.04	30.35	29.14	28.9 ± 14.4
PAC (pg/ml)	70–350	252	206	140	147	134	266	304	320	288	237	229.4 ± 69.6
$HCO3^-$ (mmol/L)	24	31.6	27.2	30.7	28.0	33.0	26.8	28.0	22.6	24.1	35.1	28.7 ± 3.9
Urine												
Creatinine (mmol/L)		10.6	9.4	7.9	5.7	7.3	2.1	7.9	6.2	4.7	5.2	8.6 ± 3.8
Sodium (mmol/L)		172	53	58	66	64	46	96	32	42	199	82.8 ± 57.1
Potassium (mmol/L)		45	21	27	48	43	26	17	56	37	49	36.9 ± 13.3
Chloride (mmol/L)		143	86	93	67	44	59	51	35	77	207	86.2 ± 52.4
Calcium (mmol/L)		0.58	0.55	0.25	1.28	0.23	0.05	0.10	0.63	0.38	0.53	0.46 ± 0.35
Magnesium (mmol/L)		3.09	2.55	2.34	3.58	3.17	0.86	0.62	2.26	1.52	4.61	2.46 ± 1.23
TTKG		7.15	7.28	7.10	10.80	12.51	12.61	7.13	41.13	22.67	6.23	13.46 ± 10.91

SBP, systolic blood pressure; DBP, diastolic blood pressure; PRA, plasma renin activity; PAC, plasma aldosterone concentration; TTKG, transtubular potassium gradient.

respectively. uEVs number was correlated strongly with urine creatinine (r^2 for 0.81, $P < 0.0001$) shown in **Figure 1C**. TEM also confirmed the quality of uEVs isolated by ultracentrifugation (**Figure 1D**). To further validate the uEVs purification protocol, we evaluated four commonly used uEVs makers including AQP2, TSG101, NSE, and CD9 in immunoblotting shown in **Figure 1E**. Expression pattern of selected renal transporters including NHE3, NKCC2, NCC, p-NCC, ENaCβ, pendrin, ROMK, and Maxi-K in healthy controls were shown in **Figure 1F**.

uEVs for Renal Tubular Na^+ and K^+ Associated Transporter Expression in GS

Compared with healthy controls, GS patients with different biallelic mutations exhibited a markedly attenuated expression of NCC and p-NCC protein isolated from their uEVs, indicative of an impaired NCC expression and function in GS (**Figures 2A,B**). The expression of NHE3, ENaCβ, and pendrin significantly increased although NKCC2 was not significantly increased. For uEVs associated renal tubular K^+ associated transporter expression, GS patients had significantly increased ROMK and Maxi-K expression.

Renal Tubular Na^+ and K^+ Associated Transporter Expression From Kidney Tissues in GS

AQP2 used for a tubular maker of CD was clearly stained. Compared with control kidney tissue, the representative kidney tissues from GS patients showed obviously diminished expression in both NCC and p-NCC. The expression of NHE3, ENaCβ and pendrin was significantly increased (**Figure 3**). The expression of ROMK was increased and the Maxi-K unexpressed in control kidney tissue without hypokalemia was also significantly enhanced in three GS patients. Overall, these finding from immunofluorescence of kidney tissues supported the findings of the isolated uEVs to examine Na^+ and K^+ associated renal transporter adaptation in GS patients.

Tubular Transporter Expression From uEVs and Kidney Tissue in Bulimic Patients

Three bulimic patients (male/female = 2/1, age 23.3 ± 4.0 years old) with normotension (systolic blood pressure 102 ± 17 mmHg, diastolic blood pressure 63 ± 5 mmHg) exhibited chronic hypokalemia (K^+ 2.73 ± 0.55 mmol/L), metabolic alkalosis ($HCO3^-$, 46.6 ± 11.9 mmol/L), with secondary hyperreninemia (PRA 4.3 ± 1.3 ng/mL/h) but normal to high PAC (127.6 ± 26.7 pg/mL). They all exhibited higher urinary K^+ excretion, high Na^+ (120.3 ± 80.4 mmol/L) but low Cl^- (18.7 ± 6.4 mmol/L), alkaline urine (bicarbonaturia), indicative of recent vomiting. As shown in **Figure 4A**, uEVs from them showed an increased abundance of NCC and p-NCC as well as NHE3, NKCC2, ENaCβ, pendrin, ROMK and Maxi-K. Immunofluorescence of the kidney tissue from a representative bulimic patient also had the similar finding to those in uEVs (**Figure 4B**).

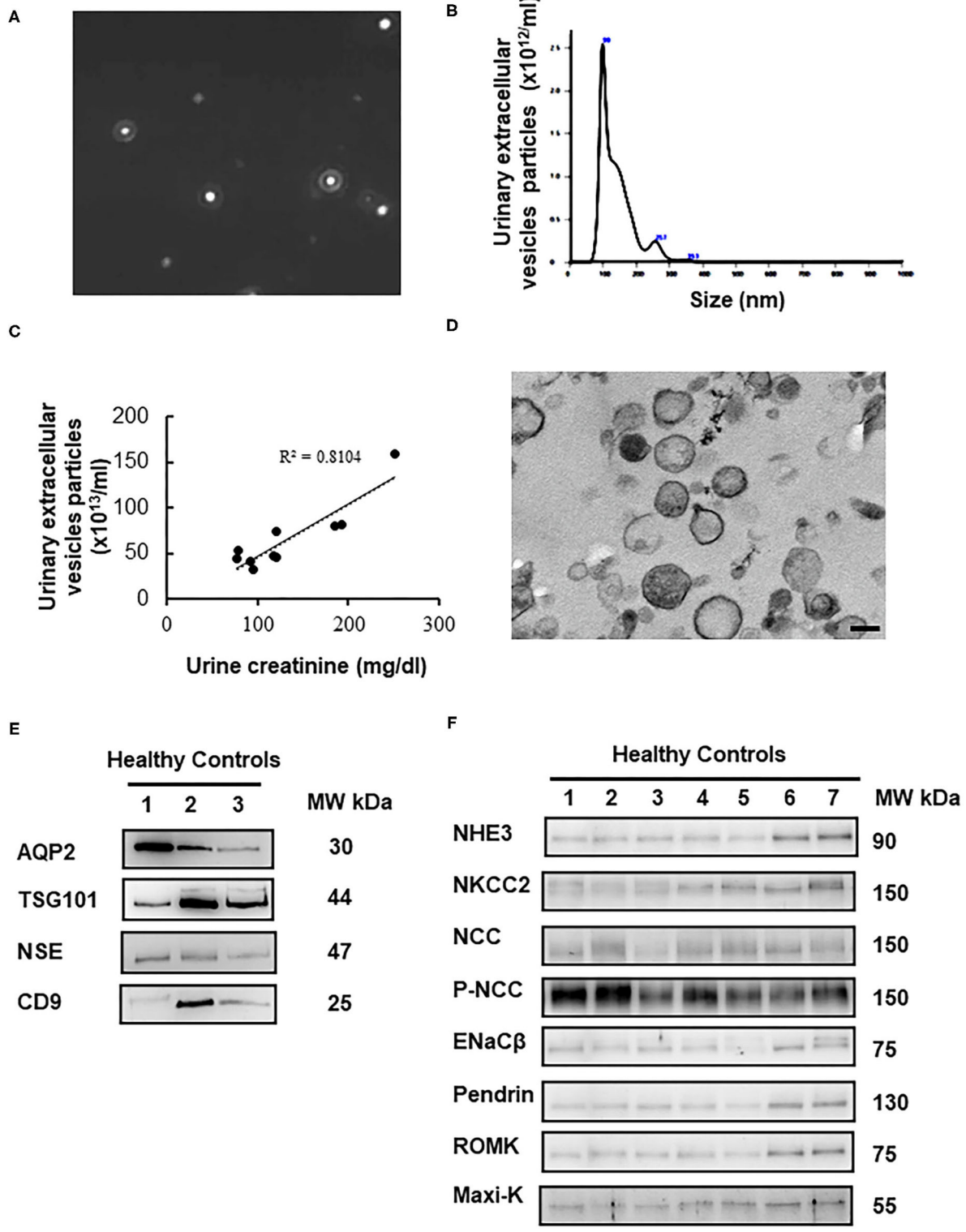

FIGURE 1 | Characterization of urinary extracellular vesicles (uEVs) from healthy controls. **(A)** Screen shot from 1:2,000 diluted urine sample reveals a range of particle sizes by nanoparticle tracking analysis (NTA). **(B)** Concentration and size distribution of uEVs (0–150 nm diameter) by NTA were shown. The concentration is expressed as number of particles per ml. **(C)** uEVs particles were correlated strongly with urine creatinine (r^2 for 0.81, $P < 0.0001$). **(D)** Transmission electron microscopy of uEVs was shown (scale bar 100 nm). **(E)** uEVs markers (AQP2, TSG101, NSE, and CD9) were assessed by immunoblotting. **(F)** Expression pattern of renal transporters including NHE3, NKCC2, NCC, p-NCC, ENaCβ, pendrin, ROMK, and Maxi-K from healthy controls was similar.

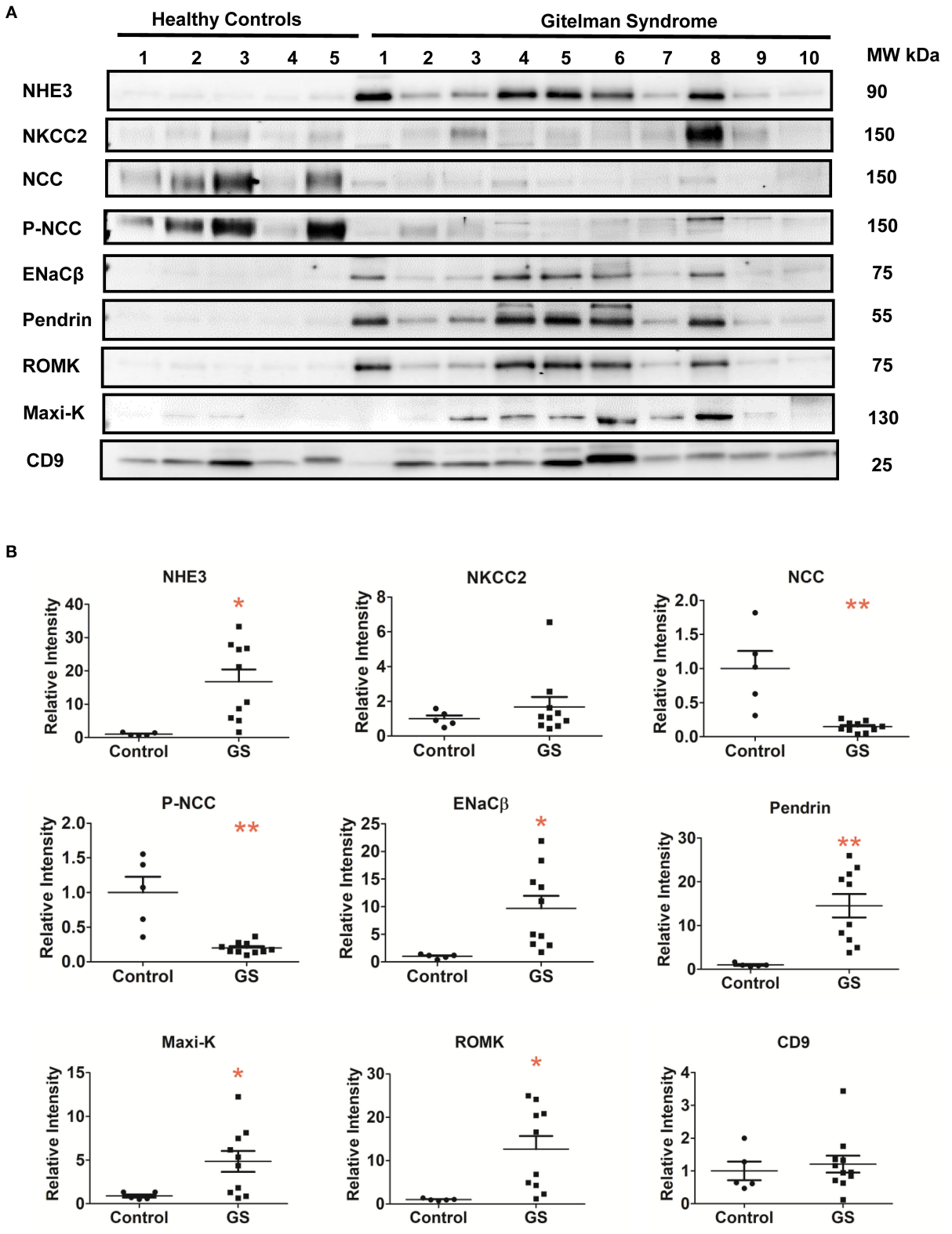

FIGURE 2 | Renal Na^+ and K^+ associated transporters expression from urinary extracellular vesicles in patients with GS ($n = 10$) compared with healthy controls. **(A)** Immunoblotting of renal transporters (NHE3, NKCC2, NCC, p-NCC, ENaCβ, pendrin, ROMK, Maxi-K, and CD9). **(B)** Quantification of immunoblotting of NHE3, NKCC2, NCC, p-NCC, ENaCβ, pendrin, ROMK, Maxi-K, and CD9. Error bars, standard deviation. $^*P < 0.05$, $^{**}P < 0.01$.

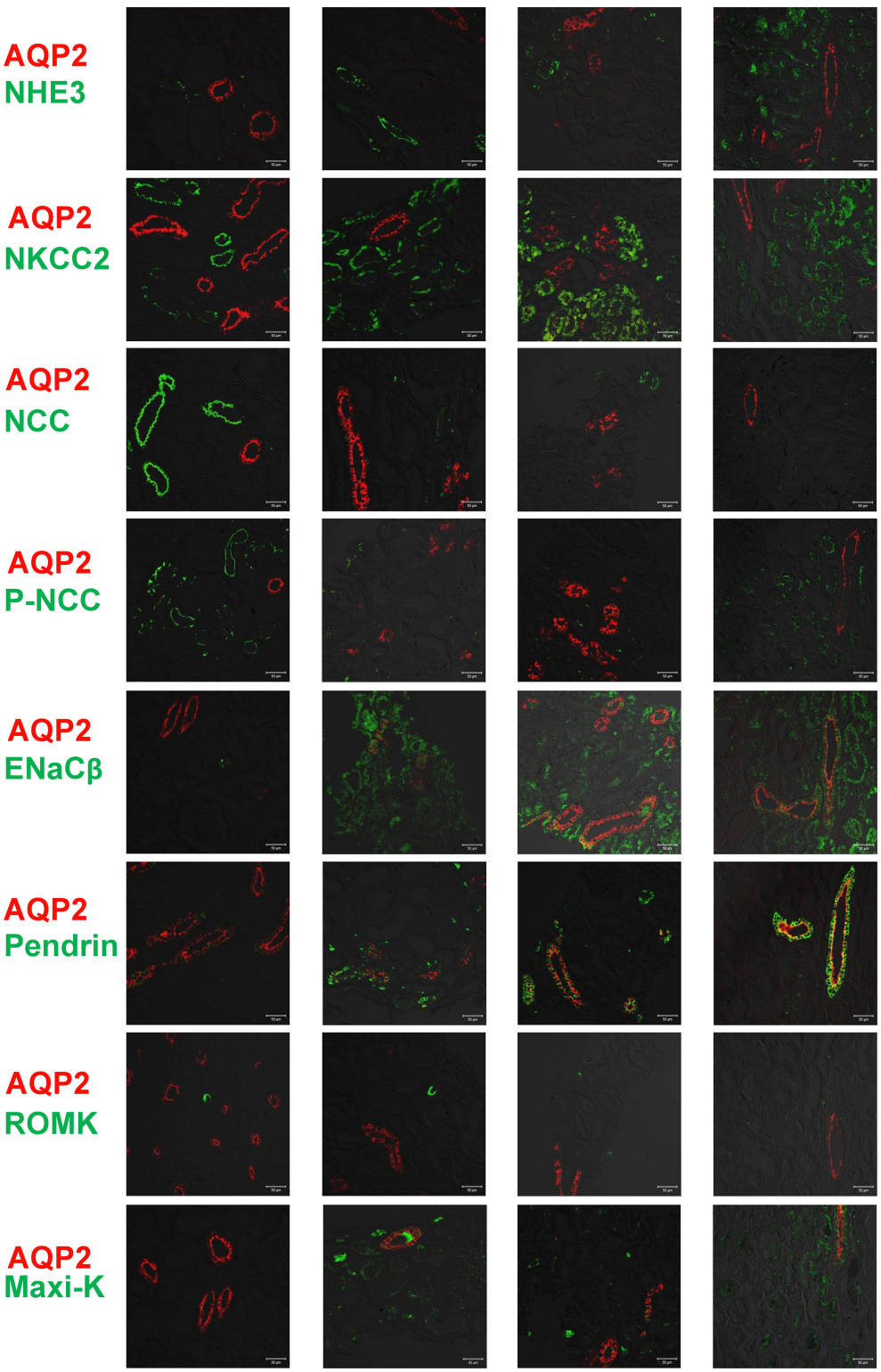

FIGURE 3 | Immunofluorescence of biopsied kidney tissues from another 3 representative GS patients (GS 1, GS 2, and GS 3) compared with the control kidney tissue. Renal transporters including NHE3, NKCC2, NCC, p-NCC, ENaCβ, pendrin, ROMK, Maxi-K were stained with green. AQP2 was stained with red for localization. Scale bar, 50 μm.

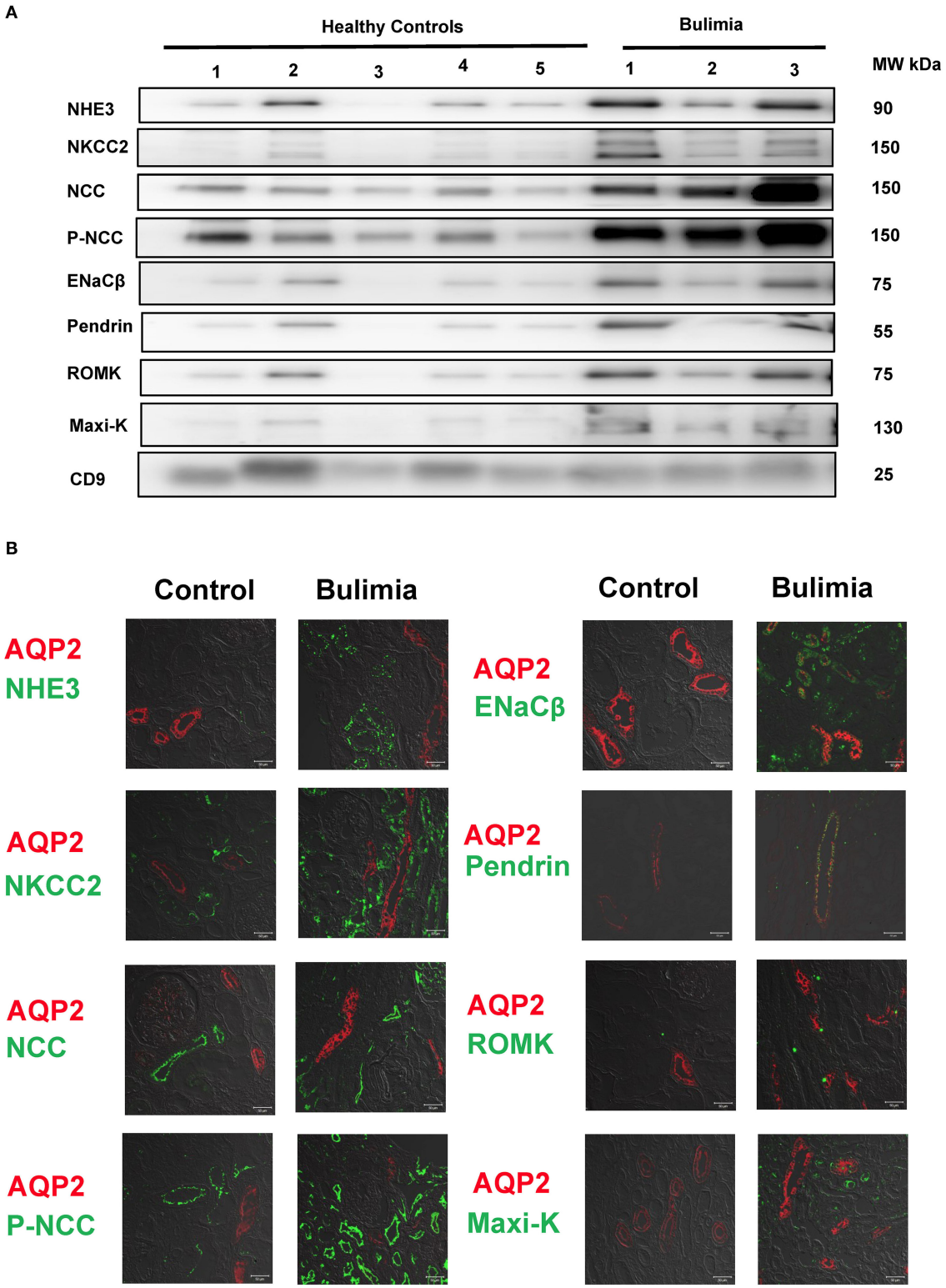

FIGURE 4 | Renal transporters expression from urinary extracellular vesicles (uEVs) and immunofluorescence of biopsied kidney tissues from bulimic patients. **(A)** Immunoblotting of renal transporters (NHE3, NKCC2, NCC, p-NCC, ENaCβ, pendrin, ROMK, Maxi-K, and CD9) from uEVs in bulimic patients ($n = 3$) compared with healthy control. **(B)** Immunofluorescence of NHE3, NKCC2, NCC, p-NCC (green, **right**) and ENaCβ, pendrin, ROMK, Maxi-K (green, **left**) from one representative bulimia patient compared with the control. AQP2 was stained with red for localization. Scale bar, 50 μm.

DISCUSSION

In this study, the isolated uEVs from GS patients with biallelic *SLC12A3* mutations showed the markedly attenuated expression of NCC and p-NCC whereas those from non-GS bulimic patients did a significantly enhanced abundance of NCC and p-NCC. In response to renal salt loss, the expression of upstream NHE3 and downstream ENaCβ, and pendrin were all accentuated. The abundance of ROMK and Maxi-K expression were also augmented for renal K^+ wasting in GS. Immunofluorescence of the representative kidney tissues from GS and bulimic patients also demonstrated similar findings to those from uEVs. This study might be the first to assess the abundance of renal tubular Na^+ and K^+ associated transporters from uEVs and kidney tissues in GS patients.

GS caused by inactivating *SLC12A3* mutations has an impaired NCC expression and/or activity as shown in both *vitro* and *vivo* studies. Although normal NCC expression with an impaired functional activity was shown in oocytes overexpressed T60M mutation at the critical NCC phosphorylation site, a markedly decreased total NCC and p-NCC protein abundance was evident in NccT58M/T58M GS knock-in mice and in the urine of human GS with homozygous T60M mutations (23). In addition, the reduced or abolished NCC abundance on the apical membrane of DCT from the human kidney tissues in GS patients with *SLC12A3* mutations were also demonstrated (24, 25). These findings supported the notion that the reduced expression of NCC was a biomarker for GS despite different mechanisms involved in the impaired NCC protein synthesis (24, 26), and sorting or trafficking defect of NCC (27). Accordingly, it is important to find a non-invasive method to faithfully represent NCC abundance in GS. Previous studies using uEVs to measure the mutated NCC by immunoblotting and enzyme-linked immunosorbent assays (ELISAs) in GS patients only showed the decreased NCC abundance (17, 18). In this study, the isolated uEVs from GS patients revealed that both NCC and p-NCC abundance were markedly diminished, also confirmed by the human kidney tissue of genetically-confirmed GS patients.

It is of great interest to understand and localize the tubular adaptation in the inherited renal tubular disorders. The traditional methods were the preparation of whole kidney sections for immunostaining and immunoblotting or biotinylating the rat or mice kidney tissues *in situ* under various chronic conditions in animal models. Tubular adaptation to renal Na^+ loss has been evaluated in the distal tubules in experimental models of GS but not human GS. Knepper et al. has used the LC-MS/MS to profile the proteome of human uEVs and suggested that uEVs analysis be a potential approach to discover adaptation in renal transporters (12). Using uEVs analysis in GS, we found that the abundance of upstream NHE3 in the proximal tubules (PT) necessary for bicarbonate reabsorption, salt and fluid homeostasis was significantly increased (28–30). Renal NHE3 abundance was markedly increased in K^+-depleted rats (31), indicating that NHE3 expression can be also regulated by the hypokalemia independent of volume depletion. Similarly, downstream ENaCβ in the principal cells of CD for tubular salt reabsorption was enhanced (32, 33). Of note, pendrin as a $Cl^-/HCO3^-$ exchanger expressed in the apical region of distal tubules and involved in the tubular Cl^- absorption and $HCO3^-$ secretion was augmented (34). Activation of pendrin-mediated Cl^- absorption has also been reported in NCC KO mice (35). Although pendrin expression has been examined in many rodent treatment models such as NCC KO mice, an aldosterone infusion or the administration of $NaHCO_3$ to regulate acid-base and salt regulation, our study suggested the increased pendrin expression from uEVs and biopsied kidney tissues be responsive to renal salt wasting and also chronic metabolic alkalosis in GS patients.

K^+ excretion in distal nephron is driven by either voltage-dependent ROMK and/or flow dependent Maxi-K (36). ROMK is an inwardly rectifying K^+ channel (37) traditionally responsible for the main renal K^+ secretory channel, dependent on Na^+ delivery and driven by electrogenic ENaC-mediated Na^+ reabsorption (38–40). Maxi-K is flow-stimulated K^+ secretion and activated by an increase in intracellular calcium and membrane depolarization (41, 42). Defective NaCl absorption in DCT leads to the increased flow rate to downstream connecting tubules (CNT) and CD to naturally stimulate both ROMK and Maxi-K. In animal model of GS (Ser707X knockin mice), an enhanced expression of both ROMK and Maxi-K has been clearly shown (6). Our uEVs for the expression of both ROMK and Maxi-K abundance were significantly increased in GS patients, akin to the findings of their representative immunofluorescence of kidney tissues. Of note, the abundance of Maxi-K was extremely low in both uEVs and biopsied kidney in controls but higher in GS patients, indicating that Maxi-K expression was more augmented at the high urinary flow rate.

The above-mentioned findings with an increased protein expression related to Na^+ reabsorption, K^+ secretion and regulation of acid/base balance at distal nephron from the uEVs in our GS patients with diminished NCC expression consisted with current idea that distal tubules including CD are highly plastic. Tubular plasticity for adaptation is defined as structural remodeling of renal tubules via cell proliferation (hyperplasia) and cell growth (hypertrophy) (43, 44). In NCC-deficient mice, early DCT showed a remarkable atrophy but CNT exhibited a marked epithelial hypertrophy accompanied by an increased apical abundance of ENaC (45). In SPAK KO mice featuring GS-like phenotypes, a distal nephron remodeling process of the CNT/CD developed to produce an increase in the numbers of principle cells and β-intercalated cells (46). These two mice models with deficient NCC clearly demonstrated the markedly attenuated DCT along with the distinctly hypertrophic and/or hyperplastic CNT/CD. Our uEVs results in GS patients were similar to those from NCC deficient animal studies, also supporting the notion of nephron plasticity with compensatory increase in the CNT/CD size.

Bulimic patients, also called pseudo-GS syndrome (47, 48), exhibiting similar laboratory and clinical features to GS, were also evaluated for disease controls. In contrast to GS patients, uEVs from bulimic patients showed a markedly enhanced abundance of NCC and p-NCC. The increased NCC and p-NCC abundance may be secondary response to volume depletion and K^+ deficiency *per se*. In rat model of K^+ deficiency, enhanced abundance NCC and p-NCC has been clearly shown (49),

closely linked to increased WNK body formation and activation of SPAK/OSR1 (50). Similarly, uEVs for upstream NHE3 and NKCC2 along with downstream ENaCβ and pendrin expression were also increased in response to salt-losing and metabolic alkalosis. Of interest, only the slightly increased ROMK and Maxi-K abundance from the isolated uEVs and biopsied kidney tissues may be associated with the interaction of bicarbonaturia to stimulate them as well as the enhanced NCC and chronic hypokalemia to suppress them.

Recently, uEVs has been emerged as a promising liquid biopsy biomarker in kidney disease research. Several novel biomarkers from uEVs including proteins, miRNA or non-coding RNA have been discovered in acute kidney injury (51, 52), chronic kidney disease (53, 54), diabetic nephropathy (55), focal segmental glomerulosclerosis (56), and lupus nephritis (57). In addition to GS and Bartter syndrome, uEVs is also utilized in some renal tubular disorders such as nephrogenic diabetes insipidus, and familial hyperkalemic hypertension due to *KLHL3* mutation (58). Accordingly, these evidence demonstrated the relevance of uEVs in understanding the pathophysiology of kidney diseases and the discovery of potential therapeutic targets. Our study provided a feasible way to analyze the differential expression proteins in renal tubular disorders and may be also applied to other non-tubular disorder such as cisplatin or drug induced tubulopathy.

There were some limitations of this study. First, the sample size of GS patients was still small due to the restricted loading wells of SDS/PAGE for immunoblotting. Second, other relevant transporters along the renal tubules such as TRPV5 and TRPM6 were not examined because of limited uEVs proteins isolated from ultracentrifugation. Third, the localization of these transporters in renal tubules could not be identified using uEVs. Finally, the specificity and sensitivity of the antibodies used for this study might affect expression of renal transporters between immunoblotting and immunofluorescence (for example NKCC2). Using the detergent for immunoblotting is another approach to enhance intracellular epitope recognition in uEVs (22).

In conclusion, uEVs could be used as non-invasive diagnostic tool to evaluate the renal tubular Na^+ or K^+ associated transporters expression in GS patients. High-throughput proteomic studies from uEVs in GS patients will be anticipated in the further investigation.

DATA AVAILABILITY STATEMENT

The original contributions presented in the study are included in the article/supplementary material, further inquiries can be directed to the corresponding author/s.

ETHICS STATEMENT

The studies involving human participants were reviewed and approved by Institutional Review Board of the Tri-Service General Hospital of Taiwan (TSGHIRB No.2-103-05-160 and TSGHIRB No.2-105-05-062). The patients/participants provided their written informed consent to participate in this study.

AUTHOR CONTRIBUTIONS

C-CS, M-HC, and S-HL substantially contributed to study conception and design, acquisition of data, and analysis and interpretation of data. Y-ChaL, Y-ChuL, Y-JL, and S-SY substantially contributed to acquisition of data, and analysis and interpretation of data. All the authors revised the paper and approved the final version of the article to be published.

FUNDING

This research was supported by grants from the Research Fund of the Ministry of Science and Technology (MOST) of Taiwan (MOST 104-2314-B-016-021-MY2 and MOST 106-2314-B-016-033-MY3) and the Research Fund of the Tri-Service General Hospital (TSGH-C107-007-S04, TSGH-C108-007-S04, and TSGH-C108-027).

ACKNOWLEDGMENTS

The authors acknowledge technical services provided by Instrument Center of National Defense Medical Center.

REFERENCES

1. Blanchard A, Bockenhauer D, Bolignano D, Calò LA, Cosyns E, Devuyst O, et al. Gitelman syndrome: consensus and guidance from a Kidney Disease: Improving Global Outcomes (KDIGO) Controversies Conference. *Kidney Int.* (2017) 91:24–33. doi: 10.1016/j.kint.2016.09.046
2. Simon DB, Nelson-Williams C, Bia MJ, Ellison D, Karet FE, Molina AM, et al. Gitelman's variant of Bartter's syndrome, inherited hypokalaemic alkalosis, is caused by mutations in the thiazide-sensitive Na-Cl cotransporter. *Nat Genet.* (1996) 12:24–30. doi: 10.1038/ng0196-24
3. Lo Y-F, Nozu K, Iijima K, Morishita T, Huang C-C, Yang S-S, et al. Recurrent deep intronic mutations in the SLC12A3 gene responsible for Gitelman's syndrome. *Clin J Am Soc Nephrol.* (2011) 6:630–9. doi: 10.2215/CJN.06730810
4. Vargas-Poussou R, Dahan K, Kahila D, Venisse A, Riveira-Munoz E, Debaix H, et al. Spectrum of mutations in Gitelman syndrome. *J Am Soc Nephrol.* (2011) 22:693–703. doi: 10.1681/ASN.2010090907
5. Tseng MH, Yang SS, Hsu YJ, Fang YW, Wu CJ, Tsai JD, et al. Genotype, phenotype, and follow-up in Taiwanese patients with salt-losing tubulopathy associated with SLC12A3 mutation. *J Clin Endocrinol Metab.* (2012) 97:E1478–82. doi: 10.1210/jc.2012-1707
6. Yang SS, Lo YF, Yu IS, Lin SW, Chang TH, Hsu YJ, et al. Generation and analysis of the thiazide-sensitive Na+ -Cl- cotransporter (Ncc/Slc12a3) Ser707X knockin mouse as a model of Gitelman syndrome. *Hum Mutat.* (2010) 31:1304–15. doi: 10.1002/humu.21364
7. van Balkom BW, Pisitkun T, Verhaar MC, Knepper MA. Exosomes and the kidney: prospects for diagnosis and therapy of renal diseases. *Kidney Int.* (2011) 80:1138–45. doi: 10.1038/ki.2011.292
8. Pisitkun T, Shen RF, Knepper MA. Identification and proteomic profiling of exosomes in human urine. *Proc Natl Acad Sci USA.* (2004) 101:13368–73. doi: 10.1073/pnas.0403453101
9. Gonzales P, Pisitkun T, Knepper MA. Urinary exosomes: is there a future? *Nephrol Dial Transplant.* (2008) 23:1799–801. doi: 10.1093/ndt/gfn058

10. Knepper MA, Pisitkun T. Exosomes in urine: who would have thought? *Kidney Int.* (2007) 72:1043–5. doi: 10.1038/sj.ki.5002510
11. Bonifacino JS, Traub LM. Signals for sorting of transmembrane proteins to endosomes and lysosomes. *Annu Rev Biochem.* (2003) 72:395–447. doi: 10.1146/annurev.biochem.72.121801.161800
12. Gonzales PA, Pisitkun T, Hoffert JD, Tchapyjnikov D, Star RA, Kleta R, et al. Large-scale proteomics and phosphoproteomics of urinary exosomes. *J Am Soc Nephrol.* (2009) 20:363–79. doi: 10.1681/ASN.2008040406
13. van der Lubbe N, Jansen PM, Salih M, Fenton RA, van den Meiracker AH, Danser AH, et al. The phosphorylated sodium chloride cotransporter in urinary exosomes is superior to prostasin as a marker for aldosteronism. *Hypertension.* (2012) 60:741–8. doi: 10.1161/HYPERTENSIONAHA.112.198135
14. Salih M, Fenton RA, Zietse R, Hoorn EJ. Urinary extracellular vesicles as markers to assess kidney sodium transport. *Curr Opin Nephrol Hypertens.* (2016) 25:67–72. doi: 10.1097/MNH.0000000000000192
15. Salih M, Bovée DM, van der Lubbe N, Danser AHJ, Zietse R, Feelders RA, et al. Increased urinary extracellular vesicle sodium transporters in Cushing syndrome with hypertension. *J Clin Endocrinol Metab.* (2018) 103:2583–91. doi: 10.1210/jc.2018-00065
16. Wolley MJ, Wu A, Xu S, Gordon RD, Fenton RA, Stowasser M. In primary aldosteronism, mineralocorticoids influence exosomal sodium-chloride cotransporter abundance. *J Am Soc Nephrol.* (2017) 28:56–63. doi: 10.1681/ASN.2015111221
17. Corbetta S, Raimondo F, Tedeschi S, Syrèn ML, Rebora P, Savoia A, et al. Urinary exosomes in the diagnosis of Gitelman and Bartter syndromes. *Nephrol Dial Transplant.* (2015) 30:621–30. doi: 10.1093/ndt/gfu362
18. Isobe K, Mori T, Asano T, Kawaguchi H, Nonoyama S, Kumagai N, et al. Development of enzyme-linked immunosorbent assays for urinary thiazide-sensitive Na-Cl cotransporter measurement. *Am J Physiol Renal Physiol.* (2013) 305:F1374–81. doi: 10.1152/ajprenal.00208.2013
19. Vahia VN. Diagnostic and statistical manual of mental disorders 5: a quick glance. *Indian J Psychiatry.* (2013) 55:220–3. doi: 10.4103/0019-5545.117131
20. Sokolova V, Ludwig AK, Hornung S, Rotan O, Horn PA, Epple M, et al. Characterisation of exosomes derived from human cells by nanoparticle tracking analysis and scanning electron microscopy. *Colloids Surf B Biointerfaces.* (2011) 87:146–50. doi: 10.1016/j.colsurfb.2011.05.013
21. Abdeen A, Sonoda H, Oshikawa S, Hoshino Y, Kondo H, Ikeda M. Acetazolamide enhances the release of urinary exosomal aquaporin-1. *Nephrol Dial Transplant.* (2016) 31:1623–32. doi: 10.1093/ndt/gfw033
22. Blijdorp CJ, Tutakhel OAZ, Hartjes TA, van den Bosch TPP, van Heugten MH, Rigalli JP, et al. Comparing approaches to normalize, quantify, and characterize urinary extracellular vesicles. *J Am Soc Nephrol.* (2021) 32:1210–26. doi: 10.1681/ASN.2020081142
23. Yang SS, Fang YW, Tseng MH, Chu PY, Yu IS, Wu HC, et al. Phosphorylation regulates NCC stability and transporter activity in vivo. *J Am Soc Nephrol.* (2013) 24:1587–97. doi: 10.1681/ASN.2012070742
24. Joo KW, Lee JW, Jang HR, Heo NJ, Jeon US, Oh YK, et al. Reduced urinary excretion of thiazide-sensitive Na-Cl cotransporter in Gitelman syndrome: preliminary data. *Am J Kidney Dis.* (2007) 50:765–73. doi: 10.1053/j.ajkd.2007.07.022
25. Jang HR, Lee JW, Oh YK, Na KY, Joo KW, Jeon US, et al. From bench to bedside: diagnosis of Gitelman's syndrome – defect of sodium-chloride cotransporter in renal tissue. *Kidney Int.* (2006) 70:813–7. doi: 10.1038/sj.ki.5001694
26. Syrén ML, Tedeschi S, Cesareo L, Bellantuono R, Colussi G, Procaccio M, et al. Identification of fifteen novel mutations in the SLC12A3 gene encoding the Na-Cl Co-transporter in Italian patients with Gitelman syndrome. *Hum Mutat.* (2002) 20:78. doi: 10.1002/humu.9045
27. De Jong JC, Van Der Vliet WA, Van Den Heuvel LP, Willems PH, Knoers NV, Bindels RJ. Functional expression of mutations in the human NaCl cotransporter: evidence for impaired routing mechanisms in Gitelman's syndrome. *J Am Soc Nephrol.* (2002) 13:1442–8. doi: 10.1097/01.ASN.0000017904.77985.03
28. Knepper MA, Brooks HL. Regulation of the sodium transporters NHE3, NKCC2 and NCC in the kidney. *Curr Opin Nephrol Hypertens.* (2001) 10:655–9. doi: 10.1097/00041552-200109000-00017
29. Bobulescu IA, Moe OW. Na^+/H^+ exchangers in renal regulation of acid-base balance. *Semin Nephrol.* (2006) 26:334–44. doi: 10.1016/j.semnephrol.2006.07.001
30. Fenton RA, Poulsen SB, de la Mora Chavez S, Soleimani M, Dominguez Rieg JA, Rieg T. Renal tubular NHE3 is required in the maintenance of water and sodium chloride homeostasis. *Kidney Int.* (2017) 92:397–414. doi: 10.1016/j.kint.2017.02.001
31. Elkjaer ML, Kwon TH, Wang W, Nielsen J, Knepper MA, Frøkiaer J, et al. Altered expression of renal NHE3, TSC, BSC-1, and ENaC subunits in potassium-depleted rats. *Am J Physiol Renal Physiol.* (2002) 283:F1376–88. doi: 10.1152/ajprenal.00186.2002
32. Khuri RN, Strieder WN, Giebisch G. Effects of flow rate and potassium intake on distal tubular potassium transfer. *Am J Physiol.* (1975) 228:1249–61. doi: 10.1152/ajplegacy.1975.228.4.1249
33. Malnic G, Berliner RW, Giebisch G. Flow dependence of K^+ secretion in cortical distal tubules of the rat. *Am J Physiol.* (1989) 256 (5 Pt 2):F932–41. doi: 10.1152/ajprenal.1989.256.5.F932
34. Wall SM, Verlander JW, Romero CA. The renal physiology of pendrin-positive intercalated cells. *Physiol Rev.* (2020) 100:1119–47. doi: 10.1152/physrev.00011.2019
35. Soleimani M, Barone S, Xu J, Shull GE, Siddiqui F, Zahedi K, et al. Double knockout of pendrin and Na-Cl cotransporter (NCC) causes severe salt wasting, volume depletion, and renal failure. *Proc Natl Acad Sci USA.* (2012) 109:13368–73. doi: 10.1073/pnas.1202671109
36. Subramanya AR, Ellison DH. Distal convoluted tubule. *Clin J Am Soc Nephrol.* (2014) 9:2147–63. doi: 10.2215/CJN.05920613
37. Hebert SC. An ATP-regulated, inwardly rectifying potassium channel from rat kidney (ROMK). *Kidney Int.* (1995) 48:1010–6. doi: 10.1038/ki.1995.383
38. Lee WS, Hebert SC. ROMK inwardly rectifying ATP-sensitive K+ channel. I. Expression in rat distal nephron segments. *Am J Physiol.* (1995) 268 (6 Pt 2):F1124–31. doi: 10.1152/ajprenal.1995.268.6.F1124
39. Giebisch G. Renal potassium transport: mechanisms and regulation. *Am J Physiol.* (1998) 274:F817–33. doi: 10.1152/ajprenal.1998.274.5.F817
40. Welling PA, Ho K. A comprehensive guide to the ROMK potassium channel: form and function in health and disease. *Am J Physiol Renal Physiol.* (2009) 297:F849–63. doi: 10.1152/ajprenal.00181.2009
41. Pluznick JL, Sansom SC. BK channels in the kidney: role in K(+) secretion and localization of molecular components. *Am J Physiol Renal Physiol.* (2006) 291:F517–29. doi: 10.1152/ajprenal.00118.2006
42. Rodan AR, Huang CL. Distal potassium handling based on flow modulation of maxi-K channel activity. *Curr Opin Nephrol Hypertens.* (2009) 18:350–5. doi: 10.1097/MNH.0b013e32832c75d8
43. Kaissling B, Bachmann S, Kriz W. Structural adaptation of the distal convoluted tubule to prolonged furosemide treatment. *Am J Physiol.* (1985) 248 (3 Pt 2):F374–81. doi: 10.1152/ajprenal.1985.248.3.F374
44. Kaissling B, Stanton BA. Adaptation of distal tubule and collecting duct to increased sodium delivery. I. Ultrastructure. *Am J Physiol.* (1988) 255 (6 Pt 2):F1256–68. doi: 10.1152/ajprenal.1988.255.6.F1256
45. Loffing J, Vallon V, Loffing-Cueni D, Aregger F, Richter K, Pietri L, et al. Altered renal distal tubule structure and renal Na^+ and Ca^{2+} handling in a mouse model for Gitelman's syndrome. *J Am Soc Nephrol.* (2004) 15:2276–88. doi: 10.1097/01.ASN.0000138234.18569.63
46. Grimm PR, Lazo-Fernandez Y, Delpire E, Wall SM, Dorsey SG, Weinman EJ, et al. Integrated compensatory network is activated in the absence of NCC phosphorylation. *J Clin Invest.* (2015) 125:2136–50. doi: 10.1172/JCI78558
47. Seyberth HW, Schlingmann KP. Bartter- and Gitelman-like syndromes: salt-losing tubulopathies with loop or DCT defects. *Pediatr Nephrol.* (2011) 26:1789–802. doi: 10.1007/s00467-011-1871-4
48. Matsunoshita N, Nozu K, Shono A, Nozu Y, Fu XJ, Morisada N, et al. Differential diagnosis of Bartter syndrome, Gitelman syndrome, and pseudo-Bartter/Gitelman syndrome based on clinical characteristics. *Genet Med.* (2016) 18:180–8. doi: 10.1038/gim.2015.56
49. Frindt G, Palmer LG. Effects of dietary K^+ on cell-surface expression of renal ion channels and transporters. *Am J Physiol Renal Physiol.* (2010) 299:F890–7. doi: 10.1152/ajprenal.00323.2010
50. Wade JB, Liu J, Coleman R, Grimm PR, Delpire E, Welling PA. SPAK-mediated NCC regulation in response to low-K+ diet. *Am J Physiol Renal Physiol.* (2015) 308:F923–31. doi: 10.1152/ajprenal.00388.2014

51. Sonoda H, Lee BR, Park K-H, Nihalani D, Yoon J-H, Ikeda M, et al. miRNA profiling of urinary exosomes to assess the progression of acute kidney injury. *Scientific Reports.* (2019) 9:4692. doi: 10.1038/s41598-019-40747-8
52. Awdishu L, Tsunoda S, Pearlman M, Kokoy-Mondragon C, Ghassemian M, Naviaux RK, et al. Identification of maltase glucoamylase as a biomarker of acute kidney injury in patients with cirrhosis. *Crit Care Res Pract.* (2019) 2019:5912804. doi: 10.1155/2019/5912804
53. Khurana R, Ranches G, Schafferer S, Lukasser M, Rudnicki M, Mayer G, et al. Identification of urinary exosomal noncoding RNAs as novel biomarkers in chronic kidney disease. *Rna.* (2017) 23:142–52. doi: 10.1261/rna.058834.116
54. Wang B, Zhang A, Wang H, Klein JD, Tan L, Wang ZM, et al. miR-26a limits muscle wasting and cardiac fibrosis through exosome-mediated microRNA transfer in chronic kidney disease. *Theranostics.* (2019) 9:1864–77. doi: 10.7150/thno.29579
55. Zang J, Maxwell AP, Simpson DA, McKay GJ. Differential expression of urinary exosomal microRNAs miR-21-5p and miR-30b-5p in individuals with diabetic kidney disease. *Sci Rep.* (2019) 9:10900. doi: 10.1038/s41598-019-47504-x
56. Gebeshuber CA, Kornauth C, Dong L, Sierig R, Seibler J, Reiss M, et al. Focal segmental glomerulosclerosis is induced by microRNA-193a and its downregulation of WT1. *Nat Med.* (2013) 19:481–7. doi: 10.1038/nm.3142
57. Garcia-Vives E, Solé C, Moliné T, Vidal M, Agraz I, Ordi-Ros J, et al. The urinary exosomal miRNA expression profile is predictive of clinical response in lupus nephritis. *Int J Mol Sci.* (2020) 21:1372. doi: 10.3390/ijms21041372
58. Salih M, Fenton RA, Knipscheer J, Janssen JW, Vredenbregt-van den Berg MS, Jenster G, et al. An immunoassay for urinary extracellular vesicles. *Am J Physiol Renal Physiol.* (2016) 310:F796–801. doi: 10.1152/ajprenal.00463.2015

Conflict of Interest: The authors declare that the research was conducted in the absence of any commercial or financial relationships that could be construed as a potential conflict of interest.

frontiers in Medicine

SYSTEMATIC REVIEW
published: 01 November 2021
doi: 10.3389/fmed.2021.728089

Effects of SGLT2 Inhibitors on Renal Outcomes in Patients With Chronic Kidney Disease: A Meta-Analysis

Ning Li[1], Dan Lv[1], Xiangjun Zhu[1], Ping Wei[1], Yuan Gui[2], Shijia Liu[1], Enchao Zhou[1], Min Zheng[1], Dong Zhou[2] and Lu Zhang[1]**

[1] Division of Nephrology, Affiliated Hospital of Nanjing University of Chinese Medicine, Jiangsu Province Hospital of Chinese Medicine, Nanjing, China, [2] Division of Nephrology, Department of Medicine, University of Connecticut, School of Medicine, Farmington, CT, United States

Introduction: The effects of sodium-glucose cotransporter-2 (SGLT2) inhibitors on renal outcomes in patients with chronic kidney disease (CKD) were initially demonstrated in recent trials. However, the magnitude of renal benefits for CKD patients with different baseline features and underlying diseases remains unclear.

Method: We systematically searched the Embase, PubMed, Web of Science, and Cochrane library databases from inception to April 15, 2021 to identify eligible trials. The primary outcome was a composite of worsening kidney function, end-stage kidney disease (ESKD), or renal death. Efficacy and safety outcomes were stratified by baseline features, such as type 2 diabetes, heart failure, atherosclerotic cardiovascular disease, proteinuria, and renal function.

Results: A total of nine studies were included. These studies included 25,749 patients with estimated glomerular filtration rate (eGFR)<60 mL/min/1.73 m² and 12,863 patients with urine albumin-to-creatinine ratio (UACR) >300 mg/g. SGLT2 inhibitors reduced the risk of the primary renal outcome by 30% in patients with eGFR<60 mL/min/1.73 m^2 (HR 0.70, [95% CI 0.58–0.83], $I^2 = 0.00\%$) and by 43% in patients with UACR > 300 mg/g (HR 0.57, [95% CI 0.48–0.67], $I^2 = 16.59\%$). A similar benefit was observed in CKD patients with type 2 diabetes. SGLT2 inhibitors had no clear effects on renal outcomes in patients with eGFR<60 mL/min/1.73 m² combined with atherosclerotic cardiovascular disease (HR 0.74, [95% CI 0.51–1.06], $I^2 = 0.00\%$). However, they reduced the risk of major renal outcomes by 46% (HR 0.54, [95% CI 0.38–0.76], $I^2 = 0.00\%$) in patients with atherosclerotic cardiovascular disease and macroalbuminuria (defined as UACR > 300 mg/g). SGLT2 inhibitors did not significantly reduce the risk of major renal outcomes in CKD patients with heart failure (eGFR<60 mL/min/1.73 m²: HR 0.81, [95% CI 0.47–1.38], $I^2 = 0.00\%$; UACR > 300 mg/g: HR 0.66, [95% CI 0.41–1.07], $I^2 = 0.00\%$). SGLT2 inhibitors showed consistent renal benefits across different levels of eGFR (P interaction = 0.48).

Conclusion: SGLT2 inhibitors significantly reduced the risk of the primary outcome in CKD patients. However, for patients with different features and underlying diseases, there exists differences in the renal protective effect.

Keywords: SGLT2 inhibitors, chronic kidney disease, renal outcome, protective effect, meta-analysis

OPEN ACCESS

Edited by:
Maik Gollasch, Charité—Universitätsmedizin Berlin, Germany

Reviewed by:
Jung Eun Lee, Yonsei University, South Korea
Atsushi Tanaka, Saga University, Japan
Husam Salah, University of Arkansas for Medical Sciences, United States

***Correspondence:**
Lu Zhang
zhanglu@njucm.edu.cn
Dong Zhou
dzhou@uchc.edu

Specialty section:
This article was submitted to Nephrology, a section of the journal Frontiers in Medicine

Received: *20 June 2021*
Accepted: *08 October 2021*
Published: *01 November 2021*

Citation:
Li N, Lv D, Zhu X, Wei P, Gui Y, Liu S, Zhou E, Zheng M, Zhou D and Zhang L (2021) Effects of SGLT2 Inhibitors on Renal Outcomes in Patients With Chronic Kidney Disease: A Meta-Analysis. Front. Med. 8:728089. doi: 10.3389/fmed.2021.728089

INTRODUCTION

Chronic kidney disease (CKD) has become a major global public health problem that imposes a heavy burden on families and society. Currently, about 700 million individuals worldwide suffer from CKD, and the incidence will continue to increase (1). Determining how to delay the progression of renal function impairment has become a global focus. Within the past two decades, the only approved renoprotective therapy for CKD patients, notably those with type 2 diabetes, has been renin-angiotensin system (RAS) blockers (2). It is encouraging that in recent years, more and more novel drugs have been developed that provide renoprotection for CKD patients (3–5), including sodium-glucose cotransporter-2 (SGLT2) inhibitors. The emergence of SGLT2 inhibitors has resulted in promising new options for renoprotection.

SGLT2 inhibitors, a new class of glucose-lowering drugs, have been proven to reduce blood glucose, blood pressure, and body mass index (6). Within the past few years, many large-scale trials have been designed to explore cardioprotection and renoprotection in patients with type 2 diabetes or heart failure (7–9). However, most of the primary outcomes of these studies were cardiovascular outcomes. Furthermore, most of the participants did not have CKD. Given these factors, the benefits of SGLT2 inhibitors for renal outcomes in patients with CKD have been questionable.

Over the last 2 years, two large studies (10, 11) that focused on patients with CKD demonstrated the renal benefits of SGLT2 inhibitors in these patients. In the CREDENCE trial (11), the first dedicated trial of an SGLT2 inhibitor in patients with type 2 diabetes and CKD, canagliflozin demonstrated substantial benefits for renal outcomes. In the DAPA-CKD trial (10), data showed that individuals with CKD who received dapagliflozin had a significantly lower risk of a composite of renal outcomes compared with those who received placebo, independent of the presence or absence of type 2 diabetes. However, whether the clinical benefits are related to baseline data, underlying diseases, or renal function remains unknown. It is difficult to draw meaningful conclusions from individual trials. Therefore, we sought to undertake a systematic review to gain more reliable evidence on the renal benefits of SGLT2 inhibitors in CKD patients with different baseline features and underlying diseases.

METHODS

Study Registration

This systematic review and meta-analysis was designed and guided according to the Preferred Reporting Items for Systematic Reviews and Meta-Analysis (PRISMA) statement (12). Moreover, this meta-analysis was registered in the PROSPERO database (CRD42021247839). No ethical approval or patient consent was required given that all analyses were conducted based on previously published studies.

Search Strategy

Without language or publication time restrictions, two authors searched for relevant randomized controlled trials that investigated the efficacy of SGLT2 inhibitors in CKD. The following electronic databases were searched: PubMed, Web of Science, Sciencedirect, Embase, and Clinical trials (http://www.clinicaltrials.gov) from their inception to April 15, 2021.

Together with Boolean logical operators, the search was conducted using medical subject headings (MeSH) incorporated with free text terms. The following terms were searched: ("Sodium-Glucose Transporter 2 Inhibitors" OR "sodium glucose transporter ii inhibitor" OR "Sodium–glucose cotransporter 2 inhibitors" OR "SGLT-2 Inhibitors" OR "Inhibitor, SGLT-2" OR "Gliflozins" OR "Canagliflozin" OR "Dapagliflozin" OR "Empagliflozin" OR "luseogliflozin" OR "Ipragliflozin" OR "Tofogliflozin" OR "Sotagliflozin" OR "Remogliflozin" OR "Sergliflozin" OR "Ertugliflozin") AND "Randomized controlled trial". Any terms related to "SGLT2i" were searched to prevent leakages.

Meanwhile, we performed several exhaustive searches of major international conference proceedings, grey literature [the non-commercial bibliography of doctors' and masters', technical documents (including government reports)] and clinical trials that may be ongoing or not yet published to minimize loss or omission of suitable articles that met our inclusion criterion. Additionally, the references in each study and meta-analysis of SGLT2 inhibitors were searched for potentially eligible studies. Details on the databases and search strategies are presented in the search strategies supplement. A check was indispensable for the integrity and veracity of studies. All records from the initial search were imported into NoteExpress v3.2.0.7535 to manage and confirm the above information, and was performed concurrently by two independent authors (NL, DL). Discrepancies during this process were resolved through discussion or mediated by a third author (LZ).

Inclusion Criteria and Literature Selection Process

Population

The included population was patients ≥18 years old with CKD, defined as estimated glomerular filtration rate (eGFR) <60 mL/min/1.73 m^2 or urine albumin-to-creatinine ratio (UACR) > 300 mg/g. There were no race or sex restrictions.

Interventions

The included trials required the intervention group to take an SGLT2 inhibitor, and there were no limits on specific doses. Trials of SGLT2 inhibitors in combination with other basic therapeutic agents (such as those for controlling blood pressure or blood sugar) were also permitted.

Comparators

Control groups without treatment or treated only with placebos were included. Control groups provided basic treatment were also included.

Outcomes

The primary outcomes of this study included: worsening kidney function (defined as doubling of serum creatinine or sustained 40% decline in eGFR), end-stage kidney disease

(ESKD) (defined as requirement for chronic dialysis or kidney transplantation, or sustained eGFR below 15 mL/min/1.73 m^2) or renal death. If the study reported both doubling of serum creatinine and sustained 40% decline in eGFR, we prioritized sustained 40% decline in eGFR as the definition of worsening kidney function. The secondary renal outcome was a composite outcome including worsening kidney function, ESKD, renal death or cardiovascular death, other secondary outcomes including MACE (cardiovascular death, myocardial infarction, and stroke), annualized eGFR slope (annualized difference in eGFR between treatment and control groups), and the percentage of reduction in UACR compared with placebo. The safety outcomes included acute kidney injury, amputation, bone fracture, and volume depletion.

Study Design

Trials were restricted to parallel-group multicenter randomized controlled trials. There were no regional or language restrictions. Repetitive studies, case reports, animal experiments, cohort studies, and retrospective studies were excluded.

Data Extraction and Quality Assessment

We focused on extracting the following information from each study: sample size, age, publication year, study and population features, outcomes of interest, and period of treatment. Data were extracted by three authors (NL, DL, YG) with use of a standardized data form. If we encountered problems during the data extraction process, we consulted two experts in this field (LZ and DZ) for resolution through discussion. For data not available in the original text or appendices, we obtained the relevant secondary analyses by contacting the authors.

The Cochrane quality assessment tool provided by RevMan was used to evaluate the risk of bias in each trial (13). Three authors (NL, DL, SL) independently assessed the risk of bias. The assessment items included random sequence generation, allocation concealment, blinding of participants and personnel, blinding of outcome assessment, incomplete outcome assessment, incomplete outcome data, selective reporting, and other biases. Each item was rated as unknown risk, low risk, or high risk. Analysis of total bias for included studies was also measured. Additionally, the Grading of Recommendations Assessment, Development, and Evaluation (GRADE) framework was used to assess the quality of each outcomes (14). Any discrepancies were adjudicated by a third author (LZ or DZ).

Data Analysis

If the studies provided corresponding hazard ratio (HR) values, we pooled HRs with 95% confidence intervals (CIs) to evaluate the effect of each trial. If the study only provided the number of events, we used the risk ratio (RR) for the calculation (HR and RR values were analyzed separately and not combined). For continuous variables, weighted mean differences (WMD) were used for analysis. Additionally, we used a random-effects models with application of the DerSimonian–Laird estimator. We assessed heterogeneity between studies using the I^2 statistics. Values of 25% or less, 25–50%, and 75% and more represented mild, moderate, and high heterogeneity, respectively (15). If the number of included studies was over 10, we conducted a publication bias analysis using the Egger test (16). For different definitions of renal outcomes among the studies, we excluded inconsistent renal outcomes and retained identical renal outcomes for sensitivity analysis. We performed subgroup analyses on primary outcomes to verify if there were any differences between different eGFR subgroups, and whether benefits changed in patients with different underlying diseases [such as type 2 diabetes, heart failure, atherosclerotic cardiovascular disease(ASCVD)]. For each outcome, patients were divided into two groups: UACR > 300 mg/g or eGFR < 60 mL/min/1.73 m^2. If several studies divided eGFR subgroups into eGFR of 60–45 mL/min/1.73 m^2 and <45 mL/min/1.73 m^2, we then combined the HR values of these different eGFR subgroups for analysis. Data were analyzed using STATA version 16.0.

RESULTS

Study Selection and Features

A total of 3,286 studies were retrieved by searching the various databases. After screening abstracts and removing duplicates, 76 studies were retrieved. We performed full-text analyses of the studies, and a total of nine were ultimately included according to our strict criteria (**Figure 1**). Among them, four (8, 9, 17, 18) included patients with type 2 diabetes, two (11, 19) included patients with diabetic kidney disease, two (7, 20) included patients with heart failure, and three (10, 11, 19) included patients with CKD. The detailed screening and retrieval process is shown in the Appendix. The intervention in all studies was SGLT2 inhibitors, and the control groups received matching placebos. All participants were CKD patients. In total, 25,749 had eGFR <60 mL/min/1.73 m^2 and 12,863 had macroalbuminuria (defined as UACR > 300 mg/g). The lowest eGFR value was 20 mL/min/1.73 m^2. Mean age among the trials ranged from 61.9 to 69 years. Median follow-up time ranged from 16 to 42 months. Features of the included studies are shown in **Table 1**.

Quality Evaluation of Included Studies

There was a certain risk of bias in some of the included studies. Sufficient generation of random sequence was observed in eight trials, while this was unspecified in one trial (19). Adequate blinding of participants and personnel was noted in all studies. Only five trials (8–10, 17, 20) mentioned allocation concealment, while this was unclear in the remaining studies. Relative completeness in the evaluation of outcomes was demonstrated in all studies. The completeness of outcome data in one trial (11) was unclear. Other biases from all of the studies were unclear. Details on overall and individual biases are shown in the **Supplementary Figures 1A,B**.

Primary Outcome

For patients with eGFR < 60 mL/min/1.73 m^2, SGLT2 inhibitors reduced the risk of primary renal outcomes by 30% (HR 0.70, [95% CI 0.58–0.83], $I^2 = 0\%$) compared with placebo (**Figure 2**). The same benefit (**Figure 2**) occurred in patients with macroalbuminuria (reduced by 43% compared with placebo, HR 0.57, [95% CI 0.48–0.67], $I^2 = 16.59\%$). Sensitivity analysis

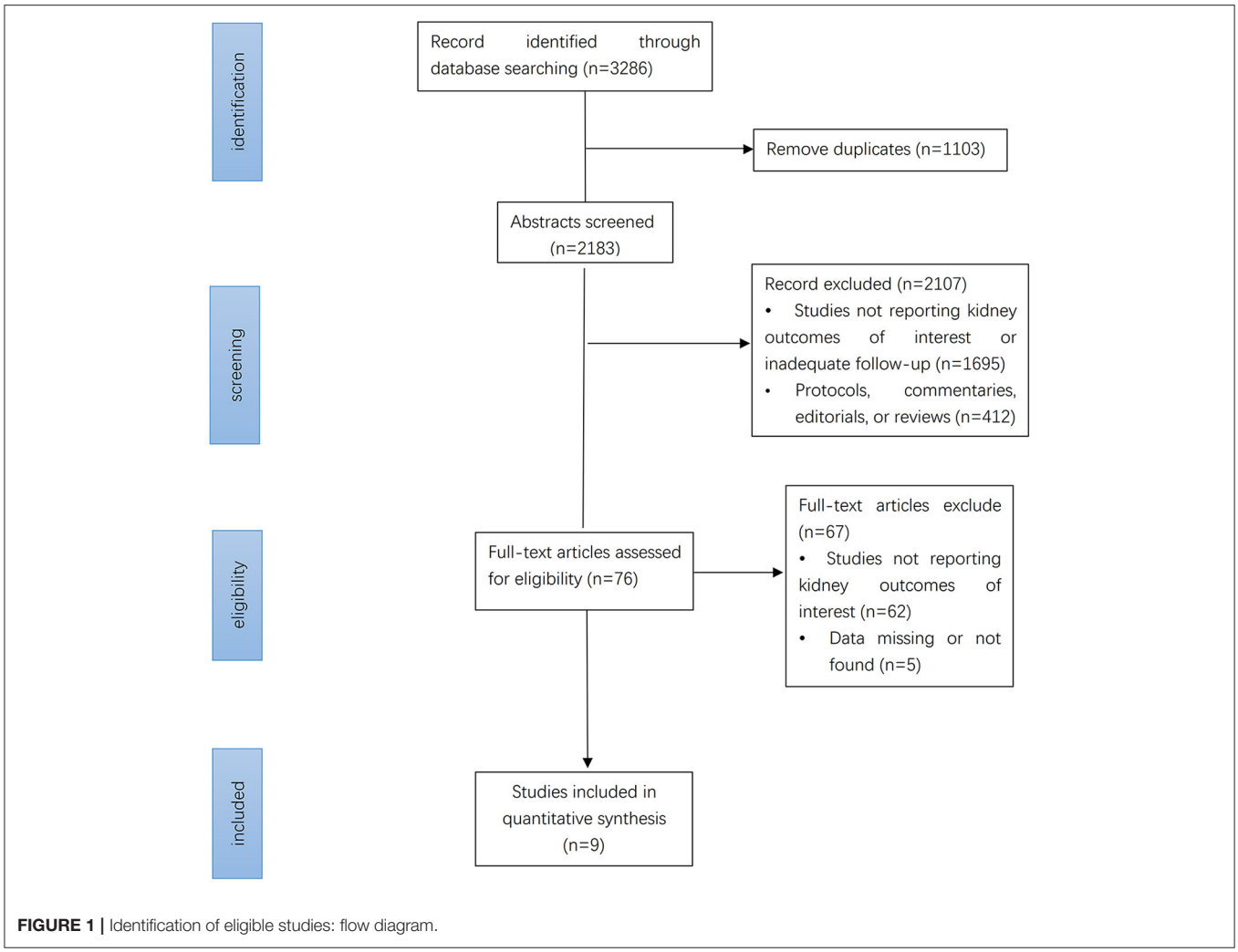

FIGURE 1 | Identification of eligible studies: flow diagram.

showed that different definitions of worsening kidney function did not alter the risk reduction of primary renal outcomes (**Supplementary Table 4**).

eGFR Subgroups

SGLT2 inhibitors reduced the risk of the primary outcome across different subgroups of eGFR (**Figure 3**). For patients with eGFR of 45–60 mL/min/1.73 m^2, the HR was reduced by 38% (HR 0.62, [95% CI 0.47–0.82], $I^2 = 3.31\%$) and by 29% in patients with eGFR of 30–45 mL/min/1.73 m^2 (HR 0.71, [95% CI 0.57–0.87], $I^2 = 0\%$). SGLT2 inhibitors also significantly reduced the risk of primary outcomes among patients with eGFR <30 mL/min/1.73 m^2 (**Figure 3**) compared with placebo (RR 0.68, [95% CI 0.49–0.96], $I^2 = 0.00\%$). The effect of reduction in primary outcomes appeared to be consistent with eGFR ≥ 30 mL/min/1.73 m^2 (P interaction = 0.37).

Subgroups for Different Underlying Diseases

Patients With Type 2 Diabetes

For patients with type 2 diabetes, SGLT2 inhibitors reduced the primary outcomes by 36% in those with eGFR < 60 mL/min/1.73 m^2 (**Figure 4**, HR 0.64, [95% CI 0.55–0.76], $I^2 = 0.00\%$) and by 44% in those with UACR > 300 mg/g (**Figure 4**, HR 0.56, [95% CI 0.46–0.68], $I^2 = 30.47\%$).

Patients With Heart Failure

For patients with heart failure, there was no significant benefit in primary outcome compared with placebo in those with eGFR <60 mL/min/1.73 m^2 (**Figure 4**, HR 0.81, [95% CI 0.47–1.38], $I^2 = 0.00\%$), or UACR > 300 mg/g (**Figure 4**, HR 0.66, [95% CI 0.41–1.07], $I^2 = 0.00\%$).

Patients With ASCVD

Although the risk of major renal outcomes was reduced by 46% in patients with macroalbuminuria with ASCVD (**Figure 4**, HR 0.54, [95% CI 0.38–0.76], $I^2 = 0.00\%$), SGLT2 inhibitors did not significantly reduce the risk in those with eGFR <60 mL/min/1.73 m^2 combined with ASCVD (**Figure 4**, HR 0.74, [95% CI 0.51–1.06], $I^2 = 0.00\%$).

Secondary Outcomes

SGLT2 inhibitors reduced the risk of the secondary renal outcome (worsening kidney function, ESKD, and renal or cardiovascular death) by 33% (**Supplementary Figure 2**) in

TABLE 1 | Baseline characteristics of patients included in different studies.

Study	Study design	Setting	Drug dose (mg/day)	Median follow up (months)	eGFR (ml/min/1.73m^2)	UACR (mg/g)	Age (yr)	Definition of renal outcomes
SGLT2i vs. placebo								
CANVAS	RCT	Multinational	Canagliflozin 300/100	29	30–59	>300	63.2 ± 8.3/63.4 ± 8.2	≥40% GFR decline, ESKD, renal death
CREDENCE	RCT	Multinational	Canagliflozin 100	31.4	30–59	>300	62.9 ± 9.2/63.2 ± 9.2	Doubling creatinine, ESKD, renal or CV death
DAPA-CKD	RCT	Multinational	Dapagliflozin 10	28.8	25–45	>1000	61.8 ± 12.1/61.9 ± 12.1	≥50% GFR decline, ESKD, renal or CV death
DAPA-HF	RCT	Multinational	Danagliflozin 10	18.2	30–59	–	66.2 ± 11.0/66.5 ± 10.8	≥50% GFR decline, ESKD, renal death
DECLARE–TIMI 58	RCT	Multinational	Danagliflozin 10	50.4	<60	>300	63.9 ± 6.8/64.0 ± 6.8	≥40% GFR decline, ESKD, renal death
EMPA-REG	RCT	Multinational	Empagliflozin 25/10	37.2	30–59	>300	63.1 ± 8.6/63.2 ± 8.8	Macroalbuminuria, doubling creatinine, ESKD, renal death
EMPEROR	RCT	Multinational	Empagliflozin 10	16	20–59	>300	67.2 ± 10.8/66.5 ± 11.2	≥40% GFR decline, ESKD
SCORED	RCT	Multinational	Sotagliflozin 200 OR 400	16.0/15.9	25–59	>300	69	≥50% GFR decline, ESKD, renal death
VERTIS CV	RCT	Multinational	ertugliflozin 15/5	42	30–59	>300	64.4 ± 8.1/64.4 ± 8.0	Doubling creatinine, ESKD, renal death

patients with eGFR <60 mL/min/1.73 m^2 (HR 0.67, [95% CI 0.58–0.78], $I^2 = 0.00\%$) and by 35% in patients with macroalbuminuria (HR 0.65, [95% CI 0.58–0.73], $I^2 = 0.00\%$). The HR for MACE was also significantly reduced (**Supplementary Figure 2**) by 16% in patients with eGFR <60 mL/min/1.73 m^2 (HR 0.84, [95% CI 0.71–0.99], $I^2 = 54.10\%$) and 23% in those with UACR > 300 mg/g (HR 0.77, [95% CI 0.67–0.89], $I^2 = 0.00\%$). The eGFR slope of the SGLT2 inhibitors group appeared to be more stable than that of the control group (**Supplementary Figure 2**) and this benefit was observed in both those with eGFR <60 mL/min/1.73 m^2 (WMD 1.67, [95% CI 0.98–2.37], $I^2 = 94.72\%$) and UACR > 300 mg/g (WMD 3.09, [95% CI 2.10–4.08], $I^2 = 74.88\%$). However, there was high heterogeneity among the different studies. The percentage of UACR (**Supplementary Figure 2**) was reduced by 26.92% (WMD 26.92, [95% CI, 7.29–46.55], $I^2 = 78.75\%$) in patients with eGFR <60 mL/min/1.73 m^2 compared with placebo and by 31.1% (WMD 31.1, [95% CI, 26.69–35.51], $I^2 = 0.00\%$) in patients with UACR > 300 mg/g. High heterogeneity was observed in patients with eGFR <60 mL/min/1.73 m^2 ($I^2 = 78.75\%$).

Safety Outcome

According to our results, there were no significant differences in adverse outcomes including amputation, fracture, volume depletion, or acute renal failure between patients with macroalbuminuria receiving SGLT2 inhibitors or placebo (**Supplementary Figure 3**, acute kidney injury: HR 0.85, [95% CI 0.67–1.08], $I^2 = 0.00\%$; amputation: HR 1.49, [95% CI 0.72–3.07], $I^2 = 67.61$; fracture: HR 0.99, [95% CI 0.74–1.34], $I^2 = 0.00\%$; volume depletion: HR 1.24, [95% CI 0.98–1.58], $I^2 = 0.00\%$), or eGFR <60 mL/min/1.73 m^2 (**Supplementary Figure 3**, acute kidney injury: HR 0.73 [95% CI 0.47–1.13], $I^2 = 0.00\%$; amputation: HR 1.10, [95% CI 0.58–2.08], $I^2 = 0.00\%$; fracture: HR 1.08 [95% CI 0.85–1.38], $I^2 = 0.00\%$; volume depletion: HR 1.41 [95% CI 0.98–2.02], $I^2 = 0.00\%$).

GRADE for the Outcomes

We evaluated all outcome indicators using GRADEpro GDT (https://gradepro.org/). The outcomes of Annualized eGFR slope (Both UACR and eGFR group) and The percentage of reduction in UACR (eGFR group) were low quality, while other outcomes were moderate or high quality (**Supplementary Table 5**).

DISCUSSION

Our meta-analysis provides evidence based on current clinical trials for the efficacy and safety of SGLT2 inhibitors on renal outcomes in patients with CKD. For the past 2 decades, only RAS blockers have been shown to exert renoprotective effects in these patients (21, 22). However, the emergence of SGLT2 inhibitors has created new possibilities for patients with CKD. Previously, a meta-analysis (23) included patients with type 2 diabetes with CKD and found that SGLT2 inhibitors significantly reduced the risk of renal outcomes. Our study not only confirmed this result, but also included patients with non-diabetes, which further confirms the efficacy of SGLT2 inhibitors in patients with CKD. We also found that across the spectrum of different

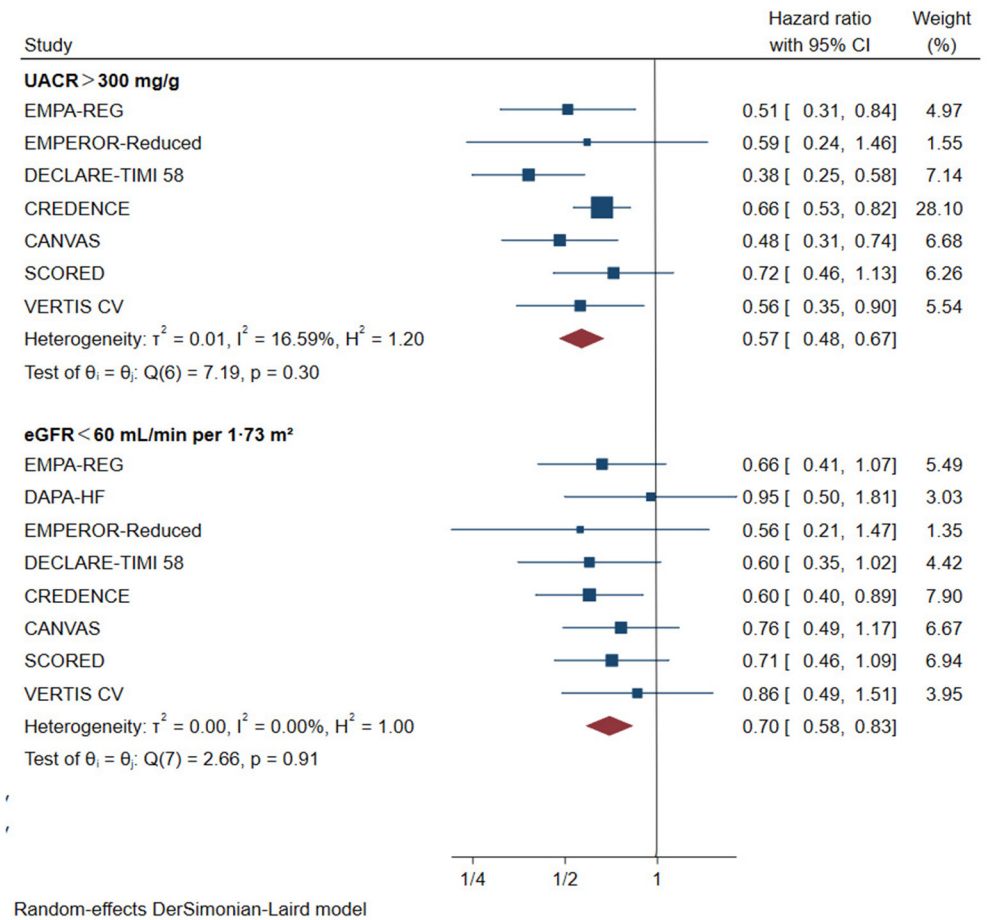

FIGURE 2 | Effect of SGLT2 inhibitors on ESKD, worsening kidney function, or death because of kidney disease. CI, confidence interval; UACR, urinary albumin-to-creatinine ratio; eGFR, estimated glomerular filtration rate. Worsening kidney function: defined as doubling of serum creatinine or sustained 40% decline in eGFR; ESKD, defined as requirement for chronic dialysis or kidney transplantation, or sustained eGFR <15 mL/min/1.73 m².

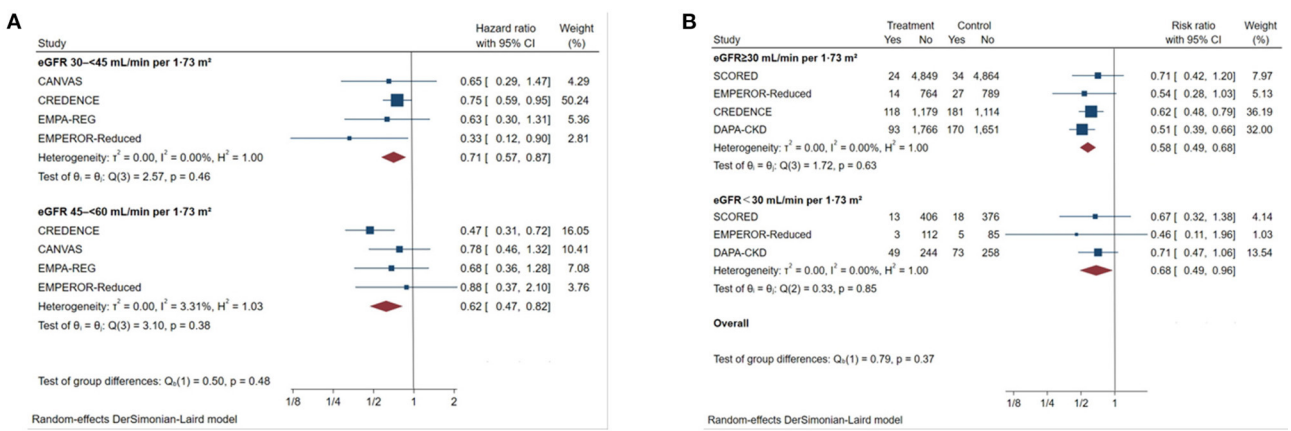

FIGURE 3 | Effect of SGLT2 inhibitors on ESKD, worsening kidney function, or death because of kidney disease across the spectrum of different levels of eGFR. **(A)** Patients with eGFR 45–60 mL/min/1.73 m²; **(B)** patients with eGFR <30 mL/min/1.73 m². CI, confidence interval; eGFR, estimated glomerular filtration rate; worsening kidney function: defined as doubling of serum creatinine or sustained 40% decline in eGFR; ESKD, defined as requirement for chronic dialysis or kidney transplantation, or sustained eGFR <15 mL/min/1.73 m².

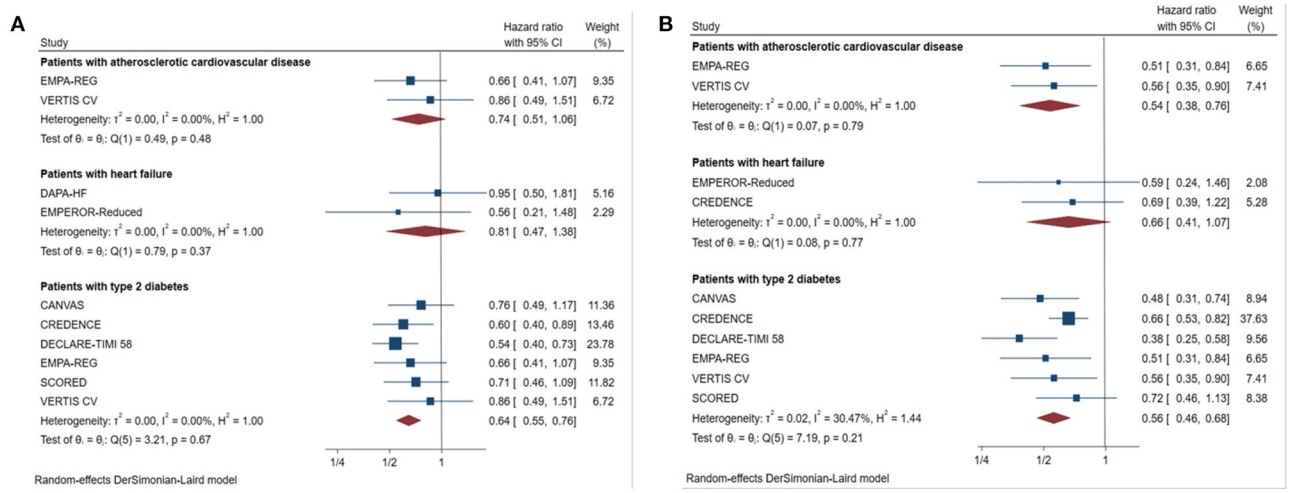

FIGURE 4 | Effect of SGLT2 inhibitors on ESKD, worsening kidney function, or death because of kidney disease in patients with different complications. **(A)** eGFR <60 mL/min/1.73 m²; **(B)** UACR > 300 mg/g; CI, confidence interval; worsening kidney function: defined as doubling of serum creatinine or sustained 40% decline in eGFR; ESKD, defined as requirement for chronic dialysis or kidney transplantation, or sustained eGFR <15 mL/min/1.73 m².

eGFR subgroup (eGFR > 30 mL/min/1.73 m²), the use of SGLT2 inhibitors was associated with significant renal benefits, and this result is consistent with those from two previous meta-studies (24, 25), which suggests that SGLT2 inhibitors can still provide renal benefits in patients with low eGFR.

Because SGLT2 inhibitors antagonize glucose reabsorption in renal tubules, the action of SGLT2 inhibitors is expected to be eGFR-dependent. For patients with low eGFR, especially those with eGFR <30 mL/min/1.73 m², the use of SGLT2 inhibitors has been controversial. Previously, a *post-hoc* analysis study (26) on canagliflozin showed that in patients with eGFR <30 mL/min/1.73 m², although canagliflozin did not confer an absolute renal benefit compared with placebo, renoprotection was consistent with that in patients with eGFR > 30 mL/min/1.73 m² (P interaction = 0.77). The results from a prespecified analysis of dapagliflozin are similar (27). These observations indicated that patients with eGFR <30 mL/min/1.73 m² may benefit from continued use of SGLT2 inhibitors. A meta-analysis (28) included patients with type 2 diabetes and stage3b-4 CKD found that patients with low eGFR also seen significant renal benefits. To further explore the renal benefits in patients with low eGFR, our study divided the population into stage 3a, 3b and 4, and showed that the protective effect did not change in patients with low eGFR, even in those with stage 4 CKD. These results provide further evidence that use of SGLT2 should be continued in patients with low eGFR population. However, the lower number of participants with eGFR <30 mL/min/1.73 m² and the different underlying diseases may have caused a certain bias.

For CKD patients with different underlying diseases, we found that there were corresponding differences in the magnitude of renal benefits from SGLT2 inhibitors. First, primary renal outcomes were reduced in patients with type 2 diabetes mellitus combined with CKD. This has been confirmed in previous meta-analyses (29). However, our study included additional new large-scale studies and, for the first time, included patients with macroalbuminuria in the analysis. This more strongly confirmed the benefit of SGLT2 inhibitors in this population. Publication of the CREDENCE trial strongly confirmed the renal benefits in patients with type 2 diabetes mellitus combined with CKD. Based on this, 2020 Kidney Disease: Improving Global Outcomes (30) guidelines for treatment of diabetic kidney disease listed SGLT2 inhibitors and RAS blockers as the primary recommendation. Second, our meta-analysis showed that patients with combined heart failure had no significant reduction in primary renal outcome (eGFR <60 mL/min/1.73 m²: HR 0.81, [95% CI 0.47–1.38], $I^2 = 0.00\%$; UACR > 300 mg/g: HR 0.66, [95% CI 0.41–1.07], $I^2 = 0.00\%$). This may be explained by the following factors: first, heart failure aggravates the progression of CKD. Therefore, the beneficial effects may be attenuated in patients with CKD complicated with heart failure; second, one study (7) included patients with ejection fraction less than 40%, and we believe that lower ejection fraction may interfere with renal outcomes to a certain degree. In addition to patients with heart failure who did not benefit, our study found that there is no significant renal benefit in patients with ASCVD combined with eGFR <60 mL/min/1.73 m² (HR 0.74, [95% CI 0.51–1.06], $I^2 = 0.00\%$). However, patients with macroalbuminuria were associated with reduced risk of major renal outcomes (HR 0.54, [95% CI 0.38–0.76], $I^2 = 0.00\%$). Combined with the results in patients with CKD complicated with heart failure, we propose that SGLT2 inhibitors may not provide clinically relevant renal benefits in patients with CKD complicated with CVD, especially those with eGFR <60 mL/min/1.73 m². However, given that the data in this population were primarily from subgroup analysis, and that most of the primary outcomes of these studies were not renal outcomes, the credibility of the results are diminished accordingly.

Regarding renal function, previously, a meta-analysis (31) which included patients with type 2 diabetes and CKD showed that there were no significant changes in eGFR associated with

SGLT2 inhibitors compared with placebo. This result is the opposite of ours. We suppose that the reason for the inconsistent results may be due to the risk of bias, and sampling error caused by the small sample size of some studies included in this meta-analysis. In contrast, the studies we included were of higher quality and had a larger sample size. Therefore, the results are of a stronger level of evidence. Currently, the potential mechanism underlying the renoprotective effect is believed to be that the proximal tubule blocks sodium uptake and leads to increased sodium concentration in the distal convoluted tubule, which delivers the sodium signal to the macula densa, leading to afferent arteriolar contraction and decreased glomerular pressure (32). This mechanism is similar to that of RAS blockers, which also exert renoprotective effects by reducing glomerular perfusion pressure (33). Proteinuria is an independent factor for risk of progression of renal disease, and our study confirmed that SGLT2 inhibitors exert a good effect on reducing proteinuria, which may also provide a protective effect for delaying the progression of renal outcomes. In addition, the antihypertensive and anti-inflammatory effects of SGLT2 inhibitors, and their ability to upregulate hypoxic-inducible factor may also have long-term protective effects on the kidney (33, 34). In addition to the renoprotective effect, we found that SGLT2 inhibitors confer favorable cardiovascular benefits in patient with CKD, which significantly reduces the risk of MACE. This suggests that SGLT2 inhibitors can also be used for cardiovascular protection in the CKD population.

Regarding safety outcomes, the results of our study showed that SGLT2 inhibitors did not increase the risk of fracture, amputation, acute kidney injury, or volume depletion. Previously, there were concerns that SGLT2 inhibitors could cause acute kidney injury by regulating hemodynamic mechanisms. Several large studies also demonstrated a significant decrease in eGFR during the early stage of use of SGLT2 inhibitors compared with placebo (8, 9). However, a previous meta-analysis (25) confirmed that SGLT2 inhibitors reduce the risk of acute kidney injury in patients with type 2 diabetes. Another study (35) that focused specifically on acute kidney injury found that use of SGLT2 inhibitors in CKD did not increase the risk of acute kidney injury. Our meta-analysis also showed the same result.

Our meta-analysis had limitations. First, we used combined data rather than individual participant data. Second, there were differences in definitions of endpoints in some studies, which may have had an impact on our results. However, after sensitivity analysis, it was proven there was no substantial impact on our results. Third, the primary outcome of most of the studies was cardiovascular outcomes. In addition, most of the data came from subgroup analyses of major trials, which may reduce the credibility of the results of this study.

CONCLUSION

In conclusion, SGLT2 inhibitors significantly reduced the risk of primary renal outcomes in patients with CKD, and this benefit was consistent across the spectrum of different levels of eGFR. Additionally, consistent benefits were observed in patients with type 2 diabetes. However, no significant renal benefit was observed in patients with CKD associated with heart failure. In the population with ASCVD, renal benefits were only observed in CKD patients with macroalbuminuria, whereas no significant benefits were observed in those with eGFR <60 mL/min/1.73 m^2. In view of the limitations of our study, in the future, additional high-quality studies are needed to confirm the renal benefits of SGLT2 inhibitors in CKD patients with different baseline features and underlying diseases.

DATA AVAILABILITY STATEMENT

The original contributions presented in the study are included in the article/**Supplementary Material**, further inquiries can be directed to the corresponding author/s.

AUTHOR CONTRIBUTIONS

NL, DL, and LZ contributed to the concept and design of this study. NL, DL, XZ, and PW contributed to the literature search. NL, DL, and YG contributed to the data extraction and risk-of-bias assessment, LZ and DZ acted as consultants for data extraction and literature screening. NL responsible for statistical analysis and writing of the report. MZ assisted in statistical analysis. DL assisted with the writing of the report. EZ reviewed the article and provided critical feedback to shape the report. NL and DL contributed equally to this work and should be considered as co-first authors. All authors read and approved the final manuscript.

FUNDING

This study was supported by Special Project of National Clinical Research Base of Traditional Chinese Medicine (No. JDZX2015094).

SUPPLEMENTARY MATERIAL

The Supplementary Material for this article can be found online at: https://www.frontiersin.org/articles/10.3389/fmed.2021.728089/full#supplementary-material

Supplementary Figure 1 | Risk of bias. Risks of bias in the included studies. **(A)** The authors reviewed the risk of bias for each item in each included study. **(B)** Risks of bias of individual studies. +, low risk of bias; –, high risk of bias; ?, unclear risk of bias.

Supplementary Figure 2 | Effect of SGLT2 inhibitors on different secondary outcomes **(A)** Worsening kidney function, ESKD, renal or cardiovascular death; **(B)** Cardiovascular death, myocardial infarction, and stroke; **(C)** Annualized eGFR slope; **(D)** The percentage of reduction in UACR; CI: confidence interval; UACR, urinary albumin-to-creatinine ratio; eGFR, estimated glomerular filtration rate; worsening kidney function: defined as doubling of serum creatinine or sustained 40% decline in eGFR; ESKD, defined as requirement for chronic dialysis or kidney transplantation, or sustained eGFR <15 mL/min/1.73 m^2.

Supplementary Figure 3 | Effect of SGLT2 inhibitors on safety outcomes **(A)** UACR > 300 mg/g; **(B)** eGFR <60 mL/min/1.73 m^2; CI, confidence interval.

Supplementary Table 1 | Kidney outcome ascertainment and adjudication across included studies.

Supplementary Table 2 | Definitions for ESKD-based kidney outcomes.

Supplementary Table 3 | Difference of slope-based outcomes.

Supplementary Table 4 | Sensitivity analyses for the outcome substantial loss of kidney function, ESKD or death due to kidney disease based on different endpoint definitions.

Supplementary Table 5 | Grade scores for each outcome.

REFERENCES

1. Webster AC, Nagler EV, Morton RL, Masson P. Chronic kidney disease. *Lancet.* (2017) 389:1238–52. doi: 10.1016/S0140-6736(16)32064-5
2. Brenner BM, Cooper ME, de Zeeuw D, Keane WF, Mitch WE, Parving HH, et al. Effects of losartan on renal and cardiovascular outcomes in patients with type 2 diabetes and nephropathy. *N Engl J Med.* (2001) 345:861–9. doi: 10.1056/NEJMoa011161
3. Kanduri SR, Kovvuru K, Hansrivijit P, Thongprayoon C, Vallabhajosyula S, Pivovarova AI, et al. SGLT2 inhibitors and kidney outcomes in patients with chronic kidney disease. *J Clin Med.* (2020) 9:92723. doi: 10.3390/jcm9092723
4. Ninčević V, Omanović KT, Roguljić H, Kizivat T, Smolić M, Bilić CI. Renal benefits of SGLT 2 inhibitors and GLP-1 receptor agonists: evidence supporting a paradigm shift in the medical management of type 2 diabetes. *Int J Mol Sci.* (2019) 20:235831. doi: 10.3390/ijms20235831
5. Bakris GL, Agarwal R, Anker SD, Pitt B, Ruilope LM, Rossing P, et al. Effect of Finerenone on chronic kidney disease outcomes in Type 2 Diabetes. *N Engl J Med.* (2020) 383:2219–29. doi: 10.1056/NEJMoa2025845
6. DeFronzo RA, Norton L, Abdul-Ghani M. Renal, metabolic and cardiovascular considerations of SGLT2 inhibition. *Nat Rev Nephrol.* (2017) 13:11–26. doi: 10.1038/nrneph.2016.170
7. Packer M, Anker SD, Butler J, Filippatos G, Pocock SJ, Carson P, et al. Cardiovascular and renal outcomes with empagliflozin in heart failure. *New Engl J Med.* (2020) 383:1413–24. doi: 10.1056/NEJMoa2022190
8. Zinman B, Wanner C, Lachin JM, Fitchett D, Bluhmki E, Hantel S, et al. Empagliflozin, Cardiovascular outcomes, and mortality in Type 2 diabetes. *New Engl J Med.* (2015) 373:2117–28. doi: 10.1056/NEJMoa1504720
9. Neal B, Perkovic V, Mahaffey KW, de Zeeuw D, Fulcher G, Erondu N, et al. Canagliflozin and cardiovascular and renal events in type 2 diabetes. *New Engl J Med.* (2017) 377:644–57. doi: 10.1056/NEJMoa1611925
10. Heerspink HJL, Stefansson BV, Correa-Rotter R, Chertow GM, Greene T, Hou F, et al. Dapagliflozin in patients with chronic kidney disease. *New Engl J Med.* (2020) 383:1436–46. doi: 10.1056/NEJMoa2024816
11. Perkovic V, Jardine MJ, Neal B, Bompoint S, Heerspink HJL, Charytan DM, et al. Canagliflozin and renal outcomes in type 2 diabetes and nephropathy. *New Engl J Med.* (2019) 380:2295–306. doi: 10.1056/NEJMoa1811744
12. Page MJ, McKenzie JE, Bossuyt PM, Boutron I, Hoffmann TC, Mulrow CD, et al. The PRISMA 2020 statement: an updated guideline for reporting systematic reviews. *J Clin Epidemiol.* (2021) 134:178–89.
13. Cumpston M, Li T, Page MJ, Chandler J, Welch VA, Higgins JP, et al. Updated guidance for trusted systematic reviews: a new edition of the cochrane handbook for systematic reviews of interventions. *Cochrane Database Syst Rev.* (2019) 10:D142. doi: 10.1002/14651858.ED000142
14. Guyatt GH, Oxman AD, Vist GE, Kunz R, Falck-Ytter Y, Alonso-Coello P, et al. GRADE: an emerging consensus on rating quality of evidence and strength of recommendations. *BMJ.* (2008) 336:924–6. doi: 10.1136/bmj.39489.470347.AD
15. Higgins JP, Thompson SG. Quantifying heterogeneity in a meta-analysis. *Stat Med.* (2002) 21:1539–58. doi: 10.1002/sim.1186
16. Egger M, Juni P, Bartlett C, Holenstein F, Sterne J. How important are comprehensive literature searches and the assessment of trial quality in systematic reviews? *Empirical study Health Technol Assess.* (2003) 7:1–76. doi: 10.3310/hta7010
17. Wiviott SD, Raz I, Bonaca MP, Mosenzon O, Kato ET, Cahn A, et al. Dapagliflozin and cardiovascular outcomes in type 2 diabetes. *N Engl J Med.* (2019) 380:347–57. doi: 10.1056/NEJMoa1812389
18. Cannon CP, Pratley R, Dagogo-Jack S, Mancuso J, Huyck S, Masiukiewicz U, et al. Cardiovascular outcomes with ertugliflozin in Type 2 diabetes. *N Engl J Med.* (2020) 383:1425–35. doi: 10.1056/NEJMoa2004967
19. Bhatt DL, Szarek M, Pitt B, Cannon CP, Leiter LA, McGuire DK, et al. Sotagliflozin in patients with diabetes and chronic kidney disease. *N Engl J Med.* (2021) 384:129–39. doi: 10.1056/NEJMoa2030186
20. McMurray JJV, Solomon SD, Inzucchi SE, Kober L, Kosiborod MN, Martinez FA, et al. Dapagliflozin in patients with heart failure and reduced ejection fraction. *New Engl J Med.* (2019) 381:1995–2008. doi: 10.1056/NEJMoa1911303
21. Ruggenenti P, Perna A, Gherardi G, Garini G, Zoccali C, Salvadori M, et al. Renoprotective properties of ACE-inhibition in non-diabetic nephropathies with non-nephrotic proteinuria. *Lancet.* (1999) 354:359–64. doi: 10.1016/S0140-6736(98)10363-X
22. Lewis EJ, Hunsicker LG, Clarke WR, Berl T, Pohl MA, Lewis JB, et al. Renoprotective effect of the angiotensin-receptor antagonist irbesartan in patients with nephropathy due to type 2 diabetes. *N Engl J Med.* (2001) 345:851–60. doi: 10.1056/NEJMoa011303
23. Salah HM. Al'Aref SJ, Khan MS, Al-Hawwas M, Vallurupalli S, Mehta JL, et al. Effects of sodium-glucose cotransporter 1 and 2 inhibitors on cardiovascular and kidney outcomes in type 2 diabetes: a meta-analysis update. *Am Heart J.* (2021) 233:86–91. doi: 10.1016/j.ahj.2020.12.007
24. Zelniker TA, Wiviott SD, Raz I, Im K, Goodrich EL, Bonaca MP, et al. SGLT2 inhibitors for primary and secondary prevention of cardiovascular and renal outcomes in type 2 diabetes: a systematic review and meta-analysis of cardiovascular outcome trials. *Lancet.* (2019) 393:31–9. doi: 10.1016/S0140-6736(18)32590-X
25. Neuen BL, Young T, Heerspink H, Neal B, Perkovic V, Billot L, et al. SGLT2 inhibitors for the prevention of kidney failure in patients with type 2 diabetes: a systematic review and meta-analysis. *Lancet Diabetes Endocrinol.* (2019) 7:845–54. doi: 10.1016/S2213-8587(19)30256-6
26. Bakris G, Oshima M, Mahaffey KW, Agarwal R, Cannon CP, Capuano G. et al. Effects of canagliflozin in patients with baseline eGFR <30 ml/min per 173 m(2): subgroup analysis of the randomized CREDENCE. *Trial Clin J Am Soc Nephrol.* (2020) 15:1705–14. doi: 10.2215/CJN.10140620
27. Chertow GM, Vart P, Jongs N, Toto RD, Gorriz JL, Hou FF. et al. POS-831 the effect of dapagliflozin in patients with eGFR <30 mL/min/173m2: findings from the dapa-ckd trial. *Kidney Int Rep.* (2021) 6:S361–2. doi: 10.1016/j.ekir.2021.03.869
28. Cao H, Liu Y, Tian Z, Lian Y, Jia J, Liu M, et al. Sodium-glucose cotransporter 2 inhibitors benefit to kidney and cardiovascular outcomes for patients with type 2 diabetes mellitus and chronic kidney disease 3b-4: a systematic review and meta-analysis of randomized clinical trials. *Diabetes Res Clin Pract.* (2021) 180:109033. doi: 10.1016/j.diabres.2021.109033
29. Toyama T, Neuen BL, Jun M, Ohkuma T, Neal B, Jardine MJ, et al. Effect of SGLT2 inhibitors on cardiovascular, renal and safety outcomes in patients with type 2 diabetes mellitus and chronic kidney disease: a systematic review and meta-analysis. *Diabetes Obes Metab.* (2019) 21:1237–50. doi: 10.1111/dom.13648
30. KDIGO. Clinical practice guideline for diabetes management in chronic kidney disease. *Kidney Int.* (2020) 98: S1-115. doi: 10.1016/j.kint.2020.06.019
31. Yu B, Dong C, Hu Z, Liu B. Effects of sodium-glucose co-transporter 2 (SGLT2) inhibitors on renal outcomes in patients with type 2 diabetes mellitus and chronic kidney disease: a protocol for systematic review and meta-analysis. *Medicine.* (2021) 100:e24655. doi: 10.1097/MD.0000000000024655
32. Cherney DZ, Perkins BA, Soleymanlou N, Maione M, Lai V, Lee A, et al. Renal hemodynamic effect of sodium-glucose cotransporter 2 inhibition in patients with type 1 diabetes mellitus. *Circulation.* (2014) 129:587–97. doi: 10.1161/CIRCULATIONAHA.113.005081
33. Chung EY, Ruospo M, Natale P, Bolignano D, Navaneethan SD, Palmer SC, et al. Aldosterone antagonists in addition to renin angiotensin system antagonists for preventing the progression

of chronic kidney disease. *Cochrane Database Syst Rev.* (2020) 10:D7004. doi: 10.1002/14651858.CD007004.pub4
34. Vallon V, Thomson SC. The tubular hypothesis of nephron filtration and diabetic kidney disease. *Nat Rev Nephrol.* (2020) 16:317–36. doi: 10.1038/s41581-020-0256-y
35. Menne J, Dumann E, Haller H, Schmidt B. Acute kidney injury and adverse renal events in patients receiving SGLT2-inhibitors: a systematic review and meta-analysis. *PLoS Med.* (2019) 16:e1002983. doi: 10.1371/journal.pmed.1002983

Conflict of Interest: The authors declare that the research was conducted in the absence of any commercial or financial relationships that could be construed as a potential conflict of interest.

Publisher's Note: All claims expressed in this article are solely those of the authors and do not necessarily represent those of their affiliated organizations, or those of the publisher, the editors and the reviewers. Any product that may be evaluated in this article, or claim that may be made by its manufacturer, is not guaranteed or endorsed by the publisher.

frontiers in Medicine

OPINION
published: 02 November 2021
doi: 10.3389/fmed.2021.737692

As Signals From the Kawasaki-Like Illness During the COVID-19 Pandemic: Is It Possible That the Incidence of IgA Nephropathy May Increase in the Future

Yasin Abdi Saed[1†], *Weiwei Xu*[1†], *Hasnaa Yaigoub*[2], *Hasna Tirichen*[2], *Lili Guo*[3,4], *Li Cheng*[3,4] *and Yafeng Li*[3,4*]

[1] Department of Nephrology, Graduate School of Shanxi Medical University, Taiyuan, China, [2] Institutes of Biomedical Sciences, Shanxi University, Taiyuan, China, [3] Shanxi Provincial Key Laboratory of Kidney Disease, Taiyuan, China, [4] Department of Nephrology, The Fifth Hospital (Shanxi Provincial People's Hospital), Taiyuan, China

Keywords: SARS-CoV-2, COVID-19, mucosal immune, Kawasaki-like disease, IgA nephropathy

OPEN ACCESS

Edited by:
Maik Gollasch, Charité – Universitätsmedizin Berlin, Germany

Reviewed by:
Samy Hakroush, University Medical Center Göttingen, Germany

****Correspondence:***
Yafeng Li
dr.yafengli@gmail.com

[†]These authors have contributed equally to this work and share first authorship

Specialty section:
This article was submitted to Nephrology, a section of the journal Frontiers in Medicine

Received: *07 July 2021*
Accepted: *01 October 2021*
Published: *02 November 2021*

Citation:
Abdi Saed Y, Xu W, Yaigoub H, Tirichen H, Guo L, Cheng L and Li Y (2021) As Signals From the Kawasaki-Like Illness During the COVID-19 Pandemic: Is It Possible That the Incidence of IgA Nephropathy May Increase in the Future. Front. Med. 8:737692. doi: 10.3389/fmed.2021.737692

INTRODUCTION

Coronavirus disease (COVID-19), caused by a novel beta coronavirus, severe acute respiratory syndrome coronavirus 2 (SARS-CoV-2), has been dominating our lives for over a year now, affecting every aspect from health, economy to social interactions. In addition to known complications of viral infections such as heightened immune responses, COVID-19 presents with serious multiorgan sequelae that need to be urgently addressed. Lucio Verdoni et al. reported that the SARS-CoV-2 epidemic is associated with a high incidence of a severe form of Kawasaki-like disease in Bergamo province in Italy on Lancet which draw attention to the complications of COVID-19 (1).

The etiology of Kawasaki disease is currently not fully understood. Direct viral infections, superantigen reactions and autoimmunity are thought to be linked to its onset. Magali Noval Rivas and colleagues observed that in the Kawasaki disease vasculitis mouse model, the intestinal barrier was damaged and, secretory immunoglobulin A (sIgA) secretion was increased. The damaged intestinal barrier caused sIgA leakage and sIgA-C3 complex in vascular tissue and glomeruli deposit, and thus promoting the occurrence of arteriovasculitis and abdominal aorta dilation (2). Patients with acute-phase Kawasaki disease have increased serum sIgA concentration and signs of intestinal barrier damaged. Intravenous immunoglobulin (IVIG) treatment can reduce the permeability of the intestinal barrier and serum sIgA concentration while reducing IgA deposition in vascular tissue (3). These evidence indicate that sIgA and intestinal barrier permeability play an important role in the occurrence and development of Kawasaki disease. The mucosal barrier immunity and mucosal barrier damage caused by SARS-COV-2 may be the cause of Kawasaki-like disease outbreak during the epidemic.

While IgM and IgG isotypes have received the most attention in the study of respiratory infection, mucosal and systemic IgA responses, which may play a crucial role in disease pathogenesis, have gotten far less consideration. knowing that viremia is a frequent complication of SARS. SARS-CoV-2 would be anticipated to produce secretory IgA (sIgA) and induce strong mucosal immunity. As well, IgA-mediated interactions with pathogenic microbes have been demonstrated to contribute to mucosal antiviral defense by preventing pathogens from adhering to the cell surface (4). Further, so recent research has discovered that sIgA can stimulate the synthesis of interleukin (IL)-6, IL-8, monocyte chemoattractant protein-1, and granulocyte-macrophage

colony-stimulating factor throughout human lung fibroblasts (5). It's also been suggested that sIgA and IgG work together to promote antibody-dependent cellular cytotoxicity (ADCC) (6). The role of serum IgA, in contrast to mucosal IgA, is mostly unknown. Previous research has revealed that IgA mediates either pro- or anti-inflammatory actions in innate immune cells, indicating that IgA may play a role in autoimmune disorders and immunological hyperactivation regulation (7). In a number of myeloid cells, monomeric binding of serum IgA to the Fc alpha receptor (FcRI) has been hypothesized to mediate inhibitory activity via receptor inhibitory signals (8). In contrast, IgA and pathogen crosslinking of FcRI allows activating signals to be sent, resulting in phagocytosis, respiratory burst, ADCC, increased antigen presentation, degranulation, and cytokine release (9).

Antibody isotype switching can be induced by cytokines such as transforming growth factor (TGF)- and interleukin-10 (10). Also increased levels of TGF- and IL-10, which drive antibody switching in SARS-CoV-2 infection, might explain the increased IgA production. Considering the roles of mucosal and systemic IgA in COVID-19, stimulating IgA synthesis (by activating canonical TGF-signaling with lactoferrin) (11). It's also worth mentioning that a new treatment for severe COVID-19 has been proposed using retinoic acid to increase lactoferrin-induced IgA responses (12).

IgA antibodies in the mucosa are polyreactive and have a low affinity for bacterial antigens. Mucosal pathogens and vaccines can cause high-affinity and T-cell-dependent IgA responses (13). SARS-CoV-2 can cause strong mucosal immunity to induce sIgA production, and the serum SARS-CoV-2-specific IgA level was found to have a significant positive association with the APACHE-II score of critically ill patients with COVID-19 (14). The production of large amounts of sIgA is an important step in the pathogenesis of Kawasaki disease.

Kawasaki disease patients with digestive tract symptoms are more likely to develop IVIG resistance and coronary artery lesions.SARS-CoV-2, generally, first attacks the respiratory system and causes serious infections. 61.3% of the 318 SARS-CoV-2-infected patients from nine hospitals in the United States reported at least one gastrointestinal symptom, the most common gastrointestinal symptoms were anorexia (34.8%), diarrhea (33.7%) and nausea (26.4 %) (15). In an *in vitro* organoid model, SARS-CoV-2 can effectively infect human small intestine organoids, and replicate. Digestive endoscopy sampling showed that in the patient's stomach, duodenum and rectum, the epithelial cells expressed the viral host receptor ACE2, and the viral nucleocapsid protein was detected in the cytoplasm, and a large amount of pulp infiltrating was visible in the lamina propria Cell, lymphocyte and interstitial edema (16). The SARS-CoV-2 can directly infect the respiratory system and digestive system causing mucosal barrier damage, which can be regarded as a high-risk factor for Kawasaki-like disease.

To sum up, we propose the hypothesis that SARS-CoV-2 invades the mucosa of the respiratory tract and digestive tract, causing damage to the mucosal barrier and increases secretion of sIgA, sIgA leaks into the blood and promotes the deposition of IgA-C3 complex in the cardiovascular lesions to cause Kawasaki-like disease.

DISCUSSION

IgA nephropathy (IgAN) is considered as the most common primary glomerulonephritis globally. The pathological feature of IgAN is the deposition of IgA in the mesangial area of the glomeruli; however, its pathogenesis is unclear. IgAN is a multifactorial disease. Recent studies have shown that respiratory and intestinal mucosal immunity is closely related to the pathogenesis of IgAN. Some IgAN patients have prodromal symptoms such as upper respiratory tract (tonsillitis, pharyngitis) and digestive tract infections within hours or days before the onset of illness. IgAN patients are more likely to have gastrointestinal symptoms such as celiac disease. Pathological changes similar to human Kawasaki-like disease and IgA Nephropathy(IgAN) were observed in the damaged intestinal mucosal barrier of the Kawasaki disease mice model.

Moreover, the spike protein of SARS-CoV-2 binds to ACE2 receptors on the surface of targeted cells (17). ACE2 is widely found in various tissues, particularly in the proximal tubules' apical brush borders and to a lesser extent in kidney podocytes (18). The link between ACE2 and COVID-19 has piqued curiosity as a result of this discovery. The presence of viral components (e.g., spike protein) in renal tissue and virus-like particles within epithelial cells was confirmed by histological results from postmortem tissues (19). Furthermore, Pan et al. assert that the kidney is predisposed to COVID-19 because of ACE2 expression (20). In the light of the Kawasaki-like disease outbreak during the COVID-19 pandemic, we hypothesized that IgAN may be another possible complication of COVID-19.

We collected urine from 864 patients with COVID-19 from Hubei Provincial People's Hospital for routine urine testing and found that 233 (30%) patients had urinary occult blood. Hematuria is the most common clinical manifestation of IgAN (21). The onset of IgAN is insidious and often manifests as asymptomatic hematuria. After the onset of gross hematuria, urinary erythrocytes can disappear or can be converted to microscopic hematuria. Some patients with IgAN often have paroxysmal gross hematuria associated with upper respiratory tract infections. Therefore, we speculate that some COVID-19 patients who presented with occult blood, this latter is caused by IgAN complications. We propose the hypothesis that SARS-CoV-2 invades the mucosa of the respiratory tract and digestive tract, causing damage to the mucosal barrier and increases secretion of sIgA, sIgA leaks into the blood and promotes the deposition of IgA-C3 complex in the mesangial area of the glomeruli to cause IgAN (**Figure 1**).

When patients with COVID-19 have hematuria, we first consider the acute kidney injury caused by SARS-COV-2 and ignore IgAN. The onset of IgAN is hidden, and the diagnosis often depends on renal puncture. During the epidemic, our focus is mainly on whether the patient's nucleic acid test turns negative and whether the symptoms of pneumonia are alleviated, and kidney pathological examinations are often ignored. In particular, the lack of experienced pathologists in developing countries is more likely to ignore IgAN diagnosis. Most patients undergo renal pathology only when they find abnormal renal function during the medical examination.

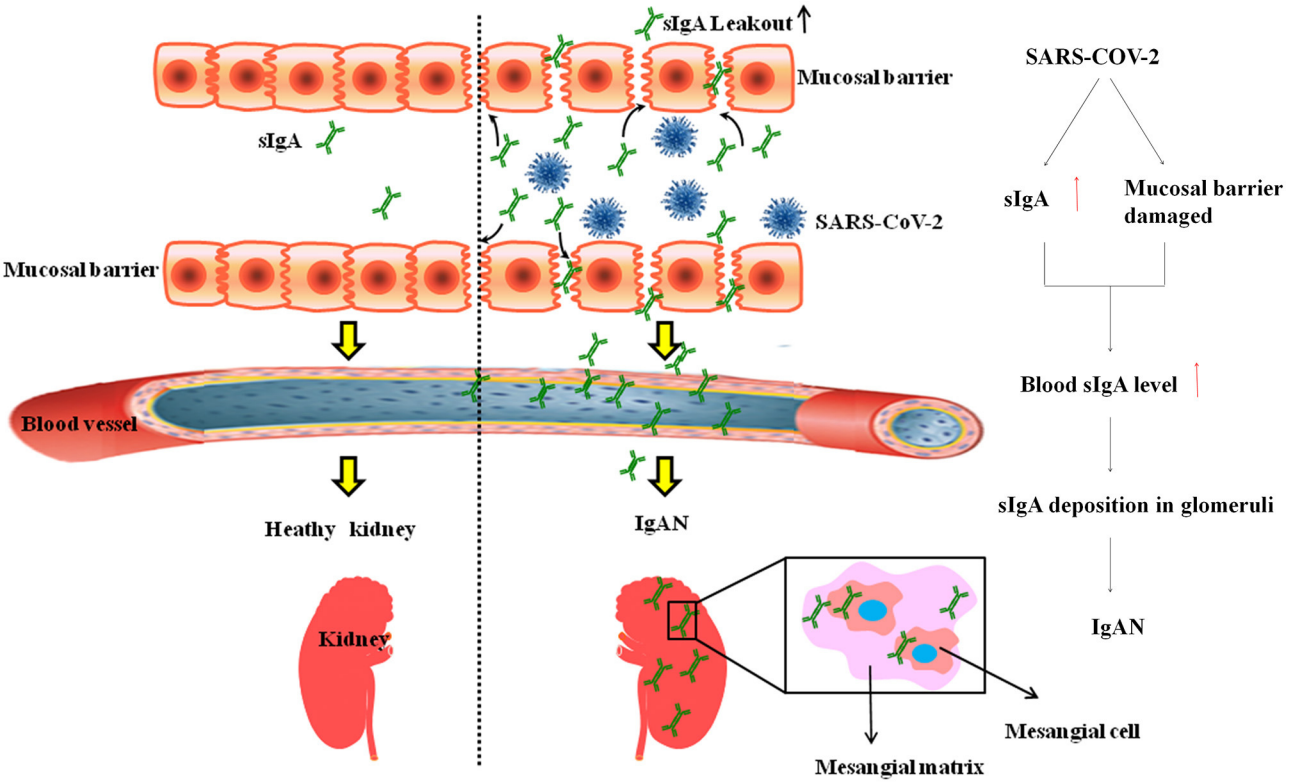

FIGURE 1 | SARS-COV-2 Lead to IgAN. SARS-CoV-2 invades the mucosa of the respiratory tract and digestive tract, increased gut permeability leads to leakage of sIgA and promotes the deposition of IgA-C3 complex in the mesangial area of the glomeruli to cause IgAN.

Therefore, we suspect that the incidence of IgAN may increase in the future.

Lately, there is an important question concerning the renal risks of vaccination against SARS-CoV-2. With the advent of mRNA-based vaccinations, concerns about the possibility of renal adverse effects have arisen. Flare-ups of nephrotic syndrome associated with minimal glomerular damage or episodes of hematuria have recently been reported in patients with IgA-deposed nephropathy following vaccination. Based on the data reported, it is currently impossible to conclude that there is a causal link. To our knowledge, nine cases of hematuria due to IgA deposit nephropathy have been reported so far (22–25).

Whilst the correlation does not necessarily imply the cause, symptoms timing should be seen as the inciting event shortly after the vaccine, The development of anti-glycan antibodies that cross-react with pre-existing under-galactosylated IgA1 is one proposed explanation for IgAN. Furthermore, an mRNA-based vaccine may stimulate higher T follicular helper and subsequent B-cell responses in the germinal center, which potentially resulting in more robust antibody production. Given elevated IgA level, another possibility is an increase in pathogenic IgA production, similar to the influenza vaccination. A recent preprint study also indicate that healthy people who received mRNA vaccinations had strong spike-specific IgA responses (26).

In conclusion, we hypothesized that IgAN may be another serious complication of COVID-19 as well COVID-19 mRNA vaccine and the incidence of IgAN may increase in the future. IgAN has a long course and poor prognosis. Early diagnosis and intervention are of great significance for improving the prognosis and quality of life of patients with COVID-19.

AUTHOR CONTRIBUTIONS

YA wrote original draft. WX, HY, HT, and LG did the review and editing. YL dealt with the project administration and supervision. All authors contributed to the article and approved the submitted version.

FUNDING

This work was supported by the National Natural Science Foundation of China (No. 82170716) and the COVID-19 Project Fund of Shanxi Province Health Commission (No. 15).

REFERENCES

1. Verdoni L, Mazza A, Gervasoni A, Martelli L, Ruggeri M, Ciuffreda M, et al. An outbreak of severe Kawasaki-like disease at the Italian epicentre of the SARS-CoV-2 epidemic: an observational cohort study. *Lancet*. (2020) 395:1771–8. doi: 10.1016/S0140-6736(20)31103-X
2. Noval Rivas M, Wakita D, Franklin MK, Carvalho TT, Abolhesn A, Gomez AC, et al. Intestinal permeability and IgA provoke immune vasculitis linked to cardiovascular inflammation. *Immunity*. (2019) 51:508–21. doi: 10.1016/j.immuni.2019.05.021
3. Onuora S. Is Kawasaki disease a form of IgA vasculitis? *Nat Rev Rheumatol*. (2019) 15:636. doi: 10.1038/s41584-019-0318-3
4. Corthésy B. Role of secretory IgA in infection and maintenance of homeostasis. *Autoimmun Rev*. (2013) 12:661–5. doi: 10.1016/j.autrev.2012.10.012
5. Arakawa S, Suzukawa M, Watanabe K, Kobayashi K, Matsui H, Nagai H, et al. Secretory immunoglobulin A induces human lung fibroblasts to produce inflammatory cytokines and undergo activation. *Clin Exp Immunol*. (2019) 195:287–301. doi: 10.1111/cei.13253
6. Shen L, Fanger MW. Secretory IgA antibodies synergize with IgG in promoting ADCC by human polymorphonuclear cells, monocytes, and lymphocytes. *Cell Immunol*. (1981) 59:75–81. doi: 10.1016/0008-8749(81)90435-4
7. Olas K, Butterweck H, Teschner W, Schwarz HP, Reipert B. Immunomodulatory properties of human serum immunoglobulin A: anti-inflammatory and pro-inflammatory activities in human monocytes and peripheral blood mononuclear cells. *Clin Exp Immunol*. (2005) 140:478–90. doi: 10.1111/j.1365-2249.2005.02779.x
8. Oortwijn BD, Roos A, van der Boog PJ, Klar-Mohamad N, van Remoortere A, Deelder AM, et al. Monomeric and polymeric IgA show a similar association with the myeloid FcalphaRI/CD89. *Mol Immunol*. (2007) 44:966–73. doi: 10.1016/j.molimm.2006.03.014
9. Leong KW, Ding JL. The unexplored roles of human serum IgA. *DNA Cell Biol*. (2014) 33:823–9. doi: 10.1089/dna.2014.2639
10. Dullaers M, Li D, Xue Y, Ni L, Gayet I, Morita R, et al. A T cell-dependent mechanism for the induction of human mucosal homing immunoglobulin A-secreting plasmablasts. *Immunity*. (2009) 30:120–9. doi: 10.1016/j.immuni.2008.11.008
11. Jang YS, Seo GY, Lee JM, Seo HY, Han HJ, Kim SJ, et al. Lactoferrin causes IgA and IgG2b isotype switching through betaglycan binding and activation of canonical TGF-β signaling. *Mucosal Immunol*. (2015) 8: 906–17. doi: 10.1038/mi.2014.121
12. Lee JM, Jang YS, Jin BR, Kim SJ, Kim HJ, Kwon BE, et al. Retinoic acid enhances lactoferrin-induced IgA responses by increasing betaglycan expression. *Cell Mol Immunol*. (2016) 13:862–70. doi: 10.1038/cmi.2015.73
13. Bunker JJ, Bendelac A. IgA responses to microbiota. *Immunity*. (2018) 49:211–24. doi: 10.1016/j.immuni.2018.08.011
14. Yu HQ, Sun BQ, Fang ZF, Zhao JC, Liu XY, Li YM, et al. Distinct features of SARS-CoV-2-specific IgA response in COVID-19 patients. *Eur Respir J*. (2020) 56:2001526. doi: 10.1183/13993003.01526-2020
15. Nobel YR, Phipps M, Zucker J, Lebwohl B, Wang TC, Sobieszczyk ME, et al. Gastrointestinal symptoms and coronavirus disease 2019: a case-control study from the United States. *Gastroenterology*. (2020). 159:373–5. doi: 10.1053/j.gastro.2020.04.017
16. Xiao F, Tang M, Zheng X, Liu Y, Li X, Shan H. Evidence for Gastrointestinal Infection of SARS-CoV-2. *Gastroenterology*. (2020) 158:1831–3. doi: 10.1053/j.gastro.2020.02.055
17. Zhou P, Yang XL, Wang XG, Hu B, Zhang L, Zhang W, et al. A pneumonia outbreak associated with a new coronavirus of probable bat origin. *Nature*. (2020) 579:270–73. doi: 10.1038/s41586-020-2012-7
18. Zou X, Chen K, Zou J, Han P, Hao J, Han Z. Single-cell RNA-seq data analysis on the receptor ACE2 expression reveals the potential risk of different human organs vulnerable to 2019-nCoV infection. *Front Med*. (2020) 14:185–92. doi: 10.1007/s11684-020-0754-0
19. Su H, Yang M, Wan C, Yi LX, Tang F, Zhu HY, et al. Renal histopathological analysis of 26 postmortem findings of patients with COVID-19 in China. *Kidney Int*. (2020) 98:219–27. doi: 10.1016/j.kint.2020.04.003
20. Pan XW, Xu D, Zhang H, Zhou W, Wang LH, Cui XG. Identification of a potential mechanism of acute kidney injury during the COVID-19 outbreak: a study based on single-cell transcriptome analysis. *Intensive Care Med*. (2020) 46:1114–6. doi: 10.1007/s00134-020-06026-1
21. Rodrigues JC, Haas M, Reich HN. IgA Nephropathy. *Clin J Am Soc Nephrol*. (2017) 12:677–86. doi: 10.2215/CJN.07420716
22. Perrin P, Bassand X, Benotmane I, Bouvier N. Gross hematuria following SARS-CoV-2 vaccination in patients with IgA nephropathy. *Kidney Int*. (2021) 100:466–8. doi: 10.1016/j.kint.2021.05.022
23. Negrea L, Rovin BH. Gross hematuria following vaccination for severe acute respiratory syndrome coronavirus 2 in 2 patients with IgA nephropathy. *Kidney Int*. (2021) 99:1487. doi: 10.1016/j.kint.2021.03.002
24. Rahim SEG, Lin JT, Wang JC. A case of gross hematuria and IgA nephropathy flare-up following SARS-CoV-2 vaccination. *Kidney Int*. (2021) 100:238. doi: 10.1016/j.kint.2021.04.024
25. Tan HZ, Tan RY, Choo J, Lim CC, Tan CS, Loh A, et al. Is COVID-19 vaccination unmasking glomerulonephritis? *Kidney Int*. (2021) 100:469–71. doi: 10.1016/j.kint.2021.05.009
26. Wisnewski AV, Campillo LJ, Redlich CA. Human IgG and IgA responses to COVID-19 mRNA vaccines. *PLoS ONE*. (2021) 16:e0249499. doi: 10.1371/journal.pone.0249499

Conflict of Interest: The authors declare that the research was conducted in the absence of any commercial or financial relationships that could be construed as a potential conflict of interest.

frontiers in Medicine

ORIGINAL RESEARCH
published: 10 February 2022
doi: 10.3389/fmed.2022.801089

Feasibility of Dialysate Bolus-Based Absolute Blood Volume Estimation in Maintenance Hemodialysis Patients

Simon Krenn[1,2,3], Michael Schmiedecker[1], Daniel Schneditz[4], Sebastian Hödlmoser[1,2], Christopher C. Mayer[3], Siegfried Wassertheurer[3], Haris Omic[1], Eva Schernhammer[2], Peter Wabel[5†] and Manfred Hecking[1†]*

[1] Division of Nephrology and Dialysis, Department of Medicine III, Medical University of Vienna, Vienna, Austria, [2] Department of Epidemiology, Center for Public Health, Medical University of Vienna, Vienna, Austria, [3] AIT Austrian Institute of Technology, Center for Health & Bioresources, Medical Signal Analysis, Vienna, Austria, [4] Division of Physiology, Otto Loewi Research Center, Medical University of Graz, Graz, Austria, [5] Independent Researcher, Rosbach, Germany

OPEN ACCESS

Edited by:
Maik Gollasch,
Charité University Medicine
Berlin, Germany

Reviewed by:
Martin K. Kuhlmann,
Vivantes Hospital, Germany
Chih-Yu Yang,
Taipei Veterans General
Hospital, Taiwan

***Correspondence:**
Manfred Hecking
manfred.hecking@meduniwien.ac.at

[†] These authors have contributed
equally to this work

Specialty section:
This article was submitted to
Nephrology,
a section of the journal
Frontiers in Medicine

Received: 24 October 2021
Accepted: 04 January 2022
Published: 10 February 2022

Citation:
Krenn S, Schmiedecker M,
Schneditz D, Hödlmoser S, Mayer CC,
Wassertheurer S, Omic H,
Schernhammer E, Wabel P and
Hecking M (2022) Feasibility of
Dialysate Bolus-Based Absolute
Blood Volume Estimation in
Maintenance Hemodialysis Patients.
Front. Med. 9:801089.
doi: 10.3389/fmed.2022.801089

Background: Absolute blood volume (ABV) is a critical component of fluid status, which may inform target weight prescriptions and hemodynamic vulnerability of dialysis patients. Here, we utilized the changes in relative blood volume (RBV), monitored by ultrasound (BVM) upon intradialytic 240 mL dialysate fluid bolus-infusion 1 h after hemodialysis start, to calculate the session-specific ABV. With the main goal of assessing clinical feasibility, our sub-aims were to (i) standardize the BVM-data read-out; (ii) determine optimal time-points for ABV-calculation, "before-" and "after-bolus"; (iii) assess ABV-variation.

Methods: We used high-level programming language and basic descriptive statistics in a retrospective study of routinely measured BVM-data from 274 hemodialysis sessions in 98 patients.

Results: Regarding (i) and (ii), we automatized the processing of RBV-data, and determined an algorithm to select the adequate RBV-data points for ABV-calculations. Regarding (iii), we found in 144 BVM-curves from 75 patients, that the average ABV $\pm$ standard deviation was 5.2 $\pm$ 1.5 L and that among those 51 patients who still had $\geq$2 valid estimates, the average intra-patient standard deviation in ABV was 0.8 L. Twenty-seven of these patients had an average intra-patient standard deviation in ABV $<$0.5 L.

Conclusions: We demonstrate feasibility of ABV-calculation by an automated algorithm after dialysate bolus-administration, based on the BVM-curve. Based on our results from this simple "abridged" calculation approach with routine clinical measurements, we encourage the use of multi-compartment modeling and comparison with reference methods of ABV-determination. Hopes are high that clinicians will be able to use ABV to inform target weight prescription, improving hemodynamic stability.

Keywords: blood volume, chronic kidney disease, fluid status, hemodialysis, renal insufficiency, chronic, renal dialysis

INTRODUCTION

Fluid homeostasis is among the most complex physiological entities known to the medical sciences (1). It can become deranged in a variety of conditions such as intensive medical care (2, 3), cardiac failure (4, 5), and chronic kidney disease (CKD) (6, 7). Even in CKD patients not yet requiring kidney replacement therapy, chronic fluid overload is associated with increased mortality (7). Once CKD patients are on dialysis, optimal fluid management is essential for avoiding deleterious consequences at both ends of fluid dysbalance (i.e., fluid overload and excessive volume depletion) (8).

Restoration of the body's delicate electrolyte and water equilibria has been a perpetual quest of nephrologists from the 19 sixties onward and is the central goal of the common "dry weight" approach (6, 9–11). Clinical "dry weight," originally defined as the target weight in a (hemo) dialysis (HD) patient at which the patient could not tolerate further fluid removal during the "probing dry weight" strategy, is not necessarily the same as the patient's euvolemic weight, determined by objective measures (9). Moreover, patients differ in their pathophysiological adoption of volume overload/depletion and susceptibility to fluid removal. Despite almost 60 years of HD experience, the physiological basis for fluid volume balance is unclear (12).

Blood volume monitoring (BVM) technology uses optical transmission/optical absorbance (13–16) or ultrasound (17–19) to measure the intradialytic concentration change of hemoglobin/hematocrit and to infer a relative change in blood volume from the hemoconcentration. The resulting BVM curve can be used to observe fluid content in the blood and thereby holds information on fluid status and optimal target weight, as steeper curves throughout HD indicate stronger intradialytic volume depletion (20). The original aim of intradialytic BVM, however, was to regulate the ultrafiltration (UF) rate based on the BVM signal to prevent intradialytic hypotension and related morbid events (21), thereby improving HD outcomes (22). In spite of some positive results regarding dialysis symptoms (23, 24), even higher mortality and hospitalization rates were initially observed with this technique (25), and the most recent large study that assessed hard outcomes was negative (12).

The main caveat of regulating the UF based on the intradialytic BVM curve during HD is that only relative blood volume (RBV) changes can currently be deduced from the BVM signal. These relative changes, however, are of little use when the absolute blood volume and its relation to the patient's overall volume status are unknown. Hecking and Schneditz compared the futility of controlling intravascular volume using only knowledge on RBV changes to a thermostat operating by temperature changes alone but ignoring the actual room temperature, which "could be anything" (21). Arguably, a measure for absolute blood volume (ABV), combined with bioimpedance-based extracellular volume assessment, could render an adapted RBV-guided UF beneficial, further enabling better explanation and control of blood pressure changes.

ABV can be measured using a variety of invasive, time-consuming methods, which are of little use in the clinical setting. Common methods range from radioactive tracer injection (26, 27) and CO-rebreathing (28, 29) to dye approaches [e.g., with indocyanine green (30, 31)]. Since 2014, Kron et al. published multiple articles on an abridged method to determine the patient's ABV during HD sessions (32–37). Utilizing the programmed "emergency function" of the Fresenius 5008 online hemodiafiltration machine (FMC, Bad Homburg, Germany) a bolus of 240 mL ultrapure dialysate was rapidly infused into the blood-stream (32). By manually reading the difference in RBV before and after this bolus administration directly from the screen of the dialysis machine, they approximated ABV and the specific blood volume in mL per kg body mass (specific blood volume, SBV) from the blood dilution caused by the injected fluid. Manual collection of the required data is too slow for clinical practice and prone to error and bias alike.

Thus, the aim of this study was to develop an automated algorithm to determine ABV by dialysate bolus (ABV-DB) from data habitually recorded by HD machines, implementing Kron et al.'s proposed method of calculation. To this end, we extracted and visualized the data recorded by the electronic interface, evaluated the correct implementation of this method in the clinical setting and assessed the intra-individual reproducibility of the resulting ABV-DB across multiple HD sessions in a cohort of CKD patients undergoing uninterrupted maintenance HD at a single tertiary care center.

METHODS

Ethics Approval, Study Setting, and Participants

Boluses of ultrapure dialysate are fast and safe, and therefore an often-preferred alternative to intravenous fluid formulations during HD. At the Chronic Hemodialysis (CHD) Unit of the Vienna General Hospital, dialysate bolus administration for ABV determination was introduced into routine clinical practice as of September 2019. During this process, the targeted UF volume was increased to account for the added volume of the bolus. We obtained study approval from the Ethics Committee of the Medical University of Vienna (EC-No. 1732/2020, Project Title: *Closing the Loop in Hemodialysis: A Precision Medicine Approach – Part A [Intradialytic Determination of Absolute Blood Volume: An Exploratory, Retrospective Study on 98 Patients]*). The study adhered to the Declaration of Helsinki.

The CHD Unit of the Vienna General Hospital has a maximum capacity to treat 144 HD patients (thrice weekly) and is divided into two equally sized subunits, each one comprising 12 positions (HD slots) and executing 3 HD shifts per day. Various HD machines from 3 manufacturers (Fresenius, Nikkiso, Gambro) are in parallel use. Only the BVM-capable Fresenius 5008 was used for the dialysate bolus administration during the period of observation. Each CHD subunit was equipped

Abbreviations: ABV, absolute blood volume; ABV-DB, absolute blood volume by dialysate bolus method; BP, blood pressure; BVM, blood volume monitoring; CHD, chronic hemodialysis; CKD, chronic kidney disease; HD, hemodialysis; KDIGO, Kidney Disease Improving Global Outcomes; r, Pearson's correlation coefficient; RBV, relative blood volume; SD, standard deviation; UF, ultrafiltration.

with one such machine, which was moved from HD slot to HD slot as required. Each HD patient was scheduled to be studied during consecutive dialysis treatments with one bolus administered at every treatment. Patients undergoing hemodialysis or hemodiafiltration at the CHD Unit of the Vienna General Hospital, who had consecutive dialysate boluses for ABV-DB calculation scheduled from September to November 2019 and who did not require hospitalization between those HD sessions were assessed for eligibility.

Data Retrieval and Visualization

All data collected by staff and HD machines (including the BVM data) were electronically stored in the hospital database by default. Nurses also routinely provided a short, informal report of each session, elaborating on irregularities and symptoms. Automatically recorded dialysis session data included BVM data, blood pressure (BP) and basic anthropometric patient information (sex, age, weight), and were extracted from the hospital database using the dialysis administration software Diamant 2 (Diasoft BV, Leusden, The Netherlands). Files containing these data were extracted for each patient using the Diamant system's individualizable reporting function. Laboratory data of quarterly routine blood work were extracted from the hospital database which operates with the clinical management software AKIM (SAP SE, Baden Württemberg, Germany). Data were parsed, pseudonymized and merged using Python 3.9 (Python Software Foundation, Beaverton, USA).

Routine Blood Sampling

Blood was drawn from the patient's hemodialysis access, after discarding at least 10 mL in patients with venous catheters to avoid contamination with catheter lock solutions. Blood was always obtained prior to the HD session to rule out contamination with heparin used for the dialysis treatment. Blood was left to clot at room temperature and was transported to the central laboratory for analyses within 60–180 min after sampling.

Blood Pressure

Systolic and diastolic BP were measured with the CHD Unit's standard BP cuffs (Philips Easy Care Adult M4555B) which are attached to the HD machines. BP measurements were triggered automatically at standard 1-h intervals, or additionally, as clinically needed. To avoid artifacts caused by the bolus injection and white coat effect, BP data collected during the dialysate bolus application itself were analyzed separately.

Absolute Blood Volume Determination

The ABV-DB at the beginning of the dialysis was determined as described in Equation (1) (32, 38):

$$\mathrm{ABV_{DB,0}\,(mL)} = \frac{\mathrm{V_{DB}\,(mL)}}{\mathrm{RBV_{after}\,(\%) - RBV_{before}\,(\%)}} \times \mathrm{RBV_0\,(\%)} \quad (1)$$

RBV_{before} was defined as the last recorded RBV value before bolus injection, RBV_{after} as the maximum RBV value within a 15-min interval after bolus injection and RBV_0 as the first RBV value recorded during HD. V_{DB} represented the volume of the dialysate bolus, in our case 240 mL as used in most publications on this method (34). Only bolus administrations of 240 mL ultrapure dialysate between 50 and 120 min after dialysis start were eligible for analysis. If RBV data expected within a 15-min window before or after bolus were missing, or if an injection of 240 mL was not completed within 3 min [considering that the average infusion time was 1 min 56 ± 20 s standard deviation [SD]], the corresponding electronic record was excluded from the study as well.

TABLE 1 | Patient characteristics (based on 86 patients).

Patient characteristics		*N* = 86
Age (years), mean (SD)		58.6 (16.5)
Sex, *n* (%)	Female	33 (38.4)
	Male	53 (61.6)
Height (cm), mean (SD)		169.3 (9.9)
Weight before dialysis (kg), mean (SD)		72.8 (15.2)
Target weight (kg), mean (SD)		70.8 (15.2)
BMI before dialysis (kg/m²), mean (SD)		25.4 (4.7)
Access type, *n* (%)	Catheter	33 (38.4)
	Shunt	53 (61.6)
Residual diuresis (mL), median [Q1, Q3]		325.0 [0.0, 800.0]
Diuresis below 200 mL/day, *n* (%)	No	49 (57.0)
	Yes	37 (43.0)
Creatinine (mg/dL), mean (SD)		9.6 (3.1)
Diabetes, *n* (%)	No	66 (76.7)
	Yes	20 (23.3)
HbA1c (%), median [Q1, Q3]		5.2 [4.8, 5.6]
Glucose (mg/dL), median [Q1, Q3]		102.0 [90.8, 117.0]
CRP (mg/dL), median [Q1, Q3]		0.6 [0.2, 1.4]
Ferritin (μg/L), median [Q1, Q3]		395.8 [193.5, 573.7]
Transferrin (mg/dL), median [Q1, Q3]		169.0 [144.0, 197.0]
Transferrin saturation (%), median [Q1, Q3]		20.9 [14.7, 28.2]
Hematocrit (%), mean (SD)		30.8 (3.8)
Hemoglobin (g/dL), mean (SD)		10.2 (1.3)
Erythrocytes (G/L), mean (SD)		3.4 (0.5)
Sodium (mmol/L), mean (SD)		139.4 (3.6)
Chloride (mmol/L), mean (SD)		99.4 (4.5)
Potassium (mmol/L), mean (SD)		5.3 (0.7)
Calcium (mmol/L), median [Q1, Q3]		2.2 [2.0, 2.3]
Inorganic phosphate (mmol/L), median [Q1, Q3]		1.9 [1.4, 2.5]
Parathyroid hormone (pg/mL), median [Q1, Q3]		298.7 [134.5, 494.1]
Urea (mg/dL), mean (SD)		64.7 (20.1)
Uric acid (mg/dL), mean (SD)		6.7 (1.4)
Total bilirubin (mg/dL), median [Q1, Q3]		0.3 [0.2, 0.4]

SD, Standard Deviation; Q1, First Quartile; Q3, Third Quartile.

Statistical Evaluation

Descriptive statistics, specifically means with SDs for normally and medians with interquartile ranges (IQRs) for non-normally distributed data were used to present patient characteristics, HD, and laboratory data (**Tables 1**–**3**). RBV curves were visualized

TABLE 2 | Fluid status, weight and blood pressure (based on 86 patients, 186 sessions).

	Measurements (*n*)	Mean	SD	Minimum	25%	Median	75%	Maximum
UF volume (ml)	186	2490.0	1132.7	10.0	1676.0	2440.0	3404.5	4800.0
Target weight (kg)	180	71.1	15.1	38.0	62.5	68.3	81.0	115.0
Weight before dialysis (kg)	181	73.1	15.1	38.9	65.0	70.6	83.8	115.9
Weight after dialysis (kg)	162	72.1	15.3	38.4	63.0	68.8	82.4	115.0
Intradialytic ABV-DB reduction (L)	186	−0.4	0.6	−1.7	−0.6	−0.4	−0.2	6.0
Intradialytic RBV reduction (%)	186	−8.4	7.5	−31.7	−13.0	−7.0	−3.4	5.5
IDWL (kg)	162	−2.0	1.1	−4.5	−2.9	−2.0	−1.1	0.3
IDWG (kg)	162	1.9	1.3	−4.2	1.1	1.8	2.7	6.6
Systolic BP before dialysis (mmHg)	172	137.0	23.3	83.0	121.0	136.0	153.0	216.0
Systolic BP after dialysis (mmHg)	145	130.9	25.9	73.0	113.0	132.0	151.0	189.0
Diastolic BP before dialysis (mmHg)	172	69.4	17.2	14.0	59.8	68.0	80.0	160.0
Diastolic BP after dialysis (mmHg)	145	67.8	16.3	26.0	58.0	69.0	79.0	128.0
Systolic BP reduction (mmHg)	139	6.5	23.2	−53.0	−8.0	8.0	18.0	119.0
Diastolic BP reduction (mmHg)	139	2.6	15.1	−53.0	−5.0	1.0	8.0	100.0
Duration of dialysis (H:M:S)	186	03:53:47	00:31:38	02:02:16	03:33:57	04:00:26	04:10:46	05:21:09

ABV-DB, Dialysate bolus derived blood volume; UF, Ultrafiltration; RBV, Relative blood volume; IDWL, Intradialytic weight loss; IDWG, Interdialytic weight gain; UF, Ultrafiltrate; BP, Blood pressure; H, Hours; M, Minutes; S, Seconds.

TABLE 3 | ABV-DB (based on 75 patients, 145 sessions).

	Measurements (*n*)	Mean	SD	Minimum	25%	Median	75%	Maximum
ABV-DB start of dialysis (L)	145	5.1	1.5	2.3	4.2	5.0	5.8	10.5
Nadler's BV before dialysis (L)	141	4.7	0.8	2.7	4.1	4.7	5.3	6.7
Nadler's BV target (L)	140	4.6	0.8	2.6	4.1	4.7	5.2	6.7
SBV Start of dialysis (ml/kg)	141	72.2	23.7	28.8	54.5	66.6	85.6	144.8
RBV before bolus (%)	145	95.7	4.0	85.4	93.1	96.0	98.6	104.8
RBV after bolus (%)	145	100.7	3.8	90.7	97.4	101.3	103.3	109.5
RBV delta caused by bolus (%)	145	5.0	1.4	2.3	4.1	4.8	5.7	10.5
RBV end of dialysis (%)	145	92.3	7.1	68.7	88.9	93.5	96.8	105.5
RBV peak delay (M:S)	145	06:14	02:16	02:00	04:56	05:34	07:04	16:32

ABV-DB, Dialysate bolus derived bolus volume; RBV, Relative blood volume; BV, Blood Volume; BP, Blood Pressure; SD, Standard Deviation; H, Hours; M, Minutes; S, Seconds; RBV peak delay denotes the time passed from bolus injection start to the maximum RBV value within 15 min after completion of the bolus injection (this includes the bolus duration ≤3 Min, hence maxima over 15 min are possible).

using line plots (**Figures 2A,B**), and blood pressure data were depicted in box-and-whisker plots (**Figure 2C**). For a statistical measure of ABV-DB reproducibility, we used the average intra-patient SD of ABV-DB (**Figure 3A**) on a range of plausible data sampling cut-offs. These cut-offs define the time windows from which the RBV values for the ABV-DB calculations are drawn. These windows always started at the bolus (bolus start or completion, respectively) and ranged back or forward in time for up to 15 min (as shown on the horizontal axes). Average intra-patient SD is a type of statistic which exhibits lower values with increasing similarity of ABV-DB values across multiple HD sessions within the same patient.

Concerning the data sampling time window before and after the bolus for the ABV-DB calculation, obviously, more RBV data points became available with greater sampling time windows and, accordingly, it would be more likely to find both a before-, as well as an after-bolus RBV value, which are both necessary for the ABV-DB calculation. Thereby, the number of curves valid for calculation increases with sampling time window size (**Figure 3B**).

For each patient with more than one RBV curve, the SD between ABV-DB estimates was calculated over all possible sampling cut combinations (which are defining the time intervals before and after bolus from which we sampled the RBV values for ABV-DB calculation) within 0 to 15 min before and 0 to 15 after bolus injection, with a granularity of 0.3 s. These intra-patient SDs were averaged over all patients for each sampling cut combination (before- and after-bolus) and then visualized using 3D surface plots (Note that, setting other constraints aside, the optimal sampling cut combination would arguably be the pair of time points before and after bolus, at which the average intra-patient SDs of ABV-DB are minimal, as this cut combination

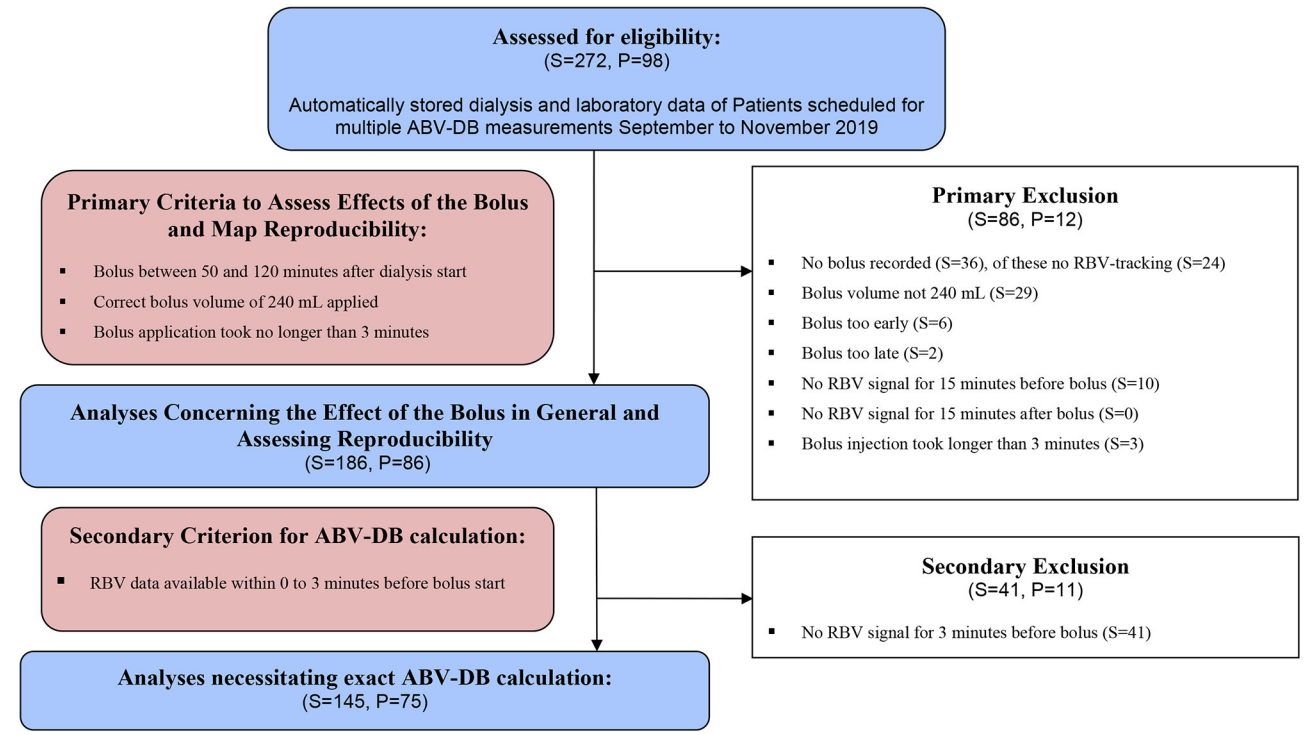

FIGURE 1 | Patient flow chart. S, Sessions; P, Patients.

on average results in the most consistent ABV-DB estimation within patients. First and foremost, however, this type of plot is suited to show sampling cut combinations that produce strong disagreement between the estimates, which clearly should be avoided.) All analyses, figures and tables were computed using Python 3.9 (Python Software Foundation, Beaverton, USA).

RESULTS

Patient Flow and Characteristics

The present analysis was separated into two parts with different exclusion criteria. For the first part we excluded 86 BVM curves from 13 patients (details of the exclusion criteria are mentioned in the Methods and reported in **Figure 1**, Primary Exclusion). The characteristics of these 86 patients are shown in **Table 1**. The average age of the patients was 58.5 ± 16.6 years, and the mean weight was 72.6 ± 15.2 kg. Patients were on average slightly overweight at a mean body mass index (BMI) of 25.3 ± 4.7 kg/m², and 23.3% were diabetic. HD was applied via the central venous catheter access prevalence in women was actually 57.6% (**Supplementary Table 1**).

For the second part of the analysis, we excluded 44 additional BVM curves from 10 patients, because no RBV data were available for 3 min before the bolus was injected (**Figure 1**, Secondary Exclusion). The ABV-DB calculations were therefore based on the remaining 145 BVM curves in 75 patients.

BVM Curve Visualization and Blood Pressure

The BVM curves of 186 complete HD sessions (primary exclusion criteria applied) are shown in **Figure 2A**. At the time of dialysate bolus injection (t = 0), a resulting spike in RBV was observable. The example of a BVM curve over a complete dialysis session is shown in **Figure 2B**, describing the entity of the bolus, and depicting also the exact points on an exemplary BVM curve where RBV values were extracted for the calculation of ABV-DB. The blood pressure values of all patients over time are provided in **Figure 2C**. We observed a narrowing of both systolic and diastolic blood pressure during the first 30 min after the bolus (boxes and whiskers). Notably, no patient exhibited systolic BP below 90 mmHg during this time.

Setting the Window for RBV Extraction

There was a need to limit the time window from which the RBV values before and after bolus were drawn for the calculation of the RBV amplitude. Otherwise, the last RBV value before bolus would have been too long before bolus to deliver reliable estimates of ABV, and the maximum RBV value after bolus might have been falsely high, due to higher local maxima not related to the bolus, and encountered at a later time point during the HD session. The range of possible data sampling time-cuts from bolus and the corresponding average intra-patient SDs of ABV-DB are shown in **Figure 3A**. The corresponding numbers of usable curves at the respective settings are reported in **Figure 3B**. As seen in **Figure 3A,** the sampling window after bolus clearly

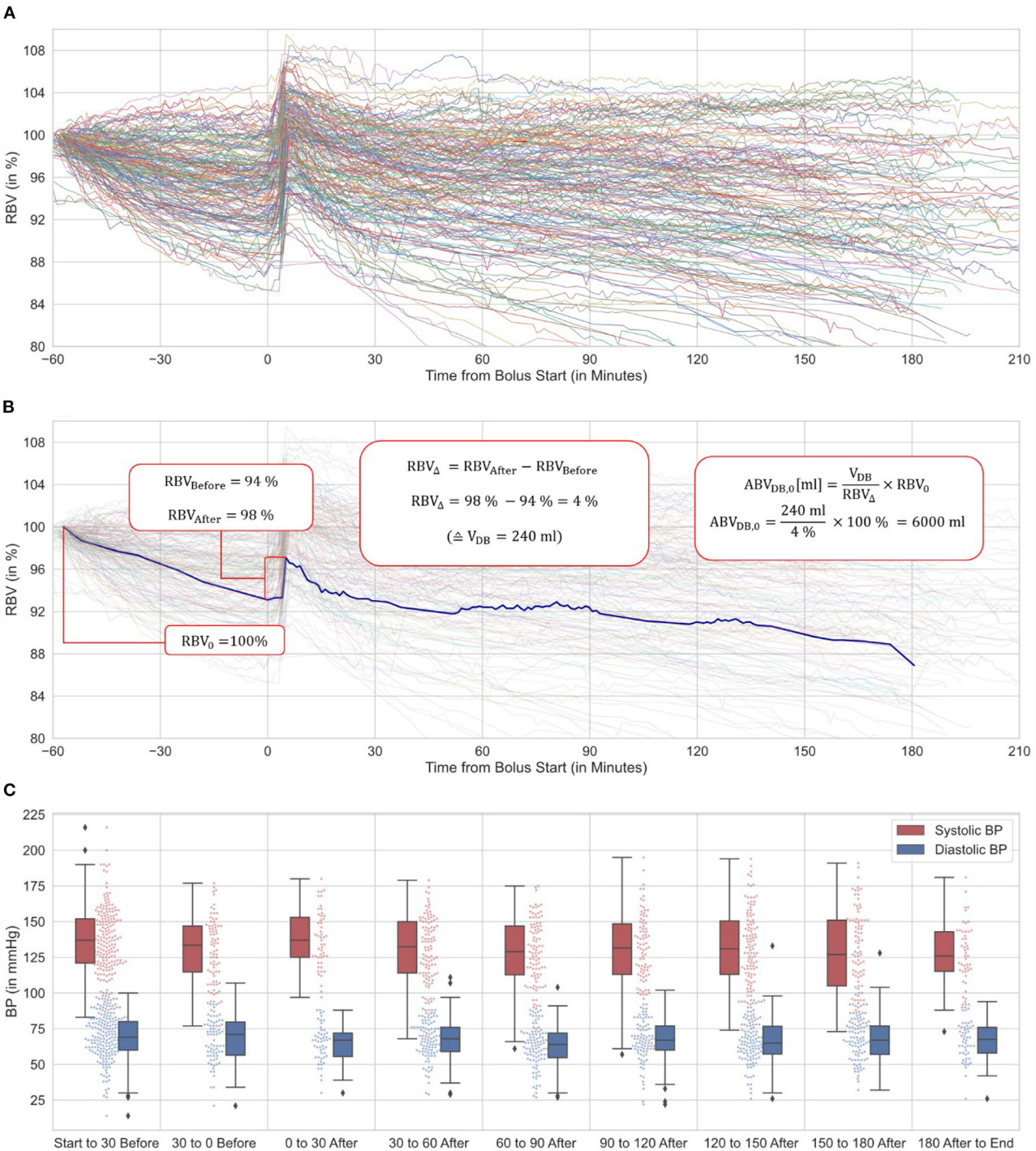

FIGURE 2 | BVM-curve variation, ABV-DB calculation details and blood pressure (based on 86 patients, 186 sessions). **(A)** 186 RBV curves showing significant divergence in curve morphology and individual progression after bolus administration. **(B)** Examplary RBV curve and ABV-DB calculation using dialysate bolus method. **(C)** Systolic and diastolic blood pressure over time relative to the dialysate bolus are depicted in box-and-whisker and jitter plots. BPs during the bolus application are omitted.

needed to be >2.5 min, but provided a robust variable for ABV-DB calculation thereafter. For the sampling cut before bolus, only small changes were observed in the ABV-DB deviation between estimates, but many calculations became impossible (because data were scarcer here) when this time-cut was set too close to the bolus, as seen in **Figure 3B**.

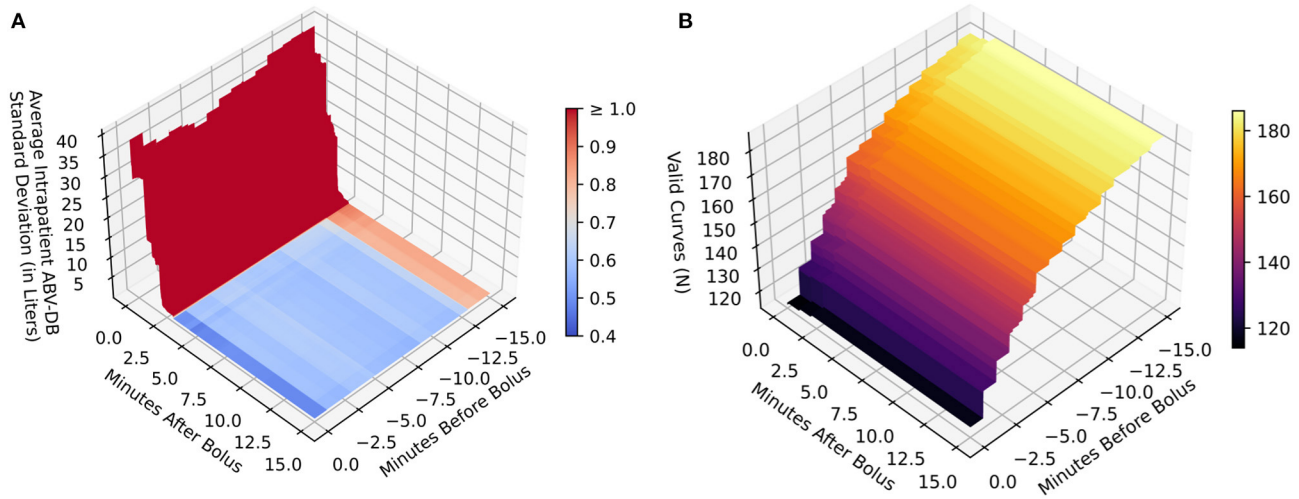

FIGURE 3 | Reproducibility and calculability mapping of all patients with at least two valid measurements (based on 86 patients, 186 sessions). **(A)** Reproducibility between measurements measured by intra-patient standard deviation of the ABV-DB (vertical axis *Z*) by time cut-offs around bolus (horizontal axes *X* and *Y*). **(B)** Amount of curves usable for ABV-DB calculation (vertical axis *Z*) by time cut-offs around bolus (horizontal axes *X* and *Y*). Color bars in **(A,B)** relate to values on the respective vertical axes *Z*. This figure maps out the reproducibility and calculability of ABV-DB by the two-point calculation method as previously used by Kron et al. when applying different time interval cut-offs from bolus for the inclusion of data. This serves to find cut-offs that produce robust results on average and do not exclude too many curves, but further methodological considerations should also inform decisions on choosing the correct cut-off intervals. Only data on the RBV curves within the cut-off interval range is used for calculations of the corresponding *Z*-axis values on these graphs. For the range before bolus, the last measured RBV value before the bolus is used. The reason, why more curves produce usable results with increasing interval size is that in some curves the last measured RBV value is outside the cut-off interval if it is too small. As the interval size is increased, these values become available for analysis and hence the number of valid curves increases. For the range after bolus, the maximum RBV value is used. A reliable RBV maximum for ABV-DB calculation occurs after the dialysate bolus is adequately distributed in the blood stream (at least 2.5 min after completion of the bolus injection) and remains robust to further interval increases thereafter.

We also observed a clear trade-off between the theoretical validity of the method and the number of usable BVM curves. As the time interval of the sampling cut before bolus was increased, more BVM curves delivered calculable results. Specifically, as more RBV values were encountered in both the before and after bolus intervals, the BVM curve was included as a "valid curve" in **Figure 3B**. However, allowing later recorded values to enter the calculation could have also led to unreliable ABV-DB estimates. In our case, if the last 3 min before bolus had generally contained no RBV data, changes in RBV would on average have resulted in an absolute difference ± SD of 0.86 ± 2.55 liters of blood. As this estimation error was expected to be cumulative over time (leading on average to an inflated ABV-DB), there was a need to collect RBV values as closely before the bolus injection as possible.

We concluded that the optimal time points for RBV extraction for Kron's abridged ABV-DB calculation method were the last measured RBV value before the bolus and the maximum RBV within 15 min after the bolus. Note that the rationale here above justifiably prompted the exclusion of those BVM curves where no RBV data were available between 3 and 0 min before bolus start (44 curves in 10 patients, as mentioned in the first paragraph of the Results Section and shown in **Figure 1**), from analyses requiring correct ABV-DB estimates.

Resulting ABV-DB

HD-specific variables are shown in **Table 2** and blood volume data (including ABV-DB and SBV) are shown in **Table 3**. We observed a very wide range of ABV-DB between patients (mean 5.2 ±1.5 L). In 64.1 % of cases, blood volume after bolus was actually greater than at the start of dialysis.

The distribution of ABV-DB between 2.2 and 7.6 liters, as well as a color-scaled measure of agreement between multiple estimates within patients, if available, are shown in a stack plot histogram in **Figure 4A**. Edge cases of very high ABV-DBs were not included in this graph, but their BVM curves and theories on why these BVM curves resulted in ABV-DB outliers are discussed in the **Supplementary Material**. The variation of the ABV-DB between estimates, depending on the average value of ABV-DB, is shown on a logarithmic scale for improved visibility in **Figure 4B**. Patients with the highest values on the average ABV-DB scale exhibited higher variation between estimates.

DISCUSSION

Here we employed a previously published method to estimate the ABV by applying an intradialytic bolus of ultrapure dialysate. In our understanding, the present study adds important information to the existing literature, not only by representing a larger population size than the earlier reports (32–37, 39), but also because repeated measurement sessions per patient were performed, and possible pitfalls regarding insufficient sampling rates using an automatic data acquisition systems were fully disclosed. To evaluate the method, we made an effort to use as much data as possible for each analysis, implementing separate, but genuine exclusion steps, as necessary for validity.

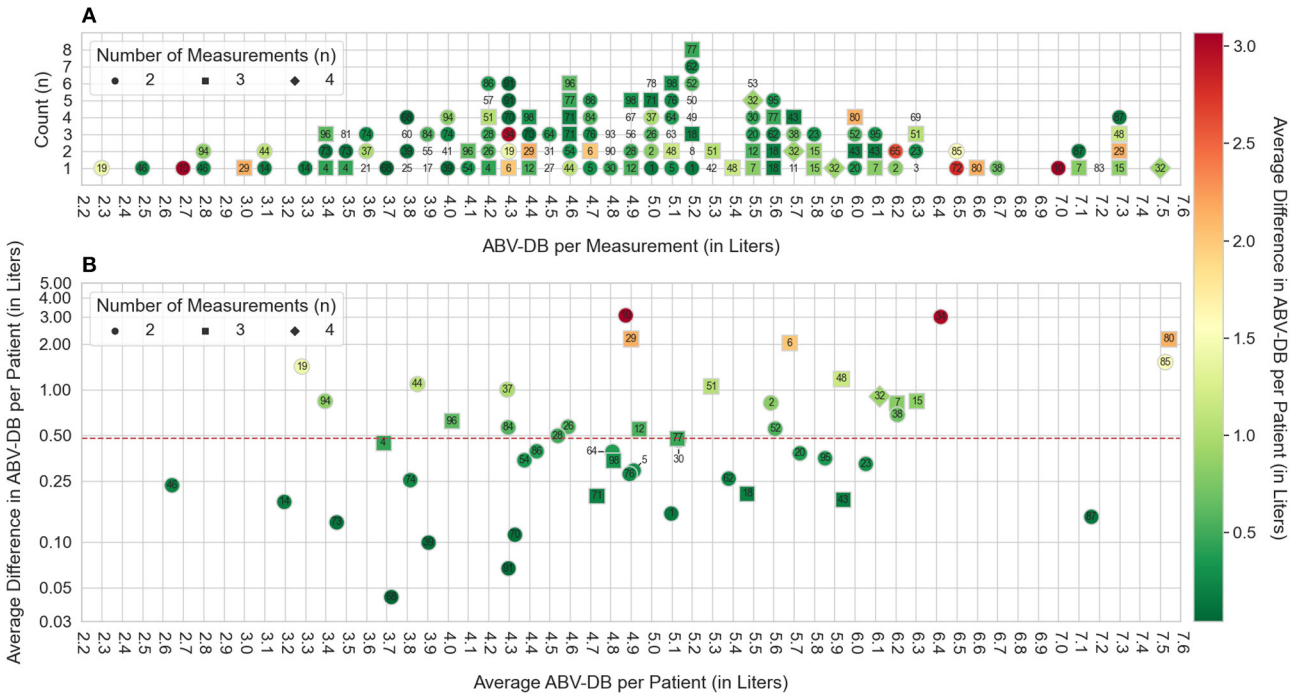

FIGURE 4 | ABV-DB distribution and standard deviation (based on 75 patients, 145 sessions). **(A)** Stacked dot-plot assessing ABV-DBs between 2.2 and 7.3 liters (70 Patients, 116 Sessions fall within this cut-off). Numeric patient identifiers are annotated for each ABV-DB estimate. The vertical axis shows the count of estimates which fall within a given 0.1 L interval of ABV-DB. Coloring of the annotation represents the average difference in ABV-DB observed in the respective patient, as specified in the color bar to the right of the figure: Green denotes high agreement between estimates, red denotes poor agreement. Patients without a colored contour marker did not have a second ABV-DB estimate available for comparison and therefore their average difference of ABV-DBs could not be calculated. **(B)** The horizontal axis here denotes the average ABV-DB for the corresponding patient. Coloring of annotations is analogous to **(A)** The vertical axis is on a logarithmic scale and denotes the average difference between ABV-BD estimates observed within the patient and is analogous to the coloring of the annotation. Patient 5, 30, and 64 were annotated with an offset to improve readability. The median average intra-patient difference in ABV-DB for all patients is denoted by a red dashed line.

ABV-DB determination using data collected in the routine clinical setting proved feasible. Nevertheless, we found that many BVM curves had to be excluded due to technical problems in the RBV sampling rate, but some also due to divergent execution in the clinical setting (e.g., non-standard bolus volume). We were able to formalize the approach for calculation provided by Kron et al. using an automated algorithm and extracting the BVM curves form the dialysis machines with a dialysis administration software. This approach is expected to provide an unbiased analysis compared to manual and direct visual inspection of data.

The manual approach described elsewhere was introduced for clinical use in want of a suitable electronic data acquisition system. Data acquisition systems recording all relevant machine data from whole dialysis units are currently not designed for data collection at high sampling rates. In our case data sampling was transmitted at increments of whole minutes, which is less than optimal. However, this sampling rate was not achieved consistently in some cases, which we expect to hold true for other standard interface systems as well. If the specified sampling period of 1 min were adequately maintained, it would still remain difficult to identify the proper concentrations required for the two-point method. In fact, analyzing the time course preceding and following the bolus dilution might be necessary. The abridged two-point approach inherently assumes instantaneous and stable distribution of indicator and a simple step change in concentrations, with stable (or steadily changing) concentrations before and after dilution. This assumption is of course idealized as blood concentrations are very variable during *in vivo* dialysis, when recorded with the precision required for BVM purposes. Nevertheless, the estimation of plausible concentrations could for example be improved by time series analysis of data points, regarding their variability and trend, and extrapolating the series of pre- and post-dilution concentrations to the time of dilution and the time of complete mixing, respectively.

Our results showed a high variability in ABV-DB, namely an average intra-patient SD of 0.78 L (median SD 0.47 L) in the 51 patients who had undergone at least two valid measurement sessions. In a quarter of repeat estimates, the intra-patient SD was 0.26 L or lower. Whether the observed variation is (at least partially) due to actual changes in blood volume between HD sessions or due to inaccuracy of the applied method cannot be determined without comparison to accepted reference methods, such as indocyanine green or radioisotope-based measurements. In future studies, we might also be able to assess whether cumulative information from a high number of BVM curves can reduce the intra-patient SD.

BP measurements performed during the dialysis sessions notably showed no drops below 90 mmHg systolic in the half-hour after bolus administration. Hospital staff also received informal feed-back from some patients who reported a positive subjective effect on overall wellbeing during and after HD sessions involving a bolus for ABV-DB estimation. As low BP and intradialytic hypotension are risk factor for outcomes, in future it might be interesting to assess the clinical outcomes of patients who receive a dialysate bolus at every dialysis session in comparison to those of a control group (even without informing dry weight adjustment or guided ultrafiltration). Whether patient-reported outcomes are purely due to placebo effect, or have some hard physiological correlate, could be an interesting side topic for future investigations applying this method. Evidence for the beneficial effect of repeated bolus infusion as used during intermittent back-filtrate infusion hemodiafiltration in reducing intradialytic hypotensive events is limited, but seems promising and could be a welcome side effect in measuring ABV-DB as well (40–42).

Concerning improved HD safety, Kron et al. observed no intradialytic morbid events, above 65 mL/kg SBV in a study encompassing 45 HD patients (33). This proposed static threshold requires further examination in larger cohorts and should probably be adapted depending on patient and treatment characteristics, as a volume-per-mass approach may be overly simplistic especially in obese subjects. We observed that an occasionally occurring sampling gap before bolus may lead to more unreliable ABV-DB estimates. For example, if RBV had not been recorded during the last 3 min before bolus in our study collective, this lack would have on average resulted in an absolute difference in ABV-DB estimation of 0.86 liters of blood with a high SD of 2.55 liters. It is therefore advisable to ensure a high sampling rate for electronic data transfer from the dialysis monitor to the data acquisition system before applying the fluid bolus.

Our study collective appeared largely representative of a standard hemodialysis population. However, a high number of patients (38.4%) received dialysis through a central catheter. This type of HD access was more prevalent in women and might have led to different results, due to the more central location of the catheter. The difference between catheters and fistulas regarding ABV-DB determination should receive special attention by investigators in the future. Especially when using a multi-compartment modeling approach, access type may be an important point to consider during model specification. In our own study ABV-DB (and SBV) was on average only 121.8 mL (1.4 mL/kg) lower in HD sessions involving a catheter access. In female patients who had a central catheter access it was 301.8 mL (8.41 mL/kg) lower, but in male patients 146.1 mL (4.3 mL/kg) higher. This result requires confirmation from future studies, and whether the location of the catheter might be causal currently remain purely speculative.

To improve accuracy and physiological plausibility, more complex models should probably be used, taking into account the intravascular/extravascular/interstitial fluid shifts. In this vein, Samandari et al. have recently published a study comparing a two compartment model to a back-extrapolation method (39). While not explicitly addressed, a main figure in their paper shows that ABV-DB values were consistently estimated lower in patients with a central catheter, using either of the modeling approaches they employed. Important points to consider during modeling include the cardiopulmonary recirculation, fluid shifts between the intravascular and interstitial spaces, as well as changes in the distribution of hematocrit between central and peripheral blood volume compartments. Future studies should also compare ABV-DB calculations with accepted reference methods [e.g., with indocyanine green (30, 31)].

In conclusion, we acknowledge the high variability in ABV-DB and a number of unreliable estimates due to a lack of BVM curve stability as the principal study limitation. Nevertheless, BVM data extraction and processing for ABV-DB calculation proved feasible. Further improvement might be made by increasing the sampling rate in the data acquisition system and by applying more sophisticated models of the cardiovascular space including whole body fluid distribution and kinetics. Establishing accuracy and reproducibility, ideally by receiving direct help from HD machine manufacturers now is the most important subsequent step along the way of enabling clinicians to use ABV-calculations such as to inform target weight prescription. Hopes are high that hemodynamic stability may be improvable once ABV estimates become more reliable and the dynamic relationship with the overall fluid status is elucidated.

DATA AVAILABILITY STATEMENT

The raw data supporting the conclusions of this article will be made available by the authors, without undue reservation.

ETHICS STATEMENT

The studies involving human participants were reviewed and approved by Ethics Committee of the Medical University of Vienna (EC No. 1732/2020, Project Title: Closing the Loop in Hemodialysis: A Precision Medicine Approach – Part A [Intradialytic Determination of Absolute Blood Volume: An Exploratory, Retrospective Study on 98 Patients]). Written informed consent for participation was not required for this study in accordance with the national legislation and the institutional requirements.

AUTHOR CONTRIBUTIONS

SK designed the study, collected data, analyzed data, and wrote the manuscript. MS and HO collected data and reviewed the manuscript. DS and PW designed the study, discussed the results, and reviewed and corrected the manuscript. SH designed the study and discussed the analysis. CM, SW, and ES discussed the results and reviewed and corrected the manuscript. MH designed the study, discussed the results, wrote the manuscript, and reviewed and corrected the manuscript. All authors contributed to the article and approved the submitted version.

FUNDING

This work was supported by the Vienna Science and Technology (WWTF) Grant LS20-079 Precision Medicine.

ACKNOWLEDGMENTS

The authors wish to thank the nursing staff at the Medical University of Vienna's CHD Units 1 and 2 for their kind cooperation. We also thank Janosch Niknam-Saeidi, Siam Hossain Mohammed, and Maximilian Waller for critically reviewing the present manuscript.

SUPPLEMENTARY MATERIAL

The Supplementary Material for this article can be found online at: https://www.frontiersin.org/articles/10.3389/fmed.2022.801089/full#supplementary-material

REFERENCES

1. Weiner DE, Brunelli SM, Hunt A, Schiller B, Glassock R, Maddux FW, et al. Improving clinical outcomes among hemodialysis patients: a proposal for a "Volume First" approach from the chief medical officers of US dialysis providers. *Am J Kidney Dis.* (2014) 64:685–95. doi: 10.1053/j.ajkd.2014.07.003
2. Basso F, Berdin G, Virzi GM, Mason G, Mason G, Day S, et al. Fluid management in the intensive care unit: bioelectrical impedance vector analysis as a tool to assess hydration status and optimal fluid balance in critically ill patients. *Blood Purif.* (2013) 36:192–9. doi: 10.1159/000356366
3. Bouchard JE, Mehta RL. Fluid balance issues in the critically ill patient. *Contrib Nephrol.* (2010) 164:69–78. doi: 10.1159/000313722
4. Available online at: http://www.infermed.com/ (accessed September 12, 2010).
5. Miller WL. Fluid volume overload and congestion in heart failure: time to reconsider pathophysiology and how volume is assessed. *Circ Heart Fail.* (2016) 9:e002922. doi: 10.1161/CIRCHEARTFAILURE.115.002922
6. Wystrychowski G, Levin NW. Dry weight: sine qua non of adequate dialysis. *Adv Chronic Kidney Dis.* (2007) 14:e10–6. doi: 10.1053/j.ackd.2007.03.003
7. Tsai YC, Chiu YW, Tsai JC, Kuo HT, Hung CC, Hwang SJ, et al. Association of fluid overload with cardiovascular morbidity and all-cause mortality in stages 4 and 5 CKD. *Clin J Am Soc Nephrol.* (2015) 10:39–46. doi: 10.2215/CJN.03610414
8. Flythe JE, Chang TI, Gallagher MP, Lindley E, Lindley E, Sarafidis PA, et al. Blood pressure and volume management in dialysis: conclusions from a kidney disease: improving global outcomes (KDIGO) controversies conference. *Kidney Int.* (2020) 97:861–76. doi: 10.1016/j.kint.2020.01.046
9. Agarwal R, Weir MR. Dry-weight: a concept revisited in an effort to avoid medication-directed approaches for blood pressure control in hemodialysis patients. *Clin J Am Soc Nephrol.* (2010) 51255–60. doi: 10.2215/CJN.01760210
10. Charra B. 'Dry weight' in dialysis: the history of a concept. *Nephrol Dial Transplant.* (1998) 13:1882–5. doi: 10.1093/oxfordjournals.ndt.a027898
11. Hecking M, Karaboyas A, Antlanger M, et al. Significance of interdialytic weight gain versus chronic volume overload: consensus opinion. *Am J Nephrol.* (2013) 38:78–90. doi: 10.1159/000353104
12. Leung KCW, Quinn RR, Ravani P, Duff H, MacRae JM. Randomized crossover trial of blood volume monitoring-guided ultrafiltration biofeedback to reduce intradialytic hypotensive episodes with hemodialysis. *Clin J Am Soc Nephrol.* (2017) 12:1831–40. doi: 10.2215/CJN.01030117
13. Steuer RR, Harris DH, Weiss RL, Biddulph MC, Conis JM. Evaluation of a noninvasive hematocrit monitor: a new technology. *Am Clin Lab.* (1991) 10:20–22.
14. Mancini E, Santoro A, Spongano M, Paolini F, Rossi M, Zucchelli P. Continuous on-line optical absorbance recording of blood volume changes during hemodialysis. *Artif Organs.* (1993) 17:691–94. doi: 10.1111/j.1525-1594.1993.tb00616.x
15. Paolini F, Mancini E, Bosetto A, Santoro A. Hemoscan: a dialysis machine-integrated blood volume monitor. *Int J Artificial Organs.* (1995) 18:487–94. doi: 10.1177/039139889501800902
16. Steuer R HD, Conis J. A new optical technique for monitoring hematocrit and circulating blood volume: its application in renal dialysis. *Dial Transplant.* (1993) 22:260–5.
17. Dasselaar JJ, Huisman RM, de Jong PE, Franssen CF. Measurement of relative blood volume changes during haemodialysis: merits and limitations. *Nephrol Dialysis Transplant.* (2005) 20:2043–9. doi: 10.1093/ndt/gfi056
18. Johner C, Chamney PW, Schneditz D, Kramer M. Evaluation of an ultrasonic blood volume monitor. *Nephrol Dialysis Transplant.* (1998) 13:2098–103. doi: 10.1093/ndt/13.8.2098
19. Schneditz D, Pogglitsch H, Horina J, Binswanger U. A blood protein monitor for the continuous measurement of blood volume changes during hemodialysis. *Kidney Int.* (1990) 38:342–6. doi: 10.1038/ki.1990.207
20. Sinha AD, Light RP, Agarwal R. Relative plasma volume monitoring during hemodialysis AIDS the assessment of dry weight. *Hypertension.* (2010) 55:305–11. doi: 10.1161/HYPERTENSIONAHA.109.143974
21. Hecking M, Schneditz D. Feedback control in hemodialysis-much ado about nothing? *Clin J Am Soc Nephrol.* (2017) 12:1730–2. doi: 10.2215/CJN.09770917
22. Keane DF, Raimann JG, Zhang H, Willetts J, Thijssen MSS, Kotanko P. The time of onset of intradialytic hypotension during a hemodialysis session associates with clinical parameters and mortality. *Kidney Int.* (2021) 99:1408–17. doi: 10.1016/j.kint.2021.01.018
23. McIntyre CW, Lambie SH, Fluck RJ. Biofeedback controlled hemodialysis (BF-HD) reduces symptoms and increases both hemodynamic tolerability and dialysis adequacy in non-hypotension prone stable patients. *Clin Nephrol.* (2003) 60:105–12. doi: 10.5414/CNP60105
24. Garzoni D, Keusch G, Kleinoeder T, Martin H, Dhondt A, Cremaschi L, et al. Reduced complications during hemodialysis by automatic blood volume controlled ultrafiltration. *Int J Artificial Organs.* (2007) 30:16–24. doi: 10.1177/039139880703000104
25. Reddan DN, Szczech LA, Hasselblad V, Lowrie EG, Lindsay RM, Himmelfarb J, et al. Intradialytic blood volume monitoring in ambulatory hemodialysis patients: a randomized trial. *J Am Soc Nephrol.* (2005) 16:2162–9. doi: 10.1681/ASN.2004121053
26. Puri S, Park J-K, Modersitzki F, Goldfarb DS. Radioisotope blood volume measurement in hemodialysis patients. *Hemodial Int.* (2014) 18:406–14. doi: 10.1111/hdi.12105
27. Malha L, Fattah H, Modersitzki F, Goldfarb DS. Blood volume analysis as a guide for dry weight determination in chronic hemodialysis patients: a crossover study. *BMC Nephrol.* (2019) 20:47. doi: 10.1186/s12882-019-1211-7
28. Ahlgrim C, Schumacher YO, Wrobel N, Waller CF, Pottgiesser T. Application of the optimized CO-rebreathing method for determination of hemoglobin mass in patients with polycythemia vera. *Ann Hematol.* (2014) 93:1159–65. doi: 10.1007/s00277-014-2020-5
29. Schmidt W, Prommer N. The optimised CO-rebreathing method: a new tool to determine total haemoglobin mass routinely. *Eur J Appl Physiol.* (2005) 95:486–95. doi: 10.1007/s00421-005-0050-3
30. Schneditz D, Haditsch B, Jantscher A, Ribitsch W, Krisper P. Absolute blood volume and hepatosplanchnic blood flow measured by indocyanine green kinetics during hemodialysis. *ASAIO J.* (2014) 60:452–8. doi: 10.1097/MAT.0000000000000075
31. Mitra S, Chamney P, Greenwood R, Farrington K. Serial determinations of absolute plasma volume with indocyanine green during hemodialysis. *J Am Soc Nephrol.* (2003) 14:2345–51. doi: 10.1097/01.ASN.0000082998.50730.FA
32. Kron J, Schneditz D, Leimbach T, Aign S, Kron S. A simple and feasible method to determine absolute blood volume in hemodialysis patients in clinical practice. *Blood Purif.* (2014) 38:180–7. doi: 10.1159/000368157

33. Kron S, Schneditz D, Czerny J, Leimbach T, Budde K, Kron J. Adjustment of target weight based on absolute blood volume reduces the frequency of intradialytic morbid events. *Hemodial Int.* (2018) 22:254–60. doi: 10.1111/hdi.12582
34. Schneditz D, Schilcher G, Ribitsch W, Krisper P, Haditsch B, Kron J. On-line dialysate infusion to estimate absolute blood volume in dialysis patients. *ASAIO J.* (2014) 60:436–42. doi: 10.1097/MAT.0000000000000086
35. Kron S, Schneditz D, Leimbach T, Aign S, Kron J. Vascular refilling is independent of volume overload in hemodialysis with moderate ultrafiltration requirements. *Hemodial Int.* (2016) 20:484–91. doi: 10.1111/hdi.12417
36. Kron S, Schneditz D, Leimbach T, Czerny J, Aign S, Kron J. Determination of the critical absolute blood volume for intradialytic morbid events. *Hemodial Int.* (2016) 20:321–6. doi: 10.1111/hdi.12375
37. Kron S, Schneditz D, Leimbach T, Kron J. Feedback control of absolute blood volume: a new technical approach in hemodialysis. *Hemodial Int.* (2020) 24:344–50. doi: 10.1111/hdi.12826
38. Erratum. *Blood Purif.* (2020). doi: 10.1159/000517063
39. Samandari H, Schneditz D, Germain MJ, Horowitz J, Hollot CV, Chait Y. Variable-volume kinetic model to estimate absolute blood volume in patients on dialysis using dialysate dilution. *ASAIO J.* (2018) 64:77–85. doi: 10.1097/MAT.0000000000000608
40. Koda Y, Aoike I, Hasegawa S, Yosawa Y, Nakagawa Y, Iwabuchi F, et al. Feasibility of intermittent back-filtrate infusion hemodiafiltration to reduce intradialytic hypotension in patients with cardiovascular instability: a pilot study. *Clin Exp Nephrol.* (2017) 21:324–32. doi: 10.1007/s10157-016-1270-z
41. Mineshima M, Eguchi K. Development of intermittent infusion hemodiafiltration using ultrapure dialysis fluid with an automated dialysis machine. *Blood Purif.* (2013) 35(Suppl. 1):55–8. doi: 10.1159/000346371
42. Koda Y, Aoike I. Prevention of intradialytic hypotension with intermittent back-filtrate infusion haemodiafiltration: insights into the underlying mechanism. *Blood Purif.* (2019) 48(Suppl. 1):1–6. doi: 10.1159/000503878

Conflict of Interest: The authors declare that the research was conducted in the absence of any commercial or financial relationships that could be construed as a potential conflict of interest.

frontiers in Medicine

ORIGINAL RESEARCH
published: 15 February 2022
doi: 10.3389/fmed.2022.799544

Frailty as an Independent Risk Factor for Depression in Patients With End-Stage Renal Disease: A Cross-Sectional Study

Chun-Yi Chi[1], *Szu-Ying Lee*[1], *Chia-Ter Chao*[2,3,4*] *and Jeng-Wen Huang*[1,4]

[1] *Nephrology Division, Department of Internal Medicine, National Taiwan University Hospital Yunlin Branch, Douliu, Taiwan,* [2] *Nephrology Division, Department of Internal Medicine, National Taiwan University Hospital, Taipei, Taiwan,* [3] *Graduate Institute of Toxicology, National Taiwan University College of Medicine, Taipei, Taiwan,* [4] *Nephrology Division, Department of Internal Medicine, National Taiwan University College of Medicine, Taipei, Taiwan*

OPEN ACCESS

Edited by:
Maik Gollasch,
Charité Universitätsmedizin Berlin, Germany

Reviewed by:
Giorgos K. Sakkas,
University of Thessaly, Greece
Malcolm Koo,
Tzu Chi University of Science and Technology, Taiwan
Abhinav Dixit,
All India Institute of Medical Sciences Jodhpur, India

***Correspondence:**
Chia-Ter Chao
b88401084@gmail.com

Specialty section:
This article was submitted to Nephrology, a section of the journal Frontiers in Medicine

Received: *21 October 2021*
Accepted: *14 January 2022*
Published: *15 February 2022*

Citation:
Chi C-Y, Lee S-Y, Chao C-T and Huang J-W (2022) Frailty as an Independent Risk Factor for Depression in Patients With End-Stage Renal Disease: A Cross-Sectional Study. Front. Med. 9:799544. doi: 10.3389/fmed.2022.799544

Background: Depression confers substantial disease burden globally, especially among those with chronic kidney disease (CKD). The presence of depression significantly impairs one's quality of life. Risk factors for depression in patients with CKD remain under-appreciated, and whether frailty, a geriatric phenotype, constitutes a risk factor for depression in this population is unknown.

Methods: We prospectively enrolled patients with end-stage renal disease (ESRD) undergoing hemodialysis for >3 months from National Taiwan University Hospital Yunlin Branch between 2019 and 2021. Clinical, physical, functional, and performance parameters were recorded, followed by frailty/sarcopenia assessment. Depression was screened for using the Geriatric Depression Scale. We analyzed the independent relationship between frailty and depression in these patients, using multiple regression analyses.

Results: Totally 151 patients with ESRD were enrolled (mean 61.1 years, 66.9% male), among whom 16.6% had screening-identified depression. ESRD participants with depression did not differ from those without regarding most parameters except serum creatinine, functional indices, and sarcopenia/frailty status. We found that having greater frail severities was independently associated with a higher probability of depression; having FRAIL- (odds ratio [OR] 5.418) and SOF-based (OR 2.858) frailty independently correlated with a higher depression probability. A linear relation exists between a greater frail severity and the probability of depression. Using a more relaxed criterion for detecting depression, higher SOF scores remained significantly associated with an increased depression risk.

Conclusions: In patients with CKD, frailty independently correlated with a higher probability of having depression. Strategies aiming to attenuate frailty may be able to benefit those with depression simultaneously in this population.

Keywords: chronic kidney disease, depression, end-stage renal disease, frailty, geriatric phenotype, malnutrition, sarcopenia

INTRODUCTION

Depression, characterized by an emotional turbulence presenting with somatic, cognitive, and behavioral symptoms, is one of the common psychiatric disorders that affect billions of people and confer substantial disease burden globally (1). Depression is frequently accompanied by loss of interest toward activities and relationships, and prominently impairs an individual's quality of life. Depression exhibits an increased incidence in patients with chronic kidney disease (CKD) and especially those with end-stage renal disease (ESRD), up to 20% to 40% depending upon countries and assessment tools (2). Depression increases CKD patients' long-term mortality by at least 50%, based on National Health and Nutrition Examination Survey (NHANES) results (3). Besides its effect on survival, depression poses a plethora of adverse influences in this population; depressed patients with CKD were found to have a higher incidence of muscle wasting and correlated with a greater degree of functional impairment, according to findings from the Dialysis Outcomes and Practice Patterns Study (DOPPS) (4, 5). Furthermore, depression and its predisposing traits likely modulate the incidence of CKD and its subsequent progression. A recent Mendelian randomization study showed that genetic alleles intimately associated with depressive symptoms conferred a greater risk of carrying lower estimated glomerular filtration rates (eGFRs) (6). Having depressive symptoms places patients at risk of developing accelerated renal function decline, rendering the identification of depression instrumental (7).

Risk factors for depression in patients with CKD or ESRD remain under-appreciated. Existing studies mostly involve patients with depression but without CKD; systematic reviews and meta-analyses indicated that smoking, higher body mass index (BMI), lower blood pressure, personal traits, chronic diseases, and sleep disturbance were associated with an increased risk of having depression in various populations (8, 9). On the other hand, these risk features may not be applicable to those with CKD. Anecdotal studies revealed that severe pain, negative illness perception, and inadequate self-esteem significantly correlated with the presence of depression in those with non-dialysis CKD (10). A longer dialysis vintage also modulated the probability of developing depression in patients with ESRD (11). Since the presence of CKD is associated with premature biological aging (12), emerging studies suggest that geriatric phenotypes demonstrate a high prevalence in this population. Frailty, in particular, is found to be highly prevalent in patients with renal insufficiency. Frailty is recently shown to correlate with the presence and severity of depression in community-dwelling older adults (13), but very few address the possibility whether frailty constitutes a risk factor for depression in patients with CKD. Such relationship has been hypothesized before (14) but never tested in this population. To answer this question, we used a prospectively collected cohort of patients with ESRD to analyze the connection between frailty and depression, using well-validated instruments.

Abbreviations: BH, body height; BMI, body mass index; BP, blood pressure; BW, body weight; CHS, cardiovascular health study; CI, confidence interval; CKD, chronic kidney disease; CNAQ, Council of Nutrition Assessment Questionnaire; DOPPS, Dialysis Outcomes and Practice Patterns Study; ECOG, eastern cooperative oncology group; EFS, Edmonton frail scale; eGFR, estimated glomerular filtration rate; ESRD, end-stage renal disease; FRAIL, fatigue, resistance, ambulation, illness, and loss of weight; GDS-15, Geriatric Depression Scale-15 items; IADL, instrumental activity of daily living; MDRD, Modification of Diet in Renal Disease; NHANES, National Health and Nutrition Examination Survey; OR, odds ratio; SOF, study of osteoporotic fracture; TCS, timed chair stand; TUG, time up and go; WC, waist circumference.

SUBJECTS, MATERIALS, AND METHODS

Ethical Statement

The protocol of the current project has been approved by the institutional review board of National Taiwan University Hospital (No. 201910100RINA). The details of the study protocol adhered to the Declaration of Helsinki, and all participants provided written informed consent.

Recruitment of Participants and Study Procedures

Patients with ESRD, defined as having an eGFR <15 mL/min/1.73 m^2, undergoing hemodialysis for more than 3 months, were prospectively enrolled from the dialysis units of National Taiwan University Hospital Yunlin Branch, Douliou and Huwei branches between August 2019 and July 2021. We used the 4-variable Modification of Diet in Renal Disease (MDRD) formula for calculating eGFR. After providing informed consent, participants underwent a 3-step assessment; first, they were interviewed by dedicated nursing staff, with their demographic information (age, gender, and education level) and morbidities recorded. Second, participants underwent physical examination, with their anthropometric parameters [body weight (BW)/body height (BH), waist circumference (WC), and arm/leg circumference] and physical examination indices [blood pressure (BP), heart rate (HR), and respiratory rate] collected (15). At this stage, participants were also instructed to complete performance assessment involving upper and lower limbs, including grip strength (using a TKK dynamometer; Takei Inc., Niigata, Japan), timed chair stand (TCS), time-up-and-go (TUG), and gait speed, according to protocols published previously (16, 17). For all performance assessment, results were obtained after averaging data from 3 repetitive tests. Finally, as the last step, dedicated staff counseled with the participants and administered self-report questionnaires including functional evaluation (eastern cooperative oncology group [ECOG], Karnofsky performance scale, Barthel index, Katz index, and Lawton-Brody instrumental activity of daily living [IADL]), sarcopenia assessment (SARC-F questionnaire), frailty status evaluation [Edmonton frail scale (EFS), Study of Osteoporotic Fractures (SOF) scale, and Fatigue, Resistance, Ambulation, Illness, Loss of weight (FRAIL) scale], and nutritional/appetite screening [Council of Nutrition Assessment Questionnaire (CNAQ)]. The validity of instruments for evaluating frailty, sarcopenia, and nutritional levels in this study has been tested and reassured in patients with CKD and ESRD based on other reports and our prior findings (17–19). Those with a SARC-F score ≥ 4 were defined as having sarcopenia, while those with a SOF, FRAIL, or EFS score ≥ 2, 3, and 8 were considered frail, respectively, according to their original schemes. Finally, at least

10 mL of peripheral blood was obtained from participants, sent for laboratory tests including hemogram, serum biochemistry and electrolytes, and metabolic parameters (glucose, lipid profile, and uric acid).

Outcome Assessment

In this study, we screened these patients regarding whether they had depression, using the Geriatric Depression Scale-15 items (GDS-15). GDS-15 has been recommended as a useful tool to screen for depression in older adults during acute and chronic settings, and also in patients with CKD (20, 21), with a score range between 0 and 15. Compared with other GDS instruments with different item counts (GDS-30, GDS-5, and GDS-4), GDS-15 exhibited a better recognition accuracy compared to others, owing to its advantages of preserving core messages while optimizing the amount of item load (22). GDS-15 assesses participants' depressive symptoms, psychosocial activities, life satisfaction, etc., all of which correlate closely with each other (23). After reassuring patients' cognitive status and literacy level, participants completed the GDS-15 questionnaire, consisting of 10 and 5 positive and negative responses to the presence of depression, respectively, with or without assistance from dedicated staff. Those with a GDS-15 score $\geq$10 were identified as potentially having depression, according to the existing literature (21–23).

Statistical Analysis

For continuous variables, we compared between groups using Student's *t*-tests (if normally distributed) or Mann-Whitney U-test (if skewed distribution). For categorical variables, we compared between groups using Chi-square tests. In all analyses, a *p*-value <0.05 was considered statistically significant. We used IBM SPSS Statistics for Windows, Version 19.0 (Armonk, NY; IBM Corp.) in all statistical analysis.

After completing all assessments in phases 1 and 2, we divided participants into those with and without potential depression, followed by comparing their demographic profiles, comorbidities, physical examination and anthropometric parameters, performance indicators, and laboratory findings. We further examined whether there were differences between those with and without depression, regarding their functional status, frailty, sarcopenia, and nutritional status based on relevant tools. Subsequently, we used multiple regression analysis with having depression or not as the dependent variable with stepwise backward variable selection, incorporating variables with significant differences in univariate analyses. Independent variables were expressed in odds ratios (ORs) with 95% confidence intervals and the associated *p*-values provided. Sensitivity analyses were planned *a priori*, including the adjustment of variable input style (categorical vs. continuous). We also tested whether the replacement of dependent variable, depression or not based on having GDS-15 $\geq$10, with depression or susceptibility status or not based on having GDS-15 $\geq$5, might influence our findings.

RESULTS

During the study period, we enrolled a total of 151 patients with ESRD under chronic hemodialysis, with a mean age of 61.1 years and 66.9% male (**Table 1**). The most common comorbidity among study participants was hypertension (80.1%), followed by diabetes mellitus (47.0%) and peptic ulcer (30.5%). Nearly half of these patients had chronic pain (43.7%). Participants exhibited on average fair upper and lower limb performance, with a mean TCS, TUG and gait speed of 14.9 s, 10.7 s, and 0.77 m/s, respectively (**Table 1**). Participants with ESRD were mildly anemic, but had normal electrolyte panels. Their serum uric acid (7.8 mg/dL) and triglyceride (172.2 mg/dL) levels were mildly increased, and participants had mild hyperglycemia (118.7 mg/dL).

Among all, 16.6% participants were found to have depression after screening questionnaire use. ESRD participants with potential depression did not differ from those without regarding their demographic profiles, comorbidities, physical examination parameters, anthropometric indices, performance indicators, and most laboratory data except lower serum creatinine levels (p = 0.02) among the former group (**Table 1**).

Functional Evaluation and Frailty/Sarcopenia Assessment for Study Participants

During functional assessment, participants with ESRD were found to have minor impairment in their activity of daily living, with an average ECOG, Karnofsky performance indicators, and Barthel index scores of 0.97 out of 4, 82.8 out of 100, and 91.3 out of 100, respectively (**Table 2**). Approximately 17.2% participants had sarcopenia, while 12.6, 19.2, and 23.8% of them had FRAIL-, EFS-, and SOF-defined frailty, respectively. Participants with depression had significantly higher ECOG (p = 0.028) and instrumental activity of daily living scores (p = 0.034) but lower Karnofsky performance indicators (p = 0.006) (**Table 2**). Those with depression were significantly more likely to have sarcopenia than those without (p = 0.032). Similarly, those with depression had a significantly higher prevalence of frailty (40–52%) compared to those without (7.1–18.3%) (**Table 2**). Participants without depression had better appetite in the form of higher CNAQ scores than those without (p = 0.033).

Independent Predictors of Depression in Patients With End-Stage Renal Disease

We then conducted multiple regression analyses to uncover independent factors associated with having depression after the screening test in study participants. After accounting for variables with significant between-group differences in univariate analysis (**Tables 1**, **2**), including serum creatinine, functional evaluation results (Karnofsky and IADL scores), SARC-F scores, frailty scores (EFS, FRAIL, and SOF scales), and CNAQ scores, we found that having a greater frail severity, including higher EFS (OR 1.365, 95% CI 1.057–1.762) and SOF scores (OR 3.076, 95% CI 1.458–6.493), was independently associated with a higher risk of developing potential depression (**Table 3**). Sensitivity analyses were done using having frailty or not based on EFS,

TABLE 1 | Baseline characteristics of patients with end-stage renal disease enrolled in this study.

	Total ($n = 151$)	Without depression ($n = 126$)	With depression ($n = 25$)	*p*-value
Basic data				
Age (years)	61.1 ± 12.0	61.0 ± 11.4	61.5 ± 14.7	*0.863*
Sex (male %)	101 (66.9)	86 (68.3)	15 (60.0)	*0.426*
Education				*0.284*
None	16 (10.6)	12 (9.5)	4 (16.0)	
Elementary school	32 (21.2)	24 (19.0)	8 (32.0)	
High school	84 (55.6)	74 (58.7)	10 (40.0)	
College or higher	19 (12.6)	16 (12.7)	3 (12.0)	
Comorbidity				
Diabetes mellitus (%)	71 (47.0)	58 (46.0)	13 (52.0)	*0.588*
Hypertension (%)	121 (80.1)	102 (81.0)	19 (76.0)	*0.574*
Cirrhosis (%)	6 (4.0)	5 (4.0)	1 (4.0)	*0.994*
Coronary artery disease (%)	32 (21.2)	25 (19.8)	7 (28.0)	*0.365*
Acute myocardial infarction (%)	8 (5.3)	6 (4.8)	2 (8.0)	*0.512*
Heart failure (%)	34 (22.5)	26 (20.6)	8 (32.0)	*0.217*
Peripheral vascular disease (%)	6 (4.0)	4 (3.2)	2 (8.0)	*0.262*
Atrial fibrillation (%)	1 (0.7)	1 (0.8)	0 (0)	*0.658*
COPD (%)	6 (4.0)	5 (4.0)	1 (4.0)	*0.994*
Rheumatology disorders (%)	5 (3.3)	4 (3.2)	1 (4.0)	*0.834*
Malignancy (%)	17 (11.3)	13 (10.3)	4 (16.0)	*0.415*
Peptic ulcer (%)	46 (30.5)	37 (29.4)	9 (36.0)	*0.513*
Prior cerebrovascular accident (%)	9 (6.0)	7 (5.6)	2 (8.0)	*0.640*
Hemiplegia (%)	2 (1.3)	2 (1.6)	0 (0)	*0.529*
Chronic pain (%)	66 (43.7)	52 (41.3)	14 (56.0)	*0.177*
Physical examination				
Blood pressure—systolic (mmHg)	147.0 ± 28.9	147.7 ± 29.1	143.6 ± 28.7	*0.516*
Blood pressure—diastolic (mmHg)	71.0 ± 13.6	71.8 ± 14.0	67.0 ± 10.9	*0.108*
Heart rate (per min)	75.8 ± 11.8	75.8 ± 11.6	75.6 ± 13.1	*0.943*
Respiratory rate (per min)	16.8 ± 1.8	16.8 ± 1.8	16.6 ± 1.5	*0.613*
Anthropometric parameters				
Body weight (kg)	63.8 ± 15.1	63.1 ± 14.5	67.1 ± 18.0	*0.226*
Body height (cm)	162.9 ± 8.3	162.7 ± 8.2	163.5 ± 8.9	*0.662*
Body mass index (kg/m^2)	23.9 ± 4.3	23.7 ± 4.2	24.8 ± 5.0	*0.215*
Waist circumference (cm)	86.8 ± 12.9	86.8 ± 13.0	87.1 ± 12.8	*0.906*
Mid-arm circumference (cm)	26.9 ± 4.1	26.9 ± 3.9	26.9 ± 4.9	*0.992*
Mid-leg circumference (cm)	31.9 ± 4.0	31.9 ± 3.8	32.0 ± 5.1	*0.913*
Performance indicators				
Grip strength (lb)	155.7 ± 66.6	159.3 ± 63.5	137.5 ± 79.3	*0.136*
Timed chair stand (s)	14.9 ± 9.8	14.8 ± 10.4	15.1 ± 5.3	*0.892*
Timed up and go (s)	10.7 ± 3.4	10.5 ± 3.0	11.4 ± 5.0	*0.243*
Gait speed (m/s)	0.77 ± 0.15	0.77 ± 0.15	0.77 ± 0.13	*0.918*
Laboratory profile				
Hemogram				
Leukocyte (K/μL)	7.1 ± 7.6	7.2 ± 8.3	6.5 ± 2.3	*0.689*
Hemoglobin (g/dL)	10.5 ± 1.5	10.5 ± 1.4	10.8 ± 1.9	*0.273*
Platelet (K/μL)	169.5 ± 54.1	167.4 ± 50.6	179.6 ± 69.6	*0.305*
Biochemistry				
Urea nitrogen (mg/dL)	85.1 ± 19.8	84.5 ± 20.3	87.8 ± 17.7	*0.445*
Creatinine (mg/dL)	12.3 ± 2.4	12.5 ± 2.2	11.3 ± 2.7	*0.020*
Albumin (mg/dL)	4.0 ± 0.3	4.0 ± 0.3	4.0 ± 0.3	*0.898*
Sodium (meq/L)	136.3 ± 3.0	136.4 ± 2.9	135.6 ± 3.7	*0.202*
Potassium (meq/L)	4.7 ± 0.7	4.7 ± 0.7	4.8 ± 0.7	*0.435*
Calcium (mmol/L)	2.4 ± 0.2	2.4 ± 0.2	2.4 ± 0.2	*0.252*
Phosphate (mg/dL)	5.2 ± 1.6	5.2 ± 1.7	5.1 ± 1.4	*0.854*
Metabolic				
Uric acid (mg/dL)	7.8 ± 1.8	7.8 ± 1.8	7.6 ± 2.1	*0.622*
Total cholesterol (mg/dL)	151.9 ± 40.7	151.0 ± 38.6	156.4 ± 50.4	*0.543*
Triglyceride (mg/dL)	172.2 ± 138.0	171.3 ± 143.7	177.2 ± 106.5	*0.845*
Low density lipoprotein cholesterol (mg/dL)	78.8 ± 29.9	78.2 ± 29.0	82.0 ± 34.8	*0.569*
Fasting glucose (mg/dL)	118.7 ± 51.8	116.1 ± 47.5	131.8 ± 69.2	*0.166*

COPD, chronic obstructive pulmonary disease.

FRAIL, and SOF scales replacing frailty-assessing scores; we similarly revealed that having FRAIL- (OR 5.418) and SOF-based (OR 2.858) frailty independently correlated with a higher depression probability (**Table 3**). Alternatively, we used a more relaxed criterion, having a GDS ≥5, as the dependent variable in another set of regression analysis; we discovered that higher SOF scores remained significantly associated with an increased risk (**Table 3**).

Based on our results that the prevalence of potential depression in those without and with SOF-defined frailty was 10.4% and 36.1%, respectively, and that the alpha value was set at 0.05, we could derive a *post-hoc* power of 91.8% for detecting difference of a dichotomous endpoint.

DISCUSSION

In this study, we prospectively enrolled a group of patients with ESRD and comprehensively assessed their baseline clinical, physical, functional, and performance status, followed by depression screening. After adjusting for potential confounders, we were able to show that frailty was an independent factor associated with having depression in these patients, in a graded fashion. This phenomenon serves to remind physicians that frailty evaluation may partially assist them in determining the probability of depression among patients with CKD, and that frailty-curbing strategy may potentially benefit CKD patients with depression as well.

The prevalence of depression ranged between 16.6 and 18.5% in the current study. Compared to results reported by others (25 to 35%) (2), the prevalence of depression was modestly lower; several reasons might be responsible for this phenomenon. First of all, the nutritional status of our study participants

TABLE 2 | Functional and geriatric syndrome evaluation results of study participants.

	Total ($n = 151$)	Without depression ($n = 126$)	With depression ($n = 25$)	*p*-value
Functional evaluation				
ECOG	0.97 ± 0.77	0.91 ± 0.73	1.28 ± 0.89	*0.028*
Karnofsky performance indicators	82.8 ± 14.6	84.2 ± 13.7	75.6 ± 16.9	*0.006*
Barthel index scores	91.3 ± 22.2	92.8 ± 20.8	83.6 ± 27.6	*0.058*
Katz index scores	5.4 ± 1.6	5.5 ± 1.5	4.9 ± 2.1	*0.083*
Lawton-Brody IADL scores	1.7 ± 2.3	1.6 ± 2.2	2.6 ± 2.6	*0.034*
Sarcopenia				
SARC-F scores	1.6 ± 2.5	1.4 ± 2.4	2.9 ± 3.0	*0.006*
Sarcopenia	26 (17.2)	18 (14.3)	8 (32.0)	*0.032*
Frailty				
Edmonton frail scale scores	5.1 ± 2.6	4.8 ± 2.4	6.8 ± 2.8	*<0.001*
EFS-defined frailty (%)	29 (19.2)	19 (15.1)	10 (40.0)	*0.004*
FRAIL scale scores	0.90 ± 1.26	0.75 ± 1.10	1.68 ± 1.68	*0.001*
FRAIL-defined frailty (%)	19 (12.6)	9 (7.1)	10 (40.0)	*<0.001*
SOF scale scores	1.00 ± 0.76	0.90 ± 0.73	1.56 ± 0.71	*<0.001*
SOF-defined frailty (%)	36 (23.8)	23 (18.3)	13 (52.0)	*<0.001*
Nutritional evaluation				
CNAQ scores	26.9 ± 3.1	27.1 ± 2.9	25.7 ± 3.8	*0.033*

CNAQ, Council on Nutrition Appetite Questionnaire; ECOG, Eastern Cooperative Oncology Group; EFS, Edmonton frail scale; IADL, instrumental activity of daily living; SOF, Study of Osteoporotic Fracture.

TABLE 3 | Independent factors associated with having depression among patients with end-stage renal disease.

Variables[&]	Odds ratio	95% confidence interval	*P*-value
Having depression, incorporating frailty scores			
EFS scores (per 1 score)	1.365	1.057–1.762	*0.017*
SOF scores (per 1 score)	3.076	1.458–6.493	*0.003*
Having depression, incorporating frailty status			
FRAIL-based frailty	5.418	1.723–17.032	*0.004*
SOF-based frailty	2.858	1.032–7.914	*0.043*
Having depression or depression susceptibility			
SOF scores (per 1 score)	3.517	1.642–7.532	*0.001*

[&] *Incorporating variables with significant differences in univariate analyses, including serum creatinine, Karnofsky score, SARC-F scores, IADL scores, Edmonton frail scale scores (or frailty status), SOF scores (or frailty status), FRAIL scale scores (or frailty status), and Council of Nutrition Assessment Questionnaire scores.*

appeared fair, with relatively good muscle power and functional status. This assertion is supported by their average BMI (23.9 ± 4.3 kg/m^2) and fair gait speed/grip strength (**Table 1**) relative to the mean values obtained previously in Taiwanese patients with ESRD (16). On the other hand, the sensitivity of our depression screening instrument may need to be optimized. There are other ways of detecting depression in patients with CKD, including Beck depression inventory, Hamilton rating scale, major depression inventory, center for epidemiological studies depression screening index, etc. (2), but heterogeneity in results is not uncommon. Specifically, it is speculated that the estimation of depression prevalence may be lower when patients are assessed by clinical interview compared to data obtained by self-report (2). Since our participants were assessed by a hybrid of self-report and clinical interview, it is likely that the prevalence estimate could be somewhat lower. Nonetheless, the relationship between depression identified by different instruments and adverse outcomes remains consistent across tools.

The paths connecting frailty to the inception of depression, though frequently under-recognized, can be complex. Frailty has been proposed to be conductive to having a mindset of suboptimal health perception and inadequate competence in self-care (24); possessing illness perceptions including a greater symptomatology, less personal control, and maladaptive coping strategies has been shown to increase the distress level of patients with CKD (25), predisposing them to the subsequent development of depression. Patients with frailty frequently report the co-presence of other geriatric syndromes such as malnutrition, polypharmacy, and functional impairment. Geriatric phenotypes, including malnutrition and polypharmacy, has been suggested to independently correlate with reporting depressive symptoms (26), serving as another rationale for linking frailty to depression. Alternatively, frailty may co-exist with a greater severity of occult inflammation; a meta-analysis showed that frail patients had significantly higher circulating levels of C-reactive protein and interleukin-6 than non-frail ones (27). Chronic inflammation, or the ingestion of a pro-inflammatory diet, potentially increases the risk of depression (28), constituting another link between frailty and depression. The strength of such link may become more prominent in patients with CKD, whose severity of inflammation outnumbers those without (29). From these arguments, we can presume that frailty may increase the risk of depression in patients with CKD, through multiple mechanisms.

We showed that results generated from one of the three frailty-assessing instruments (SOF scale) exhibited a consistent association with the risk of depression across different models, while the other two (EFS and FRAIL scale) were conditionally associated (**Table 3**). There are differences regarding the scale components, the predictive accuracy, the ease of administration, and the applicability between the 3 instruments. SOF scale has fewer items, is easier for use, and has been widely validated in various populations for outcome prediction, but it tends to over-screen frailty (30). With these features in mind, it is expectable that SOF may potentially be more sensitive for identifying those with earlier presentations of frailty compared to other instruments; indeed, we found that SOF identified a significantly higher proportion of patients with frailty in our cohort. Prior studies revealed that in certain population, SOF scale exhibited better detection ability for adverse outcomes compared to Cardiovascular Health Study (CHS) scale (31). Therefore, our findings may be reasonable in light of the inherent differences between frailty-detecting instruments.

Existing interventions to ameliorate depressive symptoms in patients with CKD include wellbeing enhancement through counseling or electronic apps (32), exercise regimens such as cycling, strengthening, pilates, jogging or home-based ones

(33), mind-body interventions such as yoga or relaxation therapies (34), pharmaceutical options (specific serotonin-selective reuptake inhibitor) (35). However, available options more or less have their disadvantages; patients with CKD already have high pill burden and multimorbidity, which renders them reluctant to receive pharmacological treatments or predisposes them to side effects. Psychiatric services, a quintessential part of depression management, may be unavailable due to staff shortage or uneven distributions, especially for those who do not live in urban areas. It would benefit patients with CKD if more treatment options can be tested for the management of depression in this population. Based on our findings, we propose that frailty-targeted interventions may an alternative choice if we aim to reduce the probability of depression in these patients. For example, dedicated exercise training, comorbidity management, senolytics, etc. may all be potential options for anti-frailty purpose (36). It would be tempting to pursue these options as adjunct options for counteracting depression in patients with CKD, although more studies are needed in this regard.

Our study has its strengths and limitations. In our study, we collected a comprehensive set of variables, ranging from demographic, morbidities, anthropometric, physical, functional, and laboratory parameters, as well as frailty, nutrition, and sarcopenia assessment results. This approach likely reduced the probability of result influenced by most residual confounding factors. We used multiple frailty-assessing instruments to evaluate frailty, and the results were robust. However, limitations do exist. Our sample size was not large, and statistical efficiency might not be sufficient. In addition, as discussed above, the sensitivity of our depression-assessing instrument might vary according to the methods of administration and possibly patient features. For confirming the diagnosis of depression, a psychiatrist evaluation and criteria fulfillment would be needed, but such service could be time-consuming and not readily available anytime. There are opinions suggesting that the utilization of depression screening tests may assist in earlier detection and potentially outcome improvement (37). Therefore, we used the widely applicable GDS to screen for depression in our patients. Our study is cross-sectional in nature, so a causal relationship cannot be ascertained between frailty and depression in these patients. There are theories and investigations showing that depression may also increase the risk of frailty (38), suggesting that a bi-directional relationship potentially exists between frailty and depression. Nonetheless, we could not derive such conclusion based on our results. Finally, our patients with ESRD were of Asian ethnicity and received chronic hemodialysis only, like in our prior experimental and clinical work (39, 40), and extrapolation of our findings to those of other ethnicities or under chronic peritoneal dialysis would not be feasible. Broader inclusion criteria and the involvement of a cohort follow-up design would better answer these questions.

CONCLUSION

We prospectively included a cohort of patients with ESRD under chronic hemodialysis and documented their baseline status of depression, using a validated instrument, along with an extensive array of interfering variables. After adjustment, we discovered that the presence of frailty was independently associated with a higher risk of exhibiting depression, while a greater frail severity correlated with an increased risk as well. Although a definitive conclusion cannot be obtained based on the current findings, we believe that the link between frailty and depression truly exists among patients with ESRD, and that strategies aiming to attenuate frailty may be able to benefit those with depression simultaneously.

ETHICS STATEMENT

The studies involving human participants were reviewed and approved by the Institutional Review Board of the National Taiwan University Hospital (No. 201910100RINA). The patients/participants provided their written informed consent to participate in this study.

AUTHOR CONTRIBUTIONS

C-TC and J-WH: study design. S-YL, C-TC, and J-WH: data analysis. C-YC, SY-L, C-TC, and J-WH: article drafting. All authors approved the final version of the manuscript.

FUNDING

The study was financially sponsored by National Taiwan University Hospital Yunlin Branch (NTUHYL 110.N004) and Ministry of Science and Technology, Taiwan (MOST 109-2314-B-002-193-MY3 and MOST 108-2314-B-002-062-MY3). The sponsors have no role in the study design, data collection, analysis, and result interpretation of this study.

ACKNOWLEDGMENTS

We are grateful to the Second Core Laboratory, Department of Medical Research of National Taiwan University Hospital and the Genomic Research Center of National Taiwan University College of Medicine for their technical input.

REFERENCES

1. GBD 2019 Diseases and injuries Collaborators. Global burden of 369 diseases and. injuries in 204 countries and territories, 1990-2019: a systematic analysis for the Global Burden of Disease Study 2019. *Lancet*. (2020) 396:1204–22. doi: 10.1016/S0140-6736(20)30925-9
2. Palmer S, Vecchio M, Craig JC, Tonelli M, Johnson DW, Nicolucci A. Prevalence of depression in chronic kidney disease: systematic review and meta-analysis of observational studies. *Kidney Int.* (2013) 84:179–91. doi: 10.1038/ki.2013.77
3. Ozieh MN, Garacci E, Walker RJ, Palatnik A, Egede LE. The cumulative impact of social determinants of health factors on mortality in adults

with diabetes and chronic kidney disease. *BMC Nephrol.* (2021) 22:76. doi: 10.1186/s12882-021-02277-2
4. Kurita N, Wakita T, Fujimoto S, Yanagi M, Koitabashi K, Suzuki T. Hopelessness and depression predict sarcopenia in advanced CKD and dialysis: a multicenter cohort study. *J Nutr Health Aging.* (2021) 25:593–9. doi: 10.1007/s12603-020-1556-4
5. Brown EA, Zhao J, McCullough K, Fuller DS, Figueiredo AE, Bieber B, et al. Burden of kidney disease, health-related quality of life, and employment among patients receiving peritoneal dialysis and in-center hemodialysis: findings from the DOPPS program. *Am J Kidney Dis*. (2021) 78:489–500.e1. doi: 10.1053/j.ajkd.2021.02.327
6. Park S, Lee S, Kim Y, Lee Y, Kang MW, Kim K. Causal effects of positive affect, life satisfaction, depressive symptoms, and neuroticism on kidney function: a mendelian randomization study. *J Am Soc Nephrol.* (2021) 32:1484–96. doi: 10.1681/ASN.2020071086
7. Zhang Z, He P, Liu M, Zhou C, Liu C, Li H. Association of depressive symptoms with rapid kidney function decline in adults with normal kidney function. *Clin J Am Soc Nephrol.* (2021) 16:889–97. doi: 10.2215/CJN.18441120
8. Chaplin AB, Daniels NF, Ples D, Anderson RZ, Gregory-Jones A, Jones PB. Longitudinal association between cardiovascular risk factors and depression in young people: a systematic review and meta-analysis of cohort studies. *Psychol Med.* (2021) 1–11. doi: 10.1017/S0033291721002488
9. Maier A, Riedel-Heller SG, Pabst A, Luppa M. Risk factors and protective factors of depression in older people 65+. *A systematic review PLoS ONE.* (2021) 16:e0251326. doi: 10.1371/journal.pone.0251326
10. Duan D, Yang L, Zhang M, Song X, Ren W. Depression and associated factors in chinese patients with chronic kidney disease without dialysis: a cross-sectional study. *Front Public Health.* (2021) 9:605651. doi: 10.3389/fpubh.2021.605651
11. Elkheir HK, Wagaella AS, Badi S, Khalil A, Elzubair TH, Khalil A. Prevalence and risk factors of depressive symptoms among dialysis patients with end-stage renal disease (ESRD) in Khartoum, Sudan: a cross-sectional study. *J Family Med Prim Care.* (2020) 9:3639–43. doi: 10.4103/jfmpc.jfmpc_1229_19
12. Kooman JP, Kotanko P, Schols AM, Shiels PG, Stenvinkel P. Chronic kidney disease and premature ageing. *Nat Rev Nephrol.* (2014) 10:732–42. doi: 10.1038/nrneph.2014.185
13. Hayajneh AA, Hammouri H, Rababa M, Al-Rawashedeh S, Wallace DC, Alsatari ES. frailty and its correlates in cognitively intact community-dwelling older adults. *Dement Geriatr Cogn Disord*. (2021) 50:357–63. doi: 10.1159/000519054
14. Wu PY, Chao CT, Chan DC, Huang JW, Hung KY. Contributors, risk associates, and complications of frailty in patients with chronic kidney disease: a scoping review. *Ther Adv Chronic Dis.* (2019) 10:2040622319880382. doi: 10.1177/2040622319880382
15. Chao CT, Han DS, Huang JW. Circulating microRNA-125b levels are associated with the risk of vascular calcification in healthy community-dwelling older adults. *Front Cardiovasc Med.* (2021) 8:624313. doi: 10.3389/fcvm.2021.624313
16. Chen SI, Chiang CL, Chao CT, Chiang CK, Huang JW. Gustatory dysfunction is closely associated with frailty in patients with chronic kidney disease. *J Ren Nutr.* (2021) 31:49–56. doi: 10.1053/j.jrn.2020.06.006
17. Sung CC, Liao MT, Chao CT. Independent determinants of appetite impairment among patients with stage 3 or higher chronic kidney disease: a prospective study. *Nutrients.* (2021) 13:2863. doi: 10.3390/nu13082863
18. Chao CT, Hsu YH, Chang PY, He YT, Ueng RS, Lai CF. Simple self-report FRAIL scale might be more closely associated with dialysis complications than other frailty screening instruments in rural chronic dialysis patients. *Nephrology.* (2015) 20:321–8. doi: 10.1111/nep.12401
19. Chao CT, Wang J, Chien KL. Both pre-frailty and frailty increase healthcare utilization and adverse health outcomes in patients with type 2 diabetes mellitus. *Cardiovasc Diabetol.* (2018) 17:130. doi: 10.1186/s12933-018-0772-2
20. Dennis M, Kadri A, Coffey J. Depression in older people in the general hospital: a systematic review of screening instruments. *Age Ageing.* (2012) 41:148–54. doi: 10.1093/ageing/afr169
21. Kondo K, Antick JR, Ayers CK, Kansagara D, Chopra P. Depression screening tools for patients with kidney failure: a systematic review. *Clin J Am Soc Nephrol.* (2020) 15:1785–95. doi: 10.2215/CJN.05540420
22. Krishnamoorthy Y, Rajaa S, Rehman T. Diagnostic accuracy of various forms of geriatric depression scale for screening of depression among older adults: systematic review and meta-analysis. *Arch Gerontol Geriatr.* (2020) 87:104002. doi: 10.1016/j.archger.2019.104002
23. Balsamo M, Cataldi F, Carlucci L, Padulo C, Fairfield B. Assessment of late-life depression via self-report measures: a review. *Clin Interv Aging.* (2018) 13:2021–44. doi: 10.2147/CIA.S114100
24. Pickard S. Health, illness and frailty in old age: a phenomenological exploration. *J Aging Stud.* (2018) 47:24–31. doi: 10.1016/j.jaging.2018.10.002
25. Muscat P, Weinman J, Farrugia E, Callus R, Chilcot J. Illness perceptions predict distress in patients with chronic kidney disease. *BMC Psychol.* (2021) 9:75. doi: 10.1186/s40359-021-00572-z
26. Chrzastek Z, Guligowska A, Soltysik B, Pigłowska M, Borowiak E, Kostka J. Association of lower nutritional status and education level with the severity of depression symptoms in older adults-a cross sectional survey. *Nutrients.* (2021) 13:515. doi: 10.3390/nu13020515
27. Marcos-Pérez D, Sánchez-Flores M, Proietti S, Bonassi S, Costa S, Teixeira JP. Association of inflammatory mediators with frailty status in older adults: results from a systematic review and meta-analysis. *Geroscience.* (2020) 42:1451–73. doi: 10.1007/s11357-020-00247-4
28. Tolkien K, Bradburn S, Murgatroyd C. An anti-inflammatory diet as a potential intervention for depressive disorders: a systematic review and meta-analysis. *Clin Nutr.* (2019) 38:2045–52. doi: 10.1016/j.clnu.2018.11.007
29. Chao CT, Lin SH. Uremic toxins and frailty in patients with chronic kidney disease: a molecular insight. *Int J Mol Sci.* (2021) 22:6270. doi: 10.3390/ijms22126270
30. Dent E, Kowal P, Hoogendijk EO. Frailty measurement in research and clinical practice: a review. *Eur J Intern Med.* (2016) 31:3–10. doi: 10.1016/j.ejim.2016.03.007
31. Henry L, Halpin L, Barnett SD, Pritchard G, Sarin E, Speir AM. Frailty in the cardiac surgical patient: comparison of frailty tools and associated outcomes. *Ann Thorac Surg.* (2019) 108:16–22. doi: 10.1016/j.athoracsur.2019.03.009
32. Dingwall KM, Sweet M, Cass A, Hughes JT, Kavanagh D, Howard K. Effectiveness of wellbeing intervention for chronic kidney disease (WICKD): results of a randomised controlled trial. *BMC Nephrol.* (2021) 22:136. doi: 10.1186/s12882-021-02344-8
33. Ferreira TL, Ribeiro HS, Ribeiro ALA, Bonini-Rocha AC, Lucena JMS, de Oliveira PA, et al. Exercise interventions improve depression and anxiety in chronic kidney disease patients: a systematic review and meta-analysis. *Int Urol Nephrol.* (2021) 53:925–33. doi: 10.1007/s11255-020-02612-w
34. Chu SWF, Yeam CT, Low LL, Tay WY, Foo WYM, Seng JJB. The role of mind-body interventions in pre-dialysis chronic kidney disease and dialysis patients - a systematic review of literature. *Complement Ther Med.* (2021) 57:102652. doi: 10.1016/j.ctim.2020.102652
35. Gregg LP, Hedayati SS. Pharmacologic and psychological interventions for depression treatment in patients with kidney disease. *Curr Opin Nephrol Hypertens.* (2020) 29:457–64. doi: 10.1097/MNH.0000000000000629
36. Lorenz EC, Kennedy CC, Rule AD, LeBrasseur NK, Kirkland JL, Hickson LJ. Frailty in CKD and transplantation. *Kidney Int Rep*. (2021) 6:2270–80. doi: 10.1016/j.ekir.2021.05.025
37. Costantini L, Costanza A, Odone A, Aguglia A, Escelsior A, Serafini G. A breakthrough in research on depression screening: from validation to efficacy studies. *Acta Biomed.* (2021) 92:e2021215. doi: 10.23750/abm.v92i3.11574
38. Soysal P, Veronese N, Thompson T, Kahl KG, Fernandes BS, Prina AM. Relationship between depression and frailty in older adults: a systematic review and meta-analysis. *Ageing Res Rev*. (2017) 36:78–87. doi: 10.1016/j.arr.2017.03.005
39. Chao CT, Wang J, Huang JW, Chan DC, Chien KL. Frailty predicts an increased risk of end-stage renal disease with risk competition by mortality among 165,461 diabetic kidney disease patients. *Aging Dis.* (2019) 10:1270–81. doi: 10.14336/AD.2019.0216

40. Chao CT, Yeh HY, Tsia YT, Chiang CK, Chen HWA. combined microRNA and target protein-based panel for predicting the probability and severity of uraemic vascular calcification: a translational study. *Cardiovasc Res.* (2021) 117:1958–73. doi: 10.1093/cvr/cvaa255

Conflict of Interest: The authors declare that the research was conducted in the absence of any commercial or financial relationships that could be construed as a potential conflict ofinterest.

Publisher's Note: All claims expressed in this article are solely those of the authors and do not necessarily represent those of their affiliated organizations, or those of the publisher, the editors and the reviewers. Any product that may be evaluated in this article, or claim that may be made by its manufacturer, is not guaranteed or endorsed by the publisher.

frontiers in Medicine

REVIEW
published: 21 March 2022
doi: 10.3389/fmed.2022.816656

Mesenchymal Stem Cell-Derived Exosomes: Toward Cell-Free Therapeutic Strategies in Chronic Kidney Disease

*Qinghua Cao, Chunling Huang, Xin-Ming Chen and Carol A. Pollock**

Renal Medicine, Kolling Institute of Medical Research, Sydney Medical School, University of Sydney, Royal North Shore Hospital, St Leonards, NSW, Australia

Chronic kidney disease (CKD) is rising in global prevalence and has become a worldwide public health problem, with adverse outcomes of kidney failure, cardiovascular disease, and premature death. However, current treatments are limited to slowing rather than reversing disease progression or restoring functional nephrons. Hence, innovative strategies aimed at kidney tissue recovery hold promise for CKD therapy. Mesenchymal stem cells (MSCs) are commonly used for regenerative therapy due to their potential for proliferation, differentiation, and immunomodulation. Accumulating evidence suggests that the therapeutic effects of MSCs are largely mediated by paracrine secretion of extracellular vesicles (EVs), predominantly exosomes. MSC-derived exosomes (MSC-Exos) replicate the functions of their originator MSCs via delivery of various genetic and protein cargos to target cells. More recently, MSC-Exos have also been utilized as natural carriers for targeted drug delivery. Therapeutics can be effectively incorporated into exosomes and then delivered to diseased tissue. Thus, MSC-Exos have emerged as a promising cell-free therapy in CKD. In this paper, we describe the characteristics of MSC-Exos and summarize their therapeutic efficacy in preclinical animal models of CKD. We also discuss the potential challenges and strategies in the use of MSC-Exos-based therapies for CKD in the future.

Keywords: exosome, chronic kidney disease, mesenchymal stem cells, therapy, new advances, regeneration

OPEN ACCESS

Edited by:
Maik Gollasch, Charité Universitätsmedizin Berlin, Germany

Reviewed by:
Mario Ollero, INSERM U955 Institut Mondor de Recherche Biomédicale (IMRB), France
Teresa Rampino, San Matteo Hospital Foundation (IRCCS), Italy

***Correspondence:**
Carol A. Pollock
carol.pollock@sydney.edu.au

Specialty section:
This article was submitted to Nephrology, a section of the journal Frontiers in Medicine

Received: *17 November 2021*
Accepted: *24 February 2022*
Published: *21 March 2022*

Citation:
Cao Q, Huang C, Chen X-M and Pollock CA (2022) Mesenchymal Stem Cell-Derived Exosomes: Toward Cell-Free Therapeutic Strategies in Chronic Kidney Disease. Front. Med. 9:816656. doi: 10.3389/fmed.2022.816656

INTRODUCTION

Chronic kidney disease (CKD) is a widespread public health problem, with adverse outcomes of kidney failure, cardiovascular disease, and premature death. CKD is more common than is widely known, affecting approximately 10% of the population worldwide (1). Although the causes of CKD may vary, diabetes and hypertension are still the leading causes (1). Irrespective of the multifactorial etiologies of the initial renal injury, progressive renal fibrosis is common to all forms of CKD (2). Although there have been recent advances in therapeutic strategies for CKD, a significant treatment gap remains. Despite targeted control of diabetes, blood pressure, hyperlipidemia and proteinuria, a large proportion of patients with CKD develop end stage kidney disease (ESKD). Kidney transplantation and dialysis are the only options for the management of ESKD, which results in a significant personal and societal burden (3). Hence innovative therapeutic strategies are urgently needed.

With potent self-renewal capabilities and great potential for differentiation and proliferation, stem cell (SC) therapy has emerged as an option for the preservation of renal function and structural repair in kidney diseases (4). Mounting evidence suggests that SCs exert therapeutic effects mostly by differentiation into tissue-specific cells to replace damaged tissue (5, 6). Amongst different types of SCs, the application of mesenchymal stem cells (MSCs) in treating kidney diseases is widely studied and has been shown to be advantageous over the application of other SCs (7). MSCs are multipotent SCs that differentiate into cells of mesenchymal cell lineages and exert important functions in tissue regeneration and repair by virtue of their wide differentiation capacity as well as anti-inflammatory and immunosuppressive properties (8–10). They can be obtained from virtually any type of tissue (tissue-derived MSCs) including bone marrow (BM), umbilical cord (UC), adipose tissue, dental pulp, amniotic fluid, placenta, Wharton's jelly (WJ), and organs including kidney, liver, spleen, pancreas, brain, lung, and thymus (11–15). MSCs can also be acquired from cells such as induced pluripotent stem cells (iPSCs)(16). Pluripotent stem cells (PSCs) are cells characterized by the capacity to self-renew and to differentiate into one of the three primary germ cell layers of the early embryo and therefore into specialized cell types (17). There are two types of PSC: embryonic stem cells (ESCs) and iPSCs (18). In 2007, it was reported by Shinya Yamanaka that induced PSCs (iPSCs) could be derived from reprogrammed adult human cells by introducing only a few genes (19). This discovery revolutionized the understanding of cell development and Shinya Yamanaka was thus awarded the Nobel Prize in Physiology or Medicine 2012.

To define MSCs with different origins, minimal criteria required include plastic adherence in standard culture conditions, expression of cluster of differentiation (CD) 105, CD73, and CD90, lack of expression of CD45, CD34, CD14 or CD11b, CD79a or CD19, and human leukocyte antigen-DR isotype (HLA-DR) surface molecules, and differentiation into osteoblasts, adipocytes, and chondroblasts *in vitro* (20). As immunoprivileged cells, MSCs rapidly home to injured kidneys and act through paracrine pathways to promote repair (21). They are reported to prevent and/or reverse kidney fibrosis and improve renal function in both experimental models and human patients (22, 23).

However, there are disadvantages in using cell based MSC therapy. These include the difficulty in maintaining a consistent source of cells with a stable phenotype (24) and in delivering large cells intravenously associated with a hazard of pulmonary microvasculature entrapment (25). Furthermore, MSCs have a risk of tumor formation through vascularization, immune regulation, and facilitating tumor interstitial remodeling (26). These disadvantages have restricted their clinical use. Thus, alternative MSC-based and complication-free therapeutic strategies are needed.

Numerous lines of evidence have supported that the therapeutic potential of MSCs is mediated by the secretion of soluble paracrine factors-extracellular vesicles (EVs) including apoptotic bodies (1–5 mm), microvesicles (MVs, 0.1–1 μm), and exosomes (30–150 nm)(27–29). Both MVs and apoptotic bodies are formed by direct budding from the plasma membrane. However, exosomes are produced after the fusion of multivesicular bodies (MVB), which are endocytic organelles containing many luminal vesicles, with the plasma membrane and are characterized by surface expression of CD9, CD63, and CD81 (30, 31). Very recent preclinical studies have identified exosomes as a dominant player in the MSC-mediated repair process of injured tissues (**Figure 1**). MSC-derived exosomes (MSC-Exos) coordinate intercellular communication and tissue repair through transfer of proteins, RNA, DNA and lipids between cells, which is likely to constitute a novel mode of intercellular communication (32, 33). In this review, we will summarize recent advances regarding the therapeutic application of MSC-Exos in preclinical studies in various experimental CKD models including diabetic kidney disease (DKD), hypertensive CKD and kidney fibrosis, aiming to provide novel insights to the treatment of CKD.

Abbreviations: AD-MSCs, adipose-derived mesenchymal stem cells; AD-MSC-Exos, AD-MSC-derived exosomes; AKI: acute kidney injury; AsFFF, asymmetrical field-flow fractionation; α-SMA, α-smooth muscle actin; Bax, Bcl-2-associated X protein; Bcl-2, B-cell lymphoma-2; BM, bone marrow; BM-MSC, bone marrow-derived mesenchymal stem cell; BM-MSC-Exos, BM-MSC-derived exosomes; BMP-7, bone morphogenetic protein-7; b-TRCP, E3 ubiquitin ligase-transducin repeats-containing protein; BUN, blood urea nitrogen; CD, cluster of differentiation; CNS, central nervous system; CK1d, casein kinase 1d; CKD, chronic kidney disease; COL-1, collagen-1; COL-4, collagen-4; DKD, diabetic kidney disease; EGF, epidermal growth factor; EMMPRIN, extracellular matrix metalloproteinase inducer; EMT, epithelial-mesenchymal transition; EPC, endothelial progenitor cells; ESC, embryonic stem cells; ESKD, end stage kidney disease; ET-1, endothelin-1; EV, extracellular vesicles; FGF, fibroblast growth factor; FN, fibronectin; GDNF, glial-derived neurotrophic factor; GF, growth factor; GFB, glomerular filtration barrier; GMCs, glomerular mesangial cells; HDAC1, histone deacetylase 1; HGF, hepatocyte growth factor; HLA-DR, human leukocyte antigen-DR isotype; HSP, heat-shock proteins; IL-6, interleukin-6; iPSC, induced pluripotent stem cells; iPSC-MSC-Exos, iPSC-MSC-derived Exosomes; IRI, ischemia-reperfusion injury; LN, lupus nephritis; MCP-1, monocyte chemoattracting protein-1; MDA, malondialdehyde; MMF, mycophenolate mofetil; MiRNAs, microRNAs; MMP-9, metalloproteinase-9; MSC, mesenchymal stem cells; MSC-Exos, MSC-derived exosomes; MSCT, MSC transplantation; mTOR, mammalian target of rapamycin; MVB, multivesicular bodies; PAI-1, plasminogen activating inhibitor-1; P-eNOS, phosphorylated endothelial nitric oxide synthase; PSC, pluripotent stem cells; RAAS, renin-angiotensin-aldosterone system; ROS, reactive oxygen species; SBP, systolic blood pressure; SC, stem cell; Scr, serum creatinine; SMC, smooth muscle cell; SEC, size exclusion chromatography; SiRNA, short interfering-RNA; Sirt6, sirtuin 6; SLE, systemic lupus erythematosus; Sox9, SRY-box transcription factor 9; SRY, sex-determining region Y; TECs, tubular epithelial cells; TEM, transmission electron microscopy; TFF, tangential flow filtration; TGF-β: transforming growth factor-beta; TSG101, tumor susceptibility gene 101; UC, umbilical cord; USC, urine-derived stem cell; UC-MSC, umbilical cord-derived mesenchymal stem cell; UC-MSC-Exos, UC-MSC-derived exosomes; UUO, unilateral ureteral obstruction; VEGF, vascular endothelial growth factor; WJ, Wharton's jelly; WJ-MSC, WJ-derived MSC; YAP, yes associated protein; 2K-1C, 2 kidney, 1 clip; 3-MA, 3-methyladenine.

EXOSOMES

Isolation, Identification, and Characterization of Natural Exosomes

Exosomes are small heterogeneous phospholipid-bilayer EVs that can be secreted by almost all type of cells via invagination of the late endosomal membrane (34). Generally, exosomes can now be isolated from conditioned cell culture media or

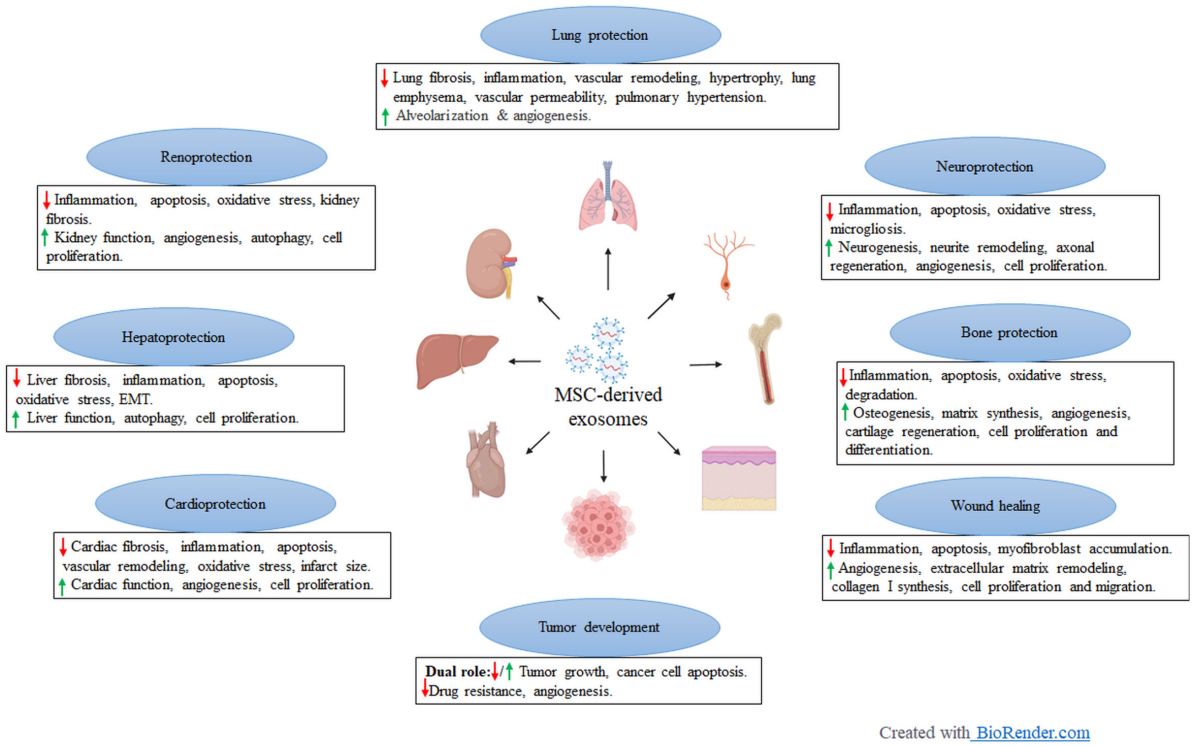

FIGURE 1 | Preclinical application of mesenchymal stem cell-derived exosomes in different disease models. Created with BioRender.com.

body fluids by differential ultracentrifugation, precipitation, size exclusion chromatography (SEC), filtration, immunoaffinity capture, commercial kits, or microfluidic technologies (35). Each approach has its advantages and disadvantages and there is lack of consensus on a gold standard of isolation. After purification, transmission electron microscopy (TEM) can be used for exosome validation (35). Exosomes contain a wide variety of cytoplasmic or membrane proteins (receptors, enzymes, transcription factors, and ECM components), nucleic acids (mitochondrial DNA, single-stranded DNA, double-stranded DNA, mRNA, and non-coding RNA) and lipids (36, 37). Of note, most exosomes have an evolutionarily conserved set of proteins including tetraspanins (CD81, CD63, and CD9), heat-shock proteins (HSP60, HSP70, and HSP90), ALIX and tumor susceptibility gene 101 (TSG101), which are used as biomarkers to identify exosomes (34).

Naturally, exosomes exhibit the characteristics of their parental cells. Thus, exosomes have been regarded as mini version of the originator cells (34). Emerging evidence has suggested that exosomes are biologically active vesicles regulating physiological and pathological pathways through delivery of functional cargos of proteins, nucleic acids and lipids (34). The cargos of exosomes vary according to the identity and physiological condition of the source cells and the extracellular environment and can be selectively taken up by neighboring or distant cells after the fusion of exosomes to the plasma membrane of recipient cells (38). Once internalized, exosomes fuse with the endosome membrane, followed by the horizontal transfer of their content to the cytoplasm of target cells and modification of their biological activities (39).

Engineered Exosomes for Drug Delivery

Recently, natural exosomes have also been engineered as drug carriers to specifically deliver a variety of bioactive molecules, such as short interfering-RNA (siRNA), antagomirs, recombinant proteins, and anti-inflammatory drugs due to their low toxicity, long-term stability, nanoscale size, cargo loading capacity, editable surface and tissue homing capability (40) (**Figure 2**). The simplest way for cargo loading is to incubate desired cargos with exosome-secreting cells or exosomes to allow diffusion of cargos into exosomes via a concentration gradient (41). Some other strategies include transfection, through which specific plasmids are transduced into cells to ectopically express desired biomolecules in exosomes. In addition to physical treatments (sonication, electroporation, extrusion, freeze-thaw, surfactant treatment and dialysis), *in situ* synthesis have also been applied to generate reconstituted exosomes (42). It is now recognized that natural exosomes spread via free diffusion and are then randomly internalized into recipient cells (43). To achieve specific targeted delivery of reconstituted exosomes, methodologies based on ligand-receptor binding, pH gradient/surface charge, and magnetism have been applied (44).

Compared with synthetic drug carriers, exosomes have several advantages. They can be obtained from patients' tissues or body fluids with excellent host bio-distribution and biocompatibility,

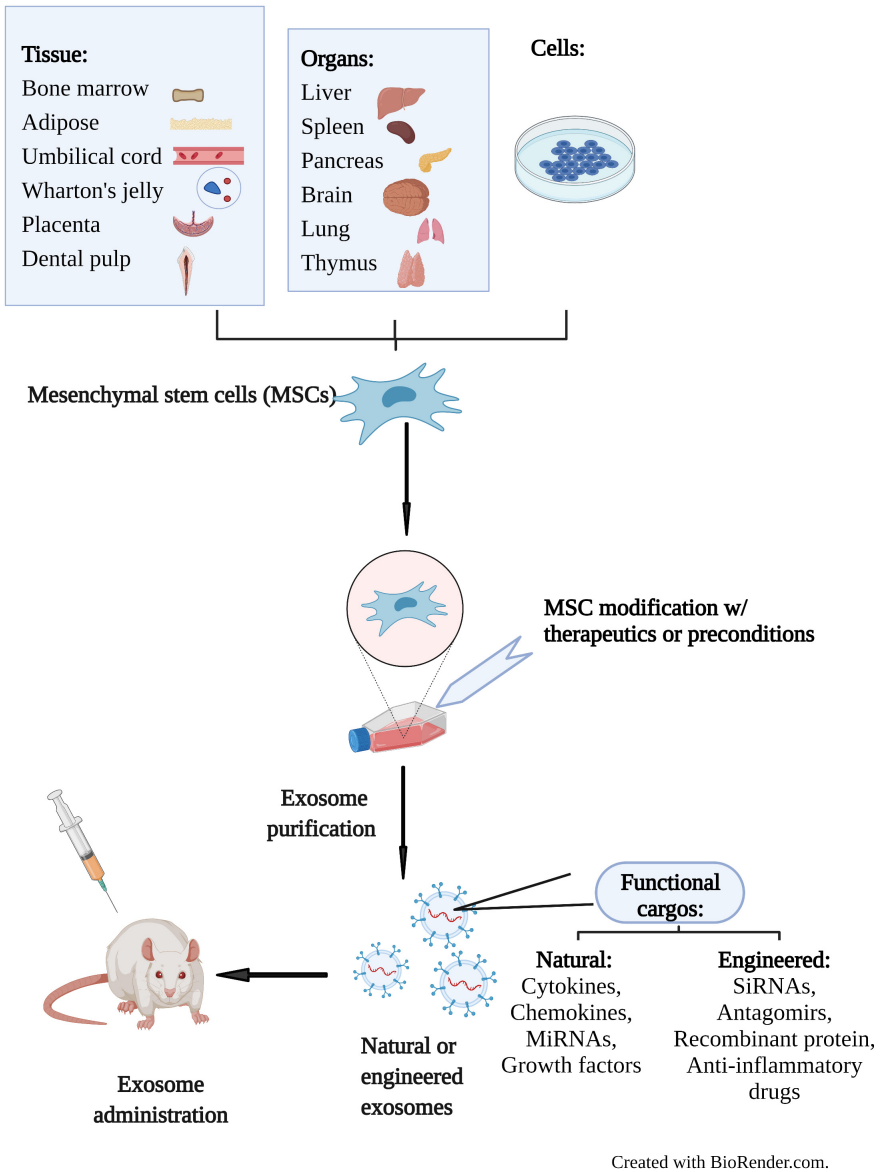

FIGURE 2 | Schematic diagram of therapeutic application of MSC-Exos in preclinical studies. MSCs can be isolated from various sources including tissues, organs, and cells. Exosomes secreted by MSCs can be engineered at the cellular or exosomal level. Natural MSC-Exos exhibit the characteristics of their parental cells through transfer of cargos such as cytokines, chemokines, miRNAs and growth factors. Engineered exosomes can also deliver bioactive siRNAs, antagomirs, recombinant proteins and anti-inflammatory drugs specifically. Administration of MSC-Exos to animal models are used to investigate their therapeutic potential in preclinical studies. Created with BioRender.com.

which minimize clearance rate and toxicity (45). For long-distance cell to cell communication, exosomes can also enter the blood and pass through additional biological barriers such as blood-brain barrier to achieve delivery throughout the body (46). Additionally, exosomes can be administrated via different routes (intranasally, intravenously, intraperitoneally, and intracranially), confirming exosome-based drug delivery is highly flexible (40).

Collectively, the utilization of exosomes in therapy has more benefits than their counterpart whole cells. MSCs have shown regenerative potential in the attenuation of kidney injury. Likewise, MSC-Exos represent attractive strategies for the treatment of various kidney diseases including CKD.

BIOCHEMISTRY AND FUNCTIONS OF MSC-EXOS

Mesenchymal stem cell-derived exosomes not only have the advantages of exosomes, but also replicate the biological characteristics of MSCs through transfer of functional cargos, mainly microRNAs (miRNAs) and proteins. MiRNAs are short

non-coding RNAs that regulate various physiological cellular processes such as cell death, differentiation, proliferation, metabolism, and pathophysiology of many diseases via regulation of target genes (47, 48). To date, more than 150 miRNAs and over 900 proteins have been identified in cargos of MSC-Exos (49, 50), resulting in the alteration of a variety of activities in target cells via different pathways. The tissue-repairing activities of MSC-Exos involve promoting cell proliferation, dedifferentiation and angiogenesis, whilst simultaneously dampening apoptosis and oxidative stress (51, 52). MiRNA cargos such as miRNA-10a, miRNA-486 were regarded as pro-regenerative miRNAs due to their capability to promote cell proliferation (53, 54) while miRNA-199a-3p was found to downregulate apoptosis-related genes and thereby suppress apoptosis (55, 56). Protein cargos like extracellular matrix metalloproteinase inducer (EMMPRIN) and metalloproteinase-9 (MMP-9) have been reported to stimulate angiogenesis (57, 58). Furthermore, MSC-Exos mitigate inflammatory responses by minimizing infiltration of immune cells such as macrophages, T cells, and NK cells (51). For instance, miRNA-155 (59), miRNA-146a (60), some cytokines such as interleukin-6 (IL-6), IL-10, and growth factor (GFs) hepatocyte growth factor (HGF), contribute to MSC-Exos-mediated immunoregulation (61). Nevertheless, exosomes of different MSC origins contain different biomolecules and thus exhibit heterogeneous characteristics (62, 63).

A comparative proteomic-based analysis through mass spectrometry on the secretome of MSCs revealed that BM-derived MSC (BM-MSCs), adipose-derived MSCs (AD-MSCs), and UC-derived MSC (UC-MSCs) differed in their secretion of anti-oxidative stress or anti-apoptosis molecules involved in central nervous system (CNS) injury (62). Another study by Hoang et al identified differential release of GFs responsible for wound healing by MSC-Exos from BM, adipose and UC (64). Notably, BM-MSC-derived exosomes (BM-MSC-Exos) was superior in inducing primary dermal fibroblasts (64). BM-MSC-Exos have enhanced regeneration capacity by virtue of induction of angiogenesis; AD-MSC-derived exosomes (AD-MSC-Exos) function as major immunomodulators and UC-MSC-derived exosomes (UC-MSC-Exos) mostly participate in tissue repair (63, 65). In spite of the heterogeneity, growing evidence demonstrate that MSC-Exos offer a novel cell-free therapeutic opportunity, as an alternative to MSCs, for treatment of various pathological conditions including neurological disorders, liver or lung damage and acute or chronic kidney injury (50, 66).

THERAPEUTIC POTENTIAL OF MSC-EXOS FOR CKD

Mesenchymal stem cells have exhibited promising efficacy in alleviating kidney injury in experimental CKD (67, 68). MSC-Exos possess repair functions similar to MSCs and have been widely used in CKD particularly DKD and kidney fibrosis to overcome the limitations of MSCs. Although the functions of MSC-Exos may vary depending on the cellular source of MSCs, they are in general therapeutic. Among all preclinical studies, heterogenous experiment settings including different doses and schedules, various routes of administration (tail infusion, organ perfusion, or the direct application in the kidney) and distinct CKD animal models were applied.

MSC-Exos for DKD

Diabetic kidney disease, a microvascular complication of diabetes mellitus (DM), is the most common form of CKD, and is likely to increase in epidemic proportions globally (69). Diabetic patients with kidney disease have a greater mortality risk than those without kidney disease. With the prevalence of DM in the global adult population expected to increase from 8.8% in 2015 to 10.4% in 2040, the impact of DKD is expected to be an increasingly prominent global health issue (69). In DKD, microalbuminuria is an early, although not invariable, clinical manifestation and portends an increased risk for progressive kidney damage. Hyperglycemia activates various inflammatory pathways through direct mechanisms to induce reactive oxygen species, oxidative stress, renin-angiotensin-aldosterone system (RAAS) activation, profibrotic cytokines, including transforming growth factor-beta (TGF-β), and advanced glycation end-products (70). This leads collectively to apoptosis, podocyte and tubular damage and associated albuminuria. The increased matrix protein production and decreased protein degradation leads to deposition of ECM proteins, including collagens and fibronectin (FN) in the glomerular mesangium and tubulointerstitium, resulting in progressive fibrosis (70, 71). To investigate the therapeutic effects of MSC-Exos in DKD, STZ-DKD *in vivo* model (mice or rats) and *in vitro* high glucose (HG)-treated cell lines of podocyte, tubular epithelial cells (TECs) and glomerular endothelial cells were commonly used. The efficacy of MSC-Exos in treating rodent DKD is summarized in **Table 1**.

Involvement of MSC-Exos From Tissues in DKD

The various cargos including GFs and therapeutic miRNAs delivered by MSC-Exos exert significant effects on restoring renal function, enhancing autophagy, attenuating podocyte injury and mitigating kidney fibrosis. MSCs originate from a wide range of sources and were first discovered from BM (72). In the study by Nagaishi et al., exosomes derived from BM-MSCs were delivered to the subcapsular region of the kidney in STZ-induced diabetic rats *in vivo* (73). These exosomes ameliorated kidney injury, inflammatory cell infiltration and TGF-β production as well as maintained the expression of tight junction protein-1 (ZO-1). Consistently, BM-MSC-Exos also suppressed apoptosis and degeneration of primary TECs from STZ-induced diabetic rats *in vitro* (73). UC, a conduit between the placenta and the developing embryo, is another popular source of MSCs due to the easy, safe and non-invasive way of collection, low immunogenicity, and high paracrine potential (74). *In vitro*, UC-MSC-Exos dramatically downregulated HG-induced pro-inflammatory cytokines including TGF-β, IL-6, IL-1β, and TNF-α in both renal TEC cell lines (NRK-52E, HK2) and human renal glomerular endothelial cell line (hrGECs) via their horizontal transfer of large amounts of GFs including epidermal growth factor (EGF), fibroblast growth factor (FGF), HGF and vascular endothelial growth factor (VEGF) (75).

TABLE 1 | Summary of therapeutic effects of MSC-Exos from various sources in preclinical models of DKD.

MSC Source	Model	Dose	Administration	Effects	Mechanism of action	References
Rat bone marrow	*In vivo*: STZ-induced DKD	Single: 5.3×10^7	Renal subcapsular	↓Renal tubule expansion, vacuolation, tubular atrophy ↓Degeneration	↓ TGF- β ZO-1 was maintained ↓Inflammatory cell infiltration	(71)
	In vitro: primary TECs	Not stated	Co-culture	↓Degeneration ↓Apoptosis		
Rat bone marrow	STZ-induced DKD	100μg/kg once per day × 4 weeks	Intravenous (Tail vein)	↑Autophagy: ↑ LC3-II/LC-I, p62, Beclin-1 ↓ BUN, Scr, Glu, proteinuria at 10 and 12 weeks ↓ Fibrosis	↓ mTOR, S6K1, p62 ↓ Collagen, FN ↓TGF-β	(77)
Mouse adipose	*In vivo*: spontaneous diabetes	Single: not stated, 12-week therapy	Intravenous (Tail vein)	↓BUN, creatinine, proteinuria ↑ Autophagy ↓ Podocyte apoptosis	↑miR-486, ↓Smad1/mTOR activation ↓Cleaved caspase 3	(79)
	In vitro: HG- treated MPC5	25 μg/ml for 48 h	Co-culture	↑Cell viability ↓Apoptosis		
Mouse adipose	*In vitro*: HG- treated MPC5	Not stated	Co-culture	↓Podocyte EMT ↑miR-215-5p, -879-5p, -3066-5p, -7a-5p	↓ ZEB2 transcription	(85)
Adipose	*In vivo*: STZ-induced DKD	50 μg twice weekly × 3	Intravenous (Caudal vein)	↓Glu, Scr, UACR, kidney/body weight ↓Mesangial hyperplasia ↓Kidney fibrosis	Delivery of miR-125a ↓HDAC1, ET-1	(88)
	IN vitro: HG-treated rat GMC	Not stated	Co-culture	↓ IL-6, Col-I and FN ↑Bcl-2 and Bax		
Human umbilical cord	*In vitro*: HG-treated HK2, NRK-52E and hrGECs	25, 50, and 100 μg/ml for 24 h	Co-culture	↓TGF-β, IL-6, IL-1β, and TNF-α	Secretion of EGF, FGF, HGF, and VEGF	(73)
Human urine	*In vivo*: STZ-induced DKD	Multiple: 100 μg weekly × 12	Intravenous (Tail vein)	↓Urine volume, albuminuria ↓Apoptosis of podocyte and tubular cells ↑Glomerular endothelial cell proliferation ↑ Angiogenesis	↓Caspase-3 Delivery of VEGF, TGF-β 1, angiogenin, BMP-7	(89)
	In vitro: HG- treated immortalized human podocytes	5, 10, and 50 μg/ml for 72 h	Co-culture	↓Podocyte apoptosis		
Human urine	*In vivo*: STZ-induced DKD	100 μg once weekly × 12	Intravenous (Tail vein)	↓Glu, KW, BUN, Scr, Ucr ↓Podocyte injury ↓Apoptosis	↓VEGFA, MCP-1, TGF-β1 and TNF-α. ↓ Bax and Caspase-3	(90)
	In vitro: HG- treated human podocytes		Co-culture	↑Cell viability ↓Apoptosis		

AD-MSCs, adipose-derived mesenchymal stem cells; Bax, Bcl-2-associated X protein; Bcl-2, B-cell lymphoma 2; BMP-7, bone morphogenetic protein-7; BUN, blood urea nitrogen; CK1d, casein kinase 1d; COL-1, collagen-1; DKD, diabetic kidney disease; EMT, epithelial-mesenchymal transition; ET-1, endothelin-1; FGF, fibroblast growth factors; FN, fibronectin; Glu, blood glucose; GMC, glomerular mesangial cell; GSH, glutathione; HDAC1, histone deacetylase 1; HG, high glucose; HGF, hepatocyte growth factor; IL-6, interleukin-6; LC3, microtubule-associated protein light chain 3; miR, microRNA; KW, kidney weight; MCP-1, monocyte chemoattractant protein-1; MSC, mesenchymal stem cells; mTOR, mammalian target of rapamycin; ROS, reactive oxygen species; S6K1, ribosomal protein S6 kinase beta-1; Scr, serum creatinine; STZ, streptozotocin; TGF-β, transforming growth factor-β; TECs, tubular epithelial cells; TGF-βR1, transforming growth factor-β type 1 receptor; TNF-α, tumor necrosis factor-α; Ucr, urine creatinine; VEGF, vascular endothelial growth factor; ZO-1, tight junction protein 1; 2K-1C, 2 kidneys, 1 clip model.

Autophagy is an intracellular lysosome-dependent degradative process, which maintains cellular homeostasis and integrity through removing damaged macromolecules and organelles (76). Additionally, autophagy is critical to provide energy and molecular building blocks by recycling macromolecules in response to nutrient and environmental stress (77). Impairment of autophagy in renal cells in patients with DM contributes to the progression of DKD via mammalian target of rapamycin (mTOR) pathway activation (78). Studies have proven that MSC-Exos can effectively restore autophagy activity by decreasing mTOR. Rats administered BM-MSC-Exos revealed significantly enhanced autophagy markers microtubule-associated protein light chain 3 (LC3)-II/LC3-I and p62 protein expression compared to the animals with DKD (79). Consistently, fibrotic markers including TGF-β and FN were also inhibited, suggesting a potent anti-fibrotic effect of MSC-Exos. The protective impact of MSC-Exos can be blocked by autophagy inhibitors including 3-methyladenine (3-MA) and chloroquine in rats, confirming the involvement of autophagy in the MSC-Exos mediated renoprotection (79).

Adipose-derived stem cells are also MSCs obtained from adipose tissue (80). Unlike BM-MSCs, AD-MSCs can be obtained by a minimally invasive procedure and thus are also promising for tissue regeneration. AD-MSC-Exos enhanced autophagy and reduced podocyte apoptosis, leading to attenuated DKD as evidenced by reduced levels of urine protein, serum creatinine (Scr) and blood urea nitrogen (BUN) in mice. Consistently, AD-MSC-Exos reversed autophagy downregulation and suppressed podocyte apoptosis *in vitro* (81).

MiRNAs as Major Bioactive Cargos of MSC-Exos

MicroRNAs have been found to be packed and protected from proteases and RNAses in EVs (82, 83) and are the most abundant content in human plasma derived exosomal RNAs (84). Investigations on mechanisms by which MSC-Exos elicit their renoprotection verify that apart from proteins such as various GFs, certain miRNAs are the main contents of exosomes contributing to their regenerative potential (32). In HG-stimulated podocyte *in vitro*, miRNA-486 from AD-MSC-Exos inhibited Smad1 and mTOR activation, leading to increased autophagy and reduced podocyte apoptosis (81). These beneficial effects can be neutralized in the presence of miRNA-486 inhibitor, further supporting that AD-MSC-Exos promoted survival of podocytes through miRNA-dependent mechanisms.

In most CKD, the breakdown of the glomerular filtration barrier (GFB) manifests as proteinuria and is subsequently associated with loss of normal kidney function (85). Podocytes, which are specialized visceral epithelial cells, are an independent component of the GFB. They plays an essential role in maintaining the integrity of GFB (85). HG induces epithelial-mesenchymal transition (EMT) and may initiate podocyte injury, resulting in GFB destruction (86). Jin et al found that AD-MSC-Exos administration mitigated HG-induced podocyte EMT due to the restoration of miRNAs including miRNA-215-5p, miRNA-879-5p, miRNA-3066-5p, and miRNA-7a-5p (87). As miRNA-215-5p mimics abrogated HG-induced EMT in podocytes and miRNA-215-5p inhibitors counteracted the protective effect of the AD-MSC-Exos, miRNA-251-5p is regarded as a main player facilitating protection of AD-MSC-Exos on podocyte damage (87). Histone deacetylase 1 (HDAC1)/endothelin-1 (ET-1) axis upregulation was observed in DKD rats and HG-stimulated glomerular mesangial cells (GMCs). High ET-1'expression induces insulin resistance and increases glomerular permeability, thereby promoting the progression of DKD (88, 89). A recent study suggested AD-MSC-Exos alleviated DKD through delivering miRNA-125a, which targeted the HDAC1/ET1 axis directly to block inflammation and fibrosis (90).

Involvement of Exosomes From Urine-Derived Stem Cells in DKD

Urine-derived stem cells (USCs) display classical features of MSCs. Importantly, they can be isolated from urine with a cheap and non-invasive procedure, whereas most adult SCs require invasive procedures (91). Moreover, USCs can differentiate into renal cells, therefore representing huge benefits for application in the treatment of kidney diseases (92, 93). Intravenous injections of USCs-derived exosomes (USC-Exos) alleviated albuminuria in diabetic rats through inhibiting podocytic apoptosis and increasing glomerular endothelial cell proliferation and mesangial angiogenesis in the early stage of DKD (94). The horizontal transfer of podocyte survival factor (bone morphogenetic protein-7, BMP-7) and proangiogenic factors (VEGF, TGF-β, and angiogenin) from USCs-Exos to resident cells mediated nephroprotection by USC-Exos (94). Another study on USC-Exos showed that USC-Exos delivered miRNA-16-5p to the injured kidney and mitigated renal functional impairment (decreased BUN, Scr, and Ucr) in the STZ-DKD rat model (95). The mechanism of renoprotection was attributed to the downregulation of VEGFA, monocyte chemoattracting protein-1 (MCP-1), TGF-β1, TNF-α, and apoptosis-associated protein including B-cell lymphoma-2 (Bcl-2), Bcl-2-associated X protein (Bax) and Caspase-3. *In vitro*, USC-Exos enriched with miRNA-16-5p also led to inhibition of VEGF and offered protection against HG-induced podocyte apoptosis (95).

MSC-Exos for Hypertensive CKD

Hypertension, a complex multifactorial disease, is also one of the leading causes of CKD due to the deleterious effects of increased blood pressure (BP) on the kidney. Chronic hypertension leads to changes in the systemic and renal macro and microvasculature, resulting in loss of renal auto-regulation, increased glomerular capillary pressure and hyperfiltration-mediated tubular injury (96). Hyperfiltration contributes to glomerular proteinuria, which promotes the release of inflammatory cytokines and GFs by GMCs and TECs (97). In addition, hypertension induces vascular stretch, endothelial dysfunction and the consequent activation of the intra-renal renin-angiotensin system (RAS), which amplifies the release of cytokines and GFs, recruitment of inflammatory cells, increased ECM production and finally progressive glomerular and tubulointerstitial fibrosis (98). Patients with diabetes commonly have hypertension due to chronic hyperglycemia-induced dysfunction of the vasculature (99).

Studies investigating the use of MSC-Exos as therapeutic agents in hypertension-associated CKD are scant. Aliotta et al found that exosomes isolated from both human and murine MSCs were effective in reversing pulmonary hypertension in a mouse model. The beneficial effects may be mediated by cargos of anti-inflammatory and anti-proliferative miRNAs (miRNAs-34a, -122, -124, and -127) that dampen angiogenesis, blunt neoplastic cell proliferation and elicit senescence of vascular smooth muscle cells (SMCs) and endothelial progenitor cells (EPCs) (100). Lindoso et al reported that multiple injections of EVs isolated from adipose-MSCs protected the kidney from hypertensive damage by downregulating the pro-inflammatory molecules MCP-1 and plasminogen activating inhibitor-1 (PAI-1) and reducing macrophage recruitment to the kidney in a hypertensive rat model. Furthermore, the miRNA-200-TGF-β axis was found to be significantly altered after EV administration, thereby reprogramming EMT signaling and preventing renal inflammation and fibrosis (101).

MSC-Exos for Kidney Fibrosis

Kidney fibrosis, and in particular tubulointerstitial fibrosis, is the final common outcome of nearly all forms of progressive CKD (2). The histopathology of tubulointerstitial fibrosis is characterized by the deposition of ECM in the interstitium associated with inflammatory cell infiltration, tubular cell damage, fibroblast activation and expansion and rarefaction of the peritubular microvasculature (2). Many studies have established TGF-β as a major profibrotic factor through various mechanisms (102). Once renal fibrosis supervenes, progressive functional decline occurs, which relentlessly progresses leading to dialysis or renal transplantation.

In recent years, apart from diabetic and hypertensive CKD models, several other rodent models of CKD such as unilateral ureteral obstruction (UUO), ischemia-reperfusion injury (IRI) and 2 kidney, 1 clip (2K-1C) unilateral renal artery stenosis model have also been utilized to assess the anti-fibrotic efficacy of MSC-Exos (**Table 2**). UUO induces severe renal injury, characterized by reduced renal blood flow and glomerular filtration rate within 24 h, followed by interstitial inflammation (peak at 2–3 days), tubular dilation, tubular atrophy and fibrosis within a week. It develops interstitial infiltration of macrophages, tubular cell death, the phenotypic transition of resident renal cells and severe interstitial renal fibrosis with excessive ECM accumulation (103). Renal IRI is one of the leading causes of acute kidney injury (AKI), which temporarily suspends the oxygen and nutrient supply to kidney, inducing robust cellular and molecular responses primarily in TECs. After IRI, the acutely damaged kidney experiences a transition from an unresolved self-healing process to maladaptive repair, resulting in incomplete recovery and progression to kidney fibrosis (104, 105). In the 2K-1C model, one renal artery is constricted to chronically reduce renal perfusion, leading to renal hypertension, hypoxia, activation of RAAS and irreversible renal impairment (106, 107).

Natural MSC-Exos

It is now well recognized that the alleviation of the inciting cause of fibrosis alone is not sufficient to restore kidney function as functional nephron tissue is damaged or lost after kidney injury (108, 109). Consequently, MSC-Exos with potential for kidney regeneration might represent an innovative strategy for kidney fibrosis alleviation. Although MSCs have been proven to be derived from virtually all tissues' adventitial progenitor cells and pericytes, UC-derived MSCs are considered one of the major MSCs sources for clinical and research applications (74). During the prenatal phase, the UC is genetically and physiologically part of the fetus and usually contains two arteries and one vein. These blood vessels are enveloped by mucous connective tissue WJ, which is derived from the extraembryonic mesoderm and exerts a protective function (13). Both UC and WJ are considered as promising sites for MSC collection (13, 74).

A notable mechanism of kidney fibrosis is injury-induced oxidative stress, which is caused by over-production of reactive oxygen species (ROS) that exceed its scavenging capacity (110). Excessive ROS repress the antioxidant enzymes and results in breakdown of cells through lipid peroxidation, DNA fragmentation and protein damage. In addition, ROS can promote the progression of renal interstitial fibrosis by regulating the infiltration of inflammatory cells such as monocytes and macrophages (111). UUO-induced renal damage is associated with oxidative stress-induced renal tubular apoptosis (112). UC-MSC-Exos administered after UUO alleviated kidney fibrosis and restored renal function (decreased BUN and Scr) through inhibition of apoptosis, malondialdehyde (MDA), ROS, and ROS-mediated P38MAPK/ERK signaling pathways. *In vitro*, similar anti-fibrotic effects were also observed in TGF-β1 treated NRK-52E cells (113). Another study investigating the anti-fibrotic effects of UC-MSC-Exos confirmed the involvement of Hippo and yes associated protein (YAP) signaling, which regulates TGF-β-Smad signaling, podocyte mesenchymal-epithelial trans-differentiation and ECM protein synthesis (114). Once the Hippo pathway is activated, it limits tissue growth and cell proliferation through the degradation of YAP. UC-MSC-Exos deliver two major ubiquitination related enzyme casein kinase 1d (CK1d) and E3 ubiquitin ligase-transducin repeats-containing protein (b-TRCP) to trigger ubiquitination and degradation of YAP in TECs. This reduced ECM deposition and attenuated fibrosis associated with UUO. Knockdown of CK1d and b-TRCP abrogated the repairing effects of UC-MSC-Exos on renal fibrosis, implying that the efficacy of UC-MSC-Exos relies on the transportation of these active proteins (114).

Sex-determining region Y-box transcription factor 9 (Sox-9) is a transcription factor of the sex-determining region Y (SRY) box family and may repair injured kidney (115). AD-MSCs-Exos upregulated Sox9 and prevented TGF-β1-induced transformation of TECs into a pro-fibrotic phenotype *in vitro*. Moreover, AD-MSC-EVs were capable of attenuating kidney fibrosis through improving kidney hypoxia, reducing inflammatory cell infiltration and inflammatory cytokine secretion, and inhibiting the TGF-β1/Smad 3 signaling pathway in mice subjected to unilateral IRI (116). IRI also occurs in donation after circulatory death (DCD) kidneys. To evaluate the renoprotective effect of MSC-EVs on isolated DCD kidney, MSC-EVs were applied as part of the hypothermic machine

TABLE 2 | Summary of anti-fibrotic effects of MSC-Exos from various sources in preclinical models of kidney fibrosis.

MSC Source	Model	Dose	Administration	Effects	Mechanism of action	References
Human umbilical cord	*In vivo*: UUO	Single: 200μg	Left renal artery	↑Renal function (↓Scr, BUN) ↓Tubular injury ↓ Tubulointerstitial fibrosis ↓ Apoptosis ↑proliferation ↓Oxidative stress	↓ ROS-mediated p38 MAPK/ERK signaling pathway ↓Bax, cleaved caspase-3 ↓ROS, MDA ↑ anti-oxidants: GSH	(111)
	In vitro: NRK52E incubated with TGF-β	Not stated	Co-incubation with isolated exosome	↓ Apoptosis ↑Proliferation ↓Oxidative stress		
Human bone marrow	*In vivo*: UUO	Single: released from 1×10^6 MSCs	Intravenous	Exosomes home to injured kidneys ↓Fibrosis	Delivery of miR-let7c ↓Collagen, MMP-9, α-SMA, TGF-βR1	(117)
	In vitro: NRK52E incubated with TGF-β	Not stated	Co-incubation with isolated exosome	↓Fibrosis		
Human bone Marrow (Transfected with anti-let-7i-5p)	*In vivo*: UUO	Single: 1 mg/kg	Intravenous	↑Renal function (↓BUN, ↓Scr, ↓Ucr, ↑eGFR) ↓ Fibrosis	↓Let-7i-5p ↓Collagen, FN, α-SMA, ↑TSC1 ↓Phosphorylation of mTORC1, p70S6K and 4E-BP1	(118)
	In vitro: NRK52E incubated with TGF-β	Not stated	MSC on Transwell with NRK52E grown on the lower chamber	↓TGF-β1-induced fibrogenic responses ↓EMT		
Human umbilical cord	*In vivo*: UUO	Single: 200 μg	Intravenous	↓Tubulointerstitial fibrosis	Exosomes delivered CK1 1δ and β-TRCP to degrade YAP	(112)
Adipose (Transfected with GDNF)	*In vivo*: UUO	Single: 200 μg	Caudal vein	↓ PTC rarefaction ↓ Tubulointerstitial fibrosis ↑ Endothelial function, angiogenesis	↑SIRT1/p-eNOS ↓α-SMA ↑ VEGF, ↓ HIF-1α	(121)
	In vitro: HUVEC against H/SD	Single: 100 μg/ml	Co-incubation with isolated exosome	↓ HUVEC injury ↓Apoptosis ↑Endothelial angiogenesis		
Adipose	*In vivo*: IRI	Single: 100 μg	Caudal vein	↑ Tubular proliferation, regeneration ↓ Interstitial fibrosis ↓Inflammation	↑Sox9 ↓α-SMA, PDGFR- β	(114)
	In vitro: primary TECs stimulated with TGF-β	Not stated	Co-incubation with isolated exosome	↓ TGF- β1-induced transformation of TECs to pro-fibrotic phenotype		

(Continued)

TABLE 2 | (Continued)

MSC Source	Model	Dose	Administration	Effects	Mechanism of action	References
Adipose	2K-1C Unilateral renal artery stenosis	Single: 100 μg	Caudal vein	↓HIF-1α Stabilised systolic blood pressure ↑ Natriuresis ↓ Fibrosis ↓ Inflammation	↓Collagen, TGF- β ↑ IL-10	(115)
Pluripotent stem cell	*In vivo*: UUO	Single: 10^{11} particles/ml	Tail vein	↓ Fibrosis ↓ Inflammation	↑SIRT6 ↓β-catenin	(126)
	In vitro: NRK-52E	$10^6/10^7/10^8$ particles/ml	Co-incubation with isolated exosome	↓Col-1, α-SMA ↑E-cadherin		

AD-MSCs, adipose-derived mesenchymal stem cells; Bax, Bcl-2-associated X protein; Bcl-2, B-cell lymphoma-2; BMP-7, bone morphogenetic protein-7; BUN, blood urea nitrogen; CK1d, casein kinase 1d; COL-1, collagen-1; DKD, diabetic kidney disease; EMT, epithelial-mesenchymal transition; ET-1, endothelin-1; FGF, fibroblast growth factors; FN, fibronectin; GDNF, glial-derived neurotrophic factor; GMC, glomerular mesangial cell; GSH, glutathione; HDAC1, histone deacetylase 1; HG, high glucose; HGF, hepatocyte growth factor; H/SD, hypoxia/serum deprivation; HUVECs, human umbilical vein endothelial cells; IL-6, interleukin-6; IRI, ischemia/reperfusion injury; LC3, microtubule-associated protein light chain 3; miR, microRNA; KW, kidney weight; MCP-1, monocyte chemoattractant protein-1; MDA, malondialdehyde; MSC, mesenchymal stem cells; mTOR, mammalian target of rapamycin; mTORC1, mammalian target of rapamycin complex 1; PDGFR-β, platelet derived growth factor receptor beta; ROS, reactive oxygen species; S6K1, ribosomal protein S6 kinase beta-1; Scr, serum creatinine; SIRT1, sirtuin-1; Sox9, SRY-box transcription factor 9; STZ, streptozotocin; TECs, tubular epithelial cells; TGF-β, transforming growth factor-β; TGF-βR1, transforming growth factor-β type 1 receptor; TNF-α, tumor necrosis factor-α; Ucr, urine creatinine; VEGF, vascular endothelial growth factor; ZO-1, tight junction protein-1; 2K-1C, 2 kidneys, 1 clip model; YAP, Yes-associated protein; UUO, unilateral ureteral obstruction.

perfusion (HMP) procedure in a rat DCD model. The addition of MSC-EVs during HMP attenuated the ischemic kidney injury through maintaining the enzymatic machinery critical for cell survival and reduced the reperfusion damage to kidney (117). Beneficial properties of AD-MSC-Exos were also reported in the 2K-1C (118), a renal artery stenosis model. Administration of AD-MSC-Exos were demonstrated to stabilize the systolic blood pressure (SBP), downregulate hypoxia marker HIF-1a and reduce profibrotic gene collogen and TGF-β expression, thus mitigating kidney fibrosis (118). Interestingly, the treatments with AD-MSC-Exos, AD-MSC or AD-MSC-EVs were equally effective in reducing the expression of the fibrotic markers collagen-1 (COL-1) and TGF-β. However, AD-MSCs were the most effective in elevating the expression of the anti-inflammatory IL-10. These difference may be ascribed to the various cargos released and/or to the ability of the vesicles to reach the damaged tissue, which requires further investigation (118). WJ-derived MSCs (WJ-MSCs) are more immune-privileged and exhibit greater immunosuppressive properties compared to BM-MSCs or AD-MSCs. WJ-MSCs mitigated kidney fibrosis triggered by IRI through downregulating HGF versus TGF-β1 expression (119).

Engineered MSC-Exos

As mentioned earlier, aside from paracrine transferring their natural biological cargos, exosomes including MSC-Exos can also be engineered to carry different biomolecules to various therapeutic targets. The engineered exosomes have a higher therapeutic potential and efficacy and more specific targeting when compared with naive exosomes (40).

Numerous studies have validated that the anti-fibrotic effect of MSC-Exos can be mediated through the transfer of miRNAs such as miRNA-let7c, which targets fibrosis-associated genes. To deliver miRNA-let7c, Wang et al., utilized lentiviral transduction to construct the engineered human BM-MSCs overexpressing miRNA-let7c.The exosomes released from engineered MSC mediated the transfer of miRNA-let7 to diseased kidney and attenuated UUO-induced kidney fibrosis through repression of fibrotic gene collagen-4 (COL-4), MMP-9, alpha-smooth muscle actin (α-SMA), TGF-β1 and its receptor (120). In another study by Jin et al., exosome-secreting MSCs were transfected with let-7i-5p antagomir (anti-let-7i-5p), and then exosomes were isolated from the transfected MSCs to deliver anti-let-7i-5p oligonucleotides to inhibit the level of let-7i-5p. These engineered exosomes reduced the level of let-7i-5p via delivery of anti-let-7i-5p, reduced ECM deposition and attenuated EMT process in TGF-β1-stimulated NRK-52E cells and in the damaged kidneys of UUO mice, thereby attenuating kidney fibrosis (121). Glial-derived neurotrophic factor (GDNF), an effective neurotrophic factor that protects nigral dopaminergic neurons, promoted the therapeutic effect of MSCs (122, 123). Chen et al transfected GDNF into human AD-MSCs via lentiviral transfection and then exosomes (GDNF-AD-MSC-Exos) were collected from those engineered MSCs. Application of the GDNF-AD-MSC-Exos led to the amelioration of kidney fibrosis in mice with UUO, which was mediated by enhancing SIRT1 signaling and its downstream target, phosphorylated endothelial nitric oxide

synthase (p-eNOS), which activated endothelial function and angiogenesis and reduced peritubular capillary loss (124).

iPSC-Derived MSC-Exos for CKD

All MSC mentioned above are from tissues. Despite promising therapeutic effects, tissue-derived MSCs have been reported to have several weaknesses, such as limited potential to proliferate, difficult to standardize, loss of differentiation capacity, and decreased regenerative efficacy with expansion (125). As mentioned earlier, MSCs can also be produced from cells such as iPSCs. Those single cell-derived MSCs have the characteristics of both MSCs and PSCs and are capable of expanding with high efficiency (17). iPSC-MSCs revealed comparable effects in renoprotection, such as reducing apoptosis and enhancing vascularization (4). EVs directly isolated from iPSC rescued rats from IRI through maintaining functional mitochondria and inhibiting oxidative stress-relevant genes (126). Sirtuin 6 (Sirt6) is an NAD-dependent deacetylase of the Sirtuin family that has been suggested to effectively reverse the fibrotic process in many organs (127, 128). More recently, a study by Liu et al established that intravenous infusion of human iPSC-derived MSC-Exos (iPSC-MSC-Exos) mitigated kidney fibrosis, reduced inflammatory responses, and improved renal function in mice subjected to UUO (129). These anti-fibrotic effects of iPSC-MSC-Exos are mediated through increasing SIRT6 while decreasing β-catenin and its downstream products (PAI-1, Fsp1 and Axin2), elucidating a novel mechanism of MSC-Exos in nephroprotection (129).

MSC-Exos in Lupus Nephritis

Systemic lupus erythematosus (SLE) is a common autoimmune disease. It is characterized by multi-organ damage resulting from abnormal activation of autoreactive T cells, the presence of pathogenic autoantibodies and deposition of immune complexes (130). LN is the most common and severe organ injury in SLE (131). Over the past decades, there has been several publications investigating the therapeutic application of MSCs in LN in both animal models and humans. BM-MSCs alleviated LN and improved mice survival rate by effectively inhibiting IL-21 production and follicular helper T cell differentiation (132). The combination of MSCs with prednisone or mycophenolate mofetil (MMF) improved survival, reduced the secretion of autoantibody and inflammatory cytokines, and decreased the infiltration of inflammatory cells in the kidney in a mouse model of lupus nephritis (133). In LN patients, allogeneic MSC transplantation (MSCT) resulted in an increased glomerular filtration rate (GFR) and renal remission over 12 months, confirming its therapeutic potential for LN (134). It has been well established that MSC-Exos exert immunomodulatory effects through delivery of immunosuppressive molecules that inhibit infiltration, proliferation, differentiation and activation of immune cells or induce anti-inflammatory cells (135). Additionally, MSC-Exos promote the chemotaxis of anti-inflammatory non-coding RNAs to accelerate tissue healing (136). However, despite the efficacy and clinical potential for therapeutic application in inflammatory glomerular disease indicated by these studies, there are few publications applying MSC-Exos directly in LN animal models or in human patients. Recently, Wei et al reported that miR-20a-containing exosomes are responsible for the alleviation of LN in the mouse lupus model through enhancing autophagy (137). In another study by Chen et al., UC-MSC-Exos attenuated SLE-associated diffuse alveolar hemorrhage (DAH) by regulating macrophage polarization in murine lupus (138). In summary, further studies are warranted for a better understanding of the application of MSC-Exos-based therapy in LN and more generally in glomerular disease.

CONCLUSION

Chronic kidney disease is a world-wide pandemic, and its prevalence is rising annually. MSC-Exos transfer a variety of growth factors and non-coding miRNAs to injured renal cells, which attenuate kidney injury and restore kidney function through promoting proliferation, autophagy and angiogenesis, and suppressing inflammation, oxidative stress, apoptosis, EMT, and tubulointerstitial fibrosis. Thus, MSC-Exos represent a novel cell-free therapeutic strategy for the treatment of CKD.

Despite advances in understanding the therapeutic capacity of MSC-Exos in CKD, major issues surrounding large-scale production and purification must be overcome before translation of MSC-Exos therapy to clinical application occurs. The amount of MSC-Exos required for clinical application is high. Recently, new technologies such as 3D culture conditions using hydrogels, spheroid or hollow fibers and bioreactors have been introduced to allow large-scale production of exosomes (139). To optimize the procedures of isolation/purification of exosomes, new approaches such as tangential flow filtration (TFF) and asymmetrical field-flow fractionation (AsFFF) have been applied (140, 141). However, there is a lack of standard techniques to quickly isolate, purify, quantitate, and identify exosomes. Moreover, it still requires further investigation to fully understand the biodistribution and clearance of MSC-Exos upon administration. Biodistribution of systemically administered exosomes is a dynamic process. Although several *in vivo* tracking strategies have been employed, current knowledge of the biodistribution of MSC-Exos is limited.

To conclude, advances in MSC-Exos studies hold a great promise for the regenerative treatment of CKD. Future studies focusing on the standardization of MSC-Exos production, purification, and characterization to improve quality and safety will enable the translation of MSC-Exos into the clinic as efficient therapeutics for CKD.

AUTHOR CONTRIBUTIONS

QC conceived and wrote the manuscript. X-MC and CH reviewed the manuscript. CP revised and reviewed the manuscript. All authors have read and agreed to the published version of the manuscript.

REFERENCES

1. Webster AC, Nagler EV, Morton RL, Masson P. Chronic kidney disease. *Lancet.* (2017) 389:1238–52. doi: 10.1016/s0140-6736(16)32064-5
2. Duffield JS. Cellular and molecular mechanisms in kidney fibrosis. *J Clin Invest.* (2014) 124:2299–306. doi: 10.1172/JCI72267
3. Levin A, Tonelli M, Bonventre J, Coresh J, Donner JA, Fogo AB, et al. Global kidney health 2017 and beyond: a roadmap for closing gaps in care, research, and policy. *Lancet.* (2017) 390:1888–917. doi: 10.1016/s0140-6736(17)30788-2
4. Rota C, Morigi M, Imberti B. Stem cell therapies in kidney diseases: progress and challenges. *Int J Mol Sci.* (2019) 20:2790. doi: 10.3390/ijms20112790
5. Ilic D, Ogilvie C. Concise review: human embryonic stem cells—what have we done? What are we doing? Where are we going? *Stem Cells.* (2017) 35:17–25. doi: 10.1002/stem.2450
6. Zakrzewski W, Dobrzyński M, Szymonowicz M, Rybak Z. Stem cells: past, present, and future. *Stem Cell Res Ther.* (2019) 10:68. doi: 10.1186/s13287-019-1165-5
7. Uccelli A, Moretta L, Pistoia V. Mesenchymal stem cells in health and disease. *Nat Rev Immunol.* (2008) 8:726–36. doi: 10.1038/nri2395
8. Campagnoli C, Roberts IA, Kumar S, Bennett PR, Bellantuono I, Fisk NM. Identification of mesenchymal stem/progenitor cells in human first-trimester fetal blood, liver, and bone marrow. *Blood.* (2001) 98:2396–402. doi: 10.1182/blood.v98.8.2396
9. Liu S, Liu F, Zhou Y, Jin B, Sun Q, Guo S. Immunosuppressive property of MSCs mediated by cell surface receptors. *Front Immunol.* (2020) 11:1076. doi: 10.3389/fimmu.2020.01076
10. Jiang W, Xu J. Immune modulation by mesenchymal stem cells. *Cell Prolif.* (2020) 53:e12712. doi: 10.1111/cpr.12712
11. Zuk PA, Zhu M, Ashjian P, De Ugarte DA, Huang JI, Mizuno H, et al. Human adipose tissue is a source of multipotent stem cells. *Mol Biol Cell.* (2002) 13:4279–95. doi: 10.1091/mbc.e02-02-0105
12. Nemeth K, Mezey E. Bone marrow stromal cells as immunomodulators. A primer for dermatologists. *J Dermatol Sci.* (2015) 77:11–20. doi: 10.1016/j.jdermsci.2014.10.004
13. Troyer DL, Weiss ML. Concise review: Wharton's jelly-derived cells are a primitive stromal cell population. *Stem Cells.* (2008) 26:591–9. doi: 10.1634/stemcells.2007-0439
14. Hassan G, Kasem I, Soukkarieh C, Aljamali M. A simple method to isolate and expand human umbilical cord derived mesenchymal stem cells: using explant method and umbilical cord blood serum. *Int J Stem Cells.* (2017) 10:184–92. doi: 10.15283/ijsc17028
15. Nancarrow-Lei R, Mafi P, Mafi R, Khan W. A systemic review of adult mesenchymal stem cell sources and their multilineage differentiation potential relevant to musculoskeletal tissue repair and regeneration. *Curr Stem Cell Res Ther.* (2017) 12:601–10. doi: 10.2174/1574888x12666170608124303
16. Lian Q, Zhang Y, Zhang J, Zhang HK, Wu X, Zhang Y, et al. Functional mesenchymal stem cells derived from human induced pluripotent stem cells attenuate limb ischemia in mice. *Circulation.* (2010) 121:1113–23. doi: 10.1161/circulationaha.109.898312
17. Tabar V, Studer L. Pluripotent stem cells in regenerative medicine: challenges and recent progress. *Nat Rev Genet.* (2014) 15:82–92. doi: 10.1038/nrg3563
18. Romito A, Cobellis G. Pluripotent stem cells: current understanding and future directions. *Stem Cells Int.* (2016) 2016:9451492. doi: 10.1155/2016/9451492
19. Takahashi K, Tanabe K, Ohnuki M, Narita M, Ichisaka T, Tomoda K, et al. Induction of pluripotent stem cells from adult human fibroblasts by defined factors. *Cell.* (2007) 131:861–72. doi: 10.1016/j.cell.2007.11.019
20. Dominici M, Le Blanc K, Mueller I, Slaper-Cortenbach I, Marini F, Krause D, et al. Minimal criteria for defining multipotent mesenchymal stromal cells. The international society for cellular therapy position statement. *Cytotherapy.* (2006) 8:315–7. doi: 10.1080/14653240600855905
21. Spees JL, Lee RH, Gregory CA. Mechanisms of mesenchymal stem/stromal cell function. *Stem Cell Res Ther.* (2016) 7:125. doi: 10.1186/s13287-016-0363-7
22. Liu D, Cheng F, Pan S, Liu Z. Stem cells: a potential treatment option for kidney diseases. *Stem Cell Res Ther.* (2020) 11:249. doi: 10.1186/s13287-020-01751-2
23. Morigi M, Imberti B, Zoja C, Corna D, Tomasoni S, Abbate M, et al. Mesenchymal stem cells are renotropic, helping to repair the kidney and improve function in acute renal failure. *J Am Soc Nephrol.* (2004) 15:1794–804. doi: 10.1097/01.asn.0000128974.07460.34
24. Musial-Wysocka A, Kot M, Majka M. The pros and cons of mesenchymal stem cell-based therapies. *Cell Transpl.* (2019) 28:801–12. doi: 10.1177/0963689719837897
25. Mäkelä T, Takalo R, Arvola O, Haapanen H, Yannopoulos F, Blanco R, et al. Safety and biodistribution study of bone marrow-derived mesenchymal stromal cells and mononuclear cells and the impact of the administration route in an intact porcine model. *Cytotherapy.* (2015) 17:392–402. doi: 10.1016/j.jcyt.2014.12.004
26. Barkholt L, Flory E, Jekerle V, Lucas-Samuel S, Ahnert P, Bisset L, et al. Risk of tumorigenicity in mesenchymal stromal cell-based therapies–bridging scientific observations and regulatory viewpoints. *Cytotherapy.* (2013) 15:753–9. doi: 10.1016/j.jcyt.2013.03.005
27. Rani S, Ryan AE, Griffin MD, Ritter T. Mesenchymal stem cell-derived extracellular vesicles: toward cell-free therapeutic applications. *Mol Ther.* (2015) 23:812–23. doi: 10.1038/mt.2015.44
28. Xin H, Li Y, Chopp M. Exosomes/miRNAs as mediating cell-based therapy of stroke. *Front Cell Neurosci.* (2014) 8:377. doi: 10.3389/fncel.2014.00377
29. Park JH, Hwang I, Hwang SH, Han H, Ha H. Human umbilical cord blood-derived mesenchymal stem cells prevent diabetic renal injury through paracrine action. *Diabetes Res Clin Pract.* (2012) 98:465–73. doi: 10.1016/j.diabres.2012.09.034
30. Yáñez-Mó M, Siljander PR, Andreu Z, Zavec AB, Borràs FE, Buzas EI, et al. Biological properties of extracellular vesicles and their physiological functions. *J Extracell Vesicles.* (2015) 4:27066. doi: 10.3402/jev.v4.27066
31. Doyle LM, Wang MZ. Overview of extracellular vesicles, their origin, composition, purpose, and methods for exosome isolation and analysis. *Cells.* (2019) 8:727. doi: 10.3390/cells8070727
32. Wei W, Ao Q, Wang X, Cao Y, Liu Y, Zheng SG, et al. Mesenchymal stem cell-derived exosomes: a promising biological tool in nanomedicine. *Front Pharmacol.* (2021) 11:590470. doi: 10.3389/fphar.2020.590470
33. Phinney DG, Pittenger MF. Concise review: MSC-derived exosomes for cell-free therapy. *Stem Cells.* (2017) 35:851–8. doi: 10.1002/stem.2575
34. Zhang Y, Liu Y, Liu H, Tang WH. Exosomes: biogenesis, biologic function and clinical potential. *Cell Biosci.* (2019) 9:19. doi: 10.1186/s13578-019-0282-2
35. Sidhom K, Obi PO, Saleem A. A review of exosomal isolation methods: is size exclusion chromatography the best option? *Int J Mol Sci.* (2020) 21:6466. doi: 10.3390/ijms21186466
36. Simpson RJ, Lim JWE, Moritz RL, Mathivanan S. Exosomes: proteomic insights and diagnostic potential. *Expert Rev Proteomics.* (2009) 6:267–83. doi: 10.1586/epr.09.17
37. Valadi H, Ekström K, Bossios A, Sjöstrand M, Lee JJ, Lötvall JO. Exosome-mediated transfer of mRNAs and microRNAs is a novel mechanism of genetic exchange between cells. *Nat Cell Biol.* (2007) 9:654–9. doi: 10.1038/ncb1596
38. Kalluri R, LeBleu VS. The biology, function, and biomedical applications of exosomes. *Science.* (2020) 367:eaau6977. doi: 10.1126/science.aau6977
39. Tian T, Wang Y, Wang H, Zhu Z, Xiao Z. Visualizing of the cellular uptake and intracellular trafficking of exosomes by live-cell microscopy. *J Cell Biochem.* (2010) 111:488–96. doi: 10.1002/jcb.22733
40. Herrmann IK, Wood MJA, Fuhrmann G. Extracellular vesicles as a next-generation drug delivery platform. *Nat Nanotechnol.* (2021) 16:748–59. doi: 10.1038/s41565-021-00931-2
41. Oskouie MN, Aghili Moghaddam NS, Butler AE. Therapeutic use of curcumin-encapsulated and curcumin-primed exosomes. *J Cell Physiol.* (2019) 234:8182–91. doi: 10.1002/jcp.27615
42. Luan X, Sansanaphongpricha K, Myers I, Chen H, Yuan H, Sun D. Engineering exosomes as refined biological nanoplatforms for drug delivery. *Acta Pharmacol Sin.* (2017) 38:754–63. doi: 10.1038/aps.2017.12
43. Lai CP, Mardini O, Ericsson M, Prabhakar S, Maguire CA, Chen JW, et al. Dynamic biodistribution of extracellular vesicles in vivo using a multimodal imaging reporter. *ACS Nano.* (2014) 8:483–94. doi: 10.1021/nn404945r

44. Fu S, Wang Y, Xia X, Zheng JC. Exosome engineering: current progress in cargo loading and targeted delivery. *Nanoimpact.* (2020) 20:100261. doi: 10.1016/j.impact.2020.100261
45. Batrakova EV, Kim MS. Using exosomes, naturally-equipped nanocarriers, for drug delivery. *J Control Release.* (2015) 219:396–405. doi: 10.1016/j.jconrel.2015.07.030
46. Elliott RO, He M. Unlocking the power of exosomes for crossing biological barriers in drug delivery. *Pharmaceutics.* (2021) 13:122. doi: 10.3390/pharmaceutics13010122
47. Chua JH, Armugam A, Jeyaseelan K. MicroRNAs: biogenesis, function and applications. *Curr Opin Mol Ther.* (2009) 11:189–99.
48. Cao Q, Chen XM, Huang C, Pollock CA. MicroRNA as novel biomarkers and therapeutic targets in diabetic kidney disease: an update. *FASEB Bioadv.* (2019) 1:375–88. doi: 10.1096/fba.2018-00064
49. Chen TS, Lai RC, Lee MM, Choo AB, Lee CN, Lim SK. Mesenchymal stem cell secretes microparticles enriched in pre-microRNAs. *Nucleic Acids Res.* (2010) 38:215–24. doi: 10.1093/nar/gkp857
50. Cheng L, Zhang K, Wu S, Cui M, Xu T. Focus on mesenchymal stem cell-derived exosomes: opportunities and challenges in cell-free therapy. *Stem Cells Int.* (2017) 2017:6305295. doi: 10.1155/2017/6305295
51. Harrell CR, Jovicic N, Djonov V, Arsenijevic N, Volarevic V. Mesenchymal stem cell-derived exosomes and other extracellular vesicles as new remedies in the therapy of inflammatory diseases. *Cells.* (2019) 8:1605. doi: 10.3390/cells8121605
52. Harrell CR, Jovicic N, Djonov V, Volarevic V. Therapeutic use of mesenchymal stem cell-derived exosomes: from basic science to clinics. *Pharmaceutics.* (2020) 12:474. doi: 10.3390/pharmaceutics12050474
53. Tapparo M, Bruno S, Collino F, Togliatto G, Deregibus MC, Provero P, et al. Renal regenerative potential of extracellular vesicles derived from miRNA-engineered mesenchymal stromal cells. *Int J Mol Sci.* (2019) 20:2381. doi: 10.3390/ijms20102381
54. Luo L, Yu Z-P, Qin H, Zhu Z-X, Liao M-H, Liao H-T, et al. Exosomal microRNA-10a is associated with liver regeneration in rats through downregulation of EphA4. *Chin Med J (Engl).* (2018) 131:454–60. doi: 10.4103/0366-6999.225057
55. Zhang R, Qin L, Shi J. MicroRNA-199a-3p suppresses high glucose-induced apoptosis and inflammation by regulating the IKKβ/NF−κB signaling pathway in renal tubular epithelial cells. *Int J Mol Med.* (2020) 46:2161–71. doi: 10.3892/ijmm.2020.4751
56. Li Z, Zhou Y, Zhang L, Jia K, Wang S, Wang M, et al. microRNA-199a-3p inhibits hepatic apoptosis and hepatocarcinogenesis by targeting PDCD4. *Oncogenesis.* (2020) 9:95. doi: 10.1038/s41389-020-00282-y
57. Abu El-Asrar AM, Ahmad A, Alam K, Siddiquei MM, Mohammad G, Hertogh GD, et al. Extracellular matrix metalloproteinase inducer (EMMPRIN) is a potential biomarker of angiogenesis in proliferative diabetic retinopathy. *Acta Ophthalmol.* (2017) 95:697–704. doi: 10.1111/aos.13284
58. Bergers G, Brekken R, McMahon G, Vu TH, Itoh T, Tamaki K, et al. Matrix metalloproteinase-9 triggers the angiogenic switch during carcinogenesis. *Nat Cell Biol.* (2000) 2:737–44. doi: 10.1038/35036374
59. Pers Y-M, Bony C, Duroux-Richard I, Bernard L, Maumus M, Assou S, et al. miR-155 contributes to the immunoregulatory function of human mesenchymal stem cells. *Front Immunol.* (2021) 12:624024. doi: 10.3389/fimmu.2021.624024
60. Tavasolian F, Hosseini AZ, Soudi S, Naderi M. miRNA-146a improves immunomodulatory effects of MSC-derived exosomes in rheumatoid arthritis. *Curr Gene Ther.* (2020) 20:297–312. doi: 10.2174/1566523220666200916120708
61. Wu H, Fan H, Shou Z, Xu M, Chen Q, Ai C, et al. Extracellular vesicles containing miR-146a attenuate experimental colitis by targeting TRAF6 and IRAK1. *Int Immunopharmacol.* (2019) 68:204–12. doi: 10.1016/j.intimp.2018.12.043
62. Assunção-Silva RC, Mendes-Pinheiro B, Patrício P, Behie LA, Teixeira FG, Pinto L, et al. Exploiting the impact of the secretome of MSCs isolated from different tissue sources on neuronal differentiation and axonal growth. *Biochimie.* (2018) 155:83–91. doi: 10.1016/j.biochi.2018.07.026
63. Pires AO, Mendes-Pinheiro B, Teixeira FG, Anjo SI, Ribeiro-Samy S, Gomes ED, et al. Unveiling the differences of secretome of human bone marrow mesenchymal stem cells, adipose tissue-derived stem cells, and human umbilical cord perivascular cells: a proteomic analysis. *Stem Cells Dev.* (2016) 25:1073–83. doi: 10.1089/scd.2016.0048
64. Hoang DH, Nguyen TD, Nguyen H-P, Nguyen X-H, Do PTX, Dang VD, et al. Differential wound healing capacity of mesenchymal stem cell-derived exosomes originated from bone marrow, adipose tissue and umbilical cord under serum- and xeno-free condition. *Front Mol Biosci.* (2020) 7:119. doi: 10.3389/fmolb.2020.00119
65. Wang Z-G, He Z-Y, Liang S, Yang Q, Cheng P, Chen A-M. Comprehensive proteomic analysis of exosomes derived from human bone marrow, adipose tissue, and umbilical cord mesenchymal stem cells. *Stem Cell Res Ther.* (2020) 11:511. doi: 10.1186/s13287-020-02032-8
66. Nikfarjam S, Rezaie J, Zolbanin NM, Jafari R. Mesenchymal stem cell derived-exosomes: a modern approach in translational medicine. *J Transl Med.* (2020) 18:449. doi: 10.1186/s12967-020-02622-3
67. Gregorini M, Corradetti V, Rocca C, Pattonieri EF, Valsania T, Milanesi S, et al. Mesenchymal stromal cells prevent renal fibrosis in a rat model of unilateral ureteral obstruction by suppressing the renin-angiotensin system via HuR. *PLoS One.* (2016) 11:e0148542. doi: 10.1371/journal.pone.0148542
68. Gregorini M, Maccario R, Avanzini MA, Corradetti V, Moretta A, Libetta C, et al. Antineutrophil cytoplasmic antibody-associated renal vasculitis treated with autologous mesenchymal stromal cells: evaluation of the contribution of immune-mediated mechanisms. *Mayo Clin Proc.* (2013) 88:1174–9. doi: 10.1016/j.mayocp.2013.06.021
69. Gheith O, Farouk N, Nampoory N, Halim MA, Al-Otaibi T. Diabetic kidney disease: world wide difference of prevalence and risk factors. *J Nephropharmacol.* (2015) 5:49–56.
70. Reidy K, Kang HM, Hostetter T, Susztak K. Molecular mechanisms of diabetic kidney disease. *J Clin Invest.* (2014) 124:2333–40. doi: 10.1172/JCI72271
71. Badal SS, Danesh FR. New insights into molecular mechanisms of diabetic kidney disease. *Am J Kidney Dis.* (2014) 63(2 Suppl. 2):S63–83. doi: 10.1053/j.ajkd.2013.10.047
72. Friedenstein AJ, Chailakhjan RK, Lalykina KS. The development of fibroblast colonies in monolayer cultures of guinea-pig bone marrow and spleen cells. *Cell Tissue Kinet.* (1970) 3:393–403. doi: 10.1111/j.1365-2184.1970.tb00347.x
73. Nagaishi K, Mizue Y, Chikenji T, Otani M, Nakano M, Konari N, et al. Mesenchymal stem cell therapy ameliorates diabetic nephropathy via the paracrine effect of renal trophic factors including exosomes. *Sci Rep.* (2016) 6:34842. doi: 10.1038/srep34842
74. Arutyunyan I, Elchaninov A, Makarov A, Fatkhudinov T. Umbilical cord as prospective source for mesenchymal stem cell-based therapy. *Stem Cells Int.* (2016) 2016:6901286. doi: 10.1155/2016/6901286
75. Xiang E, Han B, Zhang Q, Rao W, Wang Z, Chang C, et al. Human umbilical cord-derived mesenchymal stem cells prevent the progression of early diabetic nephropathy through inhibiting inflammation and fibrosis. *Stem Cell Res Ther.* (2020) 11:336. doi: 10.1186/s13287-020-01852-y
76. Chun Y, Kim J. Autophagy: an essential degradation program for cellular homeostasis and life. *Cells.* (2018) 7:278. doi: 10.3390/cells7120278
77. Filomeni G, De Zio D, Cecconi F. Oxidative stress and autophagy: the clash between damage and metabolic needs. *Cell Death Differ.* (2015) 22:377–88. doi: 10.1038/cdd.2014.150
78. Yang D, Livingston MJ, Liu Z, Dong G, Zhang M, Chen J-K, et al. Autophagy in diabetic kidney disease: regulation, pathological role and therapeutic potential. *Cell Mol Life Sci.* (2018) 75:669–88. doi: 10.1007/s00018-017-2639-1
79. Ebrahim N, Ahmed IA, Hussien NI, Dessouky AA, Farid AS, Elshazly AM, et al. Mesenchymal stem cell-derived exosomes ameliorated diabetic nephropathy by autophagy induction through the mTOR signaling pathway. *Cells.* (2018) 7:226. doi: 10.3390/cells7120226
80. Gimble JM, Katz AJ, Bunnell BA. Adipose-derived stem cells for regenerative medicine. *Circ Res.* (2007) 100:1249–60. doi: 10.1161/01.RES.0000265074.83288.09
81. Jin J, Shi Y, Gong J, Zhao L, Li Y, He Q, et al. Exosome secreted from adipose-derived stem cells attenuates diabetic nephropathy by promoting autophagy flux and inhibiting apoptosis in podocyte. *Stem Cell Res Ther.* (2019) 10:95. doi: 10.1186/s13287-019-1177-1
82. Pomatto MAC, Bussolati B, D'Antico S, Ghiotto S, Tetta C, Brizzi MF, et al. Improved loading of plasma-derived extracellular vesicles to encapsulate

antitumor miRNAs. *Mol Ther Methods Clin Dev.* (2019) 13:133–44. doi: 10.1016/j.omtm.2019.01.001
83. Ridder K, Keller S, Dams M, Rupp AK, Schlaudraff J, Del Turco D, et al. Extracellular vesicle-mediated transfer of genetic information between the hematopoietic system and the brain in response to inflammation. *PLoS Biol.* (2014) 12:e1001874. doi: 10.1371/journal.pbio.1001874
84. Huang X, Yuan T, Tschannen M, Sun Z, Jacob H, Du M, et al. Characterization of human plasma-derived exosomal RNAs by deep sequencing. *BMC Genomics.* (2013) 14:319. doi: 10.1186/1471-2164-14-319
85. Daehn IS, Duffield JS. The glomerular filtration barrier: a structural target for novel kidney therapies. *Nat Rev Drug Discov.* (2021) 20:770–88. doi: 10.1038/s41573-021-00242-0
86. Loeffler I, Wolf G. Epithelial-to-mesenchymal transition in diabetic nephropathy: fact or fiction? *Cells.* (2015) 4:631–52. doi: 10.3390/cells4040631
87. Jin J, Wang Y, Zhao L, Zou W, Tan M, He Q. Exosomal miRNA-215-5p derived from adipose-derived stem cells attenuates epithelial-mesenchymal transition of podocytes by inhibiting ZEB2. *Biomed Res Int.* (2020) 2020:2685305. doi: 10.1155/2020/2685305
88. Kasztan M, Pollock David M. Impact of ET-1 and sex in glomerular hyperfiltration in humanized sickle cell mice. *Clin Sci.* (2019) 133:1475–86. doi: 10.1042/cs20190215
89. Ahlborg G, Lindström J. Insulin sensitivity and big ET-1 conversion to ET-1 after ETA- or ETB-receptor blockade in humans. *J Appl Physiol.* (2002) 93:2112–21. doi: 10.1152/japplphysiol.00477.2002
90. Hao Y, Miao J, Liu W, Cai K, Huang X, Peng L. Mesenchymal stem cell-derived exosomes carry microRNA-125a to protect against diabetic nephropathy by targeting histone deacetylase 1 and downregulating endothelin-1. *Diabetes Metab Syndr Obes.* (2021) 14:1405–18. doi: 10.2147/DMSO.S286191
91. Bento G, Shafigullina AK, Rizvanov AA, Sardao VA, Macedo MP, Oliveira PJ. Urine-derived stem cells: applications in regenerative and predictive medicine. *Cells.* (2020) 9:573. doi: 10.3390/cells9030573
92. Zhang C, George SK, Wu R, Thakker PU, Abolbashari M, Kim T-H, et al. Reno-protection of urine-derived stem cells in a chronic kidney disease rat model induced by renal ischemia and nephrotoxicity. *Int J Biol Sci.* (2020) 16:435–46. doi: 10.7150/ijbs.37550
93. Pavathuparambil Abdul Manaph N, Al-Hawwas M, Bobrovskaya L, Coates PT, Zhou X-F. Urine-derived cells for human cell therapy. *Stem Cell Res Ther.* (2018) 9:189. doi: 10.1186/s13287-018-0932-z
94. Jiang ZZ, Liu YM, Niu X, Yin JY, Hu B, Guo SC, et al. Exosomes secreted by human urine-derived stem cells could prevent kidney complications from type I diabetes in rats. *Stem Cell Res Ther.* (2016) 7:24. doi: 10.1186/s13287-016-0287-2
95. Duan YR, Chen BP, Chen F, Yang SX, Zhu CY, Ma YL, et al. Exosomal microRNA-16-5p from human urine-derived stem cells ameliorates diabetic nephropathy through protection of podocyte. *J Cell Mol Med.* (2021) 25:10798–813. doi: 10.1111/jcmm.14558
96. Griffin KA. Hypertensive kidney injury and the progression of chronic kidney disease. *Hypertension.* (2017) 70:687–94. doi: 10.1161/HYPERTENSIONAHA.117.08314
97. Chagnac A, Zingerman B, Rozen-Zvi B, Herman-Edelstein M. Consequences of glomerular hyperfiltration: the role of physical forces in the pathogenesis of chronic kidney disease in diabetes and obesity. *Nephron.* (2019) 143:38–42. doi: 10.1159/000499486
98. Lopez-Novoa JM, Martinez-Salgado C, Rodriguez-Pena AB, Lopez-Hernandez FJ. Common pathophysiological mechanisms of chronic kidney disease: therapeutic perspectives. *Pharmacol Ther.* (2010) 128:61–81. doi: 10.1016/j.pharmthera.2010.05.006
99. de Boer IH, Bangalore S, Benetos A, Davis AM, Michos ED, Muntner P, et al. Diabetes and hypertension: a position statement by the american diabetes association. *Diabetes Care.* (2017) 40:1273–84. doi: 10.2337/dci17-0026
100. Aliotta JM, Pereira M, Wen S, Dooner MS, Del Tatto M, Papa E, et al. Exosomes induce and reverse monocrotaline-induced pulmonary hypertension in mice. *Cardiovasc Res.* (2016) 110:319–30. doi: 10.1093/cvr/cvw054
101. Lindoso RS, Lopes JA, Binato R, Abdelhay E, Takiya CM, Miranda KR, et al. Adipose mesenchymal cells-derived EVs alleviate DOCA-salt-induced hypertension by promoting cardio-renal protection. *Mol Ther Methods Clin Dev.* (2020) 16:63–77. doi: 10.1016/j.omtm.2019.11.002
102. Meng XM, Nikolic-Paterson DJ, Lan HY. TGF-beta: the master regulator of fibrosis. *Nat Rev Nephrol.* (2016) 12:325–38. doi: 10.1038/nrneph.2016.48
103. Martínez-Klimova E, Aparicio-Trejo OE, Tapia E, Pedraza-Chaverri J. Unilateral ureteral obstruction as a model to investigate fibrosis-attenuating treatments. *Biomolecules.* (2019) 9:141. doi: 10.3390/biom9040141
104. Le Clef N, Verhulst A, D'Haese PC, Vervaet BA. Unilateral renal ischemia-reperfusion as a robust model for acute to chronic kidney injury in mice. *PLoS One.* (2016) 11:e0152153. doi: 10.1371/journal.pone.0152153
105. Guan Y, Nakano D, Zhang Y, Li L, Tian Y, Nishiyama A. A mouse model of renal fibrosis to overcome the technical variability in ischaemia/reperfusion injury among operators. *Sci Rep.* (2019) 9:10435. doi: 10.1038/s41598-019-46994-z
106. Chelko SP, Schmiedt CW, Lewis TH, Lewis SJ, Robertson TP. A novel vascular clip design for the reliable induction of 2-kidney, 1-clip hypertension in the rat. *J Appl Physiol.* (2012) 112:362–6. doi: 10.1152/japplphysiol.01015.2011
107. Li L-Q, Zhang J, Wang R, Li J-X, Gu Y-Q. Establishment and evaluation of a reversible two-kidney, one-clip renovascular hypertensive rat model. *Exp Ther Med.* (2017) 13:3291–6. doi: 10.3892/etm.2017.4386
108. Allinovi M, De Chiara L, Angelotti ML, Becherucci F, Romagnani P. Anti-fibrotic treatments: a review of clinical evidence. *Matrix Biol.* (2018) 68-69:333–54. doi: 10.1016/j.matbio.2018.02.017
109. Becherucci F, Mazzinghi B, Allinovi M, Angelotti ML, Romagnani P. Regenerating the kidney using human pluripotent stem cells and renal progenitors. *Expert Opin Biol Ther.* (2018) 18:795–806. doi: 10.1080/14712598.2018.1492546
110. Liu Y. Cellular and molecular mechanisms of renal fibrosis. *Nat Rev Nephrol.* (2011) 7:684–96. doi: 10.1038/nrneph.2011.149
111. Ratliff BB, Abdulmahdi W, Pawar R, Wolin MS. Oxidant mechanisms in renal injury and disease. *Antioxid Redox Signal.* (2016) 25:119–46. doi: 10.1089/ars.2016.6665
112. Dendooven A, Ishola DA Jr, Nguyen TQ, Van der Giezen DM, Kok RJ, Goldschmeding R, et al. Oxidative stress in obstructive nephropathy. *Int J Exp Pathol.* (2011) 92:202–10. doi: 10.1111/j.1365-2613.2010.00730.x
113. Liu B, Hu D, Zhou Y, Yu Y, Shen L, Long C, et al. Exosomes released by human umbilical cord mesenchymal stem cells protect against renal interstitial fibrosis through ROS-mediated P38MAPK/ERK signaling pathway. *Am J Transl Res.* (2020) 12:4998–5014.
114. Ji C, Zhang J, Zhu Y, Shi H, Yin S, Sun F, et al. Exosomes derived from hucMSC attenuate renal fibrosis through CK1delta/beta-TRCP-mediated YAP degradation. *Cell death Dis.* (2020) 11:327. doi: 10.1038/s41419-020-2510-4
115. Kumar S, Liu J, Pang P, Krautzberger AM, Reginensi A, Akiyama H, et al. Sox9 activation highlights a cellular pathway of renal repair in the acutely injured mammalian kidney. *Cell Rep.* (2015) 12:1325–38. doi: 10.1016/j.celrep.2015.07.034
116. Zhu F, Chong Lee Shin OLS, Pei G, Hu Z, Yang J, Zhu H, et al. Adipose-derived mesenchymal stem cells employed exosomes to attenuate AKI-CKD transition through tubular epithelial cell dependent Sox9 activation. *Oncotarget.* (2017) 8:70707–26. doi: 10.18632/oncotarget.19979
117. Gregorini M, Corradetti V, Pattonieri EF, Rocca C, Milanesi S, Peloso A, et al. Perfusion of isolated rat kidney with mesenchymal stromal cells/extracellular vesicles prevents ischaemic injury. *J Cell Mol Med.* (2017) 21:3381–93. doi: 10.1111/jcmm.13249
118. Ishiy C, Ormanji MS, Maquigussa E, Ribeiro RS, da Silva Novaes A, Boim MA. Comparison of the effects of mesenchymal stem cells with their extracellular vesicles on the treatment of kidney damage induced by chronic renal artery stenosis. *Stem Cells Int.* (2020) 2020:8814574. doi: 10.1155/2020/8814574
119. Du T, Zou X, Cheng J, Wu S, Zhong L, Ju G, et al. Human Wharton's jelly-derived mesenchymal stromal cells reduce renal fibrosis through induction of native and foreign hepatocyte growth factor synthesis in injured tubular epithelial cells. *Stem Cell Res Ther.* (2013) 4:59. doi: 10.1186/scrt215
120. Wang B, Yao K, Huuskes BM, Shen HH, Zhuang J, Godson C, et al. Mesenchymal stem cells deliver exogenous microRNA-let7c via exosomes to attenuate renal fibrosis. *Mol Ther.* (2016) 24:1290–301. doi: 10.1038/mt.2016.90

121. Jin J, Qian F, Zheng D, He W, Gong J, He Q. Mesenchymal stem cells attenuate renal fibrosis via exosomes-mediated delivery of microRNA Let-7i-5p antagomir. *Int J Nanomed.* (2021) 16:3565–78. doi: 10.2147/ijn.s299969
122. Åkerud P, Canals JM, Snyder EY, Arenas E. Neuroprotection through delivery of glial cell line-derived neurotrophic factor by neural stem cells in a mouse model of Parkinson's disease. *J Neurosci.* (2001) 21:8108–18. doi: 10.1523/jneurosci.21-20-08108.2001
123. Sun S, Zhang Q, Li M, Gao P, Huang K, Beejadhursing R, et al. GDNF promotes survival and therapeutic efficacy of human adipose-derived mesenchymal stem cells in a mouse model of Parkinson's disease. *Cell Transpl.* (2020) 29:0963689720908512. doi: 10.1177/0963689720908512
124. Chen L, Wang Y, Li S, Zuo B, Zhang X, Wang F, et al. Exosomes derived from GDNF-modified human adipose mesenchymal stem cells ameliorate peritubular capillary loss in tubulointerstitial fibrosis by activating the SIRT1/eNOS signaling pathway. *Theranostics.* (2020) 10:9425–42. doi: 10.7150/thno.43315
125. Larson BL, Ylostalo J, Lee RH, Gregory C, Prockop DJ. Sox11 is expressed in early progenitor human multipotent stromal cells and decreases with extensive expansion of the cells. *Tissue Eng Part A.* (2010) 16:3385–94. doi: 10.1089/ten.tea.2010.0085
126. Zhang ZY, Hou YP, Zou XY, Xing XY, Ju GQ, Zhong L, et al. Oct-4 enhanced the therapeutic effects of mesenchymal stem cell-derived extracellular vesicles in acute kidney injury. *Kidney Blood Press Res.* (2020) 45:95–108. doi: 10.1159/000504368
127. Tian K, Chen P, Liu Z, Si S, Zhang Q, Mou Y, et al. Sirtuin 6 inhibits epithelial to mesenchymal transition during idiopathic pulmonary fibrosis via inactivating TGF-β1/Smad3 signaling. *Oncotarget.* (2017) 8:61011–24. doi: 10.18632/oncotarget.17723
128. Cai J, Liu Z, Huang X, Shu S, Hu X, Zheng M, et al. The deacetylase sirtuin 6 protects against kidney fibrosis by epigenetically blocking β-catenin target gene expression. *Kidney Int.* (2020) 97:106–18. doi: 10.1016/j.kint.2019.08.028
129. Liu L, Wu Y, Wang P, Shi M, Wang J, Ma H, et al. PSC-MSC-derived exosomes protect against kidney fibrosis in vivo and in vitro through the SIRT6/β-catenin signaling pathway. *Int J Stem Cells.* (2021) 14:310–9. doi: 10.15283/ijsc20184
130. Maidhof W, Hilas O. Lupus: an overview of the disease and management options. *P T.* (2012) 37:240–9.
131. Anders HJ, Saxena R, Zhao MH, Parodis I, Salmon JE, Mohan C. Lupus nephritis. *Nat Rev Dis Primers.* (2020) 6:7. doi: 10.1038/s41572-019-0141-9
132. Yang X, Yang J, Li X, Ma W, Zou H. Bone marrow-derived mesenchymal stem cells inhibit T follicular helper cell in lupus-prone mice. *Lupus.* (2018) 27:49–59. doi: 10.1177/0961203317711013
133. Lee HK, Kim KH, Kim HS, Kim JS, Lee JH, Ji A, et al. Effect of a combination of prednisone or mycophenolate mofetil and mesenchymal stem cells on lupus symptoms in MRL.Fas(lpr) mice. *Stem Cells Int.* (2018) 2018:4273107. doi: 10.1155/2018/4273107
134. Gu F, Wang D, Zhang H, Feng X, Gilkeson GS, Shi S, et al. Allogeneic mesenchymal stem cell transplantation for lupus nephritis patients refractory to conventional therapy. *Clin Rheumatol.* (2014) 33:1611–9. doi: 10.1007/s10067-014-2754-4
135. Shen B, Liu J, Zhang F, Wang Y, Qin Y, Zhou Z, et al. CCR2 Positive exosome released by mesenchymal stem cells suppresses macrophage functions and alleviates ischemia/reperfusion-induced renal injury. *Stem Cells Int.* (2016) 2016:1240301. doi: 10.1155/2016/1240301
136. Fatima F, Ekstrom K, Nazarenko I, Maugeri M, Valadi H, Hill AF, et al. Non-coding RNAs in mesenchymal stem cell-derived extracellular vesicles: deciphering regulatory roles in stem cell potency, inflammatory resolve, and tissue regeneration. *Front Genet.* (2017) 8:161. doi: 10.3389/fgene.2017.00161
137. Wei S, Zhang Z, Yan L, Mo Y, Qiu X, Mi X, et al. miR-20a overexpression in adipose-derived mesenchymal stem cells promotes therapeutic efficacy in murine lupus nephritis by regulating autophagy. *Stem Cells Int.* (2021) 2021:3746335. doi: 10.1155/2021/3746335
138. Chen X, Wei Q, Sun H, Zhang X, Yang C, Tao Y, et al. Exosomes derived from human umbilical cord mesenchymal stem cells regulate macrophage polarization to attenuate systemic lupus erythematosus-associated diffuse alveolar hemorrhage in mice. *Int J Stem Cells.* (2021) 14:331–40. doi: 10.15283/ijsc20156
139. Correa RR, Juncosa EM, Masereeuw R, Lindoso RS. Extracellular vesicles as a therapeutic tool for kidney disease: current advances and perspectives. *Int J Mol Sci.* (2021) 22:5787. doi: 10.3390/ijms22115787
140. Busatto S, Vilanilam G, Ticer T, Lin WL, Dickson DW, Shapiro S, et al. Tangential flow filtration for highly efficient concentration of extracellular vesicles from large volumes of fluid. *Cells.* (2018) 7:273. doi: 10.3390/cells7120273
141. Zhang H, Freitas D, Kim HS, Fabijanic K, Li Z, Chen H, et al. Identification of distinct nanoparticles and subsets of extracellular vesicles by asymmetric flow field-flow fractionation. *Nat Cell Biol.* (2018) 20:332–43. doi: 10.1038/s41556-018-0040-4

Conflict of Interest: The authors declare that the research was conducted in the absence of any commercial or financial relationships that could be construed as a potential conflict of interest.

Publisher's Note: All claims expressed in this article are solely those of the authors and do not necessarily represent those of their affiliated organizations, or those of the publisher, the editors and the reviewers. Any product that may be evaluated in this article, or claim that may be made by its manufacturer, is not guaranteed or endorsed by the publisher.

frontiers | Frontiers in Medicine

TYPE Original Research
PUBLISHED 16 August 2022
DOI 10.3389/fmed.2022.817387

OPEN ACCESS

EDITED BY
Minnie M. Sarwal,
University of California, San Francisco, United States

REVIEWED BY
Megan McFerson SooHoo,
University of Colorado, United States
Eisei Noiri,
National Center for Global Health and Medicine, Japan
Jonathan Samuel Chávez-Iñiguez,
University of Guadalajara, Mexico
Nakysa Hooman,
Iran University of Medical Sciences, Iran
Daniela Ponce,
São Paulo State University, Brazil

*CORRESPONDENCE
Rolando Claure-Del Granado
rclaure@yahoo.com

SPECIALTY SECTION
This article was submitted to Nephrology, a section of the journal Frontiers in Medicine

RECEIVED 18 November 2021
ACCEPTED 27 July 2022
PUBLISHED 16 August 2022

CITATION
Gaspar A, Iturricha-Cáceres MF, Macedo E, Mehta RL and Claure-Del Granado R (2022) The use of a medical application improves the diagnosis of acute kidney injury: A pre-post study. *Front. Med.* 9:817387. doi: 10.3389/fmed.2022.817387

The use of a medical application improves the diagnosis of acute kidney injury: A pre-post study

Andrea Gaspar[1], Maria F. Iturricha-Cáceres[2], Etienne Macedo[3], Ravindra L. Mehta[3] and Rolando Claure-Del Granado[4,5]*

[1]MedStar Franklin Square Medical Center, Baltimore, MD, United States, [2]Facultad de Medicina, Universidad Privada del Valle, Tiquipaya, Bolivia, [3]Division of Nephrology-Hypertension, University of California, San Diego, San Diego, CA, United States, [4]Facultad de Medicina, Universidad Mayor de San Simón, Cochabamba, Bolivia, [5]Hospital Obrero No 2 - CNS, Cochabamba, Bolivia

The use of mobile devices by healthcare providers has transformed many aspects of clinical practice. Mobile devices and medical applications provide many benefits, perhaps most significantly increased access to point-of-care (POC) tools, which has been shown to support better clinical decision making and improved patient outcomes. In LMICs, where computer-based technology is limited, the use of mobile technology has the potential to immensely increase access to point of care tools. In this study, we conducted an interventional, pre-post study to determine whether the use of a medical application could help healthcare providers accurately recognize and diagnose AKI. After preparing 20 clinical vignettes based on AKI cases from our center Global Snapshot study report, we asked 50 last year medical students to identify the presence and stage of AKI first without and then with the use of the IRA SLANH App (IRA SLANH app, Island of the Moon® V.1, 2014; Cochabamba-Bolivia), which was designed specifically for this study. Before the IRA SLANH app was introduced, the mean number of correctly identified cases of AKI was 14.7 ± 4.7 with a minimum of 3 and a maximum of 20. The stage of AKI was correctly identified in only 6.7 ± 4.4 of the cases. After the app was introduced, the number of correctly identified and staged cases of AKI was 20. Medical applications are useful point-of-care tools in the practice of evidence-based medicine. Their use has the potential to play a very important role in early identification and classification of AKI, particularly in LMICs potentially allowing for earlier intervention with preventive and treatment strategies to reverse kidney injury and improve recovery.

KEYWORDS

acute kidney injury, medical application, serum creatinine, mobile health, smartphones

Background

Acute kidney injury (AKI) is a common problem worldwide, affecting over 13 million people annually and causing 1.7 million deaths (1–3). AKI is caused by a multitude of etiologies (i.e., nephrotoxic medications, antibiotics, contrast, dehydration, sepsis, heart failure) and can occur in the hospital or in the community. Hospital-acquired AKI is

often multifactorial and occurs in patients that have multiple comorbidities that augment susceptibility to AKI (4–6). In contrast, community-acquired AKI usually occurs after just one inciting event, such as a diarrhea or an infectious illness, and it affects those with fewer comorbidities (6). Every episode of AKI increases the risk for progression to chronic kidney disease, end-stage kidney disease, and death - all of which can lead to diminished quality of life for patients, higher healthcare costs, and strain on healthcare systems. More severe AKI translates into a greater risk (3, 4). If identified and managed in a timely fashion, however, AKI is treatable and reversible, preventing its numerous burdensome sequelae.

AKI is particularly problematic in low-and-middle-income countries (LMICs), where rates are significantly higher compared to high-income countries (HICs) and healthcare systems are chronically resource-constrained. Nearly 85% of the world's cases of AKI occur in low-and-middle-income countries (LMICs). Despite the fact that most of these cases are caused by a single preventable insult such as a diarrheal illness or dehydration, associated morbidity and mortality is higher (1, 3, 7, 8). This is often a result of the inability to rapidly diagnose and treat AKI due to inadequate laboratory facilities, poor knowledge about risk factors for AKI and its consequences, as well as a dearth of supplies to aggressively manage AKI. Moreover, AKI more often occurs in younger patients with fewer co-morbidities, individuals whose disability from illness potentially renders a significant burden on society.

Because AKI is treatable and reversible if intervened upon early, it is important to find innovative ways to mitigate the burden of unrecognized AKI in LMICs. One potential way to do this is through using mobile technology (mHealth) to create point-of-care tools that allow healthcare providers to correctly recognize, stage, and treat AKI (3). Because mHealth bypasses the need for computers and Internet – resources which are often limited or non-existent in LMIC clinical settings - it is a promising tool to improve access to point-of-care testing and decision making (9).

In this study, we employed mHealth to help healthcare providers recognize and classify AKI. We created a Smartphone-based application (IRA SLANH app, Island of the Moon® V.1, 2014; Cochabamba-Bolivia) to assist with AKI diagnosis, and we hypothesize that its use would improve both recognition and classification of AKI.

Abbreviations: POC, point-of-care; sCr, serum creatinine; AKI, Acute kidney injury; CKD, Chronic Kidney Disease; ESKD, End Stage Kidney Disease; HICs, high-income countries; LMICs, low- and middle-income countries; RRT, renal replacement therapy; mHealth, Mobile health; KDIGO, Kidney Disease: Improving Global Outcomes.

Methods

The primary objective of this study was to evaluate the utility of a Smartphone-based mobile application in helping healthcare providers accurately diagnose and stage AKI. In order to do this, we conducted an interventional pre-post study in which last-year medical students from Cochabamba, Bolivia, were asked to identify the presence and stage of AKI both with and without the use of the IRA-SLANH application. The primary outcome was the percentage of medical students correctly identifying and staging AKI before and after use of the application.

Hospital Obrero No 2 Caja Nacional de Salud is a government-run hospital serving essential employees located in Cochabamba, Bolivia. Using the hospital's Global Snapshot Study Report, we identified twenty confirmed cases of AKI by comparing a baseline SCr to another SCr measurement within seven days of hospital admission. AKI was defined using the KDIGO guidelines of a >0.3 rise in SCr within 48 h or an increase in SCr to $>$ 1.5 times baseline occurring within the last seven days (10). Prior to initiation of the study, approval by the local ethics committee (Hospital Obrero No 2 - C.N.S, ethics committee) and written consent to participate from all participants was obtained. All procedures were in accordance with the Declaration of Helsinki.

Study participants were selected *via* convenience sampling. Any last-year medical student attending Cochabamba's medical school was eligible. All available students participated for a total of 50 students. Clinical vignettes about each of the pre-identified 20 cases of AKI were prepared (Figure 1). Patient demographics and risk factors for AKI were included in the vignettes (Table 1 shows some characteristics of patients with AKI). The medical students were asked to read the vignette and identify both the presence and stage of AKI in each case. After 72 h, they were then asked to download the IRA-SLANH application. The IRA-SLANH application is unique in that it is one of the few smart-phone based applications that assist with identifying the presence and stage of AKI as well as recommended treatment. It is free and available to all healthcare providers who have a Smartphone. All information presented in the application is based on the KDIGO criteria and guidelines of identifying and managing AKI (10). Figure 2 show the functioning of the application in greater detail.

After downloading the application, the students were asked again to identify and stage AKI, and the number of correctly identified cases and percentage of students identifying all cases correctly were compared continuous variables were expressed as the mean ± SD, or median and interquartile range. Between-group comparisons of continuous variables were performed using the independent *t*-test or Mann-Whitney *U* test, after testing for normality using the Kolmogorov-Smirnov test. Dichotomous variables were compared using chi-square test or

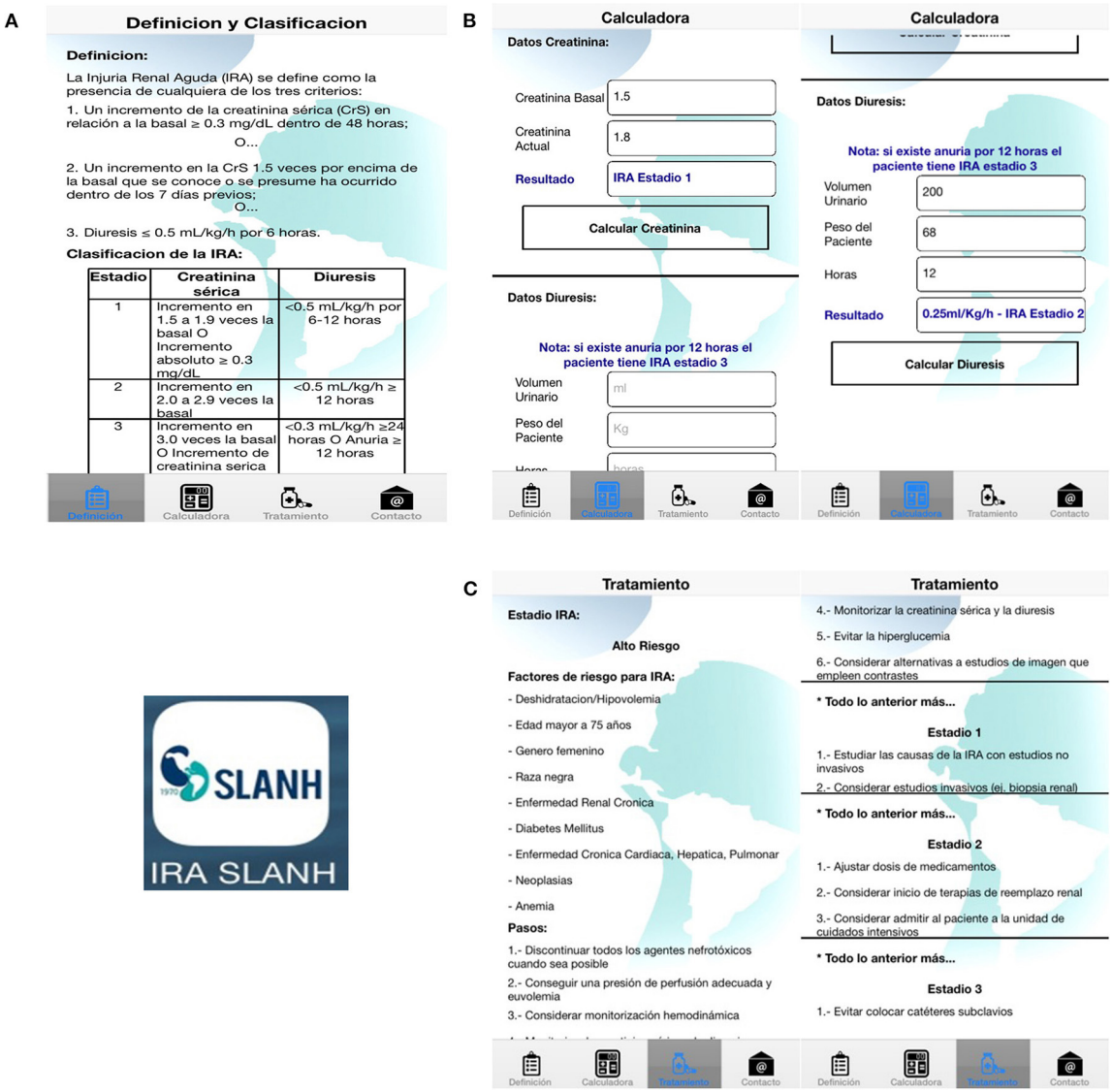

FIGURE 1
Different tabs of the IRA SLANH application. **(A)** The first tab reviews the KDIGO criteria for the definition and stages of AKI (11). **(B)** The second tab calculates the presence and stage of AKI according to these guidelines; it uses either the patient's urine output or a comparison of their baseline sCr to current sCr. **(C)** The third tab provides recommendations for clinical management according both to the level of the AKI, also based on the current KDIGO guidelines (11).

Fisher's exact test. All statistical analyses were two-tailed and performed using SPSS 22 software (SPSSFW, SPSS Inc., IBM, Armonk, NY, USA). The two-sided $P < 0.05$ was considered statistically significant.

Results

The most common co-morbidity among patients identified with AKI in the clinical cases used for this study was diabetes mellitus (28.2%). Mean baseline serum creatinine was 0.9 with a range of 0.8−1.1 mg/dL. The most common etiologies of AKI included dehydration (59%), hypotension/shock (56.4%), and nephrotoxic agents (48.7%). Just over half (56.4%) of cases occurred in the community, and the remainder (43.6%) occurred in the hospital.

Regarding some general characteristics of the medical students that participated in the survey; the mean age was 24.5 ± 1.7 years (with a minimum age of 23 years and a maximum age of 30 years), 54% of the students who answered the survey were male, and 60% of the students were from the public university (Universidad Mayor de San Simon), the rest of the students came from three different private universities (22% UNIVALLE, 14% UPAL, and 4% UNITEPC) all located in the city of Cochabamba.

TABLE 1 Characteristics of acute kidney injury.

Documented location	
	Percentage
Community-acquired AKI	(56.4%)
Hospital-acquired AKI	(43.6%)
AKI Stages	
AKI Stage 1	37.9%
AKI Stage 2	19.2%
AKI Stage 3	42.9%
Documented etiologies	
	Number (n)	**Percentage (%)**
Dehydration	11.8	59%
Hypotension/shock	11.28	56.4%
Cardiac Disease	2.56	12.8%
Liver Disease	1.54	7.7%
Urinary obstruction	2.06	10.3%
Infection	2.56	12.8%
Nephrotoxic Agents	9.74	48.7%
Animal Venom	0.52	2.6%
Sepsis	10.76	53.8%

*More than one risk factor could be present in the same patient. Community-acquired AKI is usually more common in LMICs, and usually present in more advance stages (AKI stage 2–3 in 62.1%) due to delay recognition and diagnosis. The three most common causes of AKI were dehydration, hypotension, and nephrotoxins.

Prior to the introduction of the IRA-SLANH application, 22% of medical students correctly identified the presence of AKI in all cases, and 0% identified its stage in all cases. The mean number of correctly identified AKI cases was 14.7 ± 4.7 (Table 2), and the mean number of correctly staged cases was 6.7 ± 4.4. With use of the application, 100% of students were able to correctly identify and stage AKI in all 20 cases. The use of the IRA-SLANH App improved the number of correct AKI identification answers with a mean of 5.22 ± 4.7 (95% CI 3.87 − 6.57; $p < 0.001$). The number of correct answers about AKI staging also improved after the use of this App with a mean of 13.6 ± 4.4 (95% CI 11.9 − 14.5; $p < 0.001$).

Discussion

The use of our app (IRA-SLANH) improved the ability of medical students to identify and stage AKI. The ease of access to information enabled them to quickly identify and stage AKI based on the KDIGO criteria. We showed that a simple intervention with a smartphone-based medical application can have a meaningful impact on correct diagnosis of AKI.

Several studies have demonstrated that point-of-care tools can help providers identify and appropriately manage AKI. They also have important impacts on patient care by improving time to treatment, increasing rates of renal function recovery, and decreasing mortality (12, 13). Most of these studies, however, have been conducted in high-income countries using electronic medical records (12, 13). Due to cost and high technical skills requirements, electronic medical records are not commonly used in LMICs (14). It is therefore important to find other platforms to create point-of-care tools for AKI diagnosis and treatment.

The use of mobile technology, including Smartphones, is increasing throughout the world (15). Because mobile technology bypasses the need for computers and the Internet, it is a promising and cost-effective vehicle to improve access to medical information, including point-of-care decision tools through medical applications (16, 17). Along with being widely accessible through Smartphones, medical applications are appealing because minimal training is required for their use and running costs are negligible. The IRA-SLANH application is an example of a medical application that is simple in nature but has potentially profound impacts on both short-term and long-term patient outcomes. The downstream effects of early AKI recognition in LMICs will help diminish the burden that chronic sequelae such as chronic kidney disease and end-stage renal disease have on patients, healthcare systems, and society (6, 11).

To our knowledge, this is the first LMIC-based study that examines the use of a point-of-care tool to help providers accurately diagnose AKI. It is also one of the first studies to examine Smartphone-based point-of-care decision-making tools in LMICs (17). Given the prevalence of AKI in LMICs, its disproportionate morbidity and mortality, and its often-insidious presentation, equipping healthcare providers with easily accessible, point-of-care tools to quickly and accurately diagnose and manage AKI is crucial. The results of our study are promising that medical applications can play an important role in the early identification, staging, and prompt initiation of AKI treatment.

The main strength of this study is that it is one of the first studies of its kind in many realms. It is novel in its evaluation of a Smartphone-based point-of-care tool of LMICs and its innovative approach to AKI diagnosis. It is one of the few - if not only - medical applications available that not only identifies AKI but also stages it and recommends guideline-based treatment. Additionally, the significant differences observed before and after use of the application lay a strong foundation for future studies to more extensively examine how point-of-care tools assist with diagnosis and treatment of AKI in LMIC settings and affect patient outcomes.

This study has several limitations. Although it was an interventional study, it was a non-randomized pre-post design. We did not assess knowledge of AKI prior to the study or randomize students based on other characteristics. The study

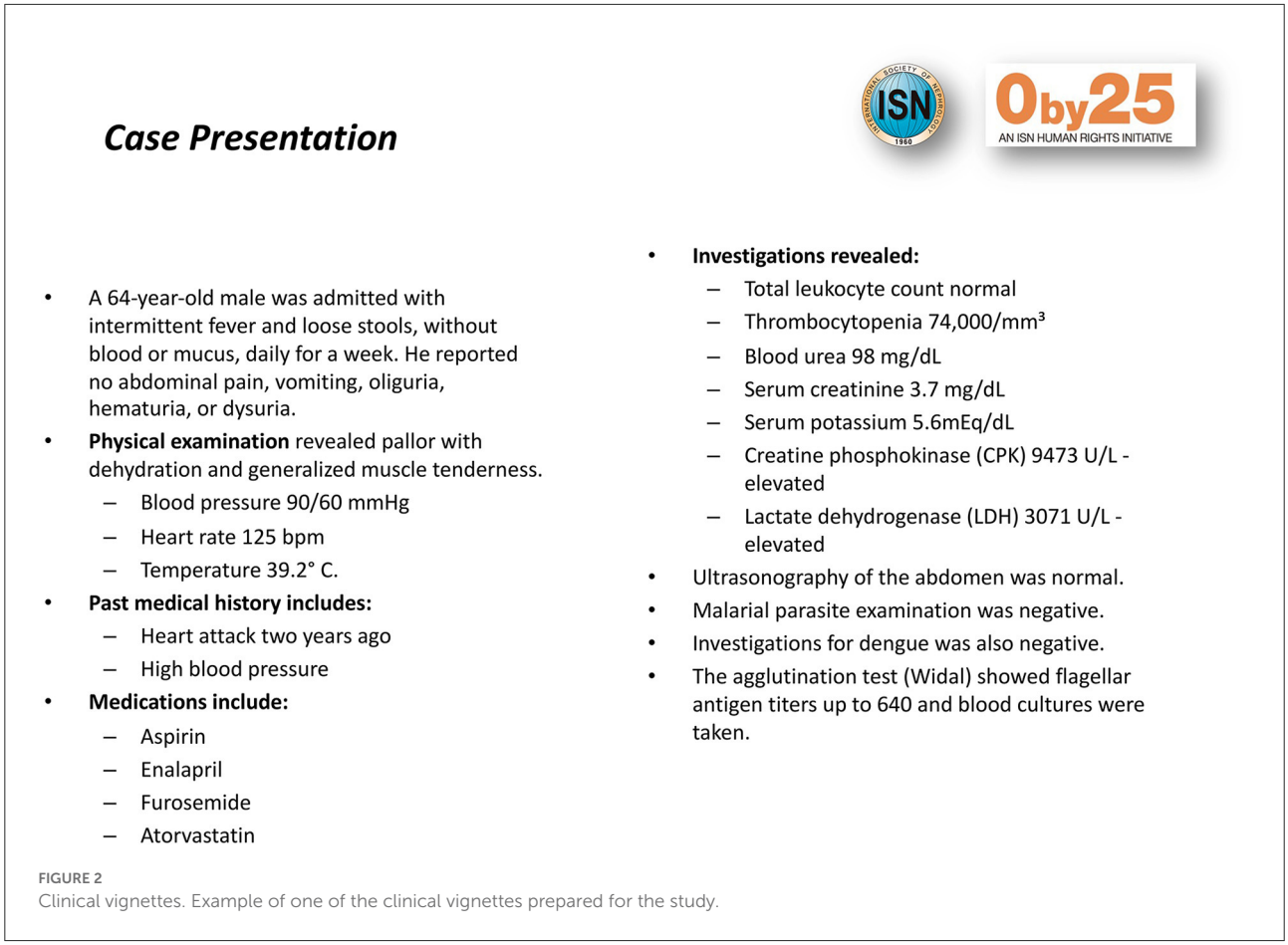

FIGURE 2
Clinical vignettes. Example of one of the clinical vignettes prepared for the study.

TABLE 2 AKI recognition and classification pre and post *IRA-SLANH App*.

	AKI recognition		AKI classification	
	Pre App	Post App	Pre App	Post App
Mean ± SD of correct answers	14.7 ± 4.7^a	20^a	6.7 ± 4.4^b	20^b
Minimum number of correct answers	3	20	0	20
Maximum number of correct answers	20	20	16	20

Only 22% of students could correctly identified AKI in all 20 cases. 0% of students could correctly classified (stages 1, 2, or 3) all AKI cases. *a and *b $p < 0.001$. The use of a the IRA-SLANH App improved the recognition and classification of AKI in a low-resource setting.

size was also small. Although the study was limited to trainees whose knowledge and skills are not as refined as fully trained providers, they were in their last year of training and most likely had gained the majority of the knowledge needed to practice independently. In addition, the study did not investigate how improved recognition of AKI impacted management or clinical outcomes. Future studies are needed to investigate these important aspects, especially since AKI is a condition whose potentially grave consequences are easily reversible if recognized early.

Conclusions

Smartphone-based medical applications have the potential to be incredibly useful point-of-care tools for helping LMIC providers apply evidence-based medicine when managing AKI. The significant improvement we saw in the ability of students to accurately diagnose AKI before and after the use of the IRA-SLANH application shows how a simple, low-cost intervention can potentially have a hugely positive impact. Although our study was small, our findings lay a strong foundation for future

studies to investigate the feasibility and impact of point-of-care tools to assist with diagnosis and management of AKI in LMIC settings.

Data availability statement

The raw data supporting the conclusions of this article will be made available by the authors, without undue reservation.

Ethics statement

The studies involving human participants were reviewed and approved by Jefatura de Enseñanza e Investigación Hospital Obrero No 2 - CNS. The patients/participants provided their written informed consent to participate in this study.

Author contributions

RC-D: study concept and design, statistical analysis, obtained funding, and study supervision. MI-C, AG, and RC-D: data acquisition, analysis, or interpretation of data. AG, MI-C, RM, EM, and RC-D: drafting of the manuscript. AG, RM, EM, and RC-D: critical revision of the manuscript for important intellectual content. MI-C and RC-D: had full access to all of the data in the study and take responsibility for the integrity of the data, the accuracy of the data analysis, the honest, accurate, and transparent reporting of the study. All authors contributed important intellectual content during manuscript drafting or revision and accepts accountability for the overall work by ensuring that questions pertaining to the accuracy or integrity of any portion of the work are appropriately investigated and resolved. All authors read and approved the final manuscript.

Funding

The clinical study reported in this publication was supported by a Sister Renal Center Program grant from the International Society of Nephrology (ISN) who provided research support for the implementation of the 0by25 pilot study at our Institution. The IRA SLANH® app development was supported by a grant provided by the Acute Kidney Injury Committee of the Latin American Society of Nephrology and Hypertension (SLANH), this grant cover the cost of the design and the development of the application by the apps developer company (Island of the Moon, Cochabamba-Bolivia).

Conflict of interest

The authors declare that the research was conducted in the absence of any commercial or financial relationships that could be construed as a potential conflict of interest.

Publisher's note

All claims expressed in this article are solely those of the authors and do not necessarily represent those of their affiliated organizations, or those of the publisher, the editors and the reviewers. Any product that may be evaluated in this article, or claim that may be made by its manufacturer, is not guaranteed or endorsed by the publisher.

References

1. Perico N, Remuzzi G. Acute kidney injury in low-income and middle-income countries: no longer a death sentence. *Lancet.* 4:e216–7. doi: 10.1016/S2214-109X(16)00065-6

2. Lunyera J, Kilonzo K, Lewington A, Yeates K, Finkelstein FO. Acute kidney injury in low-resource settings: Barriers to diagnosis, awareness, and treatment and strategies to overcome these barriers. *Am J Kidney Dis.* (2016) 6:834–40. doi: 10.1053/j.ajkd.2015.12.018

3. Mehta RL, Cerdá J, Burdmann EA, Tonelli M, García-García G, Jha V, et al. International Society of Nephrology's 0by25 initiative for acute kidney injury (zero preventable deaths by 2025): a human rights case for nephrology. *Lancet.* (2015) 385:2616–43. doi: 10.1016/S0140-6736(15)60126-X

4. Aitken E, Carruthers C, Gall L, Kerr L, Geddes C, Kingsmore D. Acute kidney injury: outcomes and quality of care. *QJ Med.* (2013) 106:323–32. doi: 10.1093/qjmed/hcs237

5. Wonnacott A, Meran S, Amphlett B, Talabani B, Phillips A. Epidemiology and outcomes in community-acquired versus Hospital-Acquired AKI. *Clin J Am Soc Nephrol.* (2014) 9:1007–14. doi: 10.2215/CJN.07920713

6. Lameire NH, Bagga A, Cruz D, De Maeseneer J, Endre Z, Kellum JA, et al. Acute kidney injury: an increasing global concern. *Lancet.* (2013) 382:170–9. doi: 10.1016/S0140-6736(13)60647-9

7. Olowu WA, Niang A, Osafo C, Ashuntantang G, Arogundade FA, Porter J, et al. Outcomes of acute kidney injury in children and adults in sub-Sabsaharan Africa: a systematic review. *The Lancet.* (2016) 4:e242–e250. doi: 10.1016/S2214-109X(15)00322-8

8. Susantitaphong P, Cruz DN, Cerda J, Abulfaraj M, Alqahtani F, Koulouridis I, et al. World Incidence of AKI: A meta-analysis. *Clin J Am Soc Nephrol.* (2013) 8:1482–93. doi: 10.2215/CJN.00710113

9. Abaza H, Marschollek M. mHealth Application Areas and Technology Combinations*. A Comparison of Literature from High and Low/Middle Income Countries. *Methods Inf Med.* (2017) 56:e105–22. doi: 10.3414/ME17-05-0003

10. Levin A, Stevens PE. Summary of recommendation statements. *Kidney Int Suppl.* (2011) 2:8–12. doi: 10.1038/kisup.2012.7

11. Xu G, Baines R, Westacott R, Selby N, Carr S. An educational approach to improve outcomes in acute kidney injury (AKI): report of a quality improvement project. *BMJ Open.* (2014) 4:e004388. doi: 10.1136/bmjopen-2013-004388

12. Colpaert K, Hoste EA, Steurbaut K, Benoit D, Van Hoecke S, De Turck F, et al. Impact of real-time electronic alerting of acute kidney injury on therapeutic intervention and progression of RIFLE class. *Crit Care Med.* (2012) 40:1164–70. doi: 10.1097/CCM.0b013e3182387a6b

13. Haase M, Kribben A, Zidek W, Floege J, Albert C, Isermann B, et al. Electronic alerts for acute kidney injury. *Dtsch Arztebl Int.* (2017) 114:1–8. doi: 10.3238/arztebl.2017.0001

14. Goldbach H, Chang AY, Kyer A, Ketshogileng D, Taylor L, Chandra A, et al. Evaluation of generic medical information accessed via mobile phones at the point of care in resource-limited settings. *J Am Med Inform Assoc*. (2014) 1:37–42. doi: 10.1136/amiajnl-2012-001276

15. Royston G, Hagar C, Long LA, McMahon D, Pakenham-Walsh N, Wadhwani N. Mobile health-care information for all: a global challenge. *The Lancet Global Health*. (2015) 3:e356–7. doi: 10.1016/S2214-109X(15)00054-6

16. Littman-Quinn R, Chandra A, Schwartz A, Chang AY, Fadlelmola FM, Ghose S, et al. mHealth applications for clinical education, decision making, and patient adherence in botswana. In *2011 IST-Africa Conference Proceedings*. IEEE. (2011). 1–8. Available online at: https://ieeexplore.ieee.org/document/6107382

17. Källander K, Tibenderana JK, Akpogheneta OJ, Strachan DL, Hill Z, ten Asbroek AH, et al. Mobile Health (mHealth) approaches and lessons for increased performance and retention of community health workers and low- and middle-income countries: a review. *J Med Internet Res*. (2013) 15:e17. doi: 10.2196/jmir.2130

Advantages of publishing in Frontiers

OPEN ACCESS
Articles are free to read for greatest visibility and readership

FAST PUBLICATION
Around 90 days from submission to decision

HIGH QUALITY PEER-REVIEW
Rigorous, collaborative, and constructive peer-review

TRANSPARENT PEER-REVIEW
Editors and reviewers acknowledged by name on published articles

Frontiers
Avenue du Tribunal-Fédéral 34
1005 Lausanne | Switzerland

Visit us: www.frontiersin.org
Contact us: frontiersin.org/about/contact

REPRODUCIBILITY OF RESEARCH
Support open data and methods to enhance research reproducibility

DIGITAL PUBLISHING
Articles designed for optimal readership across devices

FOLLOW US
@frontiersin

IMPACT METRICS
Advanced article metrics track visibility across digital media

EXTENSIVE PROMOTION
Marketing and promotion of impactful research

LOOP RESEARCH NETWORK
Our network increases your article's readership